

ADVANCED SOLAR OBSERVATORY (ASO) ACCOMMODATIONS REQUIREMENTS STUDY FINAL REPORT

May 1989

Contract No. NAS8-37128

Prepared for:
George C. Marshall Space Flight Center
Marshall Space Flight Center, AL 35812

(NASA-CR-183718) ADVANCED SOLAR OBSERVATORY N89-26885
(ASO) ACCOMMODATIONS REQUIREMENTS STUDY
Final Report (Teledyne Brown Engineering) CSCL 22B
330 p G3/18 0224021 Unclas

 **TELEDYNE
BROWN ENGINEERING**

Cummings Research Park • Huntsville, Alabama 35807

**ADVANCED SOLAR OBSERVATORY (ASO)
ACCOMMODATIONS REQUIREMENTS STUDY
FINAL REPORT**

May 1989

Contract No. NAS8-37128



TELEDYNE

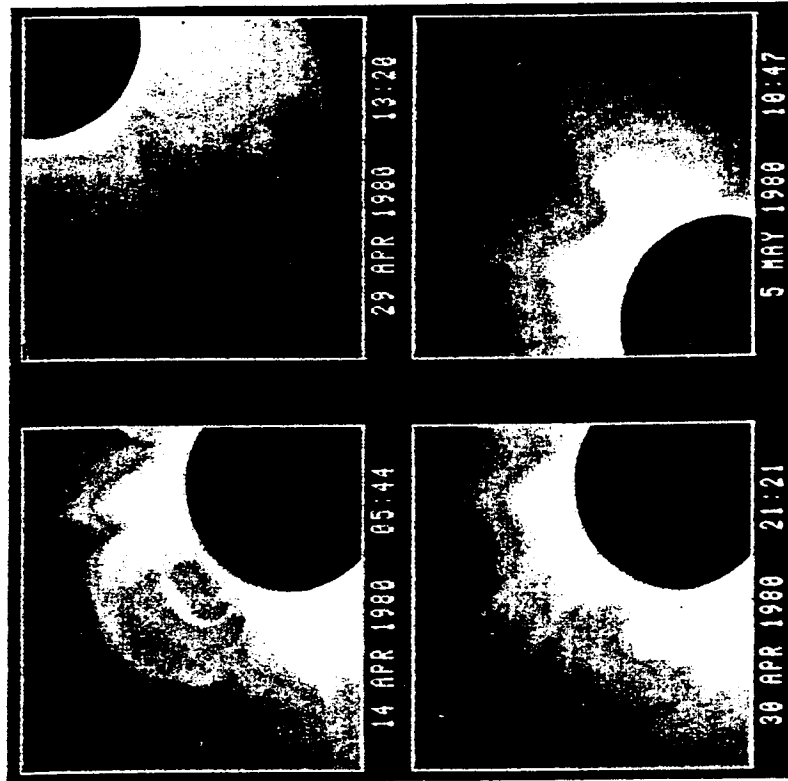
BROWN ENGINEERING

Cummings Research Park • Huntsville, Alabama 35807

Frontispiece



ORIGINAL PAGE
BLACK AND WHITE PHOTOGRAPH



A solar flare is the result of the explosive release of magnetic energy built up in the solar atmosphere by motions of the ionized gases below the Sun's photosphere. The flare associated eruption at the left is seen in the light of the Lyman- α line of Helium II, at 304 Å. The photograph was made from the first comprehensive solar space observatory, Skylab, on August 9, 1973,

with the Naval Research Laboratory's Objective Grating Spectroheliograph. The coronal mass ejection seen at the right was recorded with the High Altitude Observatory's Coronagraph/Polarimeter on the Solar Maximum Mission. The occulting disk radius is 1.5 times that of the Sun.

PREFACE

ADVANCED SOLAR OBSERVATORY SCIENTIFIC DESCRIPTION AND RATIONAL

The following is a description of the scientific requirements and program proposed for the Advanced Solar Observatory. This description was prepared by Dr. A.B.C. Walker, Stanford University. This material provided the basis for parts of the concept development and accommodations analysis.

ADVANCED SOLAR OBSERVATORY
SCIENTIFIC DESCRIPTION AND RATIONAL

1.0 Summary

1.1 Introduction: The Advanced Solar Observatory (ASO) is a comprehensive long duration solar space observatory which is planned to provide solar astronomers with the observational power (spectral, spatial, and temporal resolution, sensitivity, and breadth of wavelength coverage) necessary to address fundamental problems relating to the solar convection zone and activity cycle, the thermal and non-thermal processes which control the transport of energy, mass and magnetic flux in the solar atmosphere, the generation of the solar wind and the dynamics of the inner heliosphere. The ASO was recommended as the highest priority solar physics program for the decade of the 1980's in the report of the Astronomy Survey Committee [The Field Report (1, 2)]. The Science Working Group established as a result of the Field Report has developed an exciting concept for the evolutionary development of the Advanced Solar Observatory (3) which encompasses four instrument ensembles; (i) the Orbiting Solar Laboratory [OSL (4)] that includes visible and ultraviolet telescopes, (ii) the High Resolution Telescope Cluster [HRTC (3)] that includes extreme ultraviolet, XUV, soft x-ray and gamma ray telescopes, and Global Dynamics Instrumentation, (iii) the Pinhole/Occulter Facility [P/OF (5)] that includes Fourier transform and coded aperture x-ray and gamma ray telescopes and occulted ultraviolet and visible light coronagraphs, and (iv) the High Energy Facility [HEF (6)] that contains neutron, gamma ray and low frequency radio spectrometers. OSL is currently the highest priority moderate mission candidate within the Office of Space Science and Applications (OSSA). The ASO Science Working Group (ASOSWG) has recommended the deployment of the remaining ASO instrument ensembles on the Space Station. The ASO will operate as a facility open to the entire astronomical community.

Instrument concepts, which incorporate innovative new technologies, have been developed by the ASOSWG and others, however detailed scientific analysis, comprehensive engineering studies, and an assessment of the state of the relevant technologies critical to these updated instrument concepts is essential to the further development of the ASO. Preliminary results of an ongoing accommodation study (7) have confirmed the assessment of the ASOSWG that the ASO can be accommodated on the Space Station. However, in depth studies are required to address critical accommodation issues, notably pointing, data handling, command and control. A major goal of the concept study proposed herein is to carry out these detailed analyses, studies and assessments.

1.2 Scientific Program of the ASO: The scientific objectives of the ASO are to address fundamental questions relating to the Sun, in particular, and cool stars, in general; the specific objectives of the observatory are:

- i) *to provide instruments which are capable of observing solar phenomena on the inherent physical scales of the underlying processes that control these phenomena. For the Sun this fundamental physical scale, which is primarily that of the fine structure of the solar magnetic field, is ~70 km.*
- ii) *to allow the Sun to be studied simultaneously utilizing the entire electromagnetic spectrum, from high-energy gamma radiation to low-frequency radio waves. This capability will allow phenomena, such as solar flares, which manifest themselves at all temperatures present in the solar atmosphere, to be observed in their entirety.*
- iii) *to provide the diagnostic capability necessary to determine the detailed physical conditions extant within the solar plasma on spatial and temporal scales which will allow a direct comparison of our present understanding of physical theory with the phenomenology displayed by the solar plasma.*

1.3 Objectives and Significant Aspects of the Study: The objective of the concept study is to address the following issues related to the development of the ASO and its deployment and operation on the Space Station:

- i) definition of the requirements of the HRTC and HEF instrument ensembles to a level of detail sufficient to allow the selection of principal investigator teams for their development by the AO process. (The definition of the requirements of the P/OF is the subject of a separate Concept Study.)
- ii) definition of the facility equipment necessary to support the operation of the ASO on the Space Station. The most important issues to be addressed pertain to the pointing, data handling, and command and control requirements of the instrument ensembles.

- iii) development of a plan for the operation of the ASO, including coordinating observations of the four ASO instrument ensembles, insuring access to ASO by the astronomical community, defining the operational modes of the ASO, and the distribution and archiving of data.
- iv) development of a plan for the implementation of the ASO program, including management plans for the evolutionary construction and deployment of the ASO instrumentation, and for the management of the necessary ASO scientific and support operations. The evolution of ASO capabilities, which is essential for a long duration observing facility, will also be considered.

1.4 Investigative Approach: Our approach will be to emphasize detailed studies of the observational and operational requirements the ASO instruments must meet in order to address the major scientific questions we have posed, and the evolutionary development which the ASO must be capable of in order to meet new and as yet unforeseen requirements which will develop as the major scientific issues facing solar physics evolve. The methods we plan to use are the following:

- i) During the initial phases of the study, we will conduct a series of interactive studies of the design and operation of each ASO instrument. The design studies will be led by active solar instrumentalists and observers who will be designated as Instrument Scientists, with the assistance of consultants (who are also active members of the solar community) having expertise in areas which are critical to the design studies, such as detector technology and optics technology. The operational studies will be led by theoretical astronomers and observers, who will be designated as Mission Scientists. Subsequently, the Instrument Scientists and Mission Scientists will lead a series of scientific symposia which will provide a forum for the entire solar community to participate in the definition of observational capabilities and operational modes of the ASO instruments.
- ii) Based on the instrument design and operation studies and scientific symposia described above (and those anticipated from the parallel P/OF study mentioned earlier), we will further refine the accommodation requirements for the deployment of the ASO. This will allow the formulation of a specific set of issues pertaining to the accommodation of ASO on Space Station. We plan to initiate a number of subcontracts to address these specific issues. The issues we are able to identify now are (a) engineering analyses of the strawman ASO instrument concepts, (b) a study of alternative strategies (i.e., a fine pointing platform mounted on the Space Station Pointer, articulation of optical elements within the individual instruments, image motion compensation within the detectors, etc.) to meet the pointing requirements of the ASO instruments on Space Station, (c) a study of alternative strategies (i.e., on orbit data compression and analysis, transport of optical disks and photographic film via the Shuttle, teleoperation from the ground, control by mission specialists, etc.) to meet the operational command, control and data requirements of ASO on Space Station, and (d) a continuation of studies of the accommodation of ASO on Space Station, as the Space Station characteristics are defined in more detail.
- iii) We plan to develop a detailed plan for the operation of the ASO. Specific issues which must be addressed include the coordination of observational programs for the ASO instrument ensembles on different platforms, selection and implementation of scientific investigations for the ASO, control of observing sequences, handling and archiving of data, etc. The methods we plan to utilize include simulation of ASO observing sequences designed to address specific scientific issues of current interest, in scientific seminars to be led by the Mission Scientists.
- iv) We plan to investigate the approach used to manage the development and operation of other major NASA (ST, GRO, AXAF, SIRTf) and NSF (NOAO, NRAO) observatories as the initial step in the development of a plan to manage the development and operation of the ASO. PI's of major NASA programs, and directors of major observatories will be consulted. Based on these discussions, we plan to develop a complete management plan for the ASO, including coordination of evolutionary development of the ASO instruments, development of instrument support equipment (both flight equipment and ground-based equipment), operation of the ASO, and distribution and archiving of data.

1.5 Instrumentation: Table 1 presents an abbreviated summary of the anticipated performance of the ASO strawman instrument complement. Since the final ASO instrument complement will be selected by AO, our goal in the present study will be to model specific instrument designs to demonstrate that the performance goals that we have established can be met, and to identify the technologies that are critical to meeting those goals. Generalized specifications for the integration, and pre- and post-launch operation of ASO instruments on Space Station will be based on the detailed study of specific instrument designs. Specifications for the ground operations necessary to support the operation of the ASO on Space Station as a national facility will also be developed.

1.6 Data Acquisition Calibration Reduction, Analysis, and Archiving: It is probable that the acquisition of data by the ASO will utilize a number of media, including photoelectric detector arrays, photographic film, and storage on optical disks. The volume of data will present a formidable challenge. In order to address the issues raised by data acquisition, calibration, reduction, analysis and archiving, we will develop detailed models, of typical data sets that will be necessary to address specific problems of current interest by the use of simulations of observational campaigns. These simulations will be led by the Instrument Scientists and Mission Scientists, and will include a significant number of additional scientists from the solar community.

1.7 Role of the Crew and Payload Specialists: The interaction of the crew and payload specialists with solar instruments on Skylab, and on Spacelab 1 and 2 was an important component of the success of these missions. Definition of the role of the crew and payload specialists will be based on the past experience of major solar observatories on manned missions, and on the detailed instrument definitions and mission simulations to be carried out during the course of the study.

1.8 Cost and Management Plans: A major goal of the ASO concept study will be the development of a detailed management plan and cost model for the development, deployment and operation of the ASO facility.

Table 1 ASO Instrument Ensembles

Instrument	Spectral Range	Aperture	Resolving Power			Field of View
			Angular (Arcsec)	Spectral (g) (F/AE)	Temporal (Sec)	
High Resolution Telescope Cluster						
Soft X-Ray Telescopes ^a	1.5 - 170 Å	40 cm	0.15/0.4 ^f	10,000	0.01	3.5° x 3.5/12° x 12 ^f
XUV Telescopes ^b	150 - 310 Å	40 cm	0.1/0.4 ^f	20,000	0.01	3.5° x 3.5/12° x 12 ^f
EUV Telescope	550 - 1100 Å	40 cm	0.1/0.4 ^f	30,000	0.1	3.5° x 3.5/12° x 12 ^f
Gamma Ray Imaging Detector	2 - 1000 keV	60 cm	1.6	10	0.001	full sun
X-Ray Flare Spectrometer	1.5 - 25 Å	40 cm	1.0	10,000	0.01	full sun
Global Dynamics Instrumentation ^c	3500 - 11,000 Å	50 cm	0.5/5 ^e	100,000 ^c	1.0	full sun
Ultraviolet Telescope	1175 - 1700 Å	60 cm	0.1	30,000	0.1	3.5° x 3.5°
High Energy Facility						
Gamma Ray Line Spectrometers ^g	10 keV-10MeV	30 cm/60 cm	-	400/20	1/0.25	full sun
High Energy Gamma Ray Spectrometer	10 MeV-100 MeV	100 cm	-	5	0.001	full sun
High Energy Neutron Spectrometer	10 MeV-1000 MeV	100 cm	-	5	0.001	full sun
Low Frequency Radio Spectrograph	1 - 20 MHz	30,000	90	200	1	full sun
Pinhole/Occluder Facility						
Coded Aperture Imager	2 - 70 keV	100 cm	4.0	10	0.001	full sun
Fourier Transform Imager	2 - 1000 keV	100 cm	0.2	10	0.001	full sun
White Light Coronagraph	1100 - 11,000 Å	50 cm	1.0	5,000	1.0	full sun
EUV Coronagraph	300 - 1700 Å	50 cm	1.0	20,000	0.1	full sun
Orbiting Solar Laboratory						
Optical Telescope	2000 - 11,000 Å	100 cm	0.1	100,000	0.1	1.3° x 1.3/3° x 3°
Ultraviolet Telescope	1175 - 1700 Å	30 cm	0.5	30,000	0.1	4° x 4°

- a Our strawman configuration envisions 2 soft x-ray telescopes with spectral coverage 1.5 - 25 Å and 10 - 170 Å
b Our strawman configuration envisions 3 XUV telescopes with spectral coverage 150 - 180 Å, 190 - 210 Å, and 220 - 310 Å
c The Global Dynamics Package includes 4 small telescopes
d Possible long-term future upgrade for the OSL ultraviolet telescope
e Entries refer to high resolution and high sensitivity spectrometers respectively
f Entries refer to high resolution and wide field modes respectively
g Figure refers to highest resolution mode. Other modes may have lower resolution.

2.0 Scientific Objectives of the ASO

2.1 Scientific Motivation: The study of the Sun is an exciting and rewarding endeavor for several reasons.

- **First, the Sun is the largest and most complex physical system which we can study in detail.**

Much of the Sun's complexity arises from the interaction between plasma and magnetic fields, as is evident from the images on the cover and in the frontispiece. The diverse phenomena observable on the Sun provide an important source of inspiration for the development of physical theory and a unique environment for its testing and application, both at the microscopic level of atomic and nuclear processes and at the macroscopic level of the collective behavior of matter in the presence of gravitational and electromagnetic fields.

- **Second, the Sun occupies a central position in astrophysics.**

Because of its proximity, it is the only star which can be examined in sufficient detail to allow astrophysical phenomena to be studied at the level of the basic plasma physics and magnetohydrodynamic processes which underlie these phenomena. The Sun is, in effect, a laboratory which we can utilize to study the physics of stars and other astronomical objects.

- **Third, the Sun generates and modulates the interplanetary medium.**

The volume of space dominated by the solar wind is now generally referred to as the heliosphere to emphasize the primary role of the Sun. The solar wind, and its interaction with planetary magnetospheres, ionospheres, and atmospheres, is the subject of the discipline of space physics; the connection between solar physics and space physics is no less profound than is the connection between solar physics and astrophysics.

- **Finally, the Sun has a profound influence on the Earth's ecosphere, and hence on humanity.**

Life on Earth is possible only because of the Sun, and our lives depend on the use of solar energy, either stored or ambient. Moreover, in the past several years, evidence has steadily mounted that the variability of the Sun, which is a consequence of the Sun's magnetism, can significantly affect conditions on the Earth on time scales of centuries and millennia, and perhaps on shorter time scales as well. Our quest to understand the Sun's magnetic variability, which is represented by (but by no means limited to) the well known sunspot cycle, is therefore highly relevant to the terrestrial sciences of meteorology and climatology.

Because the solar magnetic field in and above the photosphere is strongly inhomogeneous on all scales down to well below an arcsecond, to significantly advance our knowledge and understanding of solar magnetic structure and activity, we must observe all levels of the solar atmosphere, from the photosphere to the corona, with subarcsecond resolution. This requires a set of large aperture telescopes placed above the atmosphere and observing in coordination to achieve the necessary spatial resolution across the spectral range that corresponds to the range of temperatures present in the solar atmosphere, i.e., from visible light (photosphere and chromosphere) to X-rays and gamma rays (corona). The Advanced Solar Observatory on the Space Station will realize this goal. The cluster of solar telescopes on Skylab, although not as comprehensive as those proposed for the ASO, demonstrated the power of such coordinated observations. The Skylab telescopes, with resolution of a few arcseconds, showed us that the solar magnetic field dominates the structure and behavior of the solar atmosphere; the Advanced Solar Observatory on Space station, with subarcsecond resolution, will help reveal the physical processes responsible for these structures and phenomena.

2.2 A Brief Review of Recent Advances in Solar Physics: In the past 15 years, observations of the Sun from space and from the ground have yielded discoveries which have greatly enhanced our knowledge of solar phenomena and of their connections to the other disciplines cited above. Among the most significant of these discoveries are:

- **The detection of neutrinos from the Sun (8), the first direct experimental confirmation of the central role played by thermonuclear processes in stars.**

The observed neutrino flux is a factor of 3 lower than that predicted by standard solar models. The cause of this disagreement between observation and theory remains an unsolved mystery.

- The discovery that the 5-minute oscillations of the Sun are a global seismic phenomenon that can be used as a probe of the structure and dynamical behavior of the solar interior (9).

Precise measurements of these oscillations provide a new window on the structure, transport of energy and generation of magnetic fields in a star's convective envelope.

- The discovery that the damping of compression waves driven by subphotospheric turbulent convection generates too little energy to heat the corona and drive the solar wind (10).

The correlation between the observed x-ray luminosity of other stars (that, like the Sun, have convective envelopes) and their rotation rate has reinforced the conclusion (drawn from solar observations) that magnetic effects underlie many of the active phenomena observed in stellar atmospheres.

- The discovery that, when viewed on a fine scale, the solar magnetic field is rooted in discrete flux tubes with field strengths exceeding 1000 gauss (11), and diameters of approximately 100 km (~0.1 arc sec).

The physical size of these fundamental magnetic flux elements is too small to be resolved by any present telescope. Why the solar magnetic field should be structured in this way is not understood.

- The demonstration that the large scale solar magnetic field is organized into two distinct types of structures; magnetically closed regions, in which hot plasma magnetically confined in loops largely generates the x-ray corona; and magnetically open regions, the so-called "coronal holes," which are the source of high speed streams in the solar wind (Figure 1) (12).
- The confirmation of the evidence (provided by 17th century observations) that the sunspot cycle and associated active phenomena were largely absent for a period of 70 years in the 17th century.

This episode is known as the Maunder Minimum (9,13). There is evidence that such interruptions, along with periods of heightened activity, occur quasi-periodically and that there is strong correlation between the general level of solar activity and the occurrence of climatic changes on the Earth. The cause of this modulation of the solar activity level is unknown.

- The recognition, as a result of observations of hard x-rays, gamma rays, and energetic neutrons, that the energy released during the impulsive phase of a flare is initially largely, or entirely, contained in non-thermal particles accelerated during magnetic-reconnection processes in the coronal field (14).
- The discovery that the ejection of large clouds of gas called coronal mass transients (8) (such as those shown in the frontispiece) can accompany some flares.

The profound impact of these and other discoveries on our appreciation of the complexity and diversity of solar phenomena has led to the maturing of solar physics as a scientific discipline. This new maturity has allowed solar physicists to formulate a much more precise theoretical and observational strategy for their discipline (15). The centerpiece of the observational component of this new strategy will be the Advanced Solar Observatory.

A comprehensive review of the current status of solar physics is contained in the three volume set "The Physics of the Sun" (16) which is recommended to the reader who wishes to pursue in depth any of the specific topics reviewed above.

2.3 A Scientific Strategy for Solar Physics: The report of the Solar Physics Working Group of the Astronomy Survey Committee (15) has recommended three themes or areas of concentration as potentially the most productive for solar physics over the next decade. These three themes are: (i) the development of observational techniques capable of probing the interior structure, dynamics, and composition of the Sun; (ii) the study of the "active

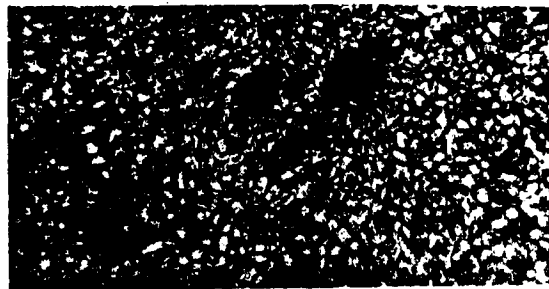


Figure 2 A wide-band (60 Å) image of the solar granulation centered on the calcium K line $\lambda 3934 \text{ Å}$. The bright granulation cells, approximately 1-2 arcseconds (700 - 1400 kilometers) in diameter, are the centers of upward moving convection cells which bring hot material from the lower photosphere to the surface. The dark boundaries contain cooler material which is flowing downward.

Figure 1 This x-ray photograph of the Sun, taken August 21, 1973, with the American Science and Engineering instrument on Skylab, shows large coronal loop structures and many small bright points though to be loops that are too small to be resolved. A large coronal hole extending from the north pole across the equator is plainly visible.

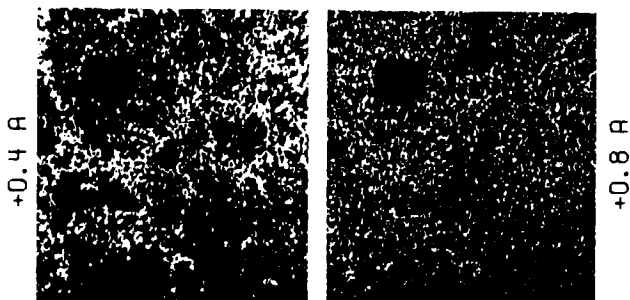


Figure 3 Narrow band images of the solar atmosphere obtained near the center of the magnesium B1 line $\lambda 5184 \text{ Å}$. In the photograph at the left (+0.4 Å from the line core) which corresponds to higher levels in the atmosphere, the supergranulation cell boundaries are visible as a bright network with a cell size of approximately 30 arcseconds (20,000 kilometers). The solar granulation is clearly visible in the image at the right taken in the wing of the line (+0.8 Å).

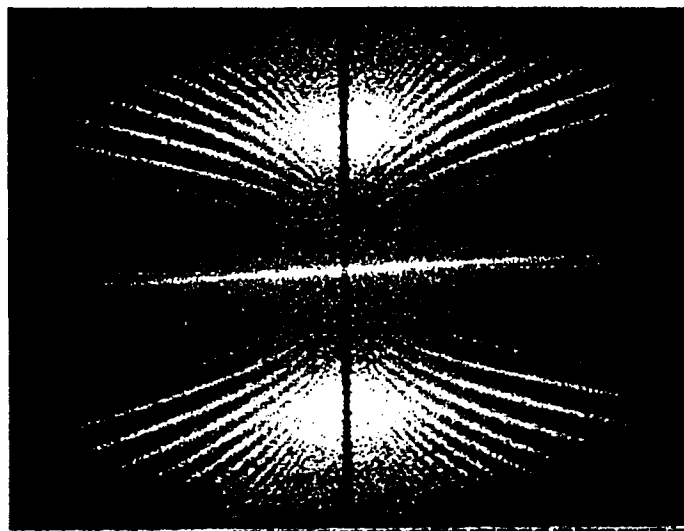


Figure 4a The power distribution over the normal modes of global oscillations of the solar surface. The vertical and horizontal axes are the temporal and spatial frequency over the ranges 0 - 0.5 cycles/min and 0 - 316 cycles/solar diameter; the brightness corresponds to the amplitude of the oscillations. The concentration of the power along these discrete ridges shows that the oscillations are the nonradial global modes in which pressure is the main restoring force.

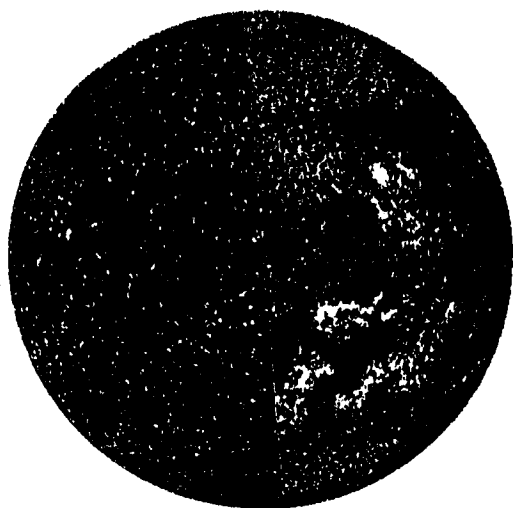


Figure 5 Montage of the magnetic structure of the quiet and active Sun. On the left is a magnetogram of half of the solar disk taken at a quiet time near minimum in the magnetic activity cycle when no major active regions were present. The right half is a magnetogram taken near the activity maximum; it shows the complex distribution of strong magnetic flux in the sunspot zones north and south of the equator.

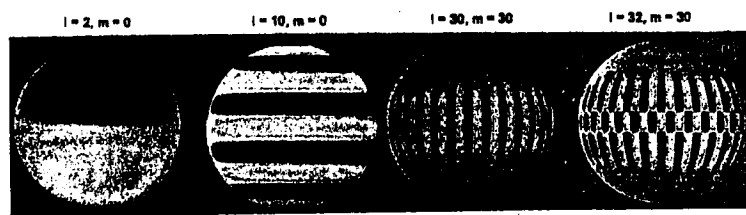


Figure 4b Oscillations of the Sun's surface are the result of sound waves resonating in its interior; here 4 of the ten million resonances that occur are modeled by computer. Surface regions that are approaching the observer are colored blue; regions that are receding are colored red. Such surface displacements are detected as Doppler shifts in the wavelengths of light absorbed by the moving gases.

phenomena" such as flares, sunspots, the activity cycle, the chromosphere, the corona, and the solar wind, which are a consequence of solar magnetic variability; and (iii) the study of the role of the Sun in shaping the three-dimensional structure and dynamics of the heliosphere. The last two themes will have important implications for our understanding of the Earth's space environment and climate (17). We can formulate a coherent scientific program which addresses these themes as a series of seven fundamental questions, which present an overview of the theoretical and observational issues which will be the focus of solar research over the next decade.

1. *What are the fundamental properties of the solar core (where energy is generated) and the radiative interior (through which energy is transported to the Sun's outer layers)? In particular, what is the Sun's internal rotation rate, chemical composition, and temperature distribution, and what is the detailed process of nuclear energy generation and energy transport? How do these properties relate to current theories of stellar evolution?*
2. *What is the magnetohydrodynamic structure of the solar convection zone, and what is the role of the three convective scales observed on the Sun, the granulation (Figure 2), the supergranulation (Figure 3), and the large scale circulation in transporting energy from the solar interior to the solar surface? Can a generalized theory of stellar convection in the presence of rotation and magnetic fields be developed which describes the structure of the Sun's convective zone and predicts the observed convective scales?*
3. *What physical mechanisms drive the solar magnetic field and activity cycle; what resulting variations in the solar radiative and particulate output follow on various time-scales; and what is the effect of this variability on the Earth's atmosphere, ionosphere, and magnetosphere? What causes the long-term variations in the solar magnetic and activity cycles, such as occurred during the Maunder Minimum? How do these phenomena relate to activity and variability on other stars?*
4. *What processes, involving small scale velocity and magnetic fields and various wave modes, determine the thermal structure and dynamics of the solar photosphere, chromosphere, and corona, and what are the implications of such processes for stellar atmospheres in general?*
5. *What are the basic plasma-physics processes responsible for metastable energy storage, magnetic reconnection, particle acceleration, and energy deposition in solar flares and related non-thermal phenomena? What are the implications of these for other high energy processes in the Universe?*
6. *What are the large scale structure and plasma dynamics of the solar corona, including the processes involved in heating various coronal structures and initiating the solar wind? What are the implications for stellar coronae and winds other astrophysical flows? What is the origin of coronal transients?*
7. *What are the implications of coronal structure for the three-dimensional structure and dynamics of the heliosphere and what are its implications for cosmic ray modulation and for the modulation of planetary atmospheres, ionospheres, and magnetospheres, including those of Earth?*

The broad scientific objectives of the Advanced Solar Observatory are those of the above fundamental questions. These objectives will be the focus of solar physics into the 21st century. The Advanced Solar Observatory will provide the new generation of improved observations needed to penetrate the entire range of problems defined by the above questions, viz., the structure and dynamics of the convection zone, the nature of solar magnetism and the activity cycle, the structure and dynamics of the chromosphere and corona, the nature of flares and other nonthermal phenomena, the generation of the solar wind, and the structure and dynamics of the Heliosphere. In addition, although the study of the composition, structure, energetics, and dynamics of the solar core are the focus of a number of other NASA and NSF programs, the Advanced Solar Observatory, by virtue of its ability to study solar oscillations, can make significant contributions there as well.

2.4 Specific Objectives of the Advanced Solar Observatory:

2.4.1 The Structure and Dynamics of the Convective Zone:

In the Sun's convective envelope, radial free convection in the presence of the rotation of the Sun is thought to give rise to differential rotation and other global flows. These global flows, perhaps in combination with smaller-scale convective motions, are the likely drivers of the dynamo process which generates the magnetic flux that emerges from the convection zone into the solar

atmosphere to produce all of the manifestations of the magnetic activity, e.g., sunspots, active regions, flares, chromospheric and coronal structure and heating, and the global behavior of the emergence and dispersal of the magnetic field. All known variations of the sun's output of radiation, particles, and magnetic flux into interplanetary space, and hence the terrestrial effect of these variation, are consequences of the sun's magnetic activity cycle. Obviously, understanding the dynamical processes in the convection zone is essential to the study of the extended solar atmosphere and its dynamics.

In the last decade, a new technique has been developed which can be used to probe the structure, composition, and dynamical behavior of the solar interior, which is, of course, not directly observable. Helioseismology involves the analysis of the radial and nonradial oscillations (Figures 4a and 4b) of the Sun from which the variation with depth of the sound speed in the Sun's interior can be determined; from the sound speed, the structure, composition, and dynamics of the solar interior can be inferred. Together with studies of the three scales of convective motions on the Sun, [the granulation (Figure 2), the supergranulation (Figure 3), and large scale flows, (by precise studies of the velocity and brightness pattern of the photosphere)], helioseismology should allow us to address the following basic questions.

- *Are there giant convective cells on scales between that of supergranules, and that of the global meridional circulation?*
- *How does the Sun's internal rotation rate vary with depth and latitude?*
- *Do the internal rotation or the cellular structure of the convective zone change systematically each solar cycle?*
- *How does the Sun's temperature vary with depth and latitude? Is this thermal structure time-dependent?*
- *How are changes in the strength and location of magnetic structures within the convection zone correlated with changes (e.g., by flux emergence) in the magnetic structure of the solar atmosphere?*
- *What is the extent and impact of turbulent phenomena (e.g. turbulent diffusion) on the convection zone?*

2.4.2 Active Phenomena on the Sun: Active phenomena on the Sun are the result of the variability of the solar magnetic field, which is a consequence of the energy transport processes operating in the convection zone (9a). We divide solar activity into four aspects: (i) magnetism and mass motion, including the activity cycle; (ii) atmospheric heating and mass transport, including the structure and dynamics of the chromosphere and corona; (iii) flares and particle acceleration; and (iv) the generation of the solar wind.

2.4.2.1 Solar Magnetism and the Activity Cycle: One of the major characteristics of the Sun (and of many other stars) (18) is a magnetic field which varies cyclically (Figure 5). The cycle period for the Sun is about 11 years without regard to magnetic polarity or 22 years taking account of polarity. There is evidence that the strength of the cycle may at times be substantially weaker or stronger than recent cycles (Figure 6). However, a remarkable analysis of 1760 years of annual sediment deposits in an ancient glacial lake provides evidence that the solar cycle was present 680 million years ago with the same period as now. Of great practical importance to mankind is the fact that the enduring magnetic activity cycle (9a) is the source of the variation of the solar radiative and particulate flux.

The currently prevailing (but not universally held) view of the basic dynamo processes that sustain the solar cycle invokes amplification of a relatively weak magnetic field by shearing motions at the base of the convection zone. This action forms buoyant flux bundles which rise fairly rapidly through the convection zone and erupt at the visible surface to produce active regions. Frequently a substantial amount of energy is released at the eruption site in the form of flares and other active Sun phenomena. The total radiative output of the Sun is also disturbed by these magnetic eruptions. Most of the magnetic flux disappears rather rapidly near the site of the eruption. The remaining flux spreads across the surface of the Sun (Figure 7) by the combined action of the granulation, supergranulation, differential rotation, and meridional flow. During this phase, the flux exists mainly in the form of small, isolated

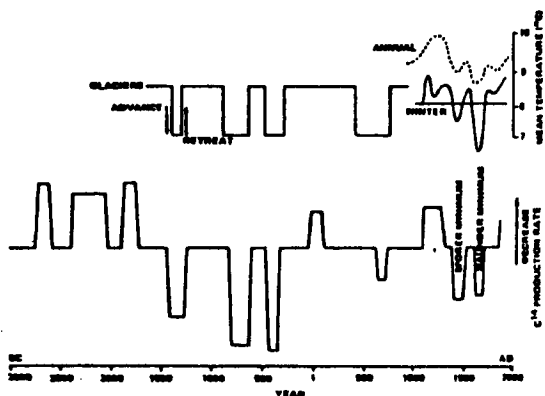


Figure 6 The apparent correlation of solar activity and climate: the lower curve, based on tree-ring data, represents the rate of production of carbon-14 by cosmic ray bombardment of the upper atmosphere. This production varies inversely with solar activity. Plotted above are measures of mean European climate: the advance and retreat of Alpine glaciers, historical inferences of mean annual temperature, and the recorded severity of northern European winters. The temporal coincidence of low solar activity and cool European climate suggests a causal connection between long-term solar behavior and climate, although other data indicate a more complex relationship.



Figure 8 Spicules are thought to be tubes of magnetic flux containing upwardly moving gas. This offband H- α photograph of the solar limb emphasizes these spike-like structures. Spicules appear at the boundaries of supergranular cells. The magnetic field is concentrated in the supergranule boundaries, which underlie a network of hot material with temperatures ranging from 10,000 to 700,000 Kelvin.

Figure 10 Solar flare gamma ray spectrum obtained by the Solar Maximum Mission, showing strong nuclear gamma ray lines. This spectrum, shown here with background and flare bremsstrahlung subtracted, was produced by the limb flare on April 27, 1981, which began at 08:05 UT. The numbered peaks are emission lines from the excited nuclear states of the isotopes Oxygen-16, carbon-12, nitrogen-14, deuterium, neon-20, iron-56, magnesium-24, beryllium-7, and lithium-7 among others, and from positron-electron annihilation. Many of the features are strongly Doppler broadened. (Courtesy of Ed Chupp, University of New Hampshire.)



Figure 7 A high resolution magnetogram of a complex of active regions. It shows that the photospheric magnetic flux in and beyond the outskirts of strong active regions is concentrated at the boundaries of supergranulation convection cells, and the field has strong fine scale structure down to the limit of resolution (2 arcsec).

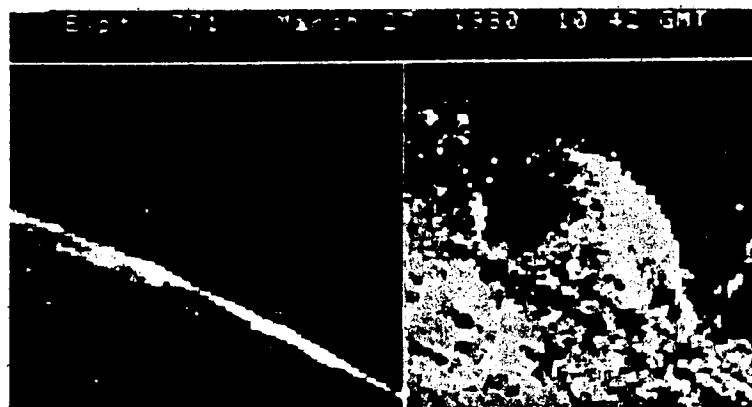
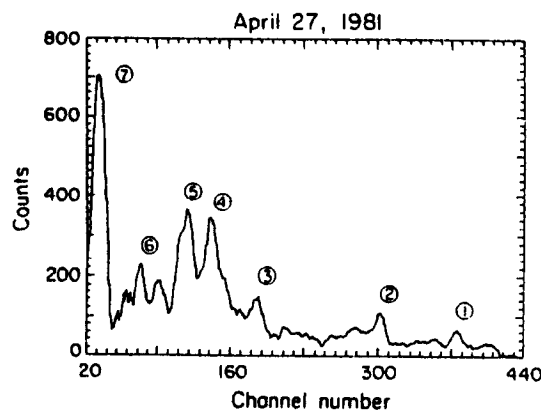


Figure 9 Complex of coronal loops at the solar limb, photographed in the light of a resonance line of C IV ($\sim 150,000$ Kelvin) at $\lambda 1548 \text{ \AA}$, with the Ultraviolet Spectrometer and Polarimeter on the Solar Maximum Mission. The photograph at the left shows the intensity, while the photograph at the right, which was obtained from the difference in intensity of the red and blue wings of the line, represents the velocity distribution within the loop. Material is apparently flowing in the loop, emphasizing the dynamic nature of the apparently static features in the solar atmosphere.



vertical bundles having a large flux density and low gas density. A substantial amount of this flux gradually disappears from our observations. The small amount of surviving flux eventually concentrates at the poles where as yet uncertain processes may operate to seed the beginnings of a new cycle.

While many of the observed aspects of the magnetic cycle have been reproduced in kinematic dynamo models, serious doubts have been raised recently about the validity of these models. What is required is a theory of the dynamical behavior of the convection zone, based on the fundamental physical principles, which can predict the convective and magnetic properties of the Sun's outer layers. The acquisition of an observational record which can guide astrophysicists in the development of such a theory and provide the observational tests required to refine the theory, is a fundamental objective of the Advanced Solar Observatory.

Among the basic questions relating to the activity cycle and the magnetic field which will be addressed by the Advanced Solar Observatory are:

- *What are the factors which control the modulation of the activity cycle (Figure 6)?*
- *What is the fine scale structure of the solar magnetic field, and what factors control this structure?*
- *What factors control the generation, transport, and dissipation of magnetic flux?*
- *How does the magnetic field modify the flow of energy in the outer layers of the convection zone and in the solar atmosphere?*

2.4.2.2 Atmospheric Heating and Mass Transport: The occurrence of a temperature reversal in the solar chromosphere, the million-degree temperatures characteristic of the corona, and the expansion of the corona into the solar wind all demonstrate that conditions in the solar atmosphere are far removed from local thermodynamic equilibrium (LTE). Non-thermal phenomena, which include the propagation and dissipation of waves, the generation and dissipation of macroscopic flows and coronal current systems, and the confinement of the plasma by magnetic forces, have a major influence on the structure, dynamics, and energy balance of the atmosphere.

Although the photosphere and chromosphere are layers of almost negligible geometrical thickness compared with the radius of the Sun (somewhat analogous to the outer skin of an onion), they are of fundamental importance to the energy balance, mass balance, and composition of the entire outer solar atmosphere, including the solar wind. The energy and mass flux that ultimately produce the corona and solar wind move through these lower atmospheric regions, leaving their signatures there; the energy dissipated in the photosphere and chromosphere is roughly 10 times greater than that required to heat the entire corona and solar wind. The photosphere is highly structured by convective and magnetic processes and is highly dynamic, with the granulation structure (Figure 2) constantly changing. The complexity of the structures which control the transport of mass and energy in the chromosphere/corona interface is illustrated by Figure 8, which shows the upward flowing columns of gas called spicules, which are confined by magnetic flux concentrated at the boundaries of the supergranulation cells. The chromospheric material is concentrated in a network of hot low-density gas, which traces out the supergranulation boundaries. This network is visible in the mottled appearance of the solar disk in the He II (304 Å) image in the frontispiece, and in EUV lines emitted at temperatures up to 7×10^5 K (cover image).

While the magnetic field is an important factor in the dynamical behavior of the chromosphere, it is the dominant factor in the corona. High resolution observations (such as that on the cover) have demonstrated that the coronal layers of active regions (within 1 to 2 solar radii of the surface) consist primarily of elemental structures in the form of magnetic flux tubes or loops in closed configurations (i.e. with both footpoints rooted in the chromosphere) which contain material ranging in temperature up to 10,000,000 Kelvin or more. One of the surprises of the 1970's was the discovery of cool loops, filled with plasma at temperatures between 100,000 K and 1,000,000 K. These loops appear to be dynamically and thermally unstable, with material flowing downward into the chromosphere (Figure 9). The exchange of mass and energy between the chromospheric and coronal levels in these structures appears to play a major role in determining the temperature-density structure of the coronal layers of active regions.

The ASO will provide the observational data required to guide the development of theoretical models of the structures and processes that control the transport and dissipation of energy and the flow of material in the photosphere, chromosphere, and inner corona, and to provide the observational tests required to refine these models. These observations will address the following fundamental issues:

- *What is the detailed structure and energy balance of the temperature minimum region in the lower chromosphere, where the rise to coronal temperature begins?*
- *What processes control the non-LTE transport of radiation through the chromosphere, and what is the effect of the atmospheric fine structure and differential velocity fields on these transport processes?*
- *Although acoustic waves have been ruled out as the principal agent responsible for the heating of the corona, they may still play an important role in the chromosphere. Among the questions which must be addressed in connection with the role of acoustic waves are: (i) how does the dynamic behavior or the solar granulation generate acoustic waves, and what are the spectral characteristics and energy flux of these waves; and (ii) how are acoustic waves dissipated in the chromosphere?*
- *What physical process cause the rising and surge-like behavior of spicules?*
- *What are the roles of the conduction of heat from the corona and direct magnetic heating (via current dissipation) in maintaining the thermal structure of the chromosphere and transition region?*
- *What is the relative role of the dissipation of magnetohydrodynamic waves and of coronal current systems in the heating of coronal loops? Do rapid reconnection processes play a significant role in heating the "quiet" corona, or are they only important in flares? What roles do thermal conduction and macroscopic mass flow play in the energy balance of coronal loops?*
- *What is the role of the newly emerging regions of magnetic flux which manifest themselves by enhanced EUV and soft x-ray emission (the bright points) in the magnetic evolution of the solar atmosphere and leakage of mass into the solar wind?*
- *Although theoretical diffusion models have predicted composition differences between the chromosphere and corona, no such differences have been observed. What processes cause the atmospheric mixing which eliminates these composition differences, and do occasional interruptions in these processes contribute to the composition anomalies observed in the solar wind?*
- *What characterizes the flows in the chromosphere that preserve mass balance in the corona, while providing leakage to the solar wind, and how does this affect the energy balance of the chromosphere?*

2.4.2.3 Flares and Particle Acceleration: The basic flare mechanism is an explosive conversion of magnetic energy into high energy particles (Figure 10), bulk mass motion (frontispiece), and heated plasma. Since the fundamental ingredient is magnetized plasma in which energy has been stored in the magnetic field through non-uniform motion of this medium, and since dynamic magnetoplasma systems in and around stars and galaxies pervade the Universe, flares are of general astrophysical importance. In solar flares, both the buildup and the release of energy appear to depend critically on the fine scale (less than 1000 kilometers) structure of the magnetic field, and involve all levels of the solar atmosphere. All flares drastically affect the low corona and chromosphere; large flares can strongly affect the outer corona and solar wind, and sometimes noticeably heat the photosphere. The accelerated particles range in energy from at least 10 keV to more than 1 GeV (1 GeV equals 1000 MeV), the heated plasma ranges in temperatures from photospheric (5,000 K) to more than 50,000,000 K. Thus, to observe the overall flare phenomenon and to identify the energy release mechanism will require the full capability of the Advanced Solar Observatory for coordinated high resolution observations spanning the pre-flare configuration of the solar atmosphere and the full range of flare outputs.

The flare phenomenon can be divided into five distinct phases. In approximate order of occurrence, these are energy storage, initiation of energy release, mass ejection and particle acceleration, energy transport and heating, and atmospheric restructuring. Among the basic questions which must be addressed by the Advanced Solar Observatory in order to develop a fundamental theoretical understanding of flares and the related non-thermal phenomena are:

- *What is the detailed structure of the magnetic configurations and current systems responsible for storage of the flare energy, and how do these configurations evolve?*
- *What changes occur in coronal current systems immediately before a flare, and what is the role of the filaments of cool chromospheric material which are observed in the low corona before many flares?*
- *What is the site of the energy release in flares that are observed to occur in coronal loops?*
- *In both filament eruption flares and coronal magnetic-loop flares, the initial release mechanism is thought to be magnetic reconnection or tearing, which is the only known way of releasing the stored energy rapidly enough. What are the details of this reconnection process, and how does it mediate the impulsive transfer of energy from the magnetic fields to a population of relativistic electrons and ions?*
- *What is the mechanism which, in many flares, causes the large scale ejection of mass (filament eruptions) into the corona?*
- *Does the presence of high-density currents during the reconnection process generate turbulence in the solar plasma? If so, does the turbulence inhibit the escape of non-thermal particles from the flare site?*
- *How is the energy released by the flare initially transported to the surrounding solar plasma, and what is its impact?*
- *What is the relative magnitude of the energy released in the impulsive reconnection process and the energy that is released more gradually after the impulsive phase?*

2.4.2.4 The Generation of the Solar Wind: Interest in the solar wind acceleration region stems from the astrophysical problem of stellar winds (and expanding hydromagnetic flows from stellar systems) and the space physics problems of the heliosphere and solar-planetary relations, as well as from the influence of this region on the energy and mass balance of the corona. Most of the acceleration of the solar wind is believed to take place within 10 solar radii of the Sun's center. It is in this region that the magnetic field changes from being mostly closed to being mostly open. Over this radial span, the coronal plasma changes from being collision-dominated to being nearly collisionless; as a result, the charge state of coronal ions entering the solar wind is expected to be frozen in the acceleration region. Variations in the chemical composition of the solar wind, measured near the Earth, may be produced here also. Because of the long thermalization times due to the low densities, non-thermal processes (e.g., magnetohydrodynamic waves) may produce detectable spectroscopic signatures for particles of different mass; this would help identify mechanisms of plasma heating and momentum deposition. In addition, flares and filament eruptions can produce coronal mass ejections (frontispiece) that disturb the corona and solar wind strongly enough to dramatically affect the Earth's magnetosphere.

The ASO will provide unprecedented capabilities for observing the generation of the solar wind and for relating structures and events in the acceleration region to their origins in the lower atmosphere. Specific issues which must be addressed in the study of the solar wind acceleration region are:

- *What are the processes that deposit energy and momentum in the outer corona to generate the solar wind?*
- *What are the processes that heat the corona in closed magnetic regions?*
- *What are the mechanisms by which the corona evolves in response to slowly varying conditions on the solar surface?*

- *What are the processes governing the expulsion of coronal mass ejections? How do they affect the solar wind?*
- *What is the role of the solar wind, and of coronal mass transients in the overall angular momentum loss and spindown of the Sun?*
- *How are the high and low speed streams observed in the solar wind generated?*

2.4.3 The Structure and Dynamics of the Heliosphere: The heliosphere is that region of space in which the physical conditions are established and controlled by the presence of the Sun; as such, it represents the largest scale organization associated with our star. Our knowledge of the heliosphere is quite limited. We do not know its extent, its detailed morphology or its evolution, although we are well aware of many features of its innermost regions, the corona and the interplanetary medium in the vicinity of the Earth. Since the flow of the solar wind is governed by conditions at the base of the corona, we expect that detailed knowledge of the corona will allow us to infer the conditions throughout the heliosphere. However, internal dynamical processes, together with the results of influences from without the heliosphere, will modify these conditions, perhaps significantly near the outermost boundary. Thus, careful and coordinated studies of coronal and other direct indicators of the condition of the heliosphere and its interface with the interstellar medium are required for an understanding of the physics of the heliosphere. The role of the Advanced Solar Observatory will be to probe the physics of the coronal phenomena which directly structure and disturb the interplanetary stretch of the heliosphere. Among the issues pertaining to the heliosphere which the Advanced Solar Observatory will address are:

- *How is the three-dimensional structure of the corona and the large scale magnetic field reflected in the structure of the heliosphere?*
- *How, and with what time delay, are changes in the corona reflected in changes in heliospheric conditions?*
- *What is the role of large scale coronal mass-ejection transients in the evolution of the corona, and what is their impact on heliospheric conditions?*
- *With regard to the effect of the Sun on the Earth by modulation of heliospheric structure, what is the relative importance of recurrent events such as the passage of coronal holes, and of more transient occurrences such as those associated with coronal mass ejection events? Is there a significant correlation between the conditions in the heliosphere and atmospheric phenomena on the Earth such as weather, or is heliospheric influence limited to phenomena such as the aurora?*

2.5 Non Solar Observations with ASO: A potentially significant aspect of the ASO program is the possibility of observing active phenomena in other stars with ASO. We plan to explore the scientific implications, and engineering impact of such observations during the Concept Study.

2.6 A Detailed Scientific Program for the High Resolution Telescope Cluster: The scientific objectives discussed above emphasize the broad nature of the problems the powerful combination of instruments that make up the ASO can address. It is important to emphasize, however, that each ASO component ensemble is a very powerful and advanced observatory, which is capable of addressing a broad range of specific and fundamental issues. Therefore, at each stage of the evolutionary ASO development, the ASO will be capable of observations at the cutting edge of astronomical research. The scientific program of OSL (formerly HRSO) has been well documented (4). Since the High Resolution Telescope Cluster is expected to be the first of the ASO instrument ensembles discussed in this proposal to be deployed, we present in Appendix A, a discussion of scientific objectives to be addressed with its high resolution X-Ray, XUV, EUV, and UV instruments. Discussions of the scientific programs of P/OF and HEF are contained in the conference proceedings edited by Tandberg-Hanssen, Wilson and Hudson (5b) and Chupp and Walker (6).

REFERENCES

1. *Astronomy and Astrophysics for the 1980s, Vol. I: Report of the Astronomy Survey Committee*, (National Academy Press, Washington, D.C., 1982.); An overview of the report of the full Survey Committee is contained in the article by George Field in *Physics Today*, 35, No. 4, 46, (April 1982.)
- 2a. *Challenges to Astronomy and Astrophysics: Working Documents of the Astronomy Survey Committee*, (National Academy Press, Washington, D.C., 1983.)
- 2b. "Astronomy and Astrophysics for the 1980s, Vol. II: Reports of the panels," (National Academy Press, Washington, D.C., 1983.); Overviews of the reports of the High Energy, Radio and Ultraviolet, Optical and Infrared Panels are contained in a special issue of *Physics Today*, 35, No. 11, (November 1982.)
3. A.B.C. Walker, Jr., R. Moore, and W. Roberts, *The Advanced Solar Observatory*, NASA Technical Publication (1986)
- 4a. Stuart B. Jordan, "The Solar Optical Telescope (SOT)," *Space Science Reviews*, 29, 333, (1981.)
- 4b. Richard B. Dunn, "SOT Instrumentation." *Ibid.*, 341.
- 4c. Alan Title, "An Overview of the Orbiting Solar Laboratory," Lockheed Palo Alto Research Laboratory preprint (1988)
- 5a. "The Pinhole/Occulter Executive Summary," *NASA Technical Paper 2089*, (October 1982.)
- 5b. E. Tandberg-Hanssen, R.M. Wilson and A.S. Hudson, "Solar Flares and Coronal Physics; Using P/O as a Research Tool," *NASA Conf. Publ. 2421*, (1986).
6. "On High-Energy Aspects of Solar Flares - A Basis for a High Energy Facility for Solar Physics", Special Issue of the Journal *Solar Physics*; Eds. E.L. Chupp and A.B.C. Walker, Jr., in press (1988)
7. W. Bailey, "Advanced Solar Observatory Accommodation Requirements Study," Teledyne Brown Engineering, Inc., Huntsville, Alabama, Sept. 1988.
8. John Bahcall, "Solar Neutrinos: Theory versus Experiment," *Space Science Reviews*, 24, 277, (October 1979.)
- 9a. Gordon Newkirk, Jr., and Kendrick Frazier, "The Solar Cycle," *Physics Today*, 35, No. 4, 25, (April 1982.)
- 9b. *Advances in Helio and Astroseismology*, IAO Symp. 123 Ed. J. Christensen, Dalgaard and S. Frandsen (D. Reidel Publ. Co. Dordrecht, 1988)
Symposium on Seismology of the Sun and Sun-like Stars, Tenerife, Spain Sept. 1988 to be published by ESA Publ. 286 Ed. E. J. Rolfe
10. R. Grant Athay and Oran R. White, "Chromospheric Oscillations Observed with OSO 8: IV. Power and Phase Spectra for C II," *The Astrophysical Journal*, 229, 1147, (May 1979.)
11. Jack Harvey, "Observations of Small-Scale Photospheric Magnetic Fields," *Highlights of Astronomy*, 4, 223-239, (1977.)
12. Jack B. Zirker, Editor, "Coronal Holes and High Speed Wind Stream,," (Colorado Associated University Press, 1977.)
13. Jack A. Eddy, "The Maunder Minimum," *Science*, 192, 1189, (June 1976.)
- 14a. Gerard Van Hoven, "Plasma Energetics in Solar Flares," *Highlights of Astronomy*, 5, 343, (1980.)
- 14b. Reuven Ramaty and Richard E. Lingenfelter, "Gamma Ray Astronomy," *Annual Review of Nuclear and Particle Science*, 32, 235, (1982.)
15. "Solar Physics: The Report of the Solar Physics Working Group of the Astronomy Survey Committee," Chapter 1 of Reference 2a (1982); An overview of the report of the Solar Physics Working Group is contained in the article by A.B.C. Walker, Jr., in *Physics Today*, 35, No. 11, (November 1982.)
16. *Physics of the Sun* (3 Volumes), edited by P.A. Sturrock, T.E. Holzer, D.M. Mihalas, and R.K. Ulrich, (D. Reidel Publishing Company, 1985.)
17. "Solar Variability, Weather, and Climate," (National Academy Press, Washington, D.C., 1982.)
- 18a. O.C. Wilson, Arthur H. Vaughn, and D.M. Mihalas, "The Activity Cycles of Stars," *Scientific American*, 224, 104, (February 1981.)
- 18b. O.C. Wilson, "Chromospheric Variations in Main Sequence Star,," *The Astrophysical Journal*, 226, 379, (December 1978.)
19. J. D. F. Bartoe and G. E. Bruckner, *J. Opt. Soc. Am.* 65, 13 (1975)
20. D. A. Schwartz et al, *Proc. SPIE* 597, 10 (1985)
21. T.W. Barbee, Jr., *Optical Engineering* 25, 898 (1986)

3.0 Instrumentation: The ASO will consist of 4 instrument clusters, the Orbiting Solar Laboratory (OSL), the High Resolution Telescope Cluster (HRTC), the Pinhole Occulter Facility (P/OF), and the High Energy Facility (HEF). The major components of the OSL, a 1.0 meter aperture visible light telescope (4) and a 0.3 meter ultraviolet telescope, the High Resolution Telescope and Spectrograph (19) are well defined, and will not be addressed during the present Concept Study (data on the OSL and HRTS are included in Appendix B, for the convenience of the reader). The P/OF is the subject of a separate Concept Study proposal, and will also not be included in the present Concept Study [The P/OF is shown in Figure 11b, as it might appear mounted on the Space Station]. We will concentrate on the High Resolution Telescope Cluster and the High Energy Facility in this Concept Study.

3.1 The High Resolution Telescope Cluster; The Advanced Solar Observatory High Resolution Telescope Cluster (HRTC) is an array of telescopes that will provide high resolution spectroheliograms in lines and continuum emitted over the full range of temperatures ($\sim 2 \times 10^4$ to 5×10^7 K) present in the outer solar atmosphere with angular resolution of ~ 0.1 arc second. The HRTC (mounted on the Space Station Payload Pointing System (PPS) is shown in Figure 11a). The full ASO HRTC consists of the following telescopes:

- A 40 - 50 cm aperture ultraviolet telescope [U-1] covering the spectral range from $\lambda\lambda$ 1200 - 3300 Å
- A 35 - 40 cm aperture EUV telescope [E-1] covering the spectral range $\lambda\lambda$ 550 - 1200 Å
- Three (3) or four (4) 35 - 40 cm aperture XUV telescopes [X-1 to X-4] covering the spectral range $\lambda\lambda$ 170 - 600 Å
- A 35 - 40 cm aperture soft x-ray/XUV telescope [S-1] covering the spectral range $\lambda\lambda$ 10 - 170 Å
- A 35 - 40 cm aperture soft x-ray telescope [S-2] covering the spectral range $\lambda\lambda$ 1.5 - 25 Å
- An X-Ray Flare Spectrometer [S-3] covering the spectral range $\lambda\lambda$ 1.5 - 150 Å
- A 50 cm aperture Gamma Ray Imaging Device [Γ-1] covering the energy range from 20 keV to 1 MeV
- A Cluster of Global Dynamics Instruments.

A possible arrangement of the major HRTC telescopes for the Space Station is shown in Figure 12. The properties of the HRTC instruments are summarized in Tables 2a and 2b.

Some of the ions whose principal lines will be observed by each telescope are shown in the footnotes to Table 1a.

3.1.1 The Soft X-Ray, XUV, EUV and Ultraviolet Telescopes: The EUV and XUV strawman telescopes both share the same optical design, a Ritchey-Chretien. Ray trace results have shown that on-axis resolution of 0.03 arc seconds can be achieved in principal, and the resolution over a 10 min arcmin field is better than 0.1 arcseconds. The wavelengths imaged will be determined by the mirror coatings or surface composition, SiC for the EUV, and Si/Mo multilayers for the XUV. The soft x-ray telescopes will both use the Wolter I configuration, but they will differ in their grazing angle. We note that one possible development approach for the S2 Telescope is to utilize the AXAF TMA mirror (20). This mirror has a focal length of ~ 6 meters and an aperture of 40 cm, which are the same as the proposed ASO S2 mirror. Slit-jaw images will be formed for all telescopes in H Ly- α , to provide information for co-registration of images from each telescope, and for an aspect signal for pointing control and stability.

The EUV and XUV Telescopes: The basic configuration of the EUV and XUV telescopes is illustrated in Figure 13. The radiation from the primary mirror is shared by two focal planes; the first is illuminated by a Cassegrain/Ritchey-Chretien secondary which intercepts $\sim 90\%$ of the light, and forms a focus behind the primary, at the aperture of a toroidal grating spectrometer. The remaining 10% of the light is allowed to proceed toward the prime focus where it is analyzed by a small Czerny-Turner monochromator to produce a full disk monochromatic image.

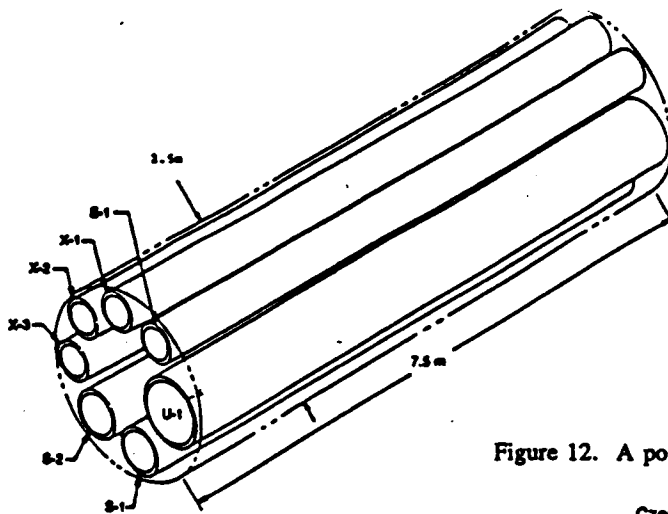


Figure 12. A possible arrangement of the ASO HRTC Telescopes

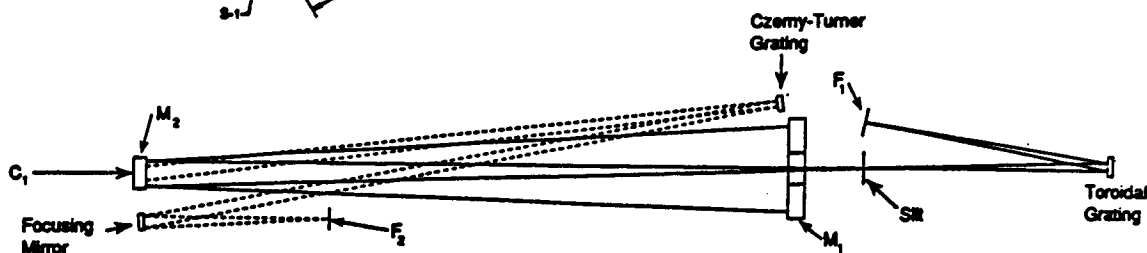


Figure 13. Optical layout of the EUV and XUV telescopes. M_1 and M_2 are the mirrors of the Ritchey-Cretien telescope, S is the aperture/slit of the toroidal grating spectrograph, and F_1 is the focal plane. C_1 is the first Czerny-Turner collimating mirror (it is nested in the center of M_2), C/TG is a flat grating, and C_2 is the Czerny-Turner focusing mirror. F_2 is the wide field focal plane. The scale is in centimeters. The envelope of E_1 , and $X1-X4$ is a cylinder 0.55 m in diameter and ~7 m long. The Czerny-Turner grating and detector will project beyond the envelope slightly.

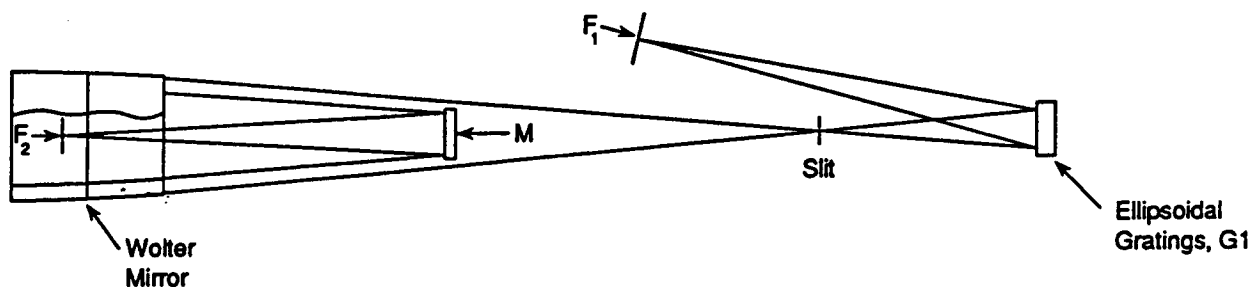


Figure 14. Optical layout of the long wavelength Wolter Telescope, S-1. The primary Wolter mirror is nested. S is the entrance aperture to the Ellipsoidal Grating Spectrometer, G_1 is an array of multilayer ellipsoidal grating, and F_1 is the focal plane. M represents an array of multilayer tertiary mirrors which provide a wide field image at F_2 . The envelope for $S1$ is a cylinder 0.55 m in diameter and ~7 m long. The ellipsoidal focal plane spectrometer will project beyond this envelope slightly.

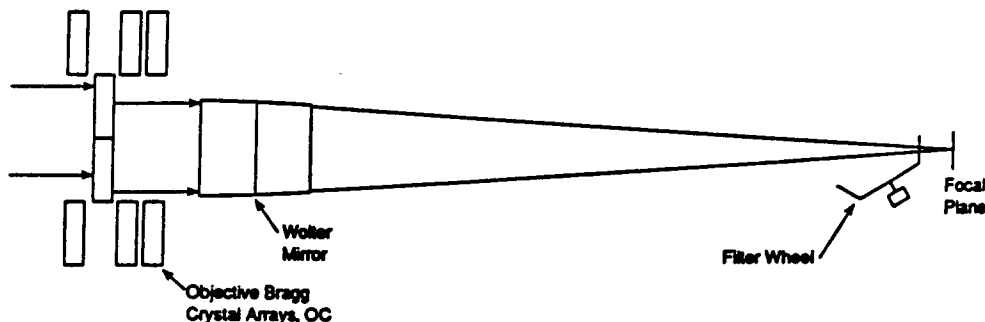


Figure 15. Optical Layout of the short wavelength Wolter Telescope, S-2. OC are the objective double crystal arrays, FW is a filter wheel, and F is the focal plane. The envelope for S-2 is a cylinder 0.55 m in diameter and ~7.2 m long.

Table 2a. Properties of the HRTC Instruments

System	Primary Optics	Bandpass Å	Primary Mirror Aperture F.L. cm mm	Spectroscopic Focus F.L. Pixel Size mm μm	Wide Field Focus F.L. Pixel Size mm μm	Mirror Coating	Major Spectroheliograph	Wide Field Spectrograph
U-1	Ritchey-Chretien	1200 - 3300 ¹	40 5000	20,000 5 (0.05")	5000 5 (0.2")	Al	Tandem Wadsworth ($\lambda/\Delta\lambda \sim 3 \times 10^4$)	Czerny-Turner
- 1	Ritchey-Chretien	550 - 1100 ²	40 5000	20,000 5 (0.05")	5000 5 (0.2")	SiC	Toroidal Grating ($\lambda/\Delta\lambda \sim 3 \times 10^4$)	Czerny-Turner
X-1	Ritchey-Chretien	167 - 177 ³	40 5000	20,000 5 (0.05")	5000 5 (0.2")	Mo/Si	Toroidal Grating ($\lambda/\Delta\lambda \sim 2 \times 10^4$)	Czerny-Turner
X-2	Ritchey-Chretien	187 - 200 ⁴	40 5000	20,000 5 (0.05")	5000 5 (0.2")	Mo/Si	Toroidal Grating ($\lambda/\Delta\lambda \sim 2 \times 10^4$)	Czerny-Turner
X-3	Ritchey-Chretien	245 - 265 ⁵	40 5000	20,000 5 (0.05")	5000 5 (0.2")	Mo/Si	Toroidal Grating ($\lambda/\Delta\lambda \sim 2 \times 10^4$)	Czerny-Turner
X-4	Ritchey-Chretien	275 - 295 ⁶	40 5000	20,000 5 (0.05")	5000 5 (0.2")	Mo/Si	Toroidal Grating ($\lambda/\Delta\lambda \sim 2 \times 10^4$)	Czerny-Turner
S-1	Wolter I	10 - 170 ⁷	40 5000	10,000 5 (0.10")	5000 5 (0.2")	Au	Ellipsoidal Grating ($\lambda/\Delta\lambda \sim 10^4$)	Cassegrain
S-2	Wolter I	1.5 - 25 ⁸	40 6000	N.A. N.A.	6000 5 (0.15")	Ni	Objective Double Crystal ($\lambda/\Delta\lambda \sim 10^4$)	N.A.
Γ-1	Collimator	20 keV-1 MeV	50 6000	N.A. N.A.	6000 90 (1.6")	N.A.	($\lambda/\Delta\lambda \sim 100$)	N.A.
S-3	N.A.	1.5-25 ⁸	N.A. N.A.	N.A. N.A.	N.A. N.A.	N.A.	($\lambda/\Delta\lambda \sim 10^4$)	N.A.

¹ H I, C IV, O V, O VI ² He I, He II, Mg X, O V, C III, O VI ³ Fe IX, Fe X, O V, O VI ⁴ Fe XI, Fe XII, Fe XIII, Fe XXIV
⁵ He II, Si X, Fe XIII, Fe XIV ⁶ Fe XV, S XI, Mg VII ⁷ O VII, O VIII, Fe XVII-Fe XXIII ⁸ Fe XVII-Fe XXVI, Si XII, XIII, Mg XI, XII, Ca XIX, XX

Table 2b Global Dynamics Instrumentation

INSTRUMENT	SPECTRAL RANGE	APERTURE (cm)	RESOLVING POWER		
			ANGULAR (arc-sec/km)	SPECTRAL (E/ΔE)	TEMPORAL (seconds)
FOURIER TACHOMETER/ MAGNETOGRAPH	3500-11,000 Å	30	0.5/350	600,000	60
DIFFERENTIAL RADIOMETER	4000-7000 Å	15	4/3000	5	60
INTEGRATED LIGHT SPECTROMETER	4000-7000 Å	10	FULL SUN	10	1
HELIOSEISMOMETER	4000-8000 Å	12	2/1500	100,000	60

EXPLODED VIEW OF GRID TELESCOPE

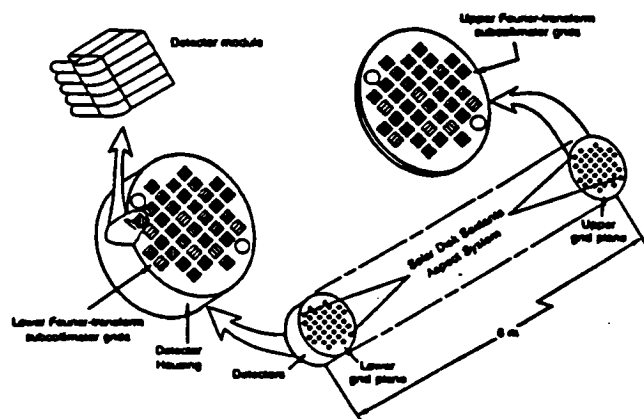


Figure 16. An exploded view of GRID showing the end plates holding the grid subcollimator pairs and the Solar Disk Sextant together with the cannister housing the detector modules.

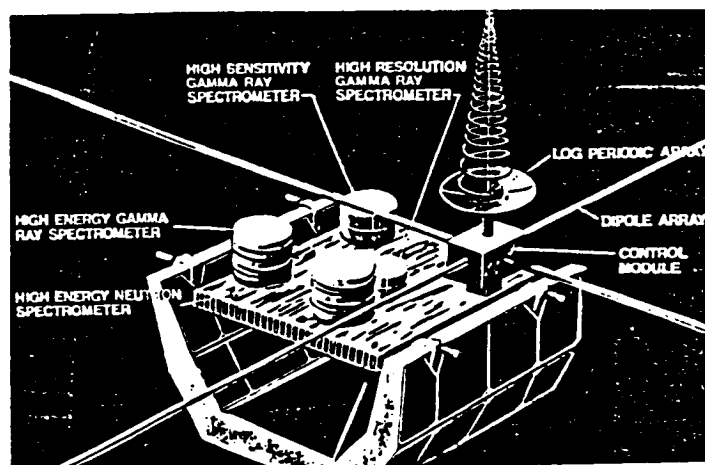


Figure 17. A view of the High Energy Facility mounted on the Space Station.

The Soft X-Ray Telescopes: Two soft X-ray telescopes are employed. The first telescope (S1) is used principally as a primary for multilayer secondary mirrors, which provide high resolution spectroheliograms. One possible configuration is illustrated in Figure 14. (This "Wolter Cassegrain" configuration is discussed in Appendix B.) The second telescope, S2 is placed behind an array of objective double crystal spectrometers (Appendix B), to provide monochromatic images of high temperature active region and flare plasmas (Figure 15).

The Ultraviolet Telescope: The primary function of the Ultraviolet Telescope on HRTC is to provide high resolution images which will allow the correlation of HRTC images with images obtained by OSL and P/OF. These are several possible approaches to the development of the HRTC Ultraviolet Telescope, including (i) a telescope/spectrometer identical to the EUV and XUV telescopes, (ii) an instrument employing the HRTS design of Bartoe and Bruckner (19), (iii) a simple high resolution telescope employing interference filters only to achieve spectral resolution. To some extent, the HRTC Ultraviolet Telescope configuration will depend on the configuration of the ultraviolet telescope on OSL. Presently, the strawman OSL ultraviolet telescope utilizes the HRTS configuration.

As Table 2a shows, the strawman x-ray, XUV, EUV and UV instruments are capable of achieving resolution of 0.1 arcsec (0.05" pixels) over the wavelength range from 10 - 3000 Å, and 0.2 arcsec resolution between 1 and 10 Å, satisfying a major ASO objective.

3.1.1.0 Technological Issues: We briefly discuss a number of technological issues raised by the strawman designs of the soft x-ray, XUV, EUV and UV telescopes, which we intend to address during our Concept Study.

3.1.1.1 Multilayer Optics: Over the past decade, significant advances have occurred in the development of normal incidence x-ray optics (21). These advances have resulted from the ability to fabricate thin film layered synthetic microstructures, "multilayers", with a level of reproducible Ångström-scale perfection which allows their use as Bragg diffractors for soft x-ray and extreme ultraviolet radiation. Multilayer structures, when deposited on substrates of sufficient smoothness, can act as optical elements in high resolution telescopes. *The resolution of the resulting mirrors is determined solely by the optical figure of the substrate.* Fabrication of these thin-film layered synthetic microstructures (multilayers) were pioneered by Eberhard Spiller at the IBM Watson Research Center (22a) and by Troy W. Barbee (22b) at Stanford University. By depositing a series of alternating layers of two different materials, one a strong x-ray scatterer with high atomic number, and the second a weak x-ray scatterer or "spacer" with low atomic number, a synthetic structure that acts as an x-ray Bragg diffractor can be fabricated. X-ray reflectivity is maximized when the condition for constructive interference is satisfied as indicated by the Bragg equation, $n\lambda = 2d_{\text{eff}}\sin\theta$, where n is the order of diffraction, θ is the angle of incidence with respect to the surface, d_{eff} is the effective layer-pair thickness (corrected for refraction effects), and λ is the wavelength of the incident radiation. Although the reflectivity at each interface is small, by the use of tens to hundreds of layer pairs, excellent reflectivities (>50% near normal-incidence) can be achieved. By proper selection of the materials and control of the thicknesses of the scatterer and spacer layers, the multilayer mirror can be tailored to reflect a desired wavelength band at maximum efficiency for a given angle of incidence. Multilayer structures can also be fabricated to have any layer pair spacing between 15 and 500 Å, thereby providing optical surfaces for radiation with $30 < \lambda < 1000$ Å. Hence, conventional astronomical imaging/spectroscopic configurations employing normal-incidence reflection optics coated with a multilayer of the appropriate layer pair spacing, can be made to operate in the soft x-ray wavelength regime where in the past only grazing-incidence reflections could be used, and in the extreme ultraviolet, where in the past only single reflection optical systems could be used. Normal-incidence x-ray optics have several distinct advantages when compared with grazing-incidence optics: (i) for a given aperture the collecting area and field of view are significantly larger; (ii) compound normal-incidence optical systems can be folded and thus be made more compact; (iii) normal-incidence optical surfaces are significantly easier and *cheaper* to manufacture; and (iv) the aberrations (resulting from violations of the Abbé Sine condition) associated with grazing-incidence optical and spectroscopic systems can be avoided; (v) image degradation due to non-specular scattering is less severe. The spectral resolution of a multilayer is determined by the number of layers that participate in the bragg-diffraction process, which in turn depends on the total number of layers present and the amount of attenuation in each layer. For multilayer-coated optics, the spectral bandpass ($\Delta\lambda/\lambda$) can be as large as 20% or as small as 1%. Normal-incidence reflection efficiencies can be made as high as 70%.

The first successful imaging experiments with normal-incidence multilayer optics were carried out in the laboratory during the early 1980's (23). Recently, Underwood et al. (24) have published a moderate resolution (~ 10 arcsec) image of a single solar active region obtained with a single-reflection (Herschellian) multilayer telescope having a bandpass centered at 44 Å (corresponding to Si XII radiation). The power of this new technology has now

been definitively demonstrated by the results obtained by Walker et al (25) in a recent rocket-borne observation of the Sun (front cover) using multilayers in the classic Cassegrain optical configuration. The success of conic multilayer telescopes demonstrates that we are able to develop a single spectroheliograph instrument design which, with the appropriate choice of mirror surface for each wavelength interval, can achieve resolution $\delta\theta \sim 0.1''$ at ultraviolet ($\sim 1000 - 2000 \text{ \AA}$), EUV ($300 - 1000 \text{ \AA}$), XUV ($100 - 300 \text{ \AA}$) and soft x-ray ($30 - 100 \text{ \AA}$) wavelengths.

Barbee (26,27) has recently successfully fabricated and tested the first multilayer gratings. Barbee has shown that these combined microstructure optical elements disperse wavelengths bragg-diffracted by the multilayer structure so that all constructive interference occurs at essentially constant angles relative to the zero order bragg-diffracted beam. The multilayers deposited on these gratings are Mo/Si layer pairs with $d_{\text{eff}} \sim 153 \text{ \AA}$. Measurements on these gratings have demonstrated resolution as high as $\lambda/\Delta\lambda \sim 2000$ at normal incidence. These very exciting results demonstrate that our strawman concept can provide the high resolution spectra required by ASO. Among the issues related to multilayer optics we propose to investigate are the improvement of reflection efficiency and the development of ellipsoidal and toroidal multilayer gratings.

3.1.1.2 The Photoelectric Detector Arrays: A fundamental requirement for the development of a compact high resolution EUV/XUV/soft x-ray spectroheliograph instrument is the availability of high resolution detector arrays. The two most widely used imaging arrays are the Charged Coupled Detector (CCD) (28) and the Multi Anode Microchannel Plate Array (MAMA) (29, 30). Both devices will be investigated. The MAMA detector has been successfully used in ground based astronomical applications, and in space, and has been selected for the second generation ultraviolet spectrometer (STIS) on Space Telescope, for two EUV instruments on SOHO, and for the stellar EUV/XUV spectroscopic explorer mission, LYMAN. The CCD has been selected for Space Telescope and AXAF, and has flown on several successful solar missions. The MAMA detector has the following advantages: (i) it is flight proven, (ii) the MAMA can have extremely fast (in principle sub-microsecond) response time, which is well matched to the dynamics of solar phenomena, (iii) the MAMA does not suffer from bias levels which vary across the array (i.e., non "flat field") as does the CCD, (iv) the nature of the MAMA (event detection by coincidence with orthogonal anode arrays) allows compensation for image motion to be achieved, at the microsecond level, within the detector, with virtually no compromise to the quality of the image [Illing et al (31)], and (v) the MAMA can be made with a photocathode that is blind to the visible, greatly simplifying the problem of suppression of scattered light in UV, EUV, XUV and soft x-ray instruments. The advantages of the CCD include wide dynamic range and availability in large size arrays (1000×1000). Three important issues related to photoelectric array detectors that we plan to address are array size, pixel size, and dynamic range.

3.1.1.3 High Resolution XUV Sensitive Films: The image shown on the cover (25) was recorded on an EUV-soft x-ray-sensitive, tabular grain (T-grain) emulsion (32) that was specially prepared by the Eastman Kodak Company. This emulsion is similar to Kodak T-MAX 100, but was prepared without a gelatin overcoat for optimum performance in the XUV. The film had a Rem-Jet backing which prevented static discharges during film transport in the vacuum and was transported in conventional Canon T-70 cameras with no adverse effects. Previous observations in the EUV/XUV region have been carried out with Schumann emulsions (33), which are extremely sensitive to contaminants and abrasions and yield a maximum photographic diffuse density no greater than 1.6. The T-grain emulsion yielded densities greater than 3.0 and high sensitivity throughout the spectral region studied during our rocket flight ($8 \text{ to } 256 \text{ \AA}$). We have extended our measurements with T-Grain 100 to 1200 \AA , using an EUV source at Los Alamos Scientific Laboratories (34). Hoover et al. (35) have discussed the advantages of these new T-grain films at soft x-ray-EUV wavelengths. More recently (34), we have carried out tests of a new XUV sensitive film based on the very high resolution type 649 emulsion used in Kodak Spectroscopic Plates. This new emulsion has been found to have excellent sensitivity over the spectral range $40 < \lambda < 1600 \text{ \AA}$. We will investigate the use of both the T-Grain 100 (resolution 200 l/mm) and the new 649 XUV sensitive emulsion (resolution 2000 l/mm) in a 70 mm format to record HRTC observations. This will allow a field of $10' \times 10'$ to be observed for the XUV and EUV spectroscopic foci, and full disk to be recorded for the wide field foci. No other presently available detector can approach film in resolution (i.e., small pixel size), array size, or storage capacity. Two important issues which we plan to investigate are photometric accuracy, and dynamic range of XUV films.

3.1.1.4 Pointing, Aspect and Stability: The pointing accuracy ($\sim 60 \text{ arc sec}$ - achieved by providing an error signal from the HRTC solar sensor) and stability ($\pm 15 \text{ arc sec/sec}$) possible with the PPS is not sufficient for the HRTC. There are three possible approaches to stabilizing the images of the HRTC telescopes and spectrographs; (i) the use of an active mirror servo for each telescope which is controlled by an error signal from a fine sun sensor; (ii) the use of the image motion compensation capability of the MAMA detector which can correct the address of each photon detected, based on an error signal [R. Illing, N. Zaum and R. Bybee (31)], or (iii) the use of a Fine Pointing Gimbal (FPG), to stabilize each HRTC telescope. We have selected, as our baseline design, the use of active

mirrors. The MAMA image motion compensation capability is very attractive, because of its simplicity (no moving parts), however it cannot achieve stabilization of images recorded on film. The possibility of a FPG system is also attractive, and will be studied further, however, insufficient data on the characteristics of the Space Station PPS is available to access this approach. One advantage of the active mirror approach is that Ball Aerospace has already successfully demonstrated the stabilization of a solar telescope mirror to an accuracy of 0.08 arc sec with a bandpass of 600 Hz, and an amplitude of ± 15 arc min, using the Lockheed Rocket derived LISS fine Sun Sensor. Different versions of this system have controlled 24", 6" and 2" mirrors to these specifications, which are adequate to stabilize HRTC images. We propose to use an active mirror for each HRTC telescope to improve the pointing accuracy and stability of the HRTC images to a fraction of an arc second. We also plan to develop a correlation tracking signal from the ultraviolet telescope H Ly α image, which can be used to further improve the stability of the active mirrors. The Ball Active Mirror Servos are described in Appendix C. We are confident that we can stabilize the HRTC images to 0.05 arc sec, and possibly 0.02 arc sec.

3.1.2 Global Dynamics Instrumentation: The ASO strawman payload was developed before the SOHO instruments were selected. The original ASO Global Dynamics Instrumentation (GDI) contained four instruments (Table 2b).

- A Helioseismometer capable of precise measurements of the global "seismic" oscillations of the Sun, in order to study the structure and dynamics of the convection zone and deeper interior.
- An Integrated Light Spectrometer capable of observing the fundamental modes of the solar oscillations.
- A magnetograph/tachometer capable of studying the large scale structure of the solar magnetic and velocity fields.
- A differential radiometer capable of studying the dynamical behavior of convective cells on the Sun.

The first two requirements appear to be met by instruments scheduled for deployment on SOHO. Our first task in regard to the Global Dynamics Instrument package will be to determine which ASO requirements can be met by SOHO instruments. The appropriate ASO GDI studies will then be undertaken.

3.1.3 Hard X-Ray and Gamma Ray Imaging: Recently, Prince et al (36) have reviewed techniques for the imaging of hard x-rays and gamma rays from solar flares. The article by Prince et al provides a detailed review of the technology of gamma ray collimators and detectors; we refer the reader to this up-to-date and comprehensive review. The GRID instrument under development for a MAX 90 balloon flight is compatible with the HRTC dimensions, and we propose to evaluate the impact of its inclusion in HRTC. The characteristics of GRID are given in Table 3 below. The P/OF will, of course, be able to achieve higher angular resolution (~ 0.1 arc sec) for hard x-rays.

Table 3 -- Characteristics and capabilities of a GRID for use on a Balloon

Detector type	Scintillation counters	Number of subcollimators	32
Detector area	80 cm ²	Sensitivity	>100 flares per week
Energy range	20keV to 1 MeV	Angular resolution	1.6 arc sec
Subcollimator material	Tungsten and tantalum	Field of view	Full Sun

3.1.4 X-Ray Flare Spectroscopy: The X-Ray Polychromator (XRP) instrument on SMM (37) demonstrated the importance of highly time resolved high resolution x-ray spectra over a series of wavelength bands containing the He-like line multiplets of ions from Fe XXV (5×10^7 K) to O VII (2×10^6 K) for the study of flares. Observations of this nature are highly complementary to the high spatial resolution narrow band observations of the HRTC soft x-ray, XUV, and EUV telescopes. These lines are emitted in the wavelength range $\lambda\lambda$ 1.5 - 25 Å and offer many diagnostic lines for density, temperature, and non-thermal excitation (38). The XRP utilized bent crystal spectrometers to obtain these highly resolved spectra; and we plan to study a similar instrument for inclusion on HRTC.

3.2 The High Energy Facility: The High Energy Facility (HEF) consists of five major spectrometers (Table 1, p. 3), (i) high and (ii) low resolution Gamma Ray Line Spectrometers (10 keV - 10 MeV), (iii) High Energy Gamma Ray Line (10 MeV - 100 MeV) and (iv) Neutron (10 MeV - 1000 MeV) spectrometers, and (v) a Low Frequency Radio Spectrograph. The parameters of the HEF Gamma Ray and Neutron instruments is given in Table 4.

Table 4
Parameters of the Four Instruments
in the High Energy Facility

X-ray and Gamma Ray Line Spectrometers (2)

Field of View:	Full Sun	Spectral Resolution:	High resolution;; 10 keV at 4.4 MeV High Sensitivity;; 200 keV at 4.4 MeV
Total Area:	High-resolution; 540 cm ² High sensitivity; 2000 cm ²	Time Resolution :	High resolution; 1 sec High Sensitivity; 0.25 sec

High Energy Gamma Ray and Neutron Spectrometers (2)

Field of View:	Full sun	Time Resolution:	1 sec
Total Area:	High Energy Gamma Ray; 1m ² High Energy Neutron; 1m ²	Spectral Range:	Gamma Ray Spectrometer 5 - 150 MeV Neutron Spectrometer 30 - 1000 MeV
Spectral Resolution:	High Energy Gamma Ray Spectrometer $\Delta E/E = 0.2$ at 50 MeV High Energy Neutron Spectrometer $\Delta E/E = 0.2$ at 100 MeV		

	<u>HEGS</u> <u>Spectrometer</u>	<u>HENS</u> <u>Spectrometer</u>	<u>High Resolution</u> <u>Gamma Spect</u>	<u>High Sensitivity</u> <u>Neutron Spec.</u>
Weight	1000 Kg	700 Kg	400 Kg	1000 Kg
Power	40 W	40 W	40 watts	60 watts
Telemetry Rate	5 Kbps	5 Kbps	80 Kbs	120 Kbs
Volume	1 m ³	1 m ³	0.7 m diam x 0.5 m	1 m diam x 0.5 m length

The proceedings of the recent "Conference on the High-Energy Aspects of Solar Flares - a Basis for a High Energy Facility for Solar Physics," are currently in press at Solar Physics (6). Contained in these proceedings are detailed reviews on the properties of the High Energy Facility gamma ray and neutron spectrometers, including papers on Hard X-Ray Gamma Ray Spectrometers (39), High Energy Gamma Ray Spectrometers (40), Polarization Measurements (41), and Neutron spectrometers (42-44). Technological questions and alternative instrument designs for HEF instruments are discussed in depth in these references, and will only be summarized here. The issues to be addressed include: (i) properties and relative advantages of scintillation materials including NaI (TI), CsI (TI), CaI (Na) and Bismuth Germanate or "BGO", (ii) the properties and relative advantages of semiconductor detector materials including Silicon, Germanium, Mercuric Iodide, and Cadmium Telluride, (iii) pulse shape discrimination (to reduce backgrounds) in semiconductor detectors, (iv) the design and construction of collimator grids for imaging instruments, and (v) imaging detectors for transform imaging instrument, including multiwire gas proportional counters, gas drift chambers, liquid Argon and Xenon detectors, and inorganic scintillators.

4.0 Data Acquisition, Calibration and Archiving:

4.1 Analysis of ASO Data Acquisition Modes: A detailed analysis of the implications of the data acquisition modes that may be employed by ASO will be undertaken. The modes to be studied are (i) compression of data from photoelectric detector arrays, (ii) storage of data on board Space Station on optical disks for transport via the Shuttle, real time telemetry via TRSS, and (iii) the use of photographic film. We plan to develop a detailed ASO data plan.

4.2 Data Reduction and Science Data Formats: This ASO data plan will define a standard data format with calibration incorporated. These formats could be generated at SSL/MSFC, and provided to ASO users, and we will investigate this possibility. The HRTC film will be microdensitometered at MSFC or at JSC.

4.3 Archiving of Data: We plan to develop a detailed plan to archive ASO reduced data in a standard format such as the NOAO (IRAF) or the NRAO formats.

5.0 Orbiter Crew Requirements: The ASO requirements for the Orbiter Crew are (i) to replace film cameras when the film has been exposed and (ii) to provide commands to select the location on the sun to which the ASO is to be pointed, (iii) to replace consumables such as cryogenic fluids or solids, and (iv) to replace defective equipment where possible, as required. We anticipate requesting active crew control of the ASO pointing on rare occasions, for special objectives such as flare observations. If a wide band link to ground is available on a sufficiently frequent basis, then requirement (ii) above is not necessary. The crew must be trained to (a) remove and replace film cameras during EVA, and (b) recognize and select solar features from the H Ly α telescope display, (c) to replace other consumables (only optical disks and cryogens are identifiable at this time) and (d) to replace electronic modules.. Skill (b) may not be required if wide band ground link is available on a sufficiently frequent basis.

6.0 Development of ASO Management and Cost Plans: We plan to carry out, at MSFC, a detailed engineering analysis of the ASO, based on the work of the Instrument Scientists, and Mission Scientists, and on the engineering analyses to be carried out by TRW, Ball Aerospace, and Brown Teledyne Engineering. Based on this analysis, we will develop detailed management and cost plans for the ASO program.

REFERENCES

1. *Astronomy and Astrophysics for the 1980s, Vol. I: Report of the Astronomy Survey Committee*, (National Academy Press, Washington, D.C., 1982.); An overview of the report of the full Survey Committee is contained in the article by George Field in *Physics Today*, 35, No. 4, 46, (April 1982.)
- 2a. *Challenges to Astronomy and Astrophysics: Working Documents of the Astronomy Survey Committee*, (National Academy Press, Washington, D.C., 1983.)
- 2b. "Astronomy and Astrophysics for the 1980s, Vol. II: Reports of the panels," (National Academy Press, Washington, D.C., 1983.); Overviews of the reports of the High Energy, Radio and Ultraviolet, Optical and Infrared Panels are contained in a special issue of *Physics Today*, 35, No. 11, (November 1982.)
3. A.B.C. Walker, Jr., R. Moore, and W. Roberts, *The Advanced Solar Observatory*, NASA Technical Publication (1986)
- 4a. Stuart B. Jordan, "The Solar Optical Telescope (SOT)," *Space Science Reviews*, 29, 333, (1981.)
- 4b. Richard B. Dunn, "SOT Instrumentation." *Ibid.*, 341.
- 4c. Alan Title, "An Overview of the Orbiting Solar Laboratory," Lockheed Palo Alto Research Laboratory preprint (1988)
- 5a. "The Pinhole/Occluder Executive Summary," *NASA Technical Paper 2089*, (October 1982.)
- 5b. E. Tandberg-Hanssen, R.M. Wilson and A.S. Hudson, "Solar Flares and Coronal Physics; Using P/OF as a Research Tool," *NASA Conf. Publ. 2421*, (1986).
6. "On High-Energy Aspects of Solar Flares - A Basis for a High Energy Facility for Solar Physics", Special Issue of the *Journal Solar Physics*; Eds. E.L. Chupp and A.B.C. Walker, Jr., in press (1988)
7. W. Bailey, "Advanced Solar Observatory Accommodation Requirements Study," Teledyne Brown Engineering, Inc., Huntsville, Alabama, Sept. 1988.
8. John Bahcall, "Solar Neutrinos: Theory versus Experiment," *Space Science Reviews*, 24, 277, (October 1979.)
- 9a. Gordon Newkirk, Jr., and Kendrick Frazier, "The Solar Cycle," *Physics Today*, 35, No. 4, 25, (April 1982.)
- 9b. *Advances in Helio and Astrogeismology*, IAO Symp. 123 Ed. J. Christensen, Dalgaard and S. Frandsen (D. Reidel Publ. Co. Dordrecht, 1988)
Symposium on Seismology of the Sun and Sun-like Stars, Tenerife, Spain Sept. 1988 to be published by ESA Publ. 286 Ed. E. J. Rolfe
10. R. Grant Athay and Oran R. White, "Chromospheric Oscillations Observed with OSO 8: IV. Power and Phase Spectra for C II," *The Astrophysical Journal*, 229, 1147, (May 1979.)
11. Jack Harvey, "Observations of Small-Scale Photospheric Magnetic Fields," *Highlights of Astronomy*, 4, 223-239, (1977.)
12. Jack B. Zirker, Editor, "Coronal Holes and High Speed Wind Stream," (Colorado Associated University Press, 1977.)
13. Jack A. Eddy, "The Maunder Minimum," *Science*, 192, 1189, (June 1976.)
- 14a. Gerard Van Hoven, "Plasma Energetics in Solar Flares," *Highlights of Astronomy*, 5, 343, (1980.)
- 14b. Reuven Ramaty and Richard E. Lingenfelter, "Gamma Ray Astronomy," *Annual Review of Nuclear and Particle Science*, 32, 235, (1982.)
15. "Solar Physics: The Report of the Solar Physics Working Group of the Astronomy Survey Committee," Chapter 1 of Reference 2a (1982); An overview of the report of the Solar Physics Working Group is contained in the article by A.B.C. Walker, Jr., in *Physics Today*, 35, No. 11, (November 1982.)
16. *Physics of the Sun* (3 Volumes), edited by P.A. Sturrock, T.E. Holzer, D.M. Mihalas, and R.K. Ulrich, (D. Reidel Publishing Company, 1985.)
17. "Solar Variability, Weather, and Climate," (National Academy Press, Washington, D.C., 1982.)
- 18a. O.C. Wilson, Arthur H. Vaughn, and D.M. Mihalas, "The Activity Cycles of Stars," *Scientific American*, 244, 104, (February 1981.)
- 18b. O.C. Wilson, "Chromospheric Variations in Main Sequence Star," *The Astrophysical Journal*, 226, 379, (December 1978.)
19. J. D. F. Bartoe and G. E. Bruckner, *J. Opt. Soc. Am.* 65, 13 (1975)
20. D. A. Schwartz et al, *Proc. SPIE* 597, 10 (1985)
21. T.W. Barbee, Jr., *Optical Engineering* 25, 898 (1986)

- 22a. E. Spiller, in *Low Energy X-Ray Diagnostics*, D.T. Attwood and B.L. Henke, Eds. *American Institute of Physics Conference Proceedings* 75, (AIP, New York, 1981) p. 124
- 22b. T.W. Barbee, Jr., *ibid.*, p. 131
23. J.H. Underwood, and T.W. Barbee, Jr., *Nature* 294, 429 (1981); J.P. Henry, E. Spiller, and M. Weisskopf, *Appl. Phys. Letters* 40, 25 (1982)
24. J.H. Underwood, M.E. Bruner, B.M. Haisch, W.A. Brown, and L.W. Acton, *Science* 238, 61 (1987)
25. A.B.C. Walker, Jr., T.W. Barbee, Jr., R.B. Hoover, and J.F. Lindblom, *Science* 241, 1781 (1988)
26. T.W. Barbee, Jr., "Combined Microstructure X-Ray Optics; Multilayer Diffraction Gratings," to be published in *Proc. Symp. D, Multilayers: Synthesis, Characterization and Non Electronic Properties*; T. Barbee, F. Spaepen and L. Green, Eds., Materials Research Society Meeting Dec 1987 Boston
27. T.W. Barbee, Jr., "The Use of Multilayer Diffraction Gratings in the Determination of X-Ray, Soft X-Ray and XUV Elemental Scattering Cross-Sections: to be published in *SPIE Proc. of the International Soc. for Optical Engineering O-E Laser 1988 meeting*. (1988)
28. R.A. Stern et al., *Optical Engineering* 26, 875 (1987)
29. J.G. Timothy and J.S. Morgan, "Status of the MAMA Detector Development Program," in *Instrumentation for Ground-based Optical Astronomy*, (Springer Verlag; Berlin, 1988), in press
30. J.G. Timothy, "Photon-Counting Detector Systems," in *Instrumentation for Ground-based Optical Astronomy*, (Springer Verlag; Berlin, 1988), in press. J.G. Timothy and R.L. Bybee, "High Resolution Pulse-Counting Array Detectors for Imaging and Spectroscopy at Ultraviolet Wavelengths", *SPIE Ultraviolet Technology* 687, 35 (1986)
31. R.M.E. Illing, N.H. Zaun, and R.L. Bybee, "Image Motion Compensation Using a Photon-Counting UUXV/Visible Detector,"
32. J.E. Maskasky, *J. Imaging Sci.* 31, 15 (1987)
33. Examples of films with Schumann emulsions include the Kodak SWR, Kodak Pathe' SC-5 and SC-7 and Kodak 101-07 films; V. Schumann, *Ann. Phys.* 5, 349 (1901); R. Audren, *Appl. Opt.* 4, 1596 (1966); M. E. Van Hoosier, J.-D. Bartoe, G.E. Breuckner, N.P. Patterson, R. Tousey, *ibid.* 16, 887 (1977); A.G. Millikan and C.E. Coykendall, *Am. Astron. Soc. Photo. Bull.* 3, 11 (1977)
34. Hoover, R.B., Lindblom, J.R., and Walker, A.B.C., Jr., (1988), unpublished results.
35. R.B. Hoover, T.W. Barbee, Jr., J.F. Lindblom, and A.B.C. Walker, Jr. *Kodak Technical Bits*, E. Eggleton, Ed. (Kodak, Rochester, summer 1988) p.1.
36. T. Prince, G.J. Hurford, H.S. Hudson, and C. Crannell, "Hard X-Ray & Gamma-Ray Imaging of Solar Flares", *Solar Physics*, in Press (1988)
37. Acton et al, *Solar Phys.* 65, 53 (1980)
38. Walker, A.B.C., Jr., in "*Solar Gamma-, X- and EUV Radiation*", S.R. Kane, Ed. (D. Reidel; Dordrecht, 1975), p. 73.
39. N. Gehrels, C.J. Drannell, P.J. Forrest, R.P. Lin, L.E. Orwig, and R. Starr, "Hard X-Ray and Low Energy Gamma Ray Spectrometers, *Solar Physics*, in Press (1988)
40. S. White, D. Forrest, P. Dunphy, C. Crannell, "Gamma Ray Spectrometers", *ibid.*
41. R. Novick, "Polarization Techniques", *ibid.*
42. G. Frye, Dunphy, "Neutron Techniques I", *ibid.*
43. G. Frye, "Neutron Techniques II", *ibid.*
44. P. Evenson, "Neutron Techniques III - Decay Proton Observations", *ibid.*

Alan Title

Lockheed Palo Alto Research Laboratory,
3251 Hanover Street, Palo Alto, California 94304

1. Introduction

August 10, 1988

The Orbiting Solar Laboratory will be a free flying, polar orbiting complement of scientific instruments to observe the surface and upper atmosphere of the sun and make precision measurements at high spatial and temporal resolution over a spectral range from the X-Ray to the near Infra-red. OSL contains a 1 meter telescope which feeds a narrowband tunable filter, a set of fixed broadband filters, and a spectrograph. These three instruments are mounted together in a common structure, share a unified science data and control system, and use a single image stabilization system for their common fields of view to form a Coordinated Instrument Package (CIP). An Ultraviolet Spectrograph and an XUV/X-Ray imager are desired co-pointing instruments which have their own independent optical systems. The CIP and the copointing instruments operate with overlapping fields of view.

The 1 meter telescope, which is optimized for 2000 - 11,000 Å, can resolve 75 km on the solar surface which is about the mean free path for photons - the coupling length of radiatively dominated processes in the solar surface. This is crucial because the surface of the sun is the interface between the region of convective and radiative transport of energy. A detailed understanding of this interface is fundamental to understanding a broad range of problems in solar and stellar physics. Not only is this the only astrophysical convection zone which can be studied in detail, but solar observations also can complement laboratory convection experiments by extension to a much higher Rayleigh number.

The surface of the sun is also the region where the solar magnetic field first becomes visible. Convective motions in the atmosphere and interior interact with the magnetic fields to provide the energy which heats the outer solar atmosphere and drives the solar wind. These magneto-convective interactions range between those driven by the pervasive granulation and supergranulation flows of the quiet sun to large scale shear flows in active regions which cause the violent events of solar activity. The solar magnetic field, which expands outward to fill the solar system, is responsible for the form of the magnetospheres of all the planets.

The Ultraviolet Spectrograph, 1175 - 1700 Å, will study the transition region between the 10,000 degree chromosphere and the 1,000,000 degree corona. The XUV/X-Ray imager, 40 - 400 Å, will allow study of the corona and of multimillion degree solar transient events.

The three year duration of the OSL means it will fly with a variety of other spacecraft which will significantly increase the joint scientific output. For example, the SoHO spacecraft has instruments that allow the study of the solar interior and the outer solar corona, while OSL is studying the critical interface region. In particular the helioseismic instrument on SoHO will obtain data on the rotational gradients in the solar interior which drive the dynamo responsible for the solar magnetic cycle. OSL and SoHO in operation together offer the promise of actually observing the invisible processes in the subsurface layers, by means of acoustic tomography, as magnetic flux tubes emerge through the surface. The corona instruments on SoHO and the fields and particle instruments on the rest of the ISTP complement of instruments will follow the effects of the magnetic field well into the environment of the earth while OSL observes the physics of the processes that convert the energy in convection to radiative and magnetohydrodynamic forms.

Figure 1 shows and artist's conception of the OSL pointing at the sun. The large central cylinder contains the 1 meter telescope, the two smaller cylinders attached on the sides indicate the volumes allocated for the Ultraviolet Spectrograph and the XUV/X-Ray imager, the CIP is seen on the top of the telescope tube. The large square panels are solar arrays and the smaller ones are phased array TDRSS antennae. Figure 2 shows an optical layout of the 1 meter telescope. The characteristics of the entire instrument package are summarized in Table 1.

The CIP instrument has been under study since 1981. It consists of the Photometric Filtergraph (PI Professor Harold Zirin, California Institute of Technology), the Tunable Filtergraph (PI Alan Title, Lockheed Palo Alto Research Laboratory), and the Klepper Institute Solar Spectrograph (PI Professor Egon Schroeter). An optical cartoon of the CIP and a series of optical mechanical drawings of the three instruments in the CIP are shown in figures 3 through 6. A top level electrical control diagram of the CIP is given in figure 7.

At present two copointing instruments are being studied for inclusion on the OSL mission. A version of the High Resolution Telescope and Spectrograph (HRTS) (PI Guenter Brueckner, Naval Research Laboratory) is being studied as the Ultraviolet Spectrograph. Figure 8 is an optical layout of the OSL/HRTS. The XUV/X-Ray Imager will probably be an array of normal incidence telescopes with multilayer coatings. These coatings have a high reflection coefficient in a spectral band of only a few angstroms and as such act as narrowband spectral filters. It is anticipated that the Air Force Geophysical Laboratory will provide the XUV/X-Ray Imager.

Figure 9 shows the fields of view of the CIP focal planes overlaid. The total science data stream of the OSL will be 16 Mbits/s proportioned 12:3:3 to the CIP:Ultraviolet Spectrograph:XUV/X-Ray Imager. The CIP data stream can be allocated in realtime but normally the rates will be allocated internally as 4.8:4.8:3 to the PF:TF:KIS9. All of the instrument focal plane detectors will be 1024 x 1024 CCD's. Those in the CIP will be front illuminated and have a full well of 200,000 electrons. The Ultraviolet instrument will probably use detectors that have been coated with a dye that absorbs in the ultraviolet and emits in the visible.

At present OSL is the number one moderate mission of NASA. If funding becomes available now or very shortly, OSL could be launched in 1994-96. Unfortunately, because of the slow recovery from the shuttle accident and funding limitations all NASA science programs have been delayed and may continue to be delayed.

The data from OSL should provide the basic physics for understanding the nature of the inputs to the Earth and its atmosphere to be studied by the Earth Observing System (EOS). Due to the significant advances in the last few years in data storage and data transmission, the OSL can act as the center piece in a network of groundbased observatories, which then can extend the total solar measurement capability with instruments in the near and far infrared and with ultra high spectral resolution. Once OSL has provided data on the basic physical processes in the solar atmosphere, a great body of information already collected as well as new ground data will be able to be correctly interpreted.

The interactions of convection, radiation, and the magnetic field - magnetohydrodynamics - are key to understanding not only the sun and other stars, but also galaxies, pulsars, neutron stars, and black holes. While the sun does not have the range of conditions of all of these objects, it provides the only place where magnetohydrodynamic process of astronomical scale can be studied in any detail.

The OSL instrument complement is summarized in section 2. Section 3 discusses the some of the operational characteristics of the OSL mission.

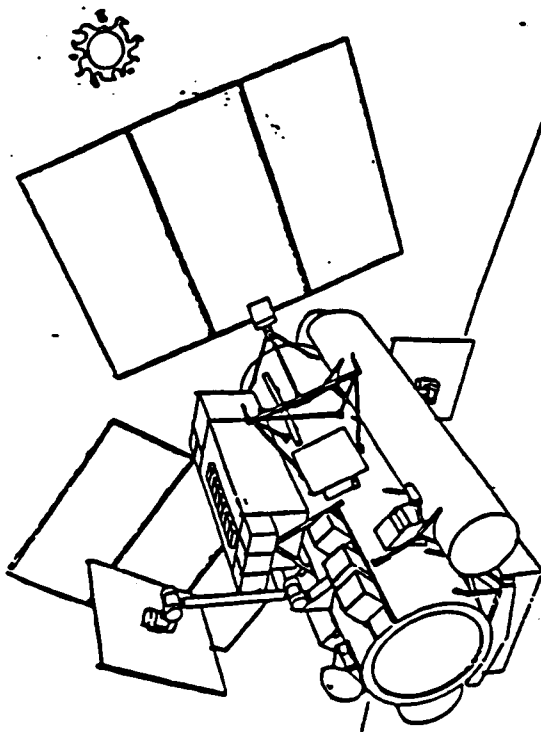


Figure 1. OSF pointing at the Sun.

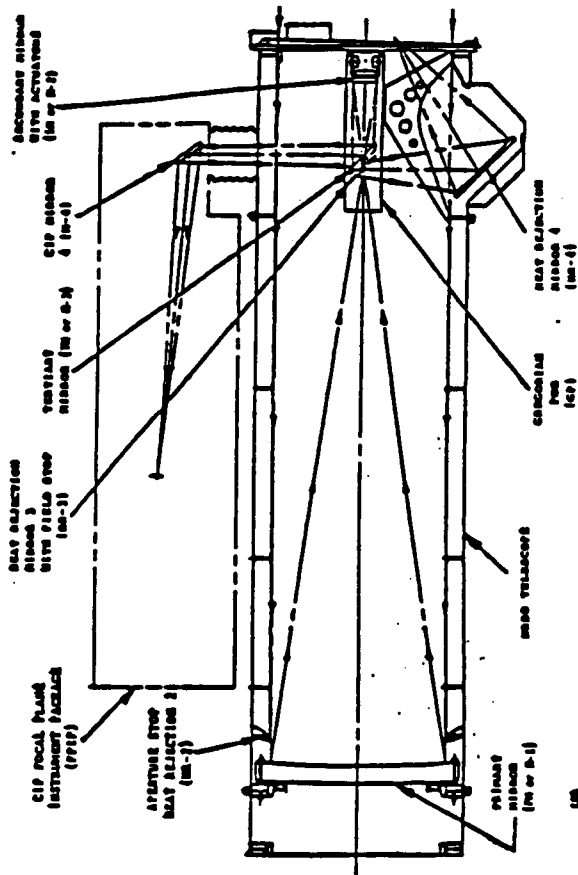


Figure 2. Optical Layout of the 1 meter telescope with CIP location indicated.

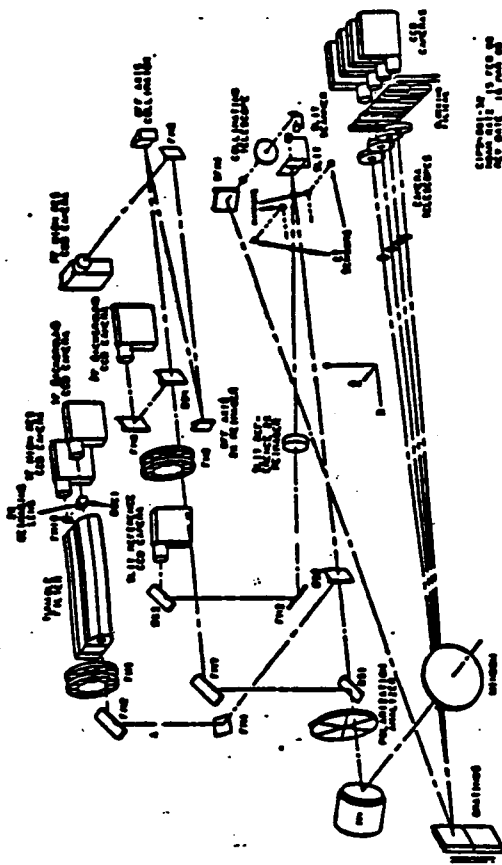


Figure 3. An optical cartoon of the CIP.

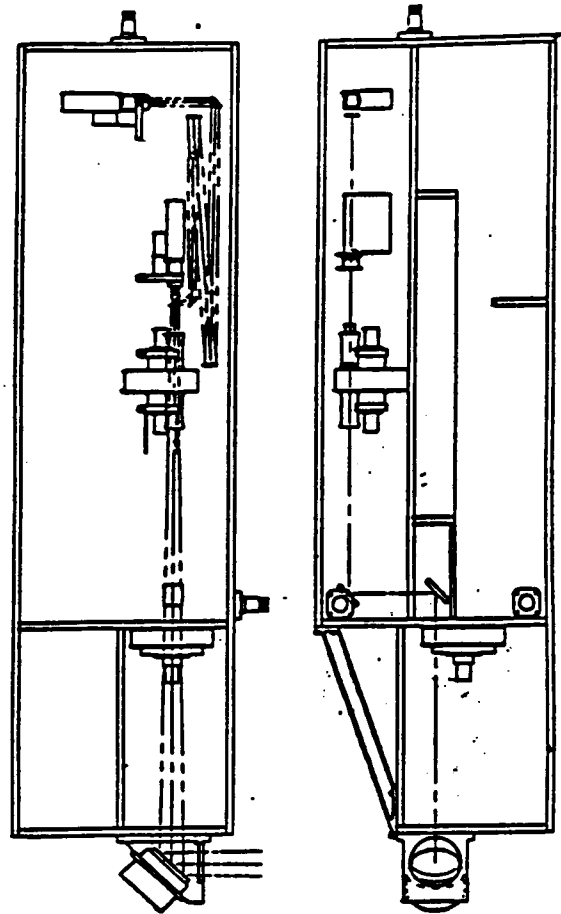


Figure 4. CIP with location of the Photometric Filtergraph components shown.

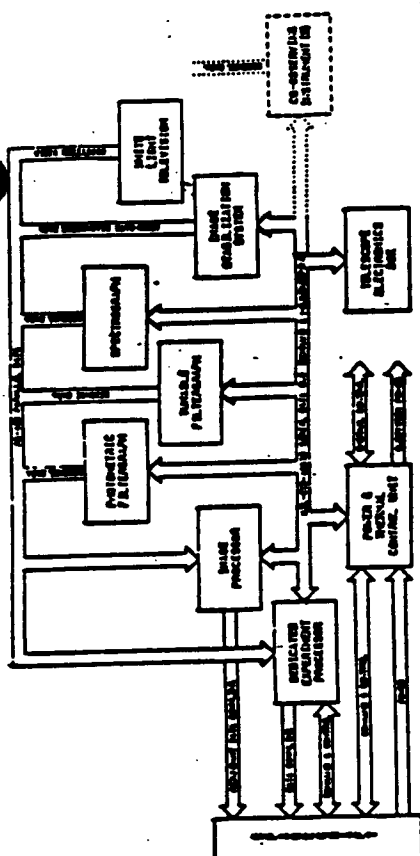


Figure 7. Top level electronic control diagram of CIP.

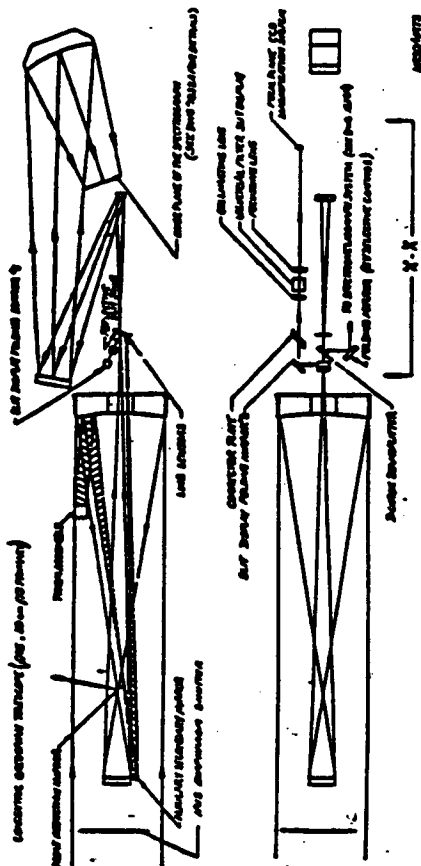


Figure 8. Optical layout of a modified HRT3 for OSL.

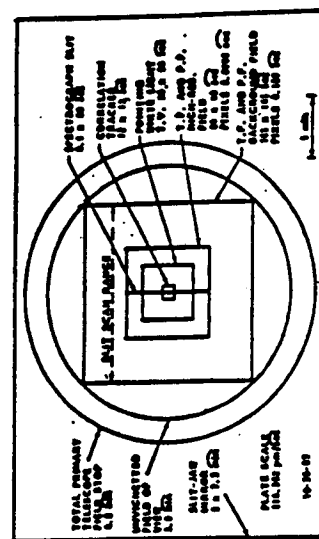


Figure 9. Fields of view of the CLP local planes.

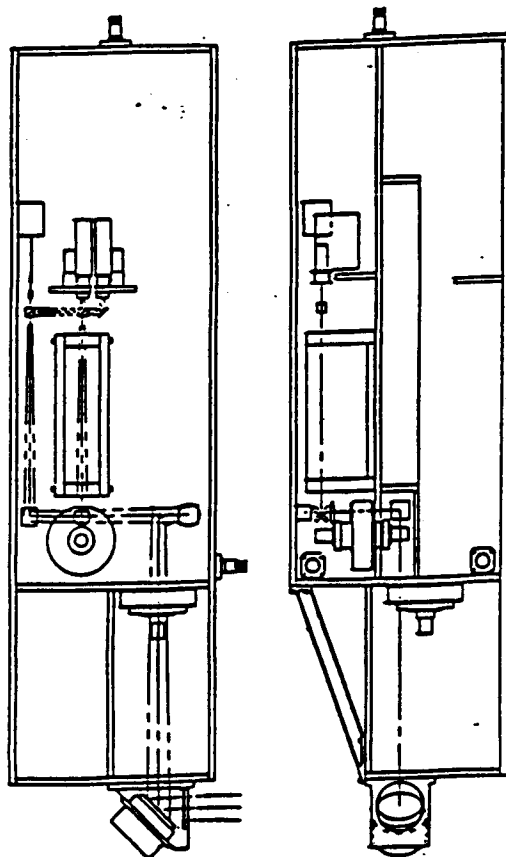


Figure 6. CLP with location of the Tunable Filtergraph components shown.

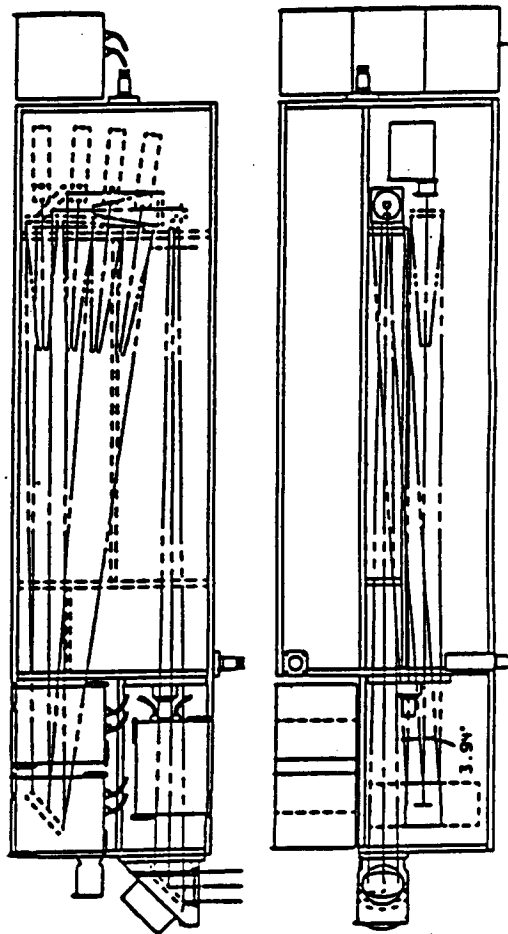


Figure 6. CIP with location of the KIS spectrograph components shown.

CIP Klepenheuer Institut Solar Spectrograph

Wavelength Range	2700 to 10,000 Å
Detectors	4 1024 x 1024 CCDs
Field of View	0.1 x 76 arc seconds
Scan Range	152 arc seconds
Resolution ($\lambda/\Delta\lambda$)	350,000
Configurations	2 grating positions, 3 sets of blocking filters
Dispersion	1.7 mm/Å (5000)

Grating 1 (188 gr/mm)

CCD-1:	Ca K	3933.7	Ca I	8502.0
	Mg K	3795.8	Ti II	4468.8
			Fe g=0	5576.1
			Fe g>0	5250.2
			Fe g>0	5247.1

Grating 2 (79 gr/mm)

CCD-1:	IR O 1	7771.9	IR O 2	7774.2
	IR O 3	7778.4	Na D 1	5895.9
	Mg I	8172.7	Ca IR	8542.1
	Fe g>0	6302.5	He I	6876.7
	Ca II	8248.8	Ca II	8254.7
	Fe II	4657.0	Ti II	4656.5
	Fe II	4657.2	Fe II	4641.5
	Fe II	4128.7	Ca II	8498.0
	Fe II	8197.6	Ti I	8193.0
	Fe II	4924.0	Cl	5032.2
	Fe I g=0	4065.4	Fe I g=0	7194.9

Grating 3 (1024 x 1024 CCD; 1 High Res, 1 Low Res)

CCD-1:	Ca K	3933.7	Ca I	8502.0
	Mg K	3795.8	Ti II	4468.8
			Fe g=0	5576.1
			Fe g>0	5250.2
			Fe g>0	5247.1

Grating 4 (1024 x 1024 CCD; 1 High Res, 1 Low Res)

CCD-1:	Ca K	3933.7	Ca I	8502.0
	Mg K	3795.8	Ti II	4468.8
			Fe g=0	5576.1
			Fe g>0	5250.2
			Fe g>0	5247.1

Grating 5 (1024 x 1024 CCD; 1 High Res, 1 Low Res)

CCD-1:	Ca K	3933.7	Ca I	8502.0
	Mg K	3795.8	Ti II	4468.8
			Fe g=0	5576.1
			Fe g>0	5250.2
			Fe g>0	5247.1

Grating 6 (1024 x 1024 CCD; 1 High Res, 1 Low Res)

CCD-1:	Ca K	3933.7	Ca I	8502.0
	Mg K	3795.8	Ti II	4468.8
			Fe g=0	5576.1
			Fe g>0	5250.2
			Fe g>0	5247.1

Grating 7 (1024 x 1024 CCD; 1 High Res, 1 Low Res)

CCD-1:	Ca K	3933.7	Ca I	8502.0
	Mg K	3795.8	Ti II	4468.8
			Fe g=0	5576.1
			Fe g>0	5250.2
			Fe g>0	5247.1

Grating 8 (1024 x 1024 CCD; 1 High Res, 1 Low Res)

CCD-1:	Ca K	3933.7	Ca I	8502.0
	Mg K	3795.8	Ti II	4468.8
			Fe g=0	5576.1
			Fe g>0	5250.2
			Fe g>0	5247.1

Grating 9 (1024 x 1024 CCD; 1 High Res, 1 Low Res)

CCD-1:	Ca K	3933.7	Ca I	8502.0
	Mg K	3795.8	Ti II	4468.8
			Fe g=0	5576.1
			Fe g>0	5250.2
			Fe g>0	5247.1

Grating 10 (1024 x 1024 CCD; 1 High Res, 1 Low Res)

CCD-1:	Ca K	3933.7	Ca I	8502.0
	Mg K	3795.8	Ti II	4468.8
			Fe g=0	5576.1
			Fe g>0	5250.2
			Fe g>0	5247.1

Grating 11 (1024 x 1024 CCD; 1 High Res, 1 Low Res)

CCD-1:	Ca K	3933.7	Ca I	8502.0
	Mg K	3795.8	Ti II	4468.8
			Fe g=0	5576.1
			Fe g>0	5250.2
			Fe g>0	5247.1

Grating 12 (1024 x 1024 CCD; 1 High Res, 1 Low Res)

CCD-1:	Ca K	3933.7	Ca I	8502.0
	Mg K	3795.8	Ti II	4468.8
			Fe g=0	5576.1
			Fe g>0	5250.2
			Fe g>0	5247.1

Grating 13 (1024 x 1024 CCD; 1 High Res, 1 Low Res)

CCD-1:	Ca K	3933.7	Ca I	8502.0
	Mg K	3795.8	Ti II	4468.8
			Fe g=0	5576.1
			Fe g>0	5250.2
			Fe g>0	5247.1

Grating 14 (1024 x 1024 CCD; 1 High Res, 1 Low Res)

CCD-1:	Ca K	3933.7	Ca I	8502.0
	Mg K	3795.8	Ti II	4468.8
			Fe g=0	5576.1
			Fe g>0	5250.2
			Fe g>0	5247.1

Grating 15 (1024 x 1024 CCD; 1 High Res, 1 Low Res)

CCD-1:	Ca K	3933.7	Ca I	8502.0
	Mg K	3795.8	Ti II	4468.8
			Fe g=0	5576.1
			Fe g>0	5250.2
			Fe g>0	5247.1

Grating 16 (1024 x 1024 CCD; 1 High Res, 1 Low Res)

CCD-1:	Ca K	3933.7	Ca I	8502.0
	Mg K	3795.8	Ti II	4468.8
			Fe g=0	5576.1
			Fe g>0	5250.2
			Fe g>0	5247.1

Grating 17 (1024 x 1024 CCD; 1 High Res, 1 Low Res)

CCD-1:	Ca K	3933.7	Ca I	8502.0
	Mg K	3795.8	Ti II	4468.8
			Fe g=0	5576.1
			Fe g>0	5250.2
			Fe g>0	5247.1

Grating 18 (1024 x 1024 CCD; 1 High Res, 1 Low Res)

CCD-1:	Ca K	3933.7	Ca I	8502.0
	Mg K	3795.8	Ti II	4468.8
			Fe g=0	5576.1
			Fe g>0	5250.2
			Fe g>0	5247.1

Grating 19 (1024 x 1024 CCD; 1 High Res, 1 Low Res)

CCD-1:	Ca K	3933.7	Ca I	8502.0
	Mg K	3795.8	Ti II	4468.8
			Fe g=0	5576.1
			Fe g>0	5250.2
			Fe g>0	5247.1

Grating 20 (1024 x 1024 CCD; 1 High Res, 1 Low Res)

CCD-1:	Ca K	3933.7	Ca I	8502.0
	Mg K	3795.8	Ti II	4468.8
			Fe g=0	5576.1
			Fe g>0	5250.2
			Fe g>0	5247.1

Grating 21 (1024 x 1024 CCD; 1 High Res, 1 Low Res)

CCD-1:	Ca K	3933.7	Ca I	8502.0
	Mg K	3795.8	Ti II	4468.8
			Fe g=0	5576.1
			Fe g>0	5250.2
			Fe g>0	5247.1

Grating 22 (1024 x 1024 CCD; 1 High Res, 1 Low Res)

CCD-1:	Ca K	3933.7	Ca I	8502.0
	Mg K	3795.8	Ti II	4468.8
			Fe g=0	5576.1
			Fe g>0	5250.2
			Fe g>0	5247.1

Grating 23 (1024 x 1024 CCD; 1 High Res, 1 Low Res)

CCD-1:	Ca K	3933.7	Ca I	8502.0
	Mg K	3795.8	Ti II	4468.8
			Fe g=0	5576.1
			Fe g>0	5250.2
			Fe g>0	5247.1

Grating 24 (1024 x 1024 CCD; 1 High Res, 1 Low Res)

CCD-1:	Ca K	3933.7	Ca I	8502.0
	Mg K	3795.8	Ti II	4468.8
			Fe g=0	5576.1
			Fe g>0	5250.2
			Fe g>0	5247.1

Grating 25 (1024 x 1024 CCD; 1 High Res, 1 Low Res)

CCD-1:	Ca K	3933.7	Ca I	8502.0
	Mg K	3795.8	Ti II	4468.8
			Fe g=0	5576.1
			Fe g>0	5250.2
			Fe g>0	5247.1

CIP Tunable Filtergraph

Wavelength Range	4600 to 6000 Å
Positional Accuracy	1 mÅ Relative, 8 mÅ Absolute
Detectors	1024 x 1024 CCD; 1 High Res, 1 Low Res
Spectral Resolution	80 mÅ (narrow mode) 100 Å (wide mode)

W-Length Species Purpose

4671	Mg I	Temperature minimum diagnostics
4924	Fe II	Zeeman triplet
4607	Br I	Weak magnetic fields via Hanle effect
5173	Mg I	Magnetic - velocities - low chromosphere
5247/5250	Fe I	Magnetic field strength pair
5324	Fe I	Strong g=0 line
5360	Cl I	Temperature diagnostic - photosphere
5394	Mn I	Temperature diagnostic - photosphere
5576	Fe I	Velocities - mid to upper photosphere
5714	Ti I	Sunspot umbral vel., g=0 (non-magnetic)
5876	He I	Prominences, spicules, activity
5896	Na I	Magnetic + vel. - low to mid chromosphere
6064	Ti I	Umbral magnetic fields
6302	Fe I	Magnetic line, low temperature sensitive
6563	H I	Chromospheric dynamics

Ultraviolet Spectrograph

Telescope

Design	Gregorian
Size	30 cm
Focal Ratio	f/15
Image Scale	20 microns/arc second
Resolution	0.5 arc second
Image Stabilisation	0.3 arc seconds RMS
Data Rate	2 Mbits/second

Spectrograph

Type	Tandem Wedgworth
Spectral Range	1176 to 1700 Å
Field of View	0.8 x 256 arc seconds
Spectral Resolution	20 x 256 arc second band
Position	3.78 seconds
Cycle time	4 1024 x 1024 CCDs
Detectors	25.6 Å per CCD

Spectrohellograph

Field of View	256 x 256 arc seconds
Spatial Resolution	(25 arc second pixels) 16 Å
Bandpass	1510 Å, 1550 Å, plus a visible band
Wavelengths	1024 x 1024 CCD
Detector	

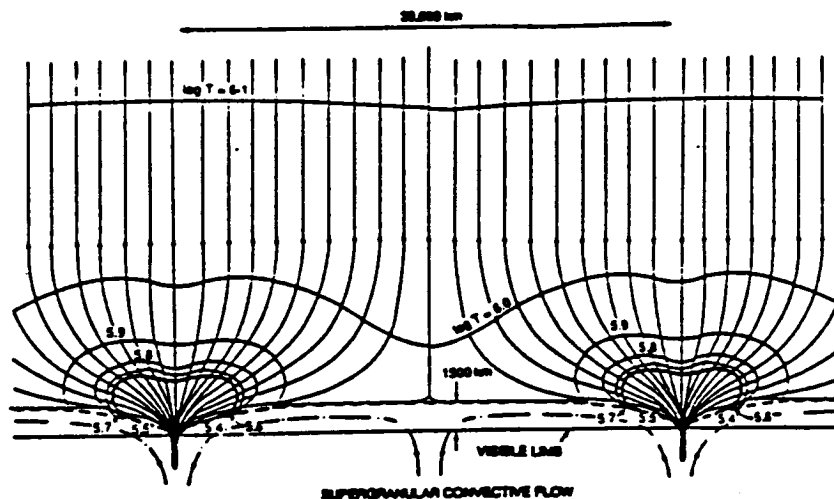
CIP Photometric Filtergraph

Wavelength Range	2000 to 11,000 Å
Detectors	1024 x 1024 CCD; 1 High Res, 1 Low Res

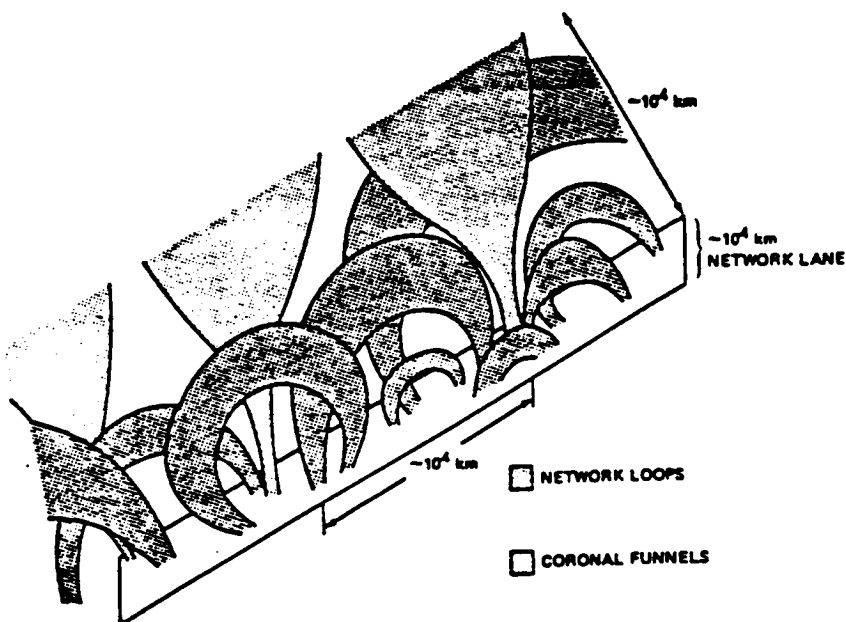
Wavelength (Å)	Band (Å)	Purpose
2100	100	UV continuum
2600	60	"Missing opacity" line blanketing
2708	12	Mg II
3300	75	H-opacity minimum
3600	40	Balmer Continuum
3862	15	Fe, CN - local opac max
3918	10	Blue continuum between deep lines
3933	0.6	Calcium K narrow band; might also use broader
4308	4	G band - CH
4508	8	4503-4611 H - opacity minimum, clean
5670	10	Clean continuum
6503	0.4	H alpha line center
6567	10	Cleanest cont < 0.06 Å lines
8170	30	Paschen Continuum
9950	100	Furthest IR - for Planck baseline

Appendix A

A Scientific Program for the ASO High Resolution Telescope Cluster



(a) Model of chromospheric network, circa 1976.



(b) Model of chromospheric network, circa 1988.

Evolution of models of the Solar Atmosphere: Figure (a) is a model of the two dimensional structure of the chromospheric (supergranulation) network proposed by Gabriel in 1976 (Ref. 4 on p. 26), which was inspired by the observation (Reeves, Ref. 3) that "transition region" ($10^5 \text{ K} < T < 10^6$) material is concentrated in the boundaries of the network. Figure (b) is a more recent model proposed by Dowdy, Rabin, Moore, and Emslie (Refs 22-26) which incorporates a more sophisticated representation of the chromospheric fine structure. It is clear that observations of the quality planned for HRTC ($\sim 0.1 \text{ arc sec} - 70 \text{ km}$) are essential to test models of chromospheric fine structure.

1.0 Introduction: A major objective of the High Resolution Telescope Cluster (HRTC) is to address fundamental problems relating to the structure and phenomenology of the solar atmosphere, including (i) the chromospheric network and magnetic fine structure, (ii) coronal loops, (iii) large scale coronal structure and dynamics, (iv) the corona-solar wind interface, and (v) flares. We discuss specific objectives which can be addressed with the HRTC instruments below. In the discussion, we will assume that the UV, XUV, and soft x-ray observations of the HRTC will allow structures in the solar atmosphere covering the entire range of temperatures present in the chromosphere and corona ($10^4\text{K} - 5 \times 10^7\text{K}$) to be observed with very high spatial ($\sim 0.1''$) and spectral ($\lambda/\Delta\lambda > 8000$) resolution simultaneously.

1.1 Chromospheric and Coronal Structure and Dynamics: In the past decade, observations made from rocket and satellites at UV, EUV/XUV and soft/x-ray wavelengths have clearly demonstrated the fundamental role that magnetic fields play in defining the structure and the flow of mass and energy in the chromosphere and corona, and have resulted in the identification of coronal holes as the source of high speed solar wind streams. Differences in the physical conditions in the chromospheric and coronal layers over different regions of the solar surface appear to be intimately related to the configuration and strength of the underlying photospheric magnetic field. We may think of the chromosphere and corona as divided into three kinds of regions, distinguished by their magnetic field structure; (i) active regions, characterized by strong local photospheric and coronal fields with closed configurations; (ii) quiet regions characterized by "chromospheric" network structure (see Frontispiece II) at transition region temperatures ($10^4 - 7 \times 10^5\text{K}$) and weak coronal magnetic fields that appear to be closed on a large scale; and (iii) coronal holes, associated with weak coronal magnetic fields having a diverging open field configuration. The regions with strong fields are characterized by enhanced radiative output, and characteristic temperatures exceeding $\sim 10^6\text{K}$. The x-ray emission of active regions is dominated by plasma confined to magnetic flux tubes, i.e., coronal loops. Quiet regions are characterized by average chromospheric radiative output and coronal temperatures near 10^6K , although cooler loops ($\sim 10^5\text{K}$) are also frequently observed. Coronal holes are characterized by somewhat lower chromospheric radiative output, low coronal radiative output and densities, and characteristic coronal temperatures generally less than 10^6K . Bright points (small bipolar regions with enhanced XUV and x-ray emission) are found in coronal holes, however, and appear to be associated with streamers and polar plumes that are sources for the solar wind. The differences in the physical conditions in these regions must be due in part to the ability of magnetic fields to channel the flow of mass and energy in the corona by the formation of loops, and in part to the role of the solar wind as a major energy loss mechanism in open field regions. Since the magnetic field plays a dominant role in the solar atmosphere, we must be able to resolve structures on scales at which the field changes significantly. For the solar atmosphere, this scale is $\sim 100 - 200\text{km}$ or less, corresponding to $0.15 - 0.30''$ when viewed from near-Earth orbit. The HRTC will be able to achieve a resolution of $\sim 0.10''$ ($0.05''$ pixels) or better.

1.1.1 The Chromospheric Network and Magnetic Fine Structure: In his comprehensive review, Athay (1) points out that the chromospheric network has been known since the late nineteenth century. SKYLAB observations have demonstrated that network structure can be observed in lines emitted by plasmas at temperatures as high as $7 \times 10^5\text{K}$ [Reeves, (2)]. The chromospheric network is characterized by fine scale ($\sim 1.0''$ or less) structures (3, 4), such as spicules (vertical magnetic flux tubes which contain cooler material and appear as dark fibers). The dynamic nature of this fine structure is demonstrated by the observation of red shifted and blue shifted line profiles in material associated with network structures such as spicules [Dere, Bartoe and Brueckner, (5a)], and small scale loops (observed in lines such as C IV $\lambda 1550\text{\AA}$ corresponding to $T \sim 10^5\text{K}$) which contain material at transition region temperatures [Dere et al., (5b)] (see Frontispiece II). Each of the network structures observed at chromospheric temperatures ($\sim 10^4\text{K}$), such as spicules, appear to have counterparts visible at ultraviolet wavelengths corresponding to emission by material at transition region temperatures ($\sim 10^5\text{K}$). In addition, distinct structures, such as the larger scale "macrospicules" and C IV emitting loops are observed at ultraviolet wavelengths. Recent Spacelab-2 observations (5c) suggest that the macrospicules, which show growth and decay on scales of minutes, are composed of very small scale structures containing upward flowing material that may counter balance down flowing material observed at lower resolution [see also Athay (1) p. 57ff]. The structure and dynamics of the network at temperatures greater than 10^5K is only now being explored at the level of 1 arc sec (6).

Two fundamental questions relating to the chromospheric network which can be addressed with the HRTC are:

- (i) *What is the relationship of microflares, bright points and spicules to magnetic flux cancellation?*

(ii) What is the relationship of microflares to spicules and coronal heating?

An unsettled observational question basic to the solar cycle is that of the removal of magnetic flux from the solar atmosphere, the process that over the course of each cycle removes all of the flux that emerges from below the photosphere. Sequences of photospheric magnetograms having nearly the best resolution that can be obtained from the ground (about 1 arcsec) have revealed examples of fine-scale merging and cancellation of positive and negative clumps of flux. Simultaneous H- α movies show that the flux cancellation was accompanied by microflare activity in the chromosphere above [Martin, Livi, and Wang (7)]. These findings are consistent with flux removal by a combination of reconnection and submergence, but the present observations do not have enough resolution to prove this [Rabin, Moore, and Hagyard (8a), Zwann (9)]. If flux is in fact removed by submergence [Moore and Rabin (8b)], then the solar cycle might be a process of recycling old magnetic field rather than a process of generating new magnetic field. On the other hand, if flux is primarily removed by either upward extraction or resistive destruction of the field [by for example, generating bright points (10 a-e) and empherical bipolar active regions (10f)], then the solar cycle may be mainly a process of generating new magnetic field rather than a recycling process. To decide between these pivotal alternatives for flux removal, we need subarcsecond resolution of the photosphere, chromosphere, transition region, and corona simultaneously to see how flux is removed or destroyed. That is, subarcsecond imaging simultaneously in visible, ultraviolet, EUV, and X-ray or XUV radiation is required to show the form of the associated fine-scale activity in the chromosphere, transition region, and corona and its role in the flux cancellation seen in the photosphere. The necessary observations of the photospheric magnetic field might be obtained by new high-resolution imaging techniques at the best ground-based sites, or from a magnetograph flown on a high-altitude balloon or in space. The HRTC will supply the necessary high-resolution imaging of the chromosphere (Ly α), transition region (UV/EUV), and corona (XUV/Soft X-ray).

Images of the transition region and corona obtained from rockets, SKYLAB, and the Solar Maximum Mission with spatial resolution in the range 1-10 arcsec, along with photospheric magnetograms and chromospheric images from the ground, have demonstrated that the heating of the corona, transition region, and chromosphere is directly tied to the magnetic field [e.g., see Parker (11)]. In active regions, studies of such data have shown that heating is strongest where the field is most nonpotential, as evidenced by shear in the field across polarity inversion lines [Orrall (12), Webb and Zirin (13), deLoach et al (14), Gary et al (15)]. This suggests that heating is accomplished by some form of current dissipation. In any case, all fields in active regions are strongly inhomogeneous on subarcsecond scales [Moore and Rabin (10), Zwann (9)], so it is likely that the basic character of the heating is hidden below the resolution of present observations. One possibility, proposed by Parker (16a,b,c,d), is that the heating is by microflaring in the fine-scale substructure of the field. Spatially unresolved microflaring has been observed in UV emission from the transition region in active regions [Porter, Toomre, and Gebbie (17a), Porter et al (17b)]. Apparently, simultaneous subarcsecond resolution of the photosphere, chromosphere, transition region, and corona is required to establish how the substructure in the field configurations with large-scale shear in active regions is involved in heating. In quiet regions, heating is concentrated in the magnetic network, the location of chromospheric spicules. It is plausible to suppose that spicules are basically smaller versions of macrospicules, the surge-like eruptions known to be generated in microflares in the small magnetic bipoles that appear as bright points in soft X-ray images of a few arcseconds resolution [Moore et al (18)]. Microflaring in UV emission from the transition region has also been observed in tiny bipoles throughout the network [Porter et al , (19)]. These observations raise the question of the role of microflares and spicules in the heating of the chromosphere, transition region, and corona (16a,b,c,d; 19; 20; 21). It will take subarcsecond resolution in visible or UV light to see the structure of chromospheric spicules and how they are generated. It will take subarcsecond resolution of the HRTC in EUV and XUV or X-ray radiation to see if and how microflares are important for spicule generation and/or coronal heating.

A third question we wish to address with the HRTC is:

(iii) What is the relationship between fine-scale magnetic structures (spicules, bright points, cool loops, etc.) and heating of the quiet transition region and corona?

From; (i) observed structural similarities of the lower transition region ($10^4 < T < 10^5$ K) with the chromosphere, (ii) the failure of coronal back-heating models of the transition region to provide enough plasma for the lower transition region, and (iii) the fine-scale mixture of polarities seen in the magnetic network in quiet regions, one is led to the view that most of the plasma in the 10^4 - 10^5 K temperature range in the quiet solar atmosphere is not

maintained by heat transfer from the corona [Rabin and Moore (22), Dowdy, Rabin, and Moore (23)]. An alternative picture, consistent with the observed fine-scale mixture of polarities in the network, is that most of this plasma is contained in small magnetic loops in the network (4), and is thereby magnetically insulated from coronal back-heating, and therefore must be heated internally (22,23). From a modeling analysis that was prompted by the observation of enhanced emission from the lower transition region at places in active regions where vector magnetograms show nonpotentiality, it has been shown that one attractive candidate for the internal heating of the lower transition region, both in active regions and in quiet regions, is resistive heating by fine-scale electric currents (14,22). It has also been pointed out that magnetograms of quiet regions imply that much of the magnetic flux linking the corona with the transition region constricts (undergoes a reduction in area) by a factor of order 100 in passing down through the transition region (23) (see the cartoon in Frontispiece II). Modeling analyses [Dowdy, Moore, and Wu (24); Dowdy Emslie, and Moore (25); Dowdy (26)] of the effect of such a large constriction on conductive heat flow and on the differential emission measure through the temperature range of the upper transition region (10^5 - 10^6 K) indicate; (i) that the conductive heat loss from the corona may be as much as an order of magnitude less than in previous such models that assume much less constriction, and (ii) that models with the larger constriction demanded by high-resolution magnetograms have too little emission measure in both the upper and lower transition region. This suggests; (i) that substantially less heating is required to sustain the corona than previously thought (because conductive losses are less), and (ii) that the upper transition region is similar to the lower transition region in that most of the solar plasma in the temperature range of the upper transition region is also heated internally rather than by heat transfer from the corona. To test the above ideas, we need to see, at subarcsecond resolution, the magnetic structure of the chromosphere, transition region, and low corona. Along with photospheric magnetograms, this will show directly; (i) the spreading out of the field that reaches up through the transition region into the corona and (ii) whether most of the solar plasma at transition region temperatures is contained in the feet of coronal loops, or instead is contained in small closed loops that are thermally insulated from the corona. The HRTC will have the necessary spatial resolution and spectral range to reveal these structures.

1.1.2 The Structure and Dynamics of Coronal Loops: A major objective of coronal studies is to significantly improve the empirical models of density, composition, structure, and temperature in coronal loops, and to use these improved models to study the energy balance, heating mechanisms and dynamical behavior of loops. The structure, dynamics and energetics of coronal loops have been discussed by a number of authors (27 - 33). Three major questions relating to coronal loops are:

- (i) *What is the nature, magnitude, spatial and temporal profile of the energy input (or inputs) which is required to establish and maintain the thermal structure of quasi-static coronal loops?*
- (ii) *How are the heating profiles related to magnetic structure: specifically, are the regions of most intense heating associated with neutral surfaces? Does the inhibition of conductive energy loss processes by the magnetic configurations of loops have a significant effect on their structure?*
- (iii) *What is the detailed physical structure of coronal loops (i.e. filling factor and density, nature and location of thermal gradients, etc.)?*

With regard to the question of the heating mechanism, there are three main classes of models that are currently being considered, a dynamic flare-type process, wave heating, and DC current dissipation. Each of these mechanisms has observable consequences that can be tested with the HRTC.

In the flare-type heating process the energy input to closed coronal loops is believed to occur in discrete impulsive events, probably related to flares. Micro-flares have been detected in both X-Rays [Lin et al, (34)] and the ultraviolet [Porter et al, (35)]. If such events occur down to very small scales [Parker (16c)] then they could account for the heating of active regions. With the HRTC active region loops can be observed from the transition region to the hottest plasma with sufficient spatial (0.10 arcseconds) and temporal (<1.0 second) resolution to observe micro-flaring directly if it is present. A key feature of the HRTC is that by virtue of the high spectral resolution of its component telescopes it will be able to obtain images of structures containing plasma in a very narrow temperature range. This is crucial for observing the solar corona since the coronal plasma is optically thin, so that a given line-of-sight necessarily traverses many different structures. Without a very fine discrimination in temperature, it is not possible to determine the true limit to the fine-scale structure of active region loops and, consequently, to the

variability of the plasma. This is a major problem with broad-band filtergrams obtained with grazing incidence telescopes such as the SKYLAB S-054 and S-056 instruments. With the HRTC, it will be possible to determine the variability of plasma at a single temperature and, hence, to test critically the micro-flare heating model.

The other possibility for coronal heating is that it is a steady-state process. For this case two general types of models have been proposed, one is that the heating is due to wave dissipation [e.g., Ionson (36), Hollweg (37), Davila (38)], the other is that it is due to the dissipation of DC currents [e.g. Parker (39), Sturrock and Uchida (40), Van Ballegoijen (41)]. Both models are similar in that the ultimate power source is the stressing of coronal magnetic fields by photospheric motions, the key difference is in the time scale of the dominant motions and of the coronal electric currents. Since the basic physics of the two processes are quite different, they predict a different dependence of the heating rate on magnetic field strength and loop length. For example, in the DC model the heating rate is expected to increase with decreasing loop length (40), whereas in the wave picture the heating is expected to be maximum at some loop length that depends on the power spectrum of the photospheric motions and the Alfvén speed in the corona. With the HRTC, it will be possible to resolve active region loops and accurately measure their lengths, to determine the differential emission measure along a loop, and to deduce the total radiative losses of the plasma. This will allow us to obtain the coronal heating rates for loops of various lengths and field strengths. Hence, we will have the necessary data for determining the relation between heating and loop length, thereby testing which of the two heating processes, if either, is supported by observations.

The second major question on active regions that the HRTC will address concerns their structure. For the high temperature coronal plasma, $T > 10^6$ K, it is known that the dominant structure is that of a loop; however, the structure of the transition region is still not known. Observations from SKYLAB [Feldman (42)] and HRTS [Dere et al., (4)] indicate that the transition region does not consist of simply the footpoints of hot coronal loops, as in the standard model, but these data do not have sufficient resolution to determine the structure. Another difficulty with the standard model for the transition region is that observed differential emission measure at these temperatures has long been recognized as being incompatible with the predictions of coronal loop models. Several theoretical models have been proposed to explain this discrepancy. Athay (43) has argued that the transition region emission originates from heated spicule material, Rabin and Moore (22) argue that it is due to plasma heated by very fine scale electric currents, and Antiochos and Noci (44a) argue for "cool loops". The question of transition region structure is important not only for understanding the solar corona but is also of great importance for stellar studies. In particular, one explanation for the observation that very-late type giants do not exhibit coronal properties (the "coronal dividing line") depends critically on whether the solar transition region is indeed due to cool loops [Antiochos, Haisch and Stern (44b)]. From the viewpoint of observations, the main distinguishing feature between the transition region models is that they predict three very distinct morphologies. With the high spatial resolution of the HRTC, it will be possible to prove or disprove all three models. Both spicules and cool loops will be fully resolvable at 0.10 arcseconds. Hence, the HRTC should finally reveal the true structure of the transition region.

For the hot coronal plasma the main outstanding morphological questions are; (a) what is the filling factor of the hot loops, (b) how are they distributed on the solar surface, and (c) what is their relation to the network? The transition region emission, $T \sim 10^5$ K, is well-known to originate from structures that are found predominantly in the chromospheric (supergranular) network. This emission is also known to have a small filling factor. (5) On the other hand the quiet coronal emission $T = 10^6$ K is believed to originate from loop structures that are unrelated to the network and that have a filling factor of order unity. The morphology is not clearly known for the hot $T > 2 \times 10^6$ K active region plasma. There is reason to believe (44a) that this material originates from low-lying loops which should have a small filling factor. In addition, the theories for coronal heating generally predict that magnetic-energy dissipation occurs in thin regions which should have very small filling factors. Hence, there appears to be disagreement between the observed structure of the corona and the predicted structure. There are also discrepancies between the structure observed for the plasma at different temperatures. Better resolved observations with high temperature discrimination are clearly needed. With the HRTC it will be possible to observe at high resolution (0.1") the corona at a variety of temperatures and to determine in detail the dependence of morphology on temperature. The HRTC high spectral resolution observations will be especially important in determining electron density [using diagnostic techniques (45)], from which the filling factor can be inferred. Such results would answer the questions raised above, and would be invaluable for furthering our understanding of both the magnetic structure of active regions and the heating of the corona.

A primary HRTC objective is to define the pre-flare morphology of the vector magnetic fields of active regions in the photosphere and their connectivity with coronal fields, and to follow the evolution of the photospheric fields and see how the coronal fields respond. Specific questions to be addressed are:

- (iv) *Can we identify dynamical processes in coronal loop structures which might be responsible for the preflare brightenings observed at soft x-ray wavelengths? If such phenomena are observed, how are they related to magnetic neutral surfaces and what is their role in the heating of coronal loops?*
- (v) *What is the relationship between the thermal structure of coronal bright points and the magnetic configuration (and possible modes of magnetic dissipation) of the corona?*

The HRTC will be a very powerful tool for the study of the correlation of nonpotential characteristics of the magnetic field with enhanced coronal heating, and the relation between x-ray emission and the morphology of the field. Using various computational models (see paragraph 1.1.3.1) we can extrapolate the measured photospheric field upwards and compare the resulting coronal field models with the field inferred from observed x-ray structures. Vector magnetograph observations show that the photospheric field in active regions exhibits nonpotential characteristics even in regions that do not produce significant flare activity [Hagyard and Rabin (46)]. X-ray images of the corona reveal enhanced emission associated with bipolar regions with strong fields [Walker et al. (6)]. These two observational results suggest a study of the correlation between areas of enhanced x-ray heating and non-potentiality of the underlying magnetic field. Three obvious objectives are: (i) investigating the relation between the intensity of the x-ray emission and the degree of nonpotentiality of the field; (ii) determining the differences between nonpotential field characteristics of regions that exhibit x-ray emission and those that do not; and (iii) looking for differences in the magnetic field in regions with x-ray heating as opposed to regions that flare. Recently, Gary and Moore (47) have drawn attention to a number of sunspots where part of the umbral region is covered by bright plages and have related this phenomenon to the morphology of the magnetic field. It seems that the marked division of plage intensity in the umbrae correlates strongly with the direction of the photospheric field there. The correlation is in the sense that the plage is associated with field lines that rise from the sunspot and fall into areas interior to the active region. The physical explanation is that the enhanced heat generated by magnetic reconnection of the strong fields interior to the active region is conducted along the magnetic field into the umbra. Since there is no equivalent heating source exterior to the active region, where the fields are much weaker, no heat is conducted along the magnetic field coming into the umbra from outside the region. Hence the sharp division of umbral emission in step with the change in direction of the field lines. An obvious extension of this correlation is to investigate this "bifurcation" phenomenon in the x-ray regime.

Investigations relating to dynamical processes and abundance anomalies in coronal loops will benefit from the HRTC spectrograph observations of line profiles. Specific questions to be addressed include:

- (vi) *What is the role of mass transport in coronal loops? Is there evidence for abundance anomalies? Is there evidence for abundance differences between coronal loops and coronal holes?*

1.1.3 Large Scale Coronal Structure and Dynamics: The large scale structure of the corona, is dominated by the solar magnetic field, as the high resolution image of the corona in the light of the emission of Fe IX and Fe X at $\sim 173 \text{ \AA}$ on the cover demonstrates. Multilayer optics have a very great advantage over grazing-incidence optics in the study of large scale coronal structure because normal incidence telescopes can achieve high resolution ($\sim 0.1 - 0.3$ arcsecond) over a field covering the entire solar disk. In contrast, grazing-incidence optics (48) have severe coma over fields exceeding $\sim 1' - 2'$, resulting in degradation of their resolution to many arcseconds at the solar limb for a Wolter I mirror pointed at sun center. We discuss the application of the high resolution spectroheliograph observations, which the HRTC will obtain, to the study of the large scale structure and dynamics of the corona.

1.1.3.1 Large Scale Magnetic Structure: Since it is difficult to measure the coronal magnetic field directly at the present time [see the discussion of coronal magnetic field determination by Walker (49)], it is generally necessary to calculate the coronal field from the boundary conditions provided by the measured vector field in the photosphere, subject to reasonable assumptions and constraints (50). In order to guide these calculations, it is desirable to compare the calculated field structure with observed coronal structures such as loops, filaments, the magnetic network, streamers, etc. Clearly, high resolution images such as the one shown on the cover, covering the full range of temperatures present in the atmosphere, will be a very valuable resource for the study of large scale coronal magnetic structure and dynamics. Using multithermal observations we will address the following question:

- (i) *What is the large scale structure of the coronal field, and how is it restructured by events such as flares and coronal mass ejections (CME's)?*

High-resolution x-ray images provide information on the morphology of the coronal field but little quantitative data can be derived from these observations. Generally, the quantitative information is derived by extrapolating upwards the measured photospheric field and comparing the computed coronal field morphology with the x-ray observations. The extrapolations can be done assuming either potential or force-free configurations for the field. The single line-of-sight component of the field is sufficient for the potential calculation and for the "constant - alpha" force-free case, but only if the region is observed near disk center. To extrapolate the field under the generalized force-free assumption and to correctly extrapolate the field for the potential or constant-alpha force-free cases for off-disk center regions, all three components of the magnetic field must be known. At MSFC, for example, the observational program with the solar vector magnetograph is supported and enhanced by a number of numerical and theoretical models and computer codes to extrapolate the photospheric field up into the corona. The three-dimensional configuration of the magnetic field above active regions can be analyzed using any of five computational approaches: (i) the Schmidt potential calculation (51), ii) the Teuber potential method (52), iii) the Nakagawa-Raadu-Welck linear force-free calculation (53), iv) Alissandrakis' linear force-free method (54), and v) Wu's nonlinear force-free calculation (55). In collaboration with Pridmore-Brown MSFC scientists are developing a second method for the nonlinear force-free problem, a variational Galerkin technique (56). To correct for off-disk center effects, MSFC scientists have developed computer programs to transform the measured vector magnetic field and image-plane coordinates into heliographic coordinates. The HRTC images will greatly enhance this type of analysis.

1.1.3.2: Coronal Dynamics: Over the past decade, accumulating knowledge shows that the sun's corona is a dynamical, interwoven, magnetic structure with rapid energy releases occurring through its volume, producing mass eruptions and million-degree temperature plasma. Coronal holes undergo continuous evolution which releases high speed solar wind flows into heliospheric space. It is evident from theoretical studies that the dynamical behavior of the corona is caused by the deformation of the magnetic field due to convective motion at the photosphere. The precise nature of these magnetic deformations and the resulting MHD waves is crucial to the understanding of the physics of these dynamical activities. These activities are also responsible for the general phenomena of solar and stellar x-ray emissions, winds, flares, and eruptive mass ejections. In order to meet the challenge of the understanding of physical processes involved in these observational phenomena, S.T. Wu has developed a number of time-dependent, multi-dimensional, non-linear magnetohydrodynamic (MHD) numerical models. These models can be formulated in either Cartesian, cylindrical or spherical coordinate allowing the analysis of observed phenomena in various geometries, and have been successfully applied to the study of a number of solar phenomena. For example, Wu and his collaborators have investigated photospheric shear motions in active regions. This work has improved the understanding of the mechanism for the storage of energy in the sheared magnetic field [Wu, et al., (57a, b)] and of the energy releases associated with eruptive phenomena [Wu, et al., (58)]. Wu et al. (59) have also studied photospheric converging and diverging motion in reference to the neutral line to understand the emerging and submerging magnetic flux. We plan to extend these studies of coronal dynamics using HRTC data, and to study large scale coronal heating and solar wind acceleration by searching for evidence of MHD waves propagation through the photosphere and chromosphere. The HRTC spectroscopic observations of line profiles will be important for this last objective.

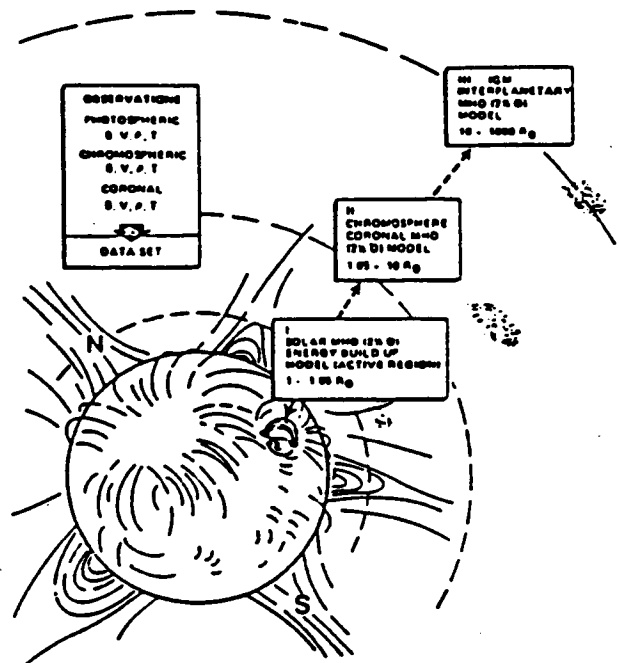
Since the discovery of coronal mass ejections (CMEs) by the coronagraphs on board the SKYLAB and SOLWIND P-78 experiments, CME's have been recognized as a major coronal phenomena; their study is essential for the understanding of coronal physics. Many fundamental questions pertaining to the initiation, acceleration and propulsion mechanisms of CMEs remain to be resolved. One main reason these fundamental questions have not been resolved is that there are no direct observations which follow ejected material from the sun's surface up through the corona with a single instrument. During the SKYLAB and SMM eras, attempts were made to carry out coordinated campaigns by using multiple instruments, however there were always key observational parameters missing. The HRTC instrument has the capability to observe CMEs from the sun's surface up through the corona. Because of this unique capability, we can address directly the following questions related to CME's:

- (ii) *What mechanisms are responsible for the initiation, acceleration and propulsion of CMEs?*
- (iii) *What are the manifestations of CME's in the corona and solar wind and their associations and correlations with solar and interplanetary events?*

- (iv) What is the role of the CMEs in entrained magnetic fields?
- (v) What is the role of CME's in the evolution of coronal holes?

For the study of coronal transients in general and CMEs in particular, a number of authors have investigated the coronal dynamical response due to a pressure pulse which models observed flaring density and temperature profiles; the calculated coronal responses do resemble observed features of coronal transients (c.f. CMEs) [Nakagawa et al (60, 61); Dryer et al.(62); Steinolfson, et al.(63); Sime and Hundhausen, (64); Wu et al., (56; 66; 67)]. A schematic description of these models in relation to their physical regions of applicability is shown in Figure 1. Employing these models as a diagnostic tool to study the physical mechanisms involved in the phenomena observed by HRTC will allow observed parameters to be used as a guide to refine the physical models.

Figure 1 Schematic representation of physical region where various models apply.



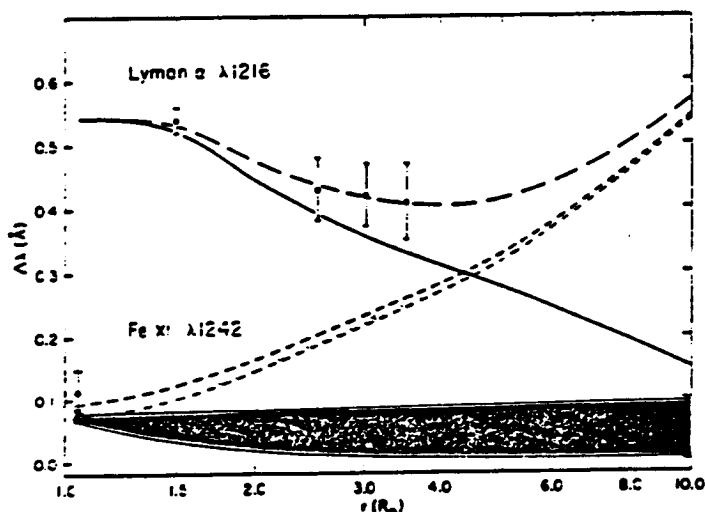
1.1.3.3 Prominences and Filaments: In both active regions and quiet regions, magnetic neutral lines across which there is strong magnetic shear are often marked by filaments (traditionally observed in absorption on the disk in lines such as H- α) of chromospheric material suspended in the low corona by the sheared field (68). The same structures can be observed as prominences in emission on the limb both in H α , and in high resolution XUV images (6,69). There is a close association between filaments and the eruption of flares in nearby active region loops (49); the filament serves as a field tracer showing that the sheared field in and around the filament erupts explosively in the impulsive phase of a flare. Quiet-region filaments mark neutral lines between opposite-polarity remnants of decayed active regions. These filaments often erupt at the onset of a two-ribbon flare and are ejected from the Sun at the core of a coronal mass ejection. Hence, it is of great interest in connection with flares and coronal mass ejections to determine the magnetic field configuration in and around quiet-region filaments, how this configuration forms and evolves, and how it changes when the sheared field holding the filament erupts. The interface between filaments, which are embedded in the corona, and hot transition region and coronal gas is also a subject of considerable interest. The filament channels that are seen in the cover image, appear to be due in at least part to absorption (6); however, suppression of coronal emission by the magnetic structure of the filament may be important as well. Among the questions involving filaments and prominences which can be effectively addressed by HRTC observations are:

- (vi) Does the field configuration in and around quiet-region filaments have a different topology than that of active-region filaments?
- (vii) Are quiet-region filament eruptions basically flares; i.e., are they just slow versions of mass-ejection flares in active regions?
- (viii) Is flux cancellation at the photospheric neutral line an important process in forming the magnetic field configuration of quiet-region filaments?

1.1.3.4 Streamers and Plumes: In coronal holes, the loss of energy and mass to the solar wind becomes an important element in the energy balance of the atmosphere. Withbroe (70) has discussed the structure and dynamics of coronal holes, and the need for high resolution observations to address questions relative to the acceleration and

heating of the solar wind. Figure 2 (70) illustrates the strong dependence of line width in the solar wind on the nature of the heating mechanisms which operate in the solar wind. The HRTC spectroscopic observations will allow line profiles to be studied in polar plumes and streamers. Since bright points are observed near the base of polar plumes, it has been suggested (71) that bright points may be the source of polar plumes and streamers. To address these fundamental questions on the nature of the solar wind/corona interface, we will require observations which combine high spatial resolution, high sensitivity, high spectral resolution (to observe line profiles), and good thermal discrimination. The cover illustrates the power of multilayer telescopes, such as those under study for HRTC, for the study of the solar wind/corona interface.

Figure 2: Spectral line widths plotted as a function of distance from Sun-center. The solid curve is for Lyman- α widths calculated for a simple two-fluid model without any Alfvén wave flux; the dashed line is for a model with Alfvén wave flux added to account more satisfactorily for the empirical Lyman- α widths measured (points) in a polar region where a coronal hole was located. From the results of the two-fluid model calculations one can estimate the behavior of a line from a heavy ion (e.g., Fe XII λ 1242). The figure shows how the width of this line would vary in a model with Alfvén waves present (the narrow cross-hatched region) and without Alfvén waves (the nearly horizontal cross-hatched area, which reflects uncertainties in the amount of electron/Fe XII and proton/Fe XII coupling). The empirical Fe XII width (point near $r = R_0$) is typical of measurements made in quiet coronal regions. Similar behavior is expected for XUV lines such as Fe XII λ 192 Å. HRTC will obtain line profiles for both Fe XII λ 192 and λ 1242.



A fundamental question related to streamers and plumes that can be addressed by the HRTC is:

- (ix) *What is the thermal and density structure of coronal streamers and polar plumes, and what is their relationship to coronal bright points? What is their contribution to the solar wind?*

1.1.3.5 Coronal Holes and the Solar Wind: Observations of the evolution of the boundaries of coronal holes are especially pertinent to the large-scale reconfiguration of the corona. X-ray images reveal the actual structures forming a hole boundary. Observations of transition region lines such as He II (λ 256 or 304 Å) reveal the boundaries of coronal holes in the transition region. Coronal holes have been established as the sources of high speed wind streams; the polar plumes observed in the polar coronal holes in white light images are thought to represent the flow of material into the solar wind.

The scientific goals of the HRTC related to Coronal Holes and the Solar Wind are: (i) *to explore the thermodynamic structure of the corona;* (ii) *to relate the structure and evolution of the corona observed in the EUV wavelengths to the global density structure;* (iii) *to investigate the regions in which the solar wind originates and is accelerated;* (iv) *to extend the knowledge of the solar corona to the interpretation of integrated flux measurements of stellar coronae;* (v) *to investigate the influence of the total coronal flux on the earth and its plasma environment.* A general discussion of the solar wind can be found in Pneuman and Orrall (72a).

Thermodynamic Structure: The design of the HRTC allows it to be sensitive to lines and to line multiplets arising in plasmas over a range of temperatures between about 10^4 K and 5×10^7 K. As a result, the global distribution of emission measure observed can be used to infer the temperature in a variety of coronal and chromospheric structures in a variety of conditions. The high resolution of the instrument coupled with its wide field of view will thus allow small scale structures to be studied in the context of their wider surroundings and the global organization of the corona. In particular, the relationship of small structures, at a variety of temperatures, to the global density structure will allow constraints to be developed on the physical processes by which the large scale

structure can be supported. High temperature lines are available which will be used to identify flares and other active phenomena. This will permit investigation of the relationship of these phenomena to the global coronal structure along with their influence on the organization of the corona and the solar wind and its heating. A specific example will be the investigation of any temperature signature in the corona associated with mass ejections which might reveal compact regions of heating before, during or after the eruptions.

Coronal Structure and Evolution : The temporal resolution of the HRTC will allow the evolution of the coronal temperature distributions to be followed, both on the long time scale (weeks to years) associated with the gradual evolution of the corona, and also on the rapid scales (minutes and tens of minutes) associated with flares, with prominence eruptions, and with mass ejections. This will provide information on the durations over which energy build up and dissipation occur for a variety of scale sizes and will indicate the time scales over which various physical processes are important.

Of particular interest will be the identification of the features on the solar disc which can reveal the development and eruption of mass ejections. This will allow the inference of imminent interplanetary disruptions in the vicinity of the earth, and will be an important step to overcoming the current restriction with conventional coronagraphs that coronal activity can only be observed above the limb. As a result, we can reasonably expect to understand more clearly the signature of such mass ejections in the interplanetary medium. This will in turn provide stronger constraints on the mechanisms by which mass ejections are formed and the physics of their propagation through the interplanetary medium. Further, by establishing a history of disc structures as they rotate towards the limb, we will have a knowledge of the development of any structure which does develop to become a mass ejection at the limb. This too will serve to place valuable constraints on candidate mechanisms for CME production.

The interaction of the long evolutionary scale and the short impulsive activity time scale in the corona will be studied with special interest. The details of this interaction should reveal whether mass ejections cause or result from the long term evolution of the coronal density and temperature distributions, or perhaps neither.

Solar Wind: The ability to infer coronal temperature in a variety of coronal structures, such as streamers and polar plumes, will permit us to investigate the physical properties of the regions in which the solar wind originates (72a) and is accelerated (72b). A specific example is in the investigation of the properties of spicules, which can be investigated both as to their global distribution and their detailed structure with HRTC. Knowledge of their distribution and physical properties compared with the relationship to the global organization of the corona should provide information to investigate more fully their role in solar wind generation. Similarly, by providing temperature estimates within coronal holes the observations from HRTC will impose constraints on a number of theories of the heating of the corona and solar wind (72b). Further, the high resolution for the instrument will minimize the effect of uncertain flow tube geometry, a feature which serves to increase uncertainty in the comparison of many theories with observations.

Since SKYLAB, it has been suggested that there may be an x-ray brightness discontinuity inside coronal holes. Some streamline geometries have been theoretically predicted to result in standing, reverse shock waves within 0.5 solar radii of the photosphere (73). This would be most likely to occur in transient coronal holes with large geometrical divergence. The very high sensitivity and dynamic range of the multilayer telescopes in the HRTC baseline design will be well suited to a search for x-rays emitted from the heated plasma downstream of these shocks -- addressing the questions of their existence and conditions of formation.

1.1.4 Flares: Walker (49) has recently reviewed the requirements for multispectral flare observations. The requirements for flare observations at XUV/EUV and soft x-ray wavelengths are summarized by Walker in a series of objectives, related to each of the five phases of the flare event. We review these requirements, and the objectives of the HRTC related to flares studies.

1.1.4.1 The Preflare State: The basic mechanism of a solar flare must involve the storage of energy in the coronal magnetic field [Spicer, Mariska and Boris, (74)]. Such field configurations are generally accepted to be force-free and to contain *in situ* electric currents [Van Hoven et al. (75)]. However, there are few direct measurements of transition region or coronal fields, and there is only indirect evidence for the existence of coronal currents. It is imperative that a knowledge of the development of the coronal magnetic field configurations which precede the impulsive phase of a flare be obtained. We may state this objective as follows:

- (i) *The dynamics and evolution of the coronal magnetic field structures associated with the flare site must be determined in sufficient detail and with sufficient precision to determine the location and magnitude of stored energy, and the location, source, and effect of associated current flows.*

Observations with the MSFC vector magnetograph have shown that, for 4 cases studied so far, flares start above the photosphere at a place where the local photospheric magnetic field has a maximum 'shear' in its azimuth [Hagyard and Smith 76]. By shear, we mean that the direction of the transverse component of the magnetic field is aligned nearly parallel to the magnetic neutral line rather than perpendicular to it as would be the case if the field were in a potential configuration. This coincidence raises some questions that are basic to understanding the flare process. First, how is this sheared configuration generated, how is it connected to the coronal fields where the flare instability occurs, and how do these coronal fields respond as the shear increases? Second, does the flare process begin as the result of a further increase in shear, presumably beyond some "critical" value, and what are the critical parameters in the coronal field? Or does the flare erupt as the result of external perturbation, such as reconnection of the flux, or submergence of flux, all of which can lead to significant changes in coronal topology in response to the formation of current sheets induced by relatively minor changes in the photosphere? Third, does the field relax from a sheared to a more potential configuration as the result of the flare, and where does this relaxation occur?

To address these questions we need a knowledge of the solar magnetic field at all levels of the solar atmosphere. However, reliable measurements can only be obtained in the photosphere and chromosphere. We propose to infer coronal fields from such observations, using the HRTC XUV coronal images (see Sec 1.1.2, p.5).

Knowledge of the physical parameters governing the preflare plasma is critical to an understanding of the conditions which must precede the energy release which signals the impulsive phase of a flare. Many of the questions which are raised by the population of non-thermal particles accelerated during the impulsive phase, such as their source, the anomalous abundances observed, and their energy spectrum [Forman, Ramaty and Zweibel (77)] may depend critically on the configuration of the preflare plasma. We may state, therefore, a second objective:

- (ii) *The preflare dynamics and evolution of the solar plasma in the vicinity of the acceleration region must be observed in sufficient detail to allow the detailed parameters [density, temperature, departure (if any) from thermal equilibrium, composition of the material which is accelerated] to be determined.*

We know from observations of magnetically confined coronal loops [Webb, (78); Withbroe, (79)] that the thermal gradients within these loops must occur on scales smaller than several thousand kilometers (2 - 5 arcseconds as viewed from the earth). In terms of the scientific problem we wish to address, a goal of observations of diagnostic quality (i.e. isolating lines excited over a narrow temperature range), with angular resolution ~ 0.1 arcseconds appears to be justified, and can be attained by the proposed HRTC strawman instruments.

1.1.4.2 Release of the Stored Energy: Kahler et al. (80) have argued that the mechanism which causes the release of the stored flare energy must be due to a rapid change in the currents which generate the magnetic field structure of the preflare region. These currents may be within the volume where particle acceleration occurs, or they may be elsewhere. Kahler et al. further argue that collision-dominated reconnection is the microscopic mechanism by which current energy is dissipated into heat. Spicer, Mariska and Boris (74) suggest that the trigger mechanism may be the non-linear excitation of the ion-acoustic instability, and resulting anomalous dissipation. Assuming that the flare energy is indeed stored *in situ* in coronal loops, we would expect that the occurrence of the flare trigger mechanism will be accompanied by rapid changes in currents within the loop, and rapid heating of the gas confined in the loop. We might expect the gas to manifest non-thermal ionization structure and electron velocity distributions. Thus, measurements of the type discussed above (Objectives i and ii) would appear to be appropriate, however temporal resolution on the order of seconds or less would appear to be necessary to follow the course of the trigger mechanism. The question of the scale on which the trigger mechanism operates has not been satisfactorily resolved theoretically. Estimates as small as 1 km or less have been discussed (74); in most cases trigger mechanism scales are expected to be no larger than 10 - 100 km. Clearly, very high resolution is essential if this aspect of the flare phenomena is to be observed in sufficient detail to allow comparison with theory. We may state the objective related to the flare trigger mechanism as follows.

- (iii) *The expected rapid change in current density that initiates the release of the stored magnetic energy causing the flare, and the anticipated heating and possible non-thermal changes in the plasma, must be observed directly on the appropriate temporal and spatial scales, which appear to be seconds and 100's of kilometers or less.*

Once again, the HRTC can provide the necessary observations.

1.1.4.3 The Impulsive Phase: The rapid variation in emission from small scale structures which characterizes the impulsive phase places the most severe requirements on multispectral observations of this phase of the flare. For example, Canfield and Gayley (81) have shown that the profile of H- α (and of course this applies to Ly α also) is sensitive to alternative models of impulsive phase energy transport, provided sufficiently high spectral ($\lambda/\Delta\lambda \sim 20,000$), temporal (~ 0.05 seconds), and spatial (~ 0.1 arcsecond or 70 km) resolution can be achieved. Similarly, very rapid, (< 0.1 seconds), but quite distinct changes in the plasma which emits the impulsive EUV radiation are predicted by models based on heating by conduction or by non-thermal electron beams [Emslie and Nagai (82)]. In order to observe the evaporation of this material, resolution of at least $\lambda/\Delta\lambda \sim 10^4$ is essential. Spatial scales should be similar to those for the H- α emission. High spectral resolution observations of the prompt soft x-ray emission have proved extremely useful in studying the heating and evaporation of chromospheric plasma to form the hot postflare loop. Electron density and deviations of the electron energy distribution from thermal equilibrium can be deduced from the ratios of satellite lines excited by inner shell excitation and dielectronic recombination [Fawcett et al., Bely-Dubau et al. (83)], provided spectral resolution of $\lambda/\Delta\lambda \sim 10^4$ is achieved. However, the spatial resolution so far obtained is inadequate. There are indications of time structure on scales of $\sim 1 - 5$ seconds, and more rapid changes may be observable on smaller spatial scales. Very rapid motion [Antonucci et al. (84)] has been observed for the x-ray emitting plasma in the impulsive phase, but the scale of these motions has not been resolved. Spatial resolution sufficient to resolve loop structures (~ 0.3 arcseconds) is necessary to understand the heating and evaporation of the hot flare plasma. We may state the objective of the multithermal impulsive phase observations as follows:

- (iv) *The testing of models of the impulsive phase of a flare requires simultaneous multithermal observations in visible, ultraviolet, EUV/XUV, and soft x-ray emission lines and continua, at wavelengths corresponding to several thermal levels in each wavelength regime. Temporal resolution must be at least on a scale of 0.1 second for the EUV/XUV and ultraviolet. Spectral resolution must be sufficient to measure line profiles, and spatial resolution should be at the 100 kilometer level on the sun.*

The HRTC can achieve both the spectral and spatial resolution required.

1.1.4.4 The Gradual Phase: A major question to be addressed in the gradual phase is the nature, duration and location of the gradual energy release mechanism. Determination of the detailed thermal, spatial and dynamical evolution of the soft x-ray emitting plasma in the postflare loop is a key observational goal [Strong et al. (85)]. The presence or absence of non-thermal electrons during this phase is also a major issue. A major objective of the study of the gradual phase is therefore:

- (v) *The flare generated thermal plasma must be observed with sufficiently high spatial (~ 0.3 arcseconds) and spectral resolution to allow a detailed model of its evolution to be constructed. Diagnostic measurements which are sensitive to non-thermal particle distributions are important during this phase.*

The HRTC is especially well suited to obtain the necessary observations, by virtue of the multithermal observations made possible by the combination of grazing incidence and normal incidence Multilayer and SiC Telescopes.

1.1.4.5 Atmospheric Restructuring: It is important to study the restructuring of the atmosphere at wavelengths sensitive to all temperature levels present in the solar atmosphere. Among the phenomena of interest are filaments (H- α or H Ly- α), chromospheric structure (Ly- α , He II, C IV), the transition region (EUV/XUV) and the corona

(soft x-rays). Of special interest are Coronal Mass Ejections (CME's), and large scale hot coronal arches [Hildner et al. (86)]. A serious deficiency in current studies of CME events is the gap between the level at which coronagraph white light images can be obtained ($\sim 1.5 R_{\odot}$ for SMM) and the height to which images of moving x-ray loops and cool filaments can be followed using non-occulted telescopes. In the case of the coronal arches, higher spatial and spectral resolution soft x-ray observations than were possible with the Hard X-Ray Imaging Spectrometer on SMM are required. The high resolution multithermal HRTC images will constitute an ideal data set for the study of these post flare phenomena. Major objectives of the study of postflare atmospheric restructuring are as follows:

- (vi) *The study of the dynamic behavior of CME events, starting in the low corona and continuing to several A.U. above the limb, is an important goal, as is the detailed study of the formation of postflare filaments and arches and the return of the solar transition region, chromosphere, photosphere, and magnetic field structure to their normal state.*

1.1.4.6 Discussion: Observations of flare phenomena clearly require simultaneous high angular resolution observations of the solar magnetic field and the solar plasma covering a broad range of temperature ($10^4 < T < 10^8$ K) or excitation (for non-thermal phenomena). In most cases, high spectral and temporal resolution is also essential. The HRTC will achieve 0.1 arcsecond resolution, and thermal coverage from 10^4 K (H Ly- α) to 5×10^7 (Fe XXVI Ly- α). In addition, the Grating Spectrographs which are part of the HRTC can resolve line profiles, allowing powerful thermal and dynamical diagnostic observations.

REFERENCES

1. R.G. Athay in *Physics of the Sun, Vol II*, P.A. Sturrock, T.E. Holzer, D.M. Mimihalas, R.K. Ulrich, Eds., (D. Reidel; Dordrecht, The Netherlands, 1985), p. 51
2. E.M. Reeves, *Solar Phys.* 46, 53 (1976)
3. Bonnet, R.M., Brunner, E.C., Acton, L.W., Brown, W.A., and Decaudin, M., *Astrophys. J. (Letters)* 237, 247 (1980); Fontenla, J., Reichmann, E.J., and E. Tandberg-Hanssen, *Astrophys. J.*, 329, 464 (1988)
4. Gariel, A.H., in R.-M. Bonnet and Ph. Delache (eds.) *IAU Colloq. No., 36, The Mass and Energy Balance and Hydrodynamics of the Solar Chromosphere and Corona*, Nice, (1976) p. 375; A.H. Gabriel, *Phil. Trans. Roy. Soc. London A* 281, 339 (1976)
- 5a. K.P. Dere, J.-D.F. Bartoe and G.E. Brueckner, *Astrophys. J.* 310, 456 (1986)
- 5b. K.P. Dere, J.-D.F. Bartoe and G.E. Brueckner, *ibid.*, 305, 947 (1986)
- 5c. K.P. Dere, J.-D. Bartoe, G.E. Brueckner, J.W. Cook, and D.G. Socker, *Science*, 238, 1267 (1987)
6. A.B.C. Walker, Jr., T.W. Barbee, Jr., R.B. Hoover, and J.F. Lindblom, *Science* 241, 1781 (1988)
7. Martin, S.F., Livi, S.H.B., and Wang, J., *Aust. J. Phys.*, 38, 855 (1985)
- 8a. Rabin, D., Moore, R., and Hagyard, M.J., *Astrophys. J.*, 287, 404 (1984)
- 8b. Moore, R., and Rabin, D., *Ann. Rev. Astron. Astrophys.*, 23, 239 (1985)
9. Zwann, C., *Ann. Rev. Astron. Astrophys.*, 25, 83 (1987)
- 10a. A.S. Kreiger, G.S. Varana, and L. Van Spegbroeck in *Solar Magnetic Fields*, Ed. R. Howard, IAU Symposium No. 3 (Reidel: Dordrecht, 1971) p. 397.
- 10b. J.M. Davis, L. Golub and A.S. Krieger, *Astrophys. J. (Letters)*, 214, L141 (1977)
- 10c. L. Golub in *The Sun and the Interplanetary Medium*, Royal Society of London (1979)
- 10d. N.O. Weiss, in *Study of the Solar Cycle From Space*, NASA Conf. Publ. 2098, p. 55 (1979)
- 10e. L. Golub, J.W. Harvey, A.S. Krieger, and G. S. Varana, *Solar Phys.*, 53, 79 (1977)
- 10f. K.L. Harvey, J.W. Harvey and S.F. Martin, *Solar Phys.*, 40, 87 (1975)
11. Parker, E.N. 1988, *Astrophys. J.* 330 (474)
12. Orrall, E.Q. (ed.), *Solar Active Regions*, 350 pages, Colorado Associated University Press, Boulder, Colorado (1981)
13. Webb, D., and Zirin, H., *Solar Phys.*, 69, 99 (1981)
14. deLoach, A.C., Hagyard, M.J., Rabin, D., Moore, R.L., Smith, J.B., Jr., West, E.A., and Tandberg-Hanssen, E., 1984, *Solar Phys.*, 91 (235)
15. Gary, G. A. Moore, R. L., Hagyard, M.J., and Haisch, B.M., *Astrophys. J.*, 314, 782 (1987)
- 16a. Parker, E.N., *Astrophys. J.*, 264, 635 (1983)
- 16b. Parker, E.N., *Astrophys. J.*, 264, 642 (1983)
- 16c. Parker, E.N., "The Origins of the Stellar Corona," in *Solar and Stellar Coronal Structure and Dynamics*, ed. R.C. Altrock, National Solar Observatory, Sacramento Peak, Sunspot, New Mexico, in press (1988)
- 16d. Parker, E.N., *Astrophys. J.*, 330, 474 (1988)
- 17a. Porter, J.G., Moore, R.L., Reichmann, E.J., and Fontenla, J.M., *Bull. Am. Astron. Soc.*, 20, 711 (1988)
- 17b. Porter, J.G., Toomre, J., and Gebbie, K.B., *Astrophys. J.*, 283, 879 (1984)
18. Moore, R.L., Tang, F., Bohlin, J.D., and Golub, L., *Astrophys. J.*, 218, 286 (1977)
19. Porter, J.G., Moore, R.L., Reichmann, E.J., Engvold, O., and Harvey, K.L., *Astrophys. J.*, 323, 380 (1987)
20. Rabin, D., and Moore, R.L., *Astrophys. J.*, 241, 394 (1980)
21. Porter, J.G., and Moore, R.L., "Coronal Heating by Microflares," in *Solar and Stellar Coronal Structure and Dynamics*, ed. R.C. Altrock, National Solar Observatory, Sacramento Peak, Sunspot, New Mexico, in press (1988)
- 22a. Rabin, D. and Moore, R.L., *Astrophys. J.* 285, 359 (1984)
- 22b. Dowdy, J.F., Jr., Rabin, D., and Moore, R.L., *Solar Phys.*, 105, 35 (1986)
24. Dowdy, J.F., Jr., Moore, R.L., and Wu, S.T., *Solar Phys.*, 99, 79 (1985)
25. Dowdy, J.F., Jr., Emslie, A.G., and Moore, R.L., *Solar Phys.*, 112, 255 (1987)
26. Dowdy, J.F., Jr., "On the Magnetic Structure and Energy Balance of EUV-emitting Plasma in the Quiet Sun," *Marshall Space Flight Center Science Laboratory Preprint No. 88-119* (Ph.D. dissertation, Physics Department, University of Alabama in Huntsville) (1988)
27. J.F. Vesecky, S.K. Antiochos and J.H. Underwood, *Astrophys. J.* 233, 987 (1979)

28. R. Rosner, W.H. Tucker, and G.S. Vaiana, *Astrophys. J.* 226, 643 (1978)
29. S.K. Antiochos, and K.R. Krall, *Astrophys. J.* 229 788 (1979)
30. M.A. Wrang and E.R. Priest, *Solar Phys.* 69, 257 (1981)
31. C.C. Chang, J.B. Smith, and E. Tandberg-Hanssen, *Solar Phys.* 67 (1981)
32. I.J.D. Craig and A.N. McClymant, *Solar Phys.* 70, 97 (1981)
33. S. Martin, S. Lavi and J. Warg, *R.G. Giovanelli Commemorative Colloquium Part II.* (January 1985)
34. Lin, R.P., Schwartz, R.A., Kane, S.R., Pelling, R.M., and Hurley, K.C., *Astrophys. J.* 283, 421 (1984)
35. Porter, J.G., Moore, R.L., Reicmann, E.J., Engvold, O., and Harvey, K.L., *Astrophys. J.* 323, 380 (1987)
36. Ionson, J.A., *Astrophys. J.* 276, 357 (1984)
37. Hollweg, J.V., *Astrophys. J.* 277, 392 (1984)
38. Davila, J.M., *Astrophys. J.* 317, 514 (1987)
39. Parker, E.N., *Astrophys. J.* 264, 642 (1983)
40. Sturrock, P.A. and Uchida, Y., *Astrophys. J.* 246, 331 (1981)
41. Van Ballegooijen, A.A., *Astrophys. J.* 298, 421 (1985)
42. Feldman, U., *Astrophys. J.* 275, 367 (1983)
43. Athay, R.G., *Astrophys. J.* 287, 412 (1984)
- 44a. Antiochos, S.K. and Noci, G., *Astrophys. J.* 301, 440 (1986)
- 44b. Antiochos, S.K., Haisch, B.M., and Stern, R.A., *Astrophys. J. (Lett.)* 307, L55 (1986)
45. Walker, A.B.C. Jr., *Space Sci. Rev.* 13, 672 (1972); *Space Sci. Instr.* 2, 9 (1972)
46. Hagyard, M.J., and Rabin, D.M., *Adv. Space Res.*, 6 (6), 7 (1986)
47. Gary, G.A., and Moore, R.L., *Bull. Am. Astron. Soc.*, 20 (2), 704 (1988)
48. R.B. Hoover, R.J. Thomas, and J.H. Underwood, *Adv. in Space Sce. & Tech.* 11, p. 150ff (1972)
49. A.B.C. Walker, Jr., to be published in *Solar Phys.* (1988)
50. R.H. Levine and M.D. Altschuler, *Solar Phys.* 36, 345 (1974); Nakagawa, Y., *Space Sci. Rev.* 19, 459 (1976)
51. Schmidt, H.U., in *AAS-NASA Symposium on Physics of Solar Flares*, W.N. Hess (ed.), NASA SP-50, 107 (1964)
52. Teuber, D., Tandberg-Hanssen, E., and Hagyard, M.J., *Solar Phys.*, 53, 97 (1977)
53. Nakagawa, Y., and Raadu, M.A., *Solar Phys.*, 127, 135 (1972)
54. Alissandrakis, C.E., *Astron. Astrophys.*, 100, 197 (1981)
55. Wu, S.T., Chang, H.M., and Hagyard, M.J., in *Measurements of Solar Vector Magnetic Fields*, M.J. Hagyard (ed.), NASA CP-2374, 17 (1985)
56. Pridmore-Brown, D.C., *Aerospace Corp. Report ATR-81 (7813) - I* (1981)
- 57a. Wu, S.T., Wang, S., Dryer, M., Poland, A.I., Sime, D.G., Wolfson, C.J., Orwing, L., and Maxwell, A., "Magnetohydrodynamic Simulation of the Coronal Transient Associated with the Solar Limb Flare of 1980, June 29, 18:21 UT", *Solar Phys.*, 85, 351 (1983)
- 57b. Wu, S.T., Hu, Y.Q., Krall, K., Hagyard, M.J., and Smith, Jr., J.B., "Modeling of Energy Buildup for a Flare-Productive Region", *Solar Phys.*, 90, 117 (1984)
58. Wu, S.T., Bao, J.J., and Wang, J.F., "Numerical Simulation of Flare Energy Build-up and Release Via Joule Dissipation", *Adv. Space Research*, 6, No. 6, 53 (1986)
59. Wu, S.T., Hu, Y.Q., Nakagawa, Y., and Tandberg-Hanssen, E., "Induced Mass and Wave Motions in the Lower Solar Atmosphere. II. Effects of Converging and Diverging Photospheric Motions", *Astrophys. J.*, 306, 751 (1986)
60. Nakagawa, Y., Wu, S.T. and Han, S.M., "Magnetohydrodynamics of Atmospheric Transients I. Basic Results of Two-Dimensional Plane Analyses", *Astrophys. J.*, 219, 314 (1978)
61. Nakagawa, Y., Wu, S.T., and Han, S.M., "Magnetohydrodynamics of Atmospheric Transients III. Basic Results of Nonplane Two-Dimensional Analysis", *Astrophys. J.*, 244, 331 (1981)
62. Dryer, M., Wu, S.T., Steinolfson, R.S., and Wilson, R., "Magnetohydrodynamic Models of Coronal Transients in the Meridional Plane II. Simulation of the Coronal Transient of 1973 August 21", *Astrophys. J.*, 227, 1059 (1979)
63. Steinolfson, R.S., Wu, S.T., Dryer, M., and Tandberg-Hanssen, E., "Magnetohydrodynamic Models of Coronal Transients in the Meridional Plane I. The Effect of the Magnetic Field," *Astrophys. J.*, 225, 259 (1978)

64. Sime, D.G., and A.J. Hundhausen, "The Coronal Mass Ejection of July 6, 1980: A Candidate for Interpretation as a Coronal Shock Wave", *J. Geophys. Res.*, **92**, 1049 (1987)
65. Wu, S.T., Dryer, M., Nakagawa, Y., and Han, S.M., "Magnetohydrodynamics of Atmospheric Transients II. Two-dimensional Numerical Results for a Model Solar Corona", *Astrophys. J.*, **219**, 324 (1978)
66. Wu, S.T., Hu, Y.Q., Nakagawa, Y., and Tandberg-Hanssen, E., "Induced Mass and Wave Motions in the Lower Solar Atmosphere. I. Effects of Shear Motion of Flux Tubes", *Astrophys. J.*, **266**, 866 (1983)
67. Wu, S.T., Song, M.T., and Dryer, M., "Photospheric Shear-Induced Non-Equilibrium and Arch-Filament Eruption/Coronal Mass Ejection", *EOS* **69**, 454, Also, *Astrophys. J.*, (to be submitted, 1988)
68. E. Tandberg-Hanssen, *Solar Prominences*, (D. Reidel; Dordrecht-Holland, 1974)
- 69a. J. Lindblom, A.B.C. Walker, Jr., R.B. Hoover and T.W. Barbee, Jr., "Soft X-Ray/EUV images of the Solar Atmosphere with Normal Incidence Multilayer Optics," to be published in *Proc. SPIE* (1988)
- 69b. J.F. Lindblom, T.W. Barbee, Jr., R.B. Hoover and A.B.C. Walker, Jr., to be submitted to *Nature* (1988)
70. G.L. Withbroe, in *Solar Flares and Coronal Physics Using PIOF as a Research Tool*, E. Tandberg-Hanssen, R.M. Wilson, and H.S. Hudson, Eds. (NASA Conf. Publ. 2421, 1986) p. 221
71. J.D. Bohlin in *Coronal Holes and High Speed Solar Wind Streams*, J. Zirker, Ed., (Colorado Assoc. Univ. Press, Boulder, 1977) p. 27
- 72a. G.W. Pneuman and F.Q. Orrall in *The Physics of the Sun*, Vol. II; P.A. Sturrock, T.E. Holzer, D.M. Mihalos and R.K. Ulrich, Eds. (D. Reidel, Dordrecht, 1986) p. 71.
- 72b. R. Rosner, B.C. Low and T.E. Holzer, *ibid.*, p. 135.
73. S.T. Suess and R.S. Steinolfson, *IOS* **46**, 1011 (1985)
74. D.S. Spicer, J.T. Mariska, and J.P. Boris; in *Physics of the Sun Vol. II*, P.A. Sturrock, T.E. Hoelzer, D.M. Mihalas, and R.K. Ulrich (Eds.) (D. Reidel Publishing Co., Dordrecht, 1986), p. 181
75. G. Van Hoven, in *Solar Flares*, P. Sturrock Ed., (Colorado Associated University Press, Boulder, 1980), p. 17
76. Hagyard, M.J., and Smith, J.B., Jr., *Bull. Am. Astron. Soc.*, **20** (2), 711 (1988)
77. M.S. Forman, K.R. Ramaty and E.G. Zweibel, in *Physics of the Sun, Vol. II*, P.S. Sturrock, D.M. Mihalas and R.K. Ulrich Eds., (D. Reidel, Dordrecht, 1986), p. 249
78. D.F. Webb, *AFGL Tech. Rep. AFGL-TR-83-0126* (1983)
79. G.L. Withbroe, in *Solar Active Regions*, F.Q. Orrall, Ed., (Colorado Associated University Press, Boulder 1980), p. 17
80. Kahler, D. Spicer, Y. Uchida and H. Zirin; in *Solar Flares*, P.A. Sturrock Ed. (Colorado Associated University Press, Boulder, 1981), p. 83
81. R.C. Canfield and K.G. Gayley, in *Rapid Fluctuations in Solar Flares*, B.R. Dennis, L.E. Orwig and A.L. Kiplinger Eds., NASA Conf. Publ. 2449, p. 249 (1987)
82. A.G. Emslie and F. Nagai, *Astrophys. J.* **279**, 896 (1984)
83. B.C. Fawcett, C. Jordan, J.R. Lemen, and K.H.J. Phillips, *Mon. Not. Royal Astron. Soc.* **225** No. 4, 1013, (1987); F. Bely-Debau, J. Debau, P. Faucher and A.H. Gabriel, *Mon. Not. Royal Astron. Soc.*, **198**, 239 (1982)
84. E. Antonucci et al., *Solar Phys.* **78**, 107 (1982); E. Antonucci et al., *Astron. and Astrophys.* **133**, 239 (1984); E. Antonucci, B.R. Dennis, A.H. Gabriel, and G.M. Simnett, *Solar Phys.* **96**, 129 (1985)
85. K.T. Strong et al. in *Energetic Phenomena on the Sun*, M. Kundu and B. Woodgate Eds., NASA Conf. Publ. 2439, p. 5-20 (1986)
86. E. Hildner et al. in *Energetic Phenomena on the Sun*, M. Kundu and B. Woodgate Eds., NASA Conf. Publ. 2439, p. 6-1., (1986)

INTRODUCTION

OBJECTIVES

Teledyne Brown Engineering began this Advanced Solar Observatory (ASO) Accommodations Requirements Study in March 1988 under contract NAS8-37128 with NASA Marshall Flight Center. The contract was under the technical direction of William T. Roberts, PS02.

The objectives of the study were to define the accommodations required to implement ASO on the Space Station, identify areas of concern related to the feasibility of accommodating ASO, develop approaches to deal with the critical issues generated by these concerns, and develop a concept to accommodate ASO on the Space Station.

We began by identifying a baseline ASO concept which incorporated the scientific requirements. A preliminary accommodations analysis was performed, addressing each of the accommodations areas: structural/mechanical, electrical, thermal, command & data handling, pointing/stabilization, safety, contamination, transportation, and operations. The results showed that accommodation would be straight-forward in several areas (electrical power, thermal control, for example), while serious concerns arose in other areas (e.g. data handling & communications, safety). The remainder of the study concentrated on the major areas of concern. We have not explicitly addressed the costs associated with implementing ASO.

OBJECTIVES

- o Define the accommodation requirements of ASO on the Space Station
- o Develop approaches to deal with the critical issues
- o Develop a concept for accommodating ASO on the Space Station

APPROACH

We have taken a systematic approach to the ASO Accommodations Requirements Study. This approach consisted of:

1. Defining the instrument and facility requirements based on the science requirements. These requirements were established with the assistance of a group of solar physicists, in particular Drs. E. Chupp, H. Hudson, & A.B.C. Walker.
2. Develop an initial concept for the ASO facility for use in the accommodations analyses.
3. Identify critical areas through analysis of accommodations for the initial facility concept.
4. Analyze critical area accommodations in detail.
5. Develop accommodation concepts which alleviate the areas of concern.
6. Create an updated ASO concept, including the changes necessary to alleviate concerns, which is feasible to implement on the Space Station.

APPROACH

- o Define instrument and facility requirements
- o Develop ASO facility concept
- o Identify critical areas
- o Perform analyses for critical areas
- o Develop concepts to accommodate ASO
- o Update ASO facility concept

TASK SUMMARY

This chart lists the tasks specified in the contract statement of work. The first two tasks listed define the requirements which the accommodations must satisfy and provide the basis for the remaining tasks. The last four tasks define the accommodations analyses required.

TASK SUMMARY

- o Define instrument accommodation data
- o Define buildup, maintenance, servicing, and upgrade scenarios for ASO facility
- o Assess operational requirements for ASO and develop operational concept
- o Evaluate effect on ASO of Transverse Boom and Dual Keel Space Station concepts
- o Assess pointing requirements of ASO and define a pointing system to satisfy them
- o Assess telemetry, command, and control requirements and develop a concept to meet them

COMPONENTS OF ADVANCED SOLAR OBSERVATORY

The Advanced Solar Observatory is composed of three major facilities: The High Resolution Telescope Cluster (HRTC); the Pinhole Occulter Facility (P/OFF); and the High Energy Facility. Each of these facilities is, in turn, composed of several individual instruments. Accommodation requirements are distinctly different for each facility. These requirements are presented in detail in the appropriate following sections.

COMPONENTS OF ADVANCED SOLAR OBSERVATORY

- o High Resolution Telescope Cluster (HRTC)
- o Pinhole/Occulter Facility (POF)
- o High Energy Facility

CRITICAL AREAS

This chart summarizes the critical areas identified in the course of this study.

Data rate and volume create an accommodation issue for the High Resolution Telescope Cluster. This is basically a result of multiple imaging sensor within the facility. Potential solutions for this concern include: operation tailoring, data compression, on-board recording, and use of photographic film.

The Pinhole/Occulter Facility boom leads to concerns about performance and safety. The boom concept is inherently flexible, but this does not introduce insurmountable problems. The length of P/OF, and the resulting large moment of inertia introduce concerns about the ability of the Payload Pointing System (PPS) to point and stabilize the facility. Our analyses indicate that the performance is adequate and that, in addition, alternatives (such as a stiff cylindrical shell, or an upgraded Spacelab IPS) exist which also can accommodate P/OF. Potential interference with the Space Station or other payloads due to the length of P/OF introduces a safety concern. Redundant safety measures are possible to eliminate this concern. They are described in the appropriate section. There is also the possibility that some experience with a similar boom will have been gained prior to P/OF if the Control and Astrophysics Structures Experiment in Space (CASES) flies on the Shuttle.

The contamination/debris environment is a concern for any sensitive instrument in space. Deployable covers and contamination monitors are among the standard solutions. Viewing into the ram direction is a result of the desire to observe the sun whenever possible. Transparent covers are one possible solution for the x-ray telescopes in the HRTC. Orbital debris does not appear to be a problem, but the evolution of the debris environment bears watching.

Pointing accommodations are driven by the high accuracy/stability requirements of HRTC and the large moment of inertia of P/OF. Image motion compensation can be used to satisfy HRTC. Our analysis indicates that performance of the PPS will be adequate.

CRITICAL AREAS

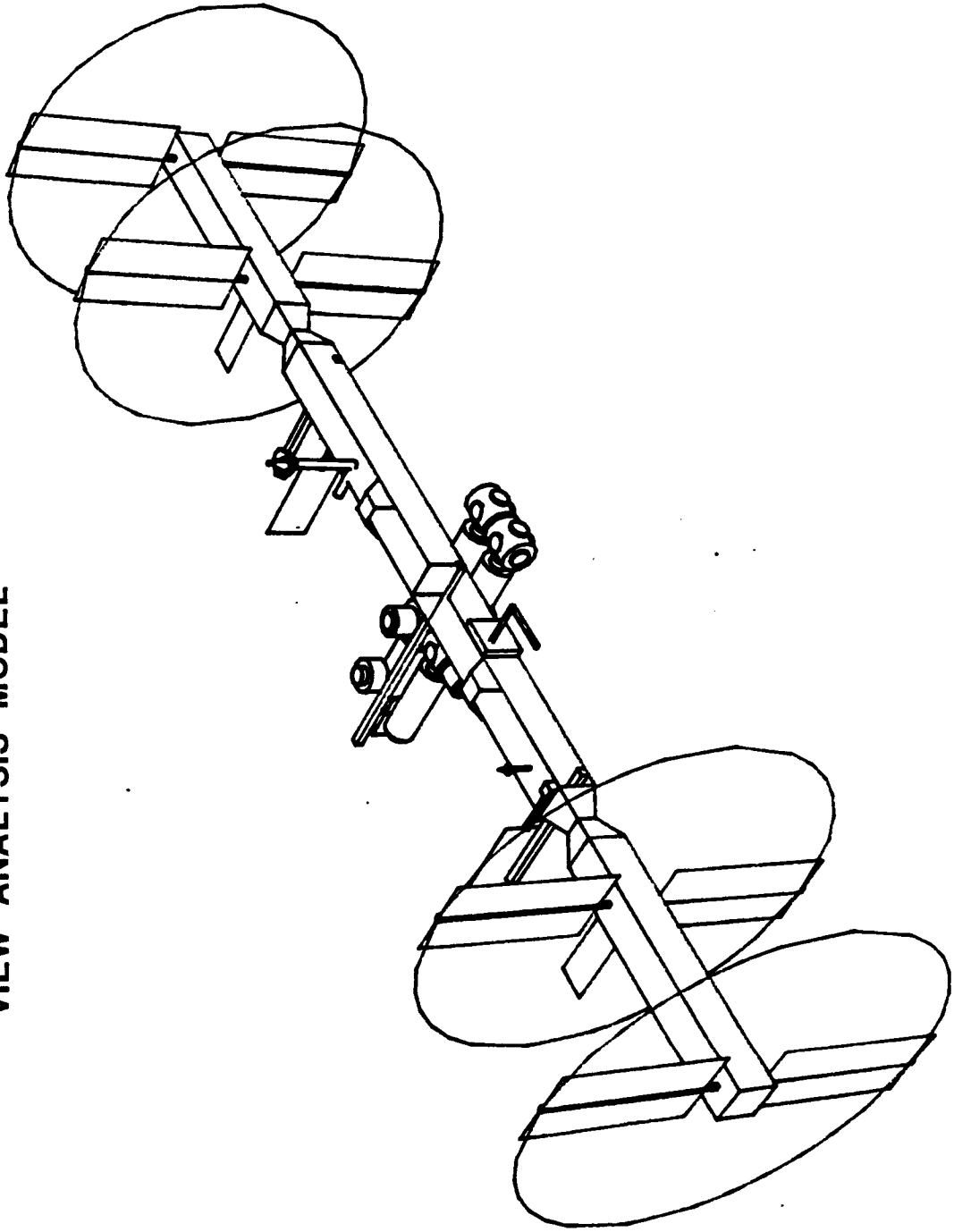
- o HRTC Data Rate and Volume
 - operations
 - data compression
 - on-board recording
 - film
- o P/OF Boom
 - dynamics
 - performance
 - collision avoidance
- o Contamination/Debris Environment
 - contamination protection
 - viewing into ram
 - orbital debris/micrometeoroid damage
- o Pointing
 - accuracy and stability
 - physical accommodations

SPACE STATION VIEW ANALYSIS

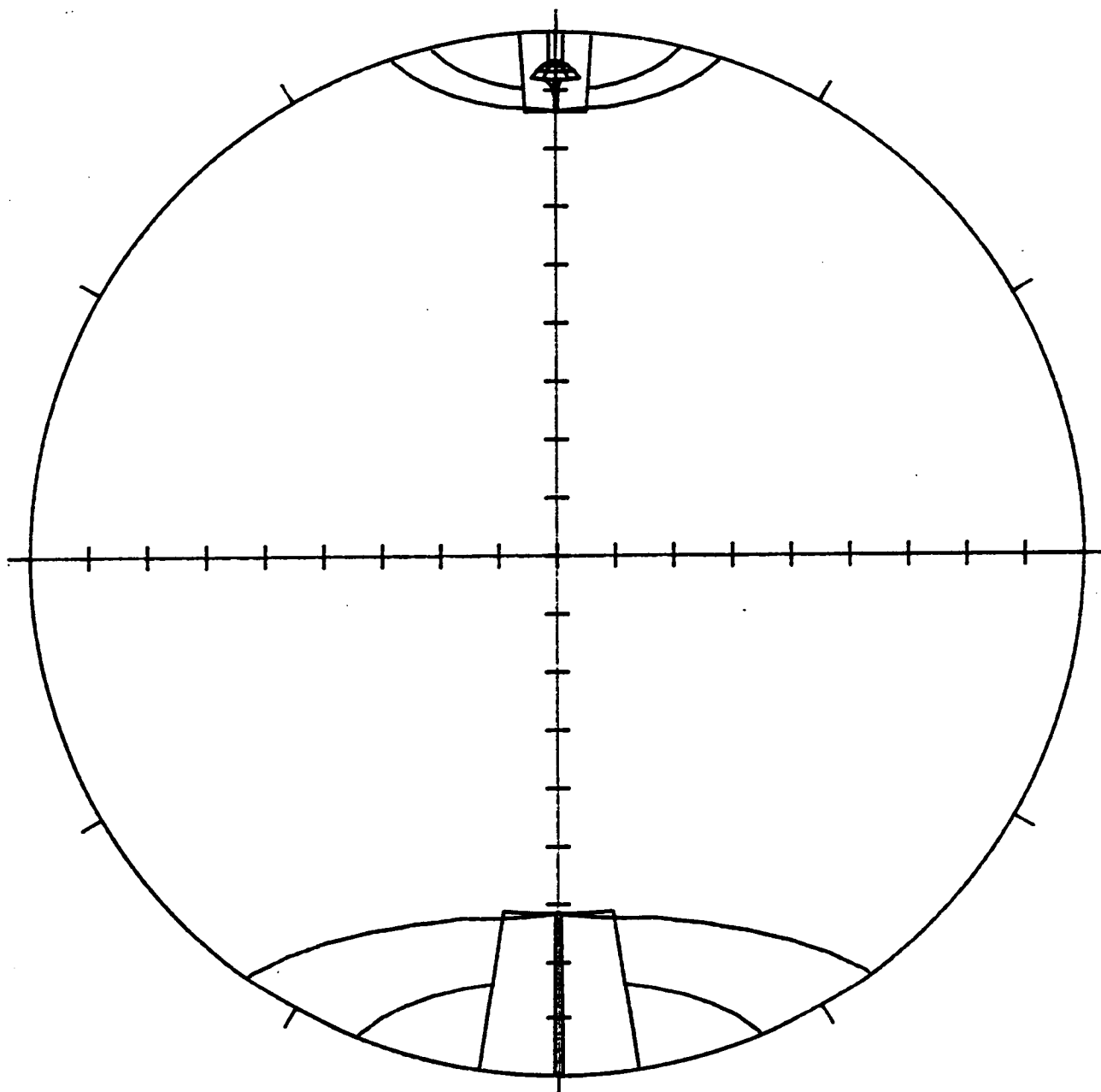
This chart shows a perspective view of the computer model used for the view analyses illustrated on the following four charts.

The following four charts show various views from potential ASO mounting locations. The illustrations are hemispherical ($+90$ degree field of view), fish-eye views from the PPS center of rotation, in the specified view direction. Recognizing that the Space Station solar arrays will be oriented normal to the ASO line of sight during operations, and that the sun remains within 52 degrees of the orbit plane, there is very little (except possibly other payloads) which impinges on the ASO field of view. Tick marks on the vertical and horizontal axes indicate 10 degree intervals. The outer circle is the plane 90 degrees from the line of sight and is divided by tick marks into 30 degree intervals.

SPACE STATION
VIEW ANALYSIS MODEL

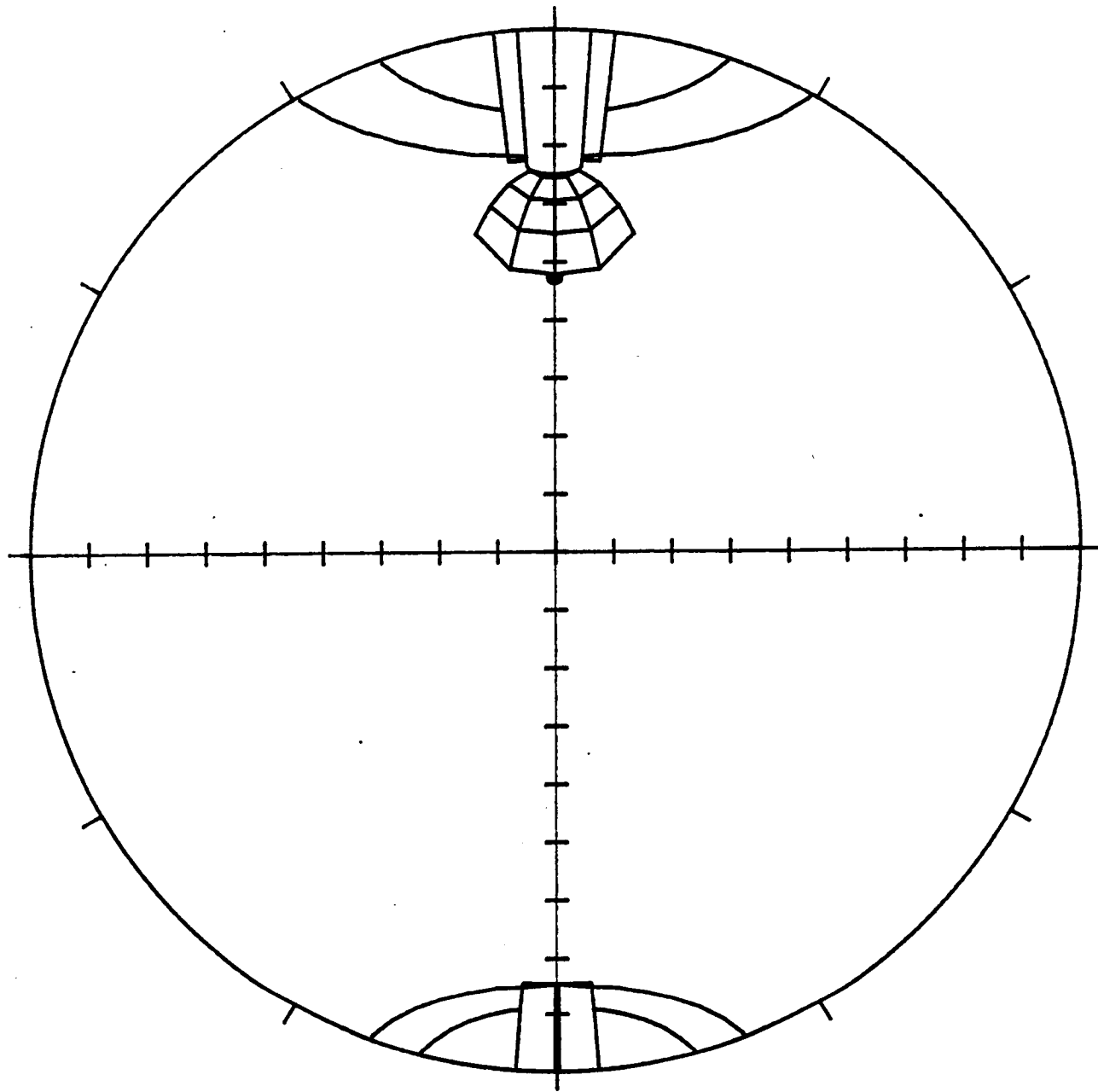


VIEW FROM SPACE STATION



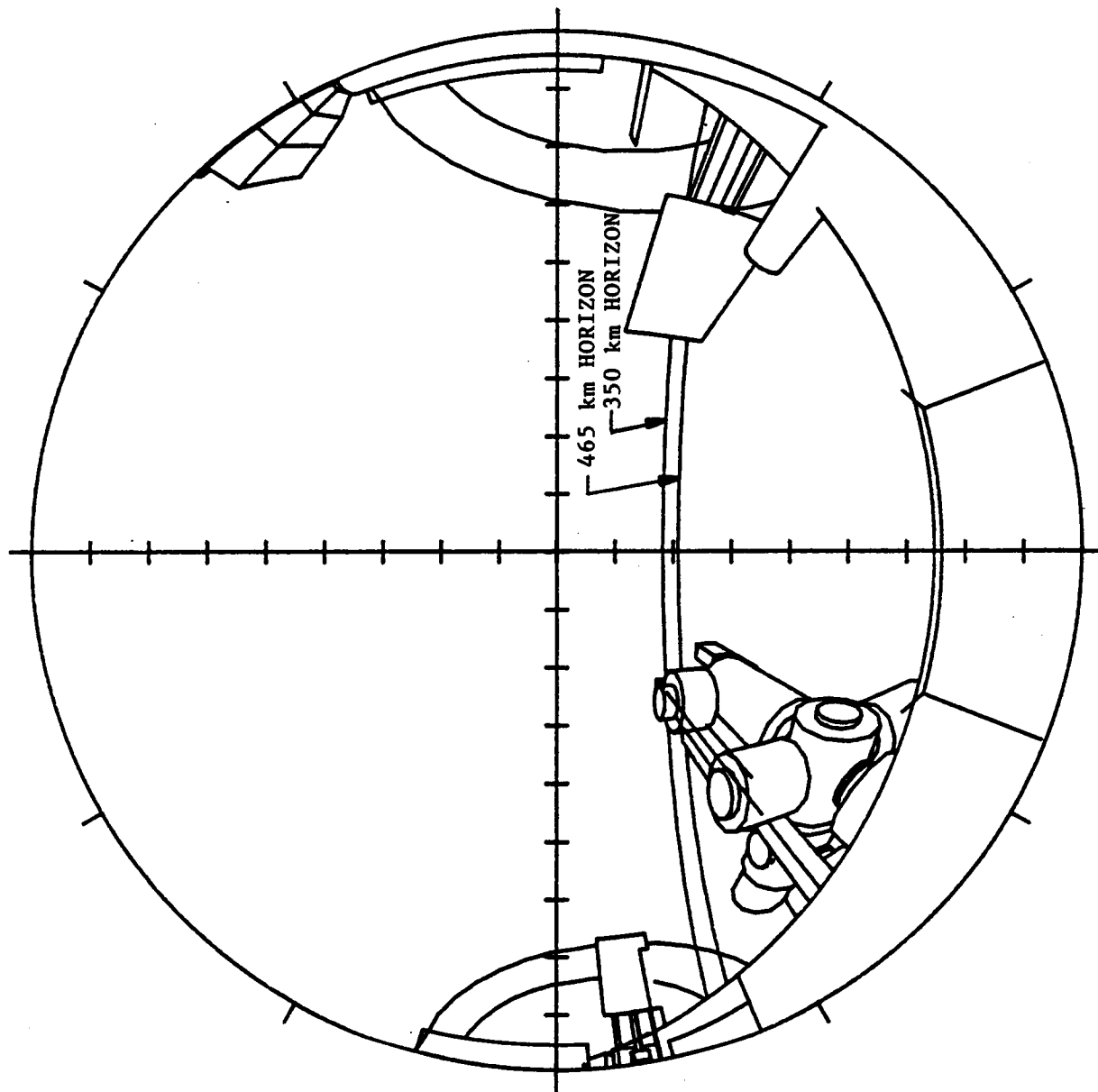
- VIEW POINT
TOP OF TRUSS
PORT SIDE
PPS CENTER OF
ROTATION
- VIEW DIRECTION
UP
- HEMISPHERICAL
FIELD OF VIEW

VIEW FROM SPACE STATION



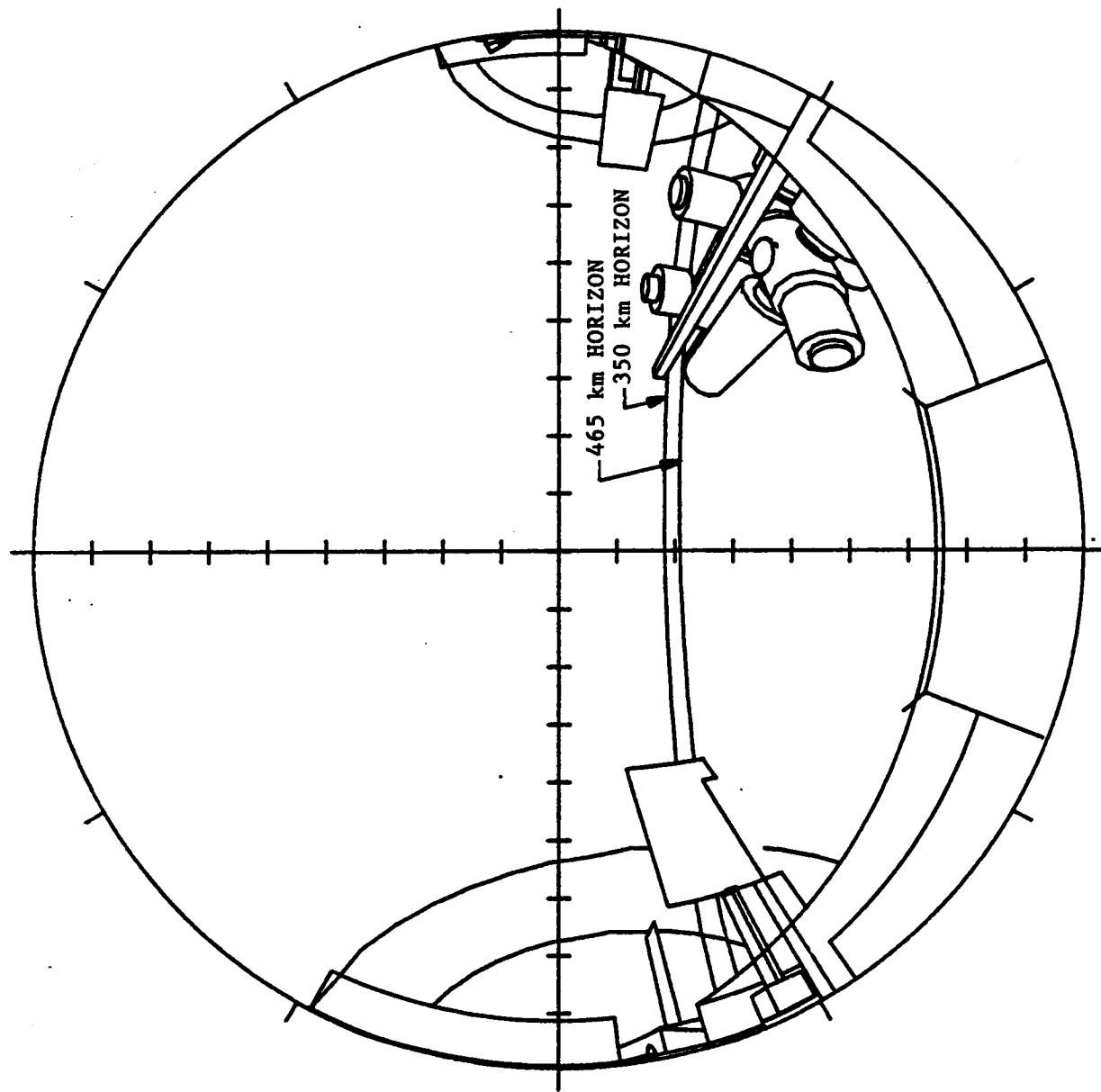
- VIEW POINT
TOP OF TRUSS
STARBOARD SIDE
PPS CENTER OF
ROTATION
- VIEW DIRECTION
UP
- HEMISPHERICAL
FIELD OF VIEW

VIEW FROM SPACE STATION



- VIEW POINT
TOP OF TRUSS
PORT SIDE
PPS CENTER OF ROTATION
- VIEW DIRECTION
AFT
- HEMISPHERICAL FIELD
OF VIEW
- HORIZON INDICATED FOR
465 km AND 350 km
ALTITUDES

VIEW FROM SPACE STATION

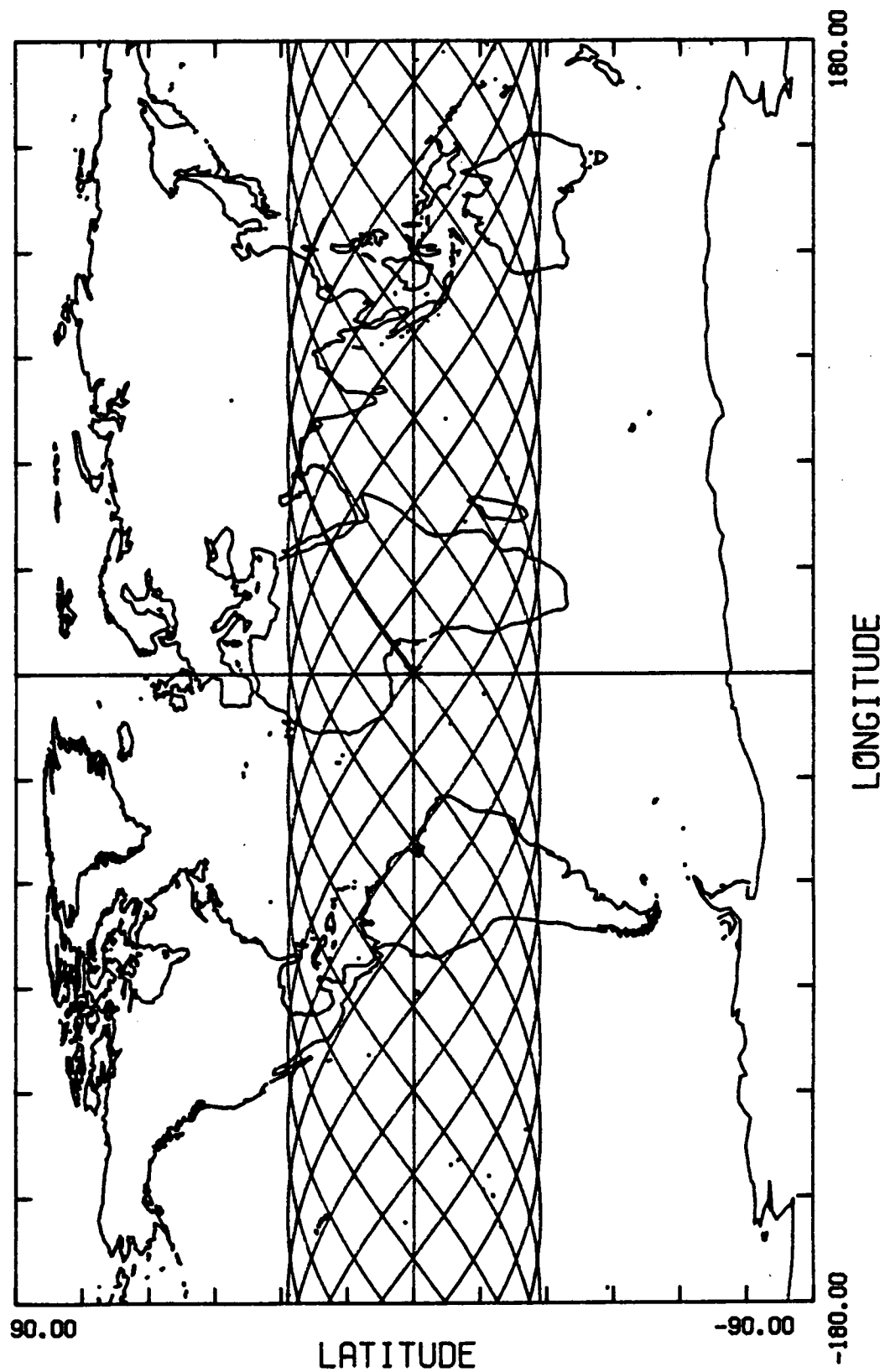


- VIEW POINT
TOP OF TRUSS
STARBOARD SIDE
PPS CENTER OF ROTATION
- VIEW DIRECTION
AFT
- HEMISPHERICAL FIELD
OF VIEW
- HORIZON INDICATED FOR
465 km AND 350 km
ALTITUDES

SPACE STATION GROUND TRACK

This chart shows a typical 24 hour ground track for the Space Station. It is intended primarily for comparison with the following charts of energetic particle flux.

SPACE STATION GROUND TRACK



ENERGETIC PARTICLE FLUX

The following four charts show contour plots of predicted electron and proton fluxes for 465 and 350 km altitude orbits. The shaded area is the range of the Space Station orbit.

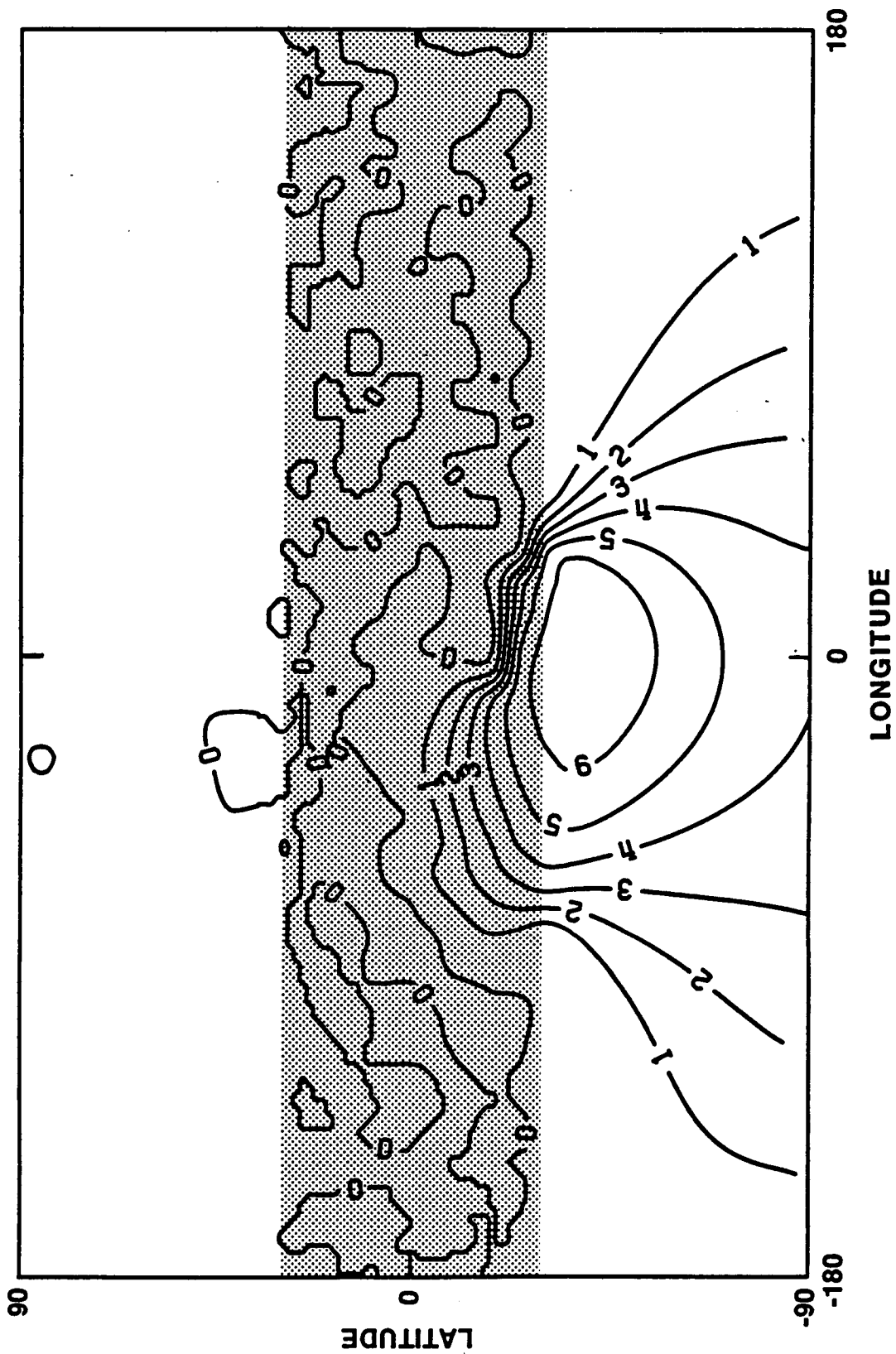
ENERGETIC PARTICLE FLUX

(LOG #/cm **2/sec)

ELECTRONS >0.1 MeV

SOLAR MAXIMUM

465 km



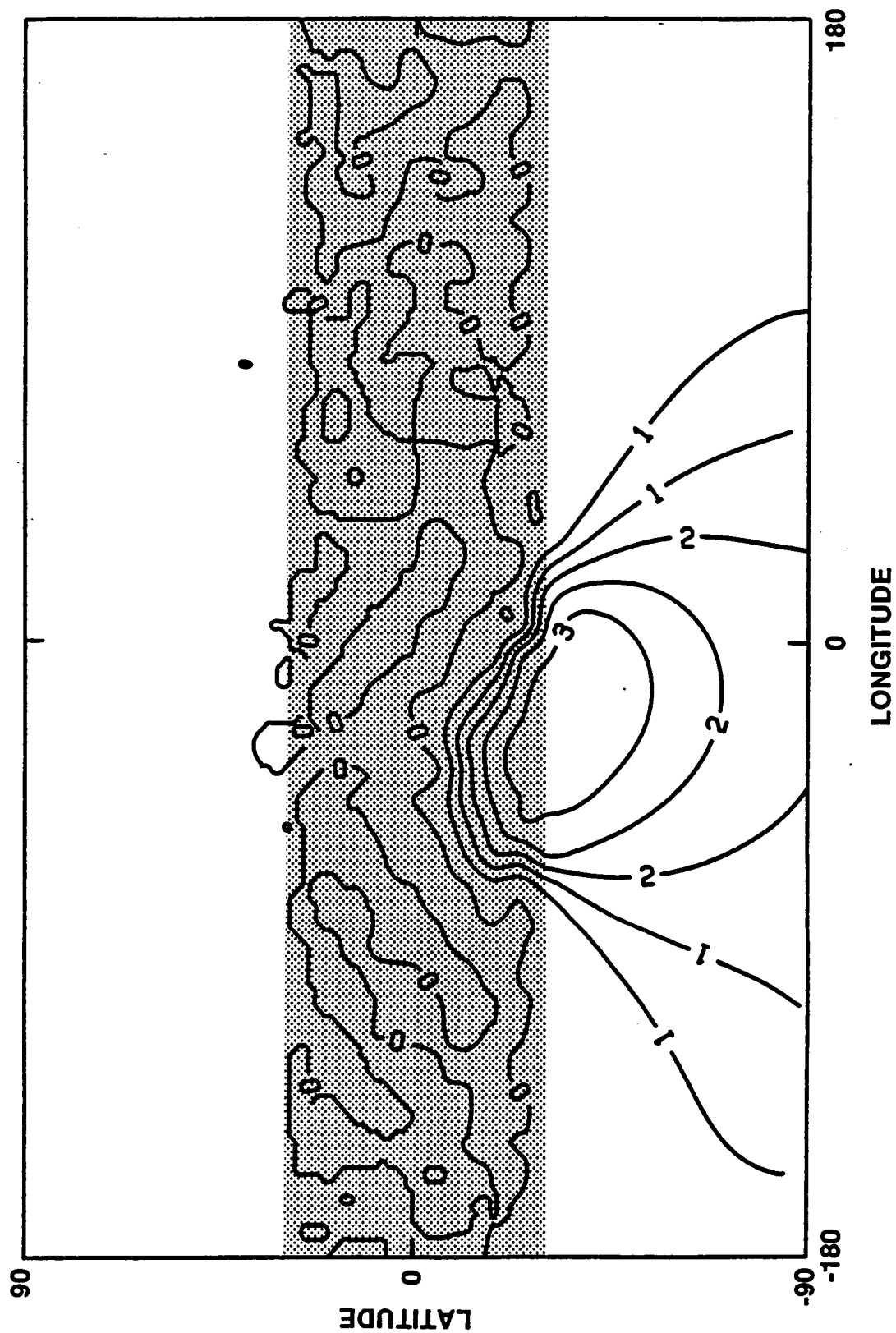
ENERGETIC PARTICLE FLUX

(LOG #/cm **2/sec

PROTONS >2 MeV

SOLAR MAXIMUM

465 km



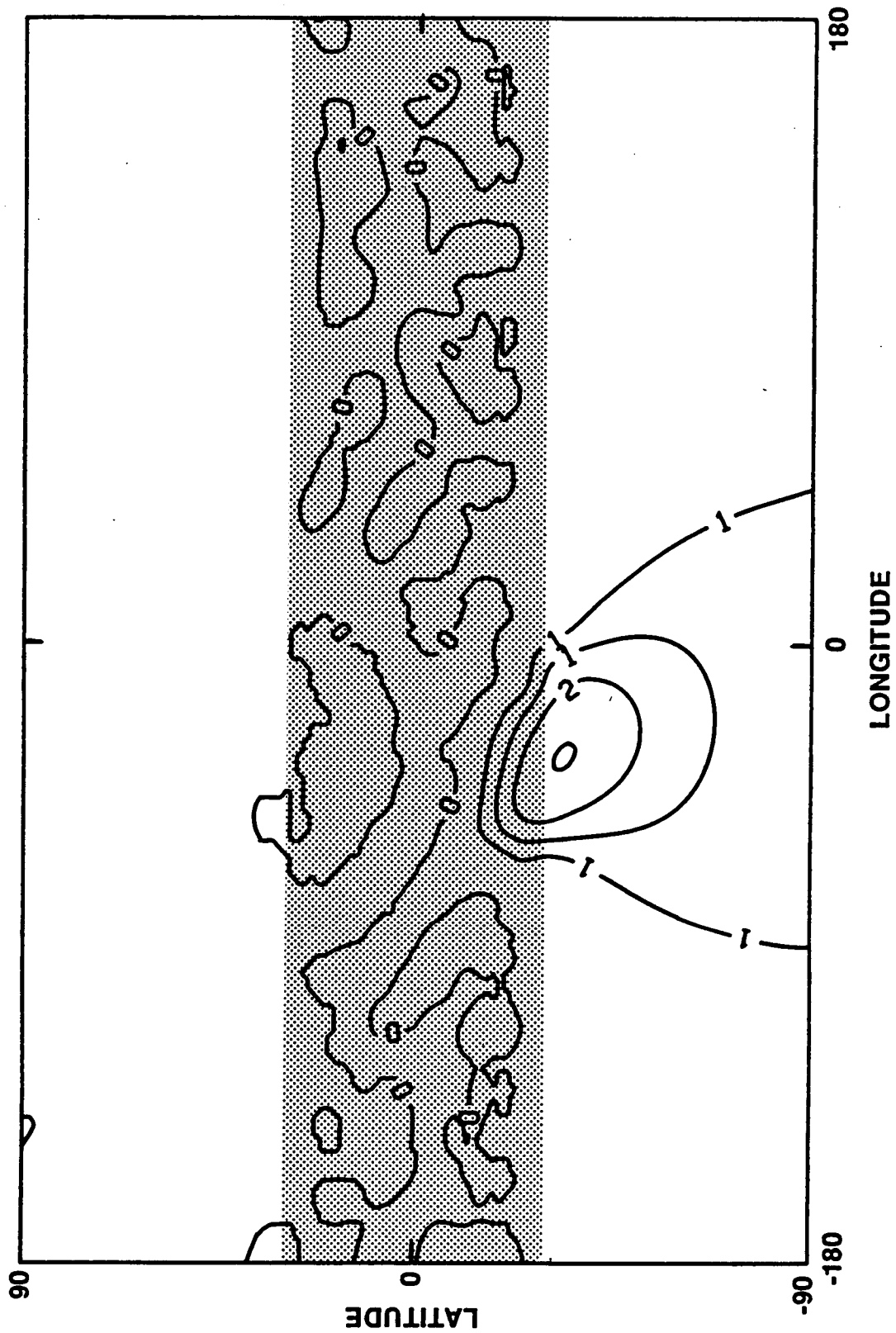
ENERGETIC PARTICLE FLUX

(LOG #/cm **2/sec)

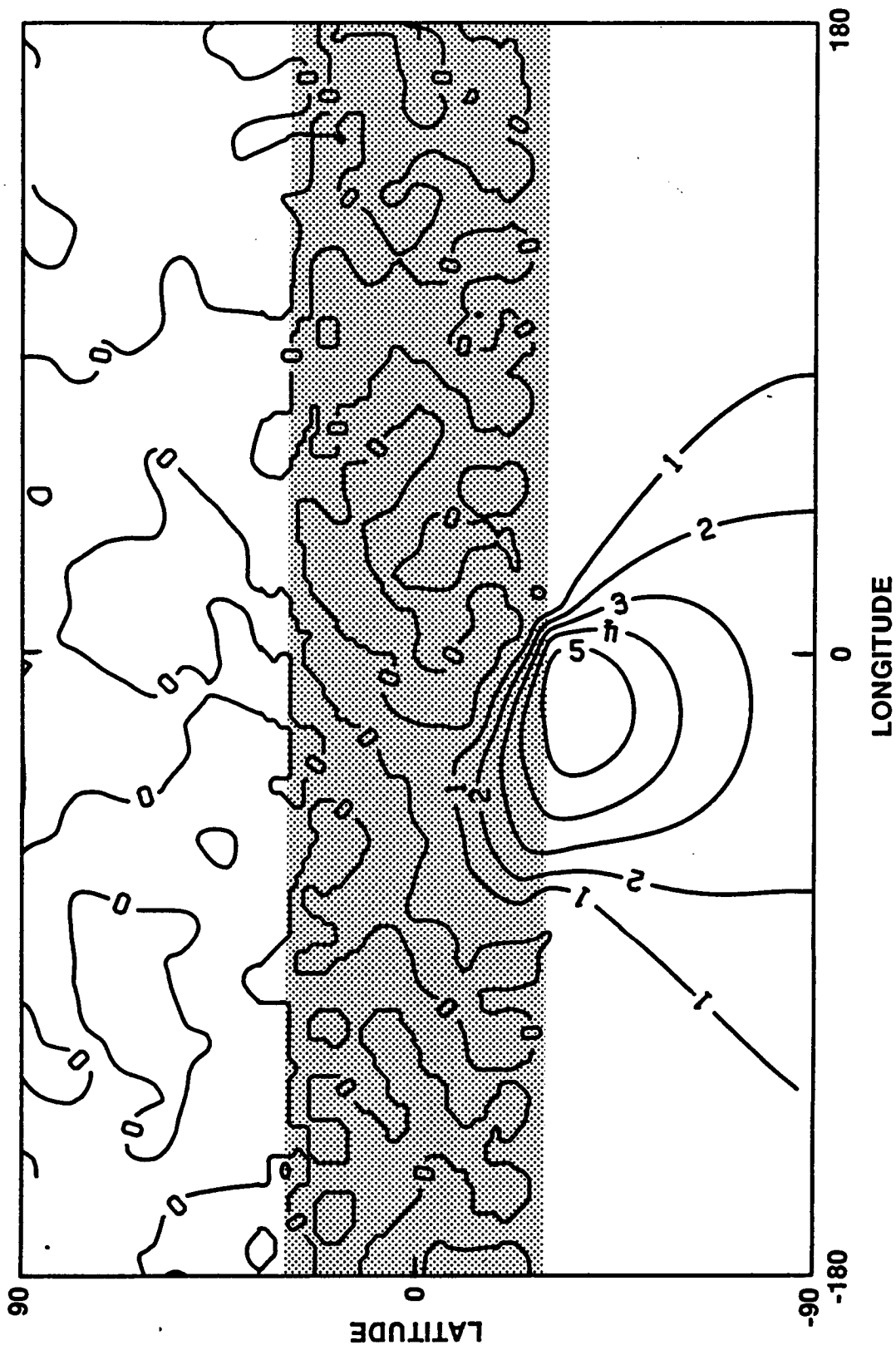
PROTONS >2 MeV

SOLAR MAXIMUM

350 km



ENERGETIC PARTICLE FLUX
 (LOG #/cm **2/sec)
 ELECTRONS >0.1 MeV
 SOLAR MAXIMUM
 350 km

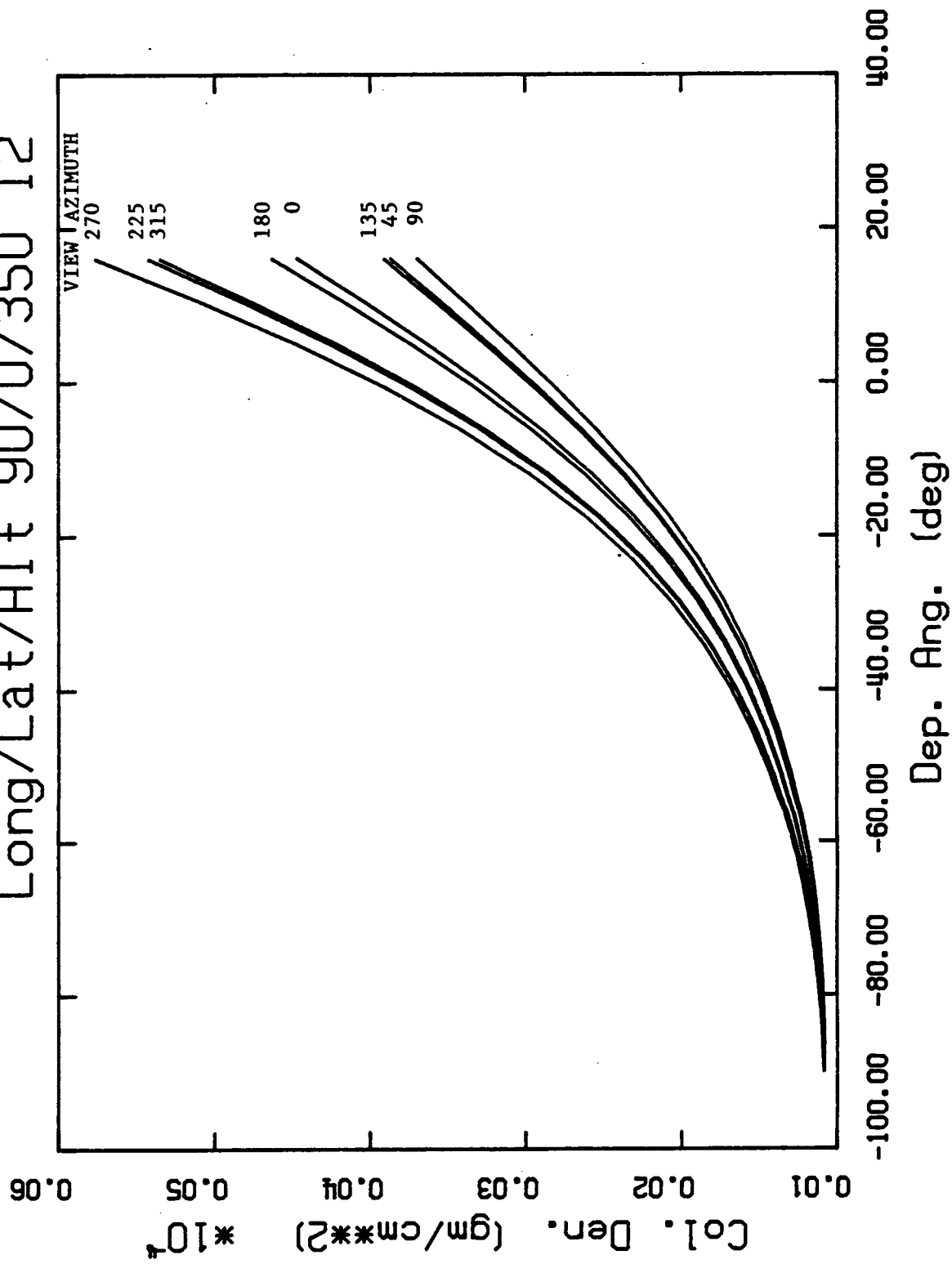


LINE OF SIGHT DENSITY

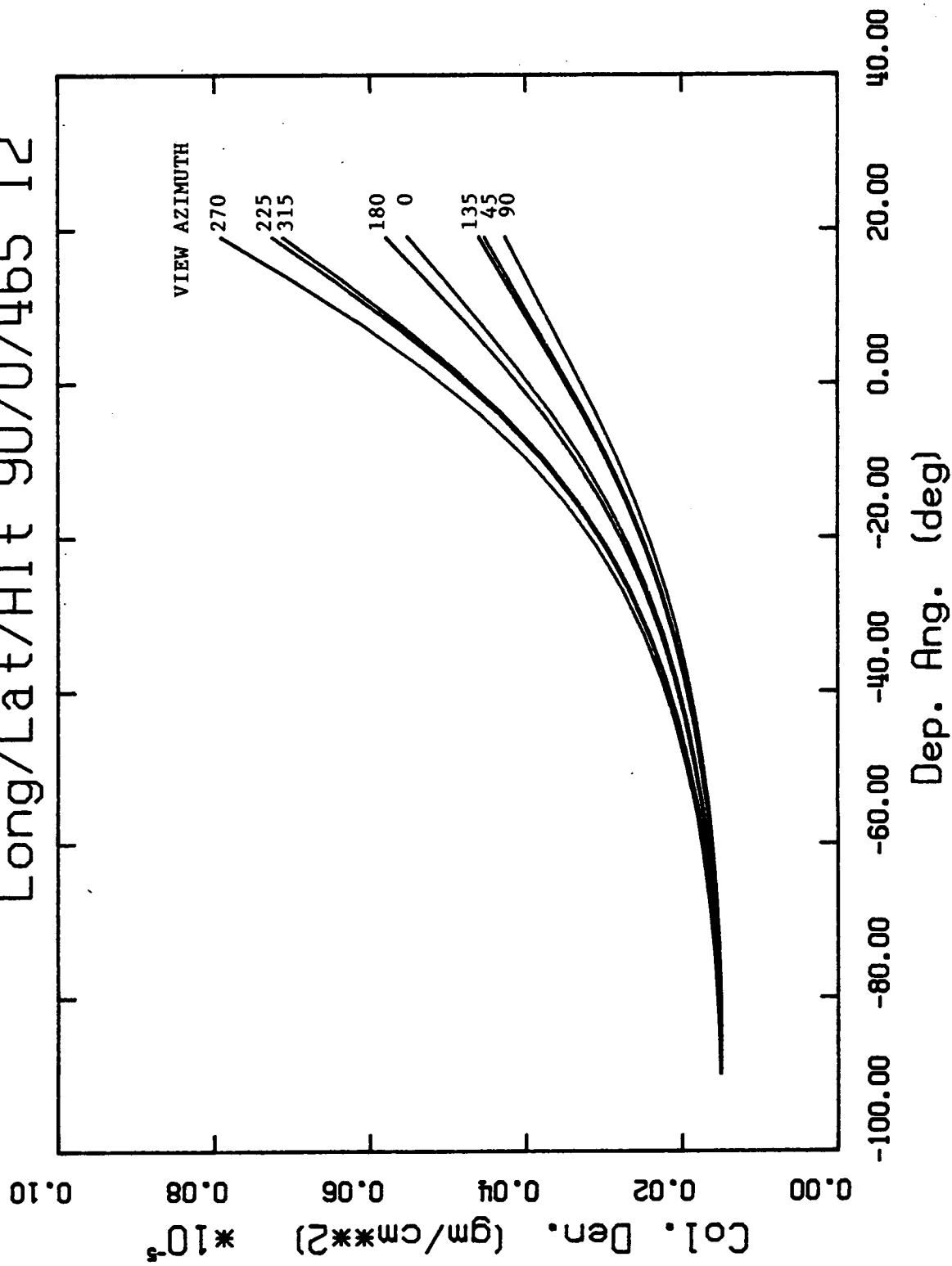
*The next seven charts illustrate the line of sight atmospheric column density for various conditions. All are based on the Marshall Engineering Thermosphere model. The abscissa on these charts is depression angle, measured positive below horizontal. All curves end at the depression angle where the tangent point altitude is 90 km, since this is the lower altitude limit of the model. The second line of the title gives longitude, latitude, altitude, and local time at the Space Station. Various curves represent different viewing azimuths (measured eastward from north). Note that the ordinate scales vary between charts by more than an order of magnitude.

Although the pointing analyses performed during this study assumed that observation of the sun is required from horizon to horizon, these charts may be useful in determining useful observational limits.

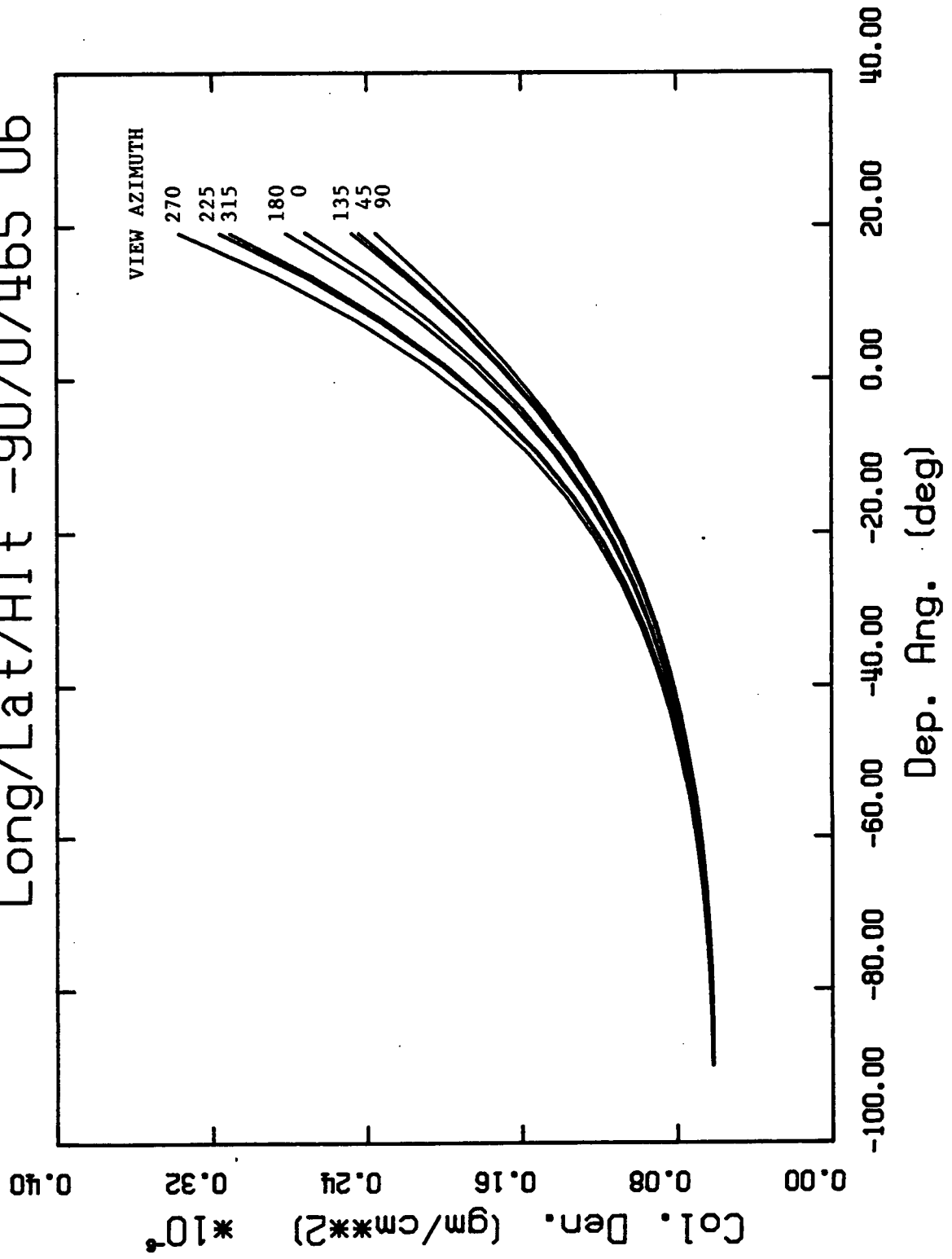
Line of Sight Density
Long/Lat/Alt 90/0/350 12



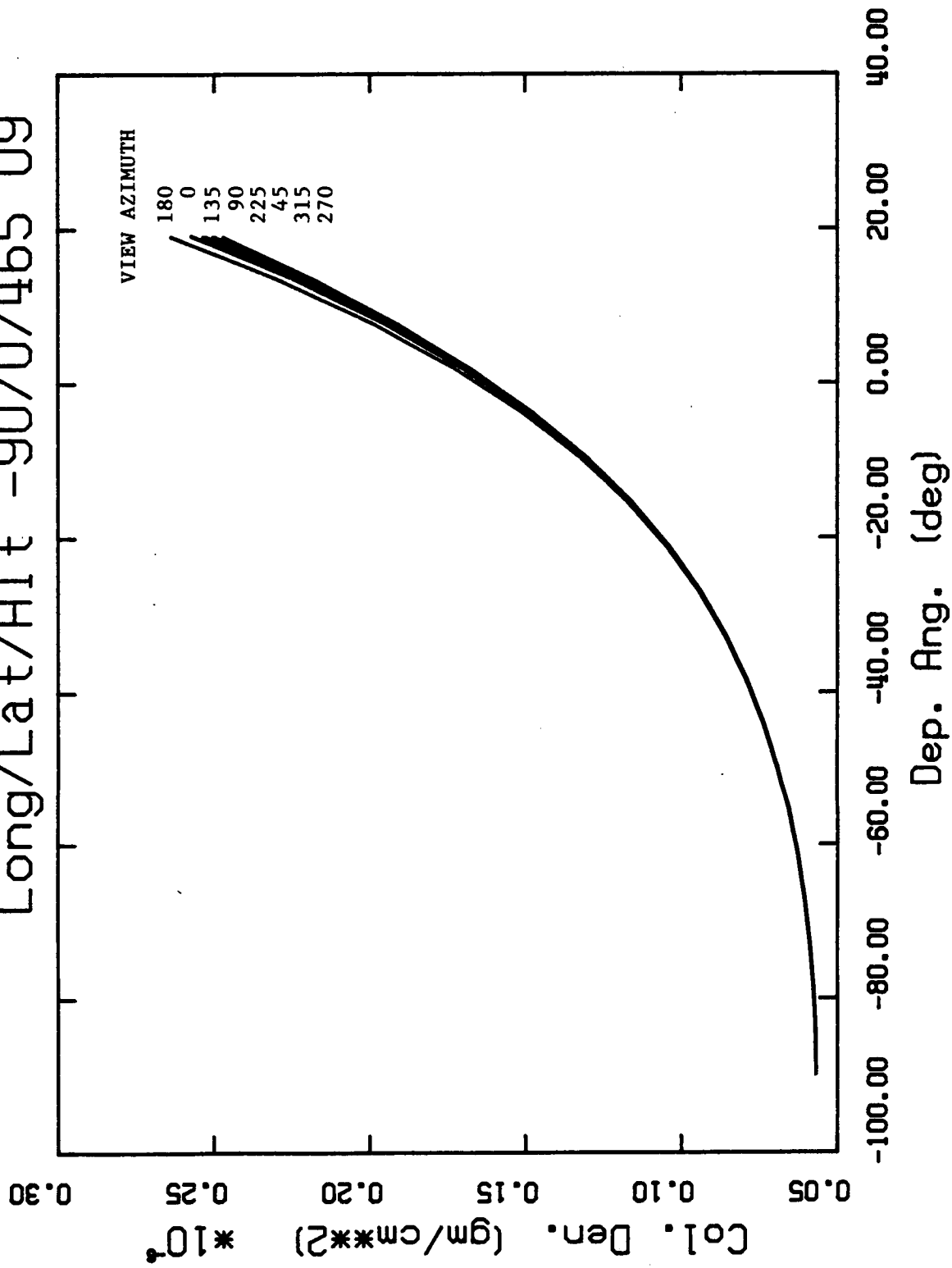
Line of Sight Density
Long/Lat/Alt 90/0/465 12



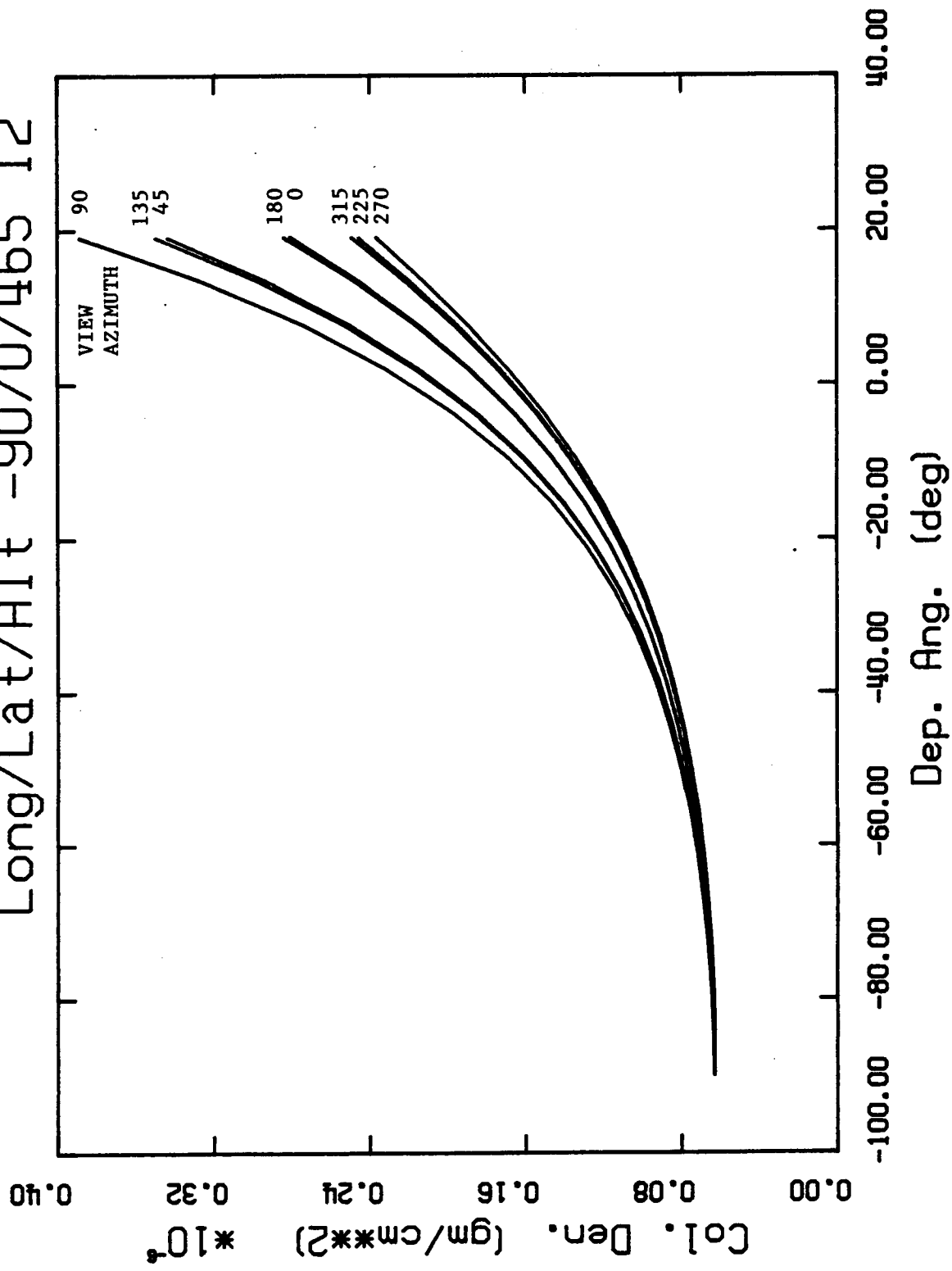
Line of Sight Density
Long/Lat/Alt -90/0/465 06



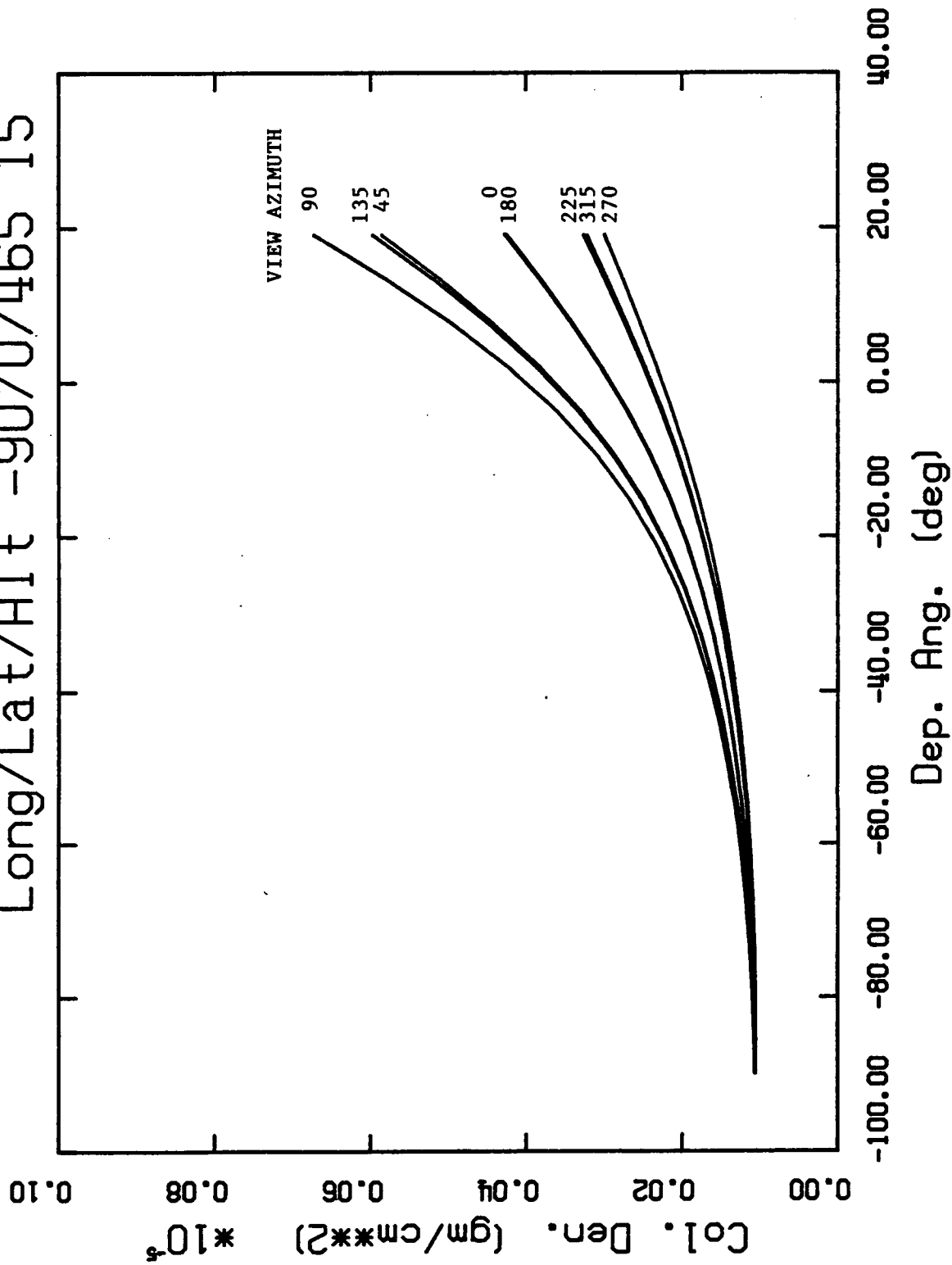
Line of Sight Density
Long/Lat/Alt -90/0/465 09



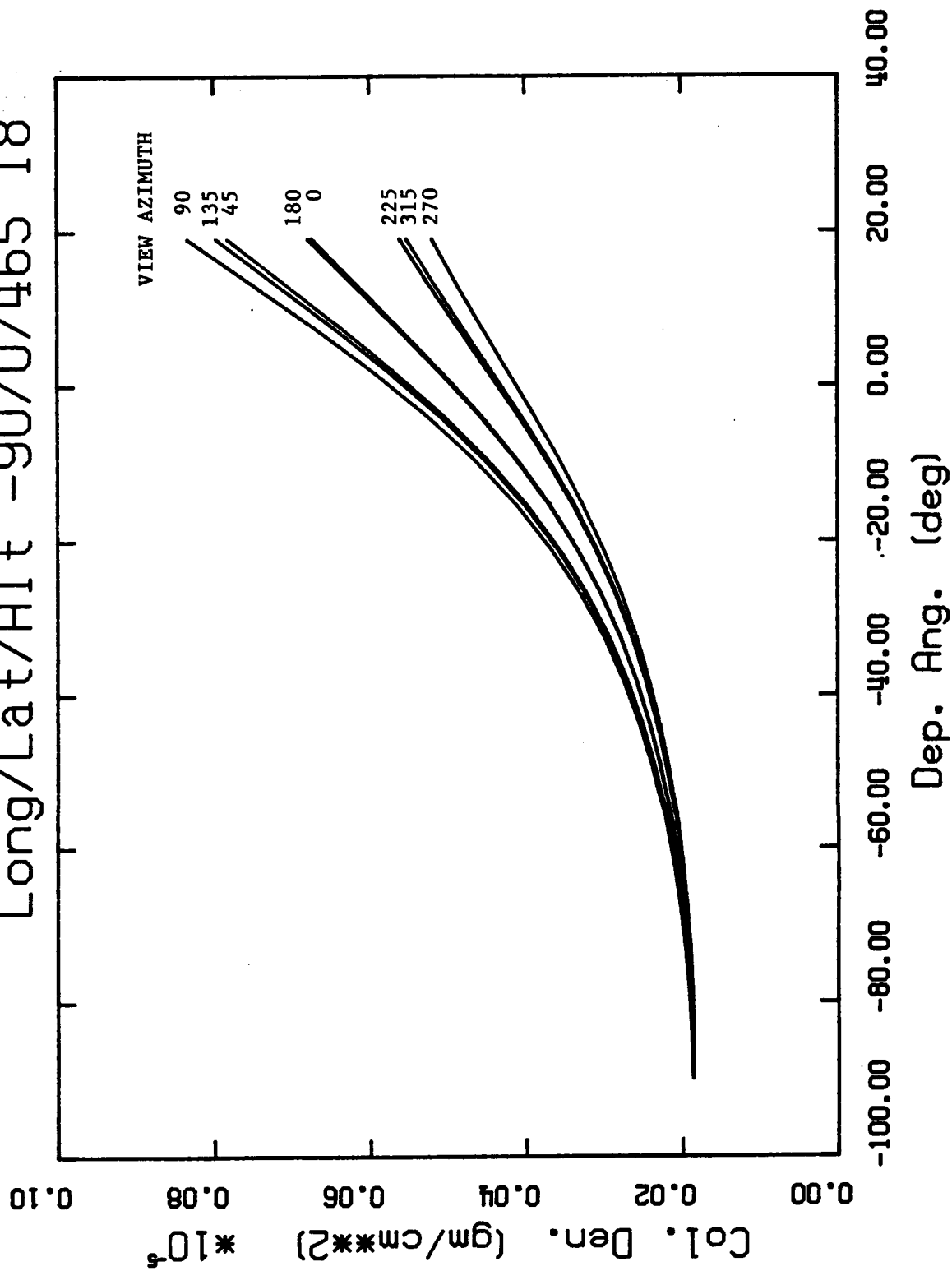
Line of Sight Density
Long/Lat/Alt -90/0/465 12



Line of Sight Density
Long/Lat/Alt -90/0/465 15



Line of Sight Density
Long/Lat/Alt -90/0/465 18



INSTRUMENT BASELINES

THREE ASO COMPONENTS

Three components have been baselined for the Advanced Solar Observatory; 1) The High Resolution Telescope Cluster, 2) The Pinhole Occulter Facility, and 3) The High-Energy Facility. Issues which need further study are the data rate requirement for the High Resolution Telescope Cluster and the boom dynamics for The Pinhole Occulter Facility.

THREE ASO COMPONENTS

High-Resolution Telescope Cluster

Critical Issue: Data Rates

Pinhole Occulter Facility

Critical Issue: Boom Dynamics

High-Energy Cluster

HRTC INSTRUMENT LIST

The High Resolution Telescope Cluster consists of seven independent instruments which will occupy the same housing. Each of these instruments will look at a different portion of the spectrum. Spectral coverage for the cluster will be approximately from 1.5 Å to 3300 Å. Mass and electrical requirements are well within those provided for by the space station.

HRTC INSTRUMENT LIST

TELESCOPE	BANDPASS (nm)	MASS (kg)	ELECTRICAL REQUIREMENTS (W)	APERTURE/ FOCAL LENGTH (cm)
U-1	120 to 330	154	190	65/500
E-1	55 to 110	96.5	190	40/500
X-1	16.7 to 17.7	96.5	190	40/500
X-2	18.7 to 20	96.5	190	40/500
X-3	24.5 to 26.5	96.5	190	40/500
S-1	1 to 17	147	190	40/500
S-2	0.15 to 2.5	184	190	40/600

TELESCOPE SIZES

This chart summarizes the gross dimensions of the HRTC telescopes. Projections beyond the cylindrical outline exist, but are not described here. They are taken into account in the structural layouts.

TELESCOPE SIZES

TELESCOPE	PHYSICAL ENVELOPE LENGTH/DIA. (m)
U-1	7.0/0.75
E-1	7.5/0.67
X-1	7.5/0.67
X-2	7.5/0.67
X-3	7.5/0.67
S-1	7.0/0.55
S-2	7.2/0.55

TWO OPERATIONAL MODES FOR HRTC

The High Resolution Telescope Cluster will be designed to operate in two separate modes. The first of these is the "normal operation" mode. In this configuration the telescopes will be alternately observing the sun and the resulting data rate will be lower than for simultaneous observations. The second mode is the "special event" mode. When an event (such as a flare) is identified the telescopes will concentrate their observations on that particular area and data rates will increase due to simultaneous viewing by the individual instruments.

TWO OPERATIONAL MODES FOR HRTC

(Sheet 1 of 2)

Normal Operation

IMAGES	DESCRIPTION	DATA RATE (BITS PER FRAME)
U-1	SHG	1.2×10^9
E-1	SHG	3.0×10^8
X-1	SHG	1.5×10^8
X-2	SHG	1.5×10^8
X-3	SHG	1.5×10^8
S-1	SHG (Ellipsoidal Focus)	4.0×10^7
S-2	SHG (Prime Focus)	1.5×10^8
Cyclic	Full Disk (1/7 per frame)	1.3×10^8
Cyclic	Slit Jawed (1/7 per frame)	1.4×10^6
Total = 2271 mbpf		

TWO OPERATIONAL MODES FOR HRTC (Sheet 2 of 2)

Special Event Mode

IMAGES	DESCRIPTION	DATA RATE (BITS PER FRAME)
U-1	Wide-Field	1.5×10^8
E-1	Wide-Field	1.5×10^8
X-1	Wide-Field	1.5×10^8
X-2	Wide-Field	1.5×10^8
X-3	Wide-Field	1.5×10^8
S-1	Wide-Field	4.0×10^7
S-2	Wide-Field	1.5×10^8
U-1	SHG	1.2×10^9
E-1	SHG	3.0×10^8
X-1	SHG	1.5×10^8
X-2	SHG	1.5×10^8
X-3	SHG	1.5×10^8
S-1	SHG (Ellipsoidal Focus)	4.0×10^7
U-1	UV Spectrum	4.0×10^5
U-1	Split Jawed (2 Images)	2.0×10^7
S-1	Wolter-I SHG	4.0×10^7
Total = 2990 mbpf		

OPERATION IN ROUTINE MODE

This diagram depicts the routine operational mode of the High Resolution Telescope Cluster. Each column represents one frame (assumed to be one second). In this mode one spectroheliographic image is sent down for each telescope each frame in addition to a wide-field image which is required only once every few frames.

OPERATION IN ROUTINE MODE

1 2 3 4 5 6 7

(Frame Number)

U-1

E-1

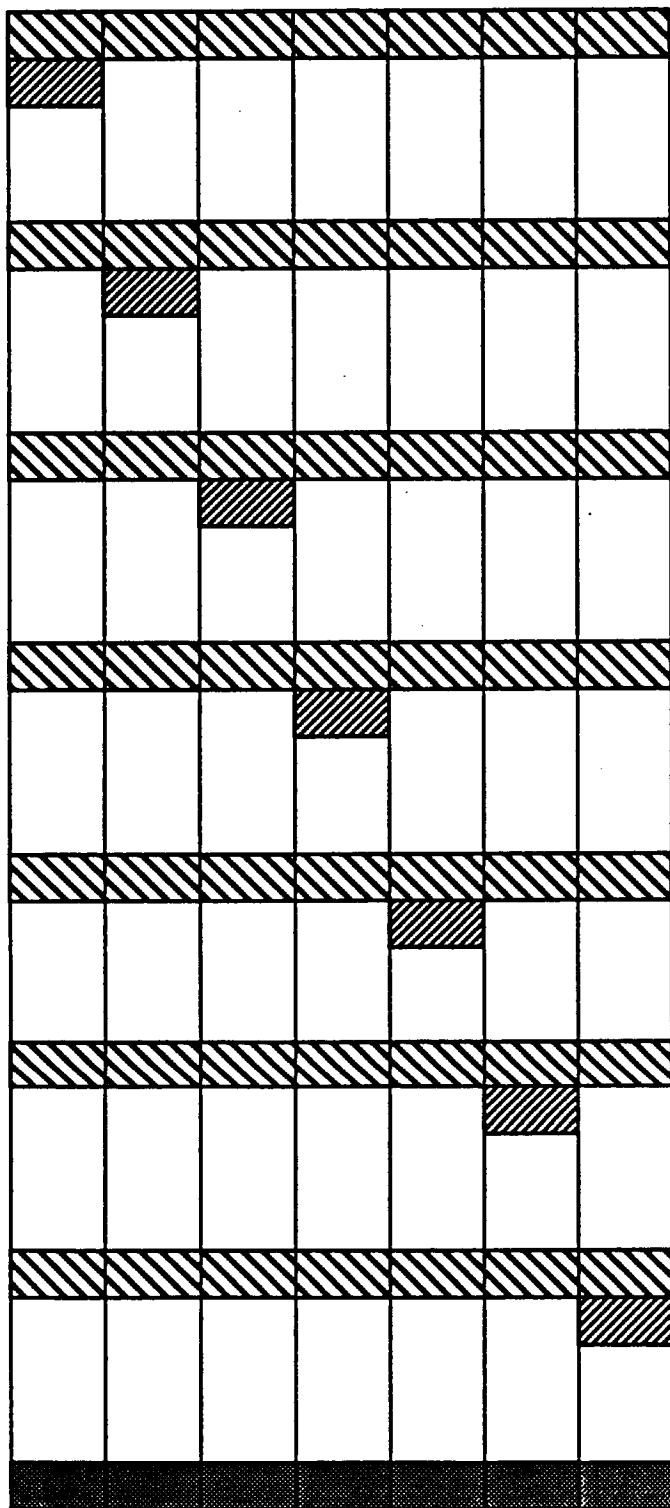
X-1

X-2

X-3

S-1

S-2



- Spectrohrliographic Focus



- Slit Jaw






























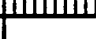
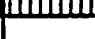

























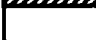
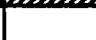

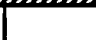






















































- Wide Field (1/7 per frame)

OPERATION IN SPECIAL EVENT MODE

This diagram depicts the special event operational mode of the High Resolution Telescope Cluster. Each column represents one frame (assumed to be one second). In this mode several images are sent down from each instrument thereby increasing the demand on the data transfer system.

OPERATION IN SPECIAL EVENT MODE

	1	2	3	4	5	6	7	(Frame Number)
U-1								
								
								
								
E-1								
								
								
X-1								
								
X-2								
								
X-3								
								
S-1								
								
								
S-2								



- Wide-Field Focus



- Spectroheliographic Focus



- Ultraviolet Spectrum



- Silt Jaw (2 Images)



- Wolter-I Spectroheliogram

P/OF INSTRUMENT LIST

The Pinhole Occulter Facility consists of six instruments which will be fixed to a baseplate/boom/occulting mask assembly. Each of these instruments will operate independently. Power and data rate requirements are well within space station limits but the mass properties of the assembly remain a critical issue.

POF INSTRUMENT LIST

INSTRUMENT	APERTURE (m ²)	POWER (W)	DATA RATE (Mbps)
FTI			
(6) 0.45 x 0.45 m	0.44	150	1.44
(11) 0.2 x 0.2 m	0.13	275	2.64
(9) 0.45 x 0.45 m	0.66	225	2.16
Coded			
(9) 0.45 x 0.45 m	0.66	225	1.8
(9) 0.4 x 0.4 m	0.56	225	1.8
(16) 0.45 x 0.45 m	1.17	400	3.2
WLSI	0.20	130	1
SLIS		0.20	140 1
Bragg		0.25	70 0.2
RMC	1.17	500	1.5

FTI	Fourier-Transform Imager	CAI	Coded Aperture Imager
SLIS	Solar Limb Imager/Spectrograph	WLSLI	White Light Solar Limb Imager
Bragg Imaging Bragg Spectrometer		RMC	Rotating Modulation Collimator

HIGH-ENERGY CLUSTER

The High-Energy Cluster will consist of four separate instruments. Because of the nature of these instruments, pointing requirements are less stringent than in the other facilities. Mass, power, and data requirements are well within station capabilities.

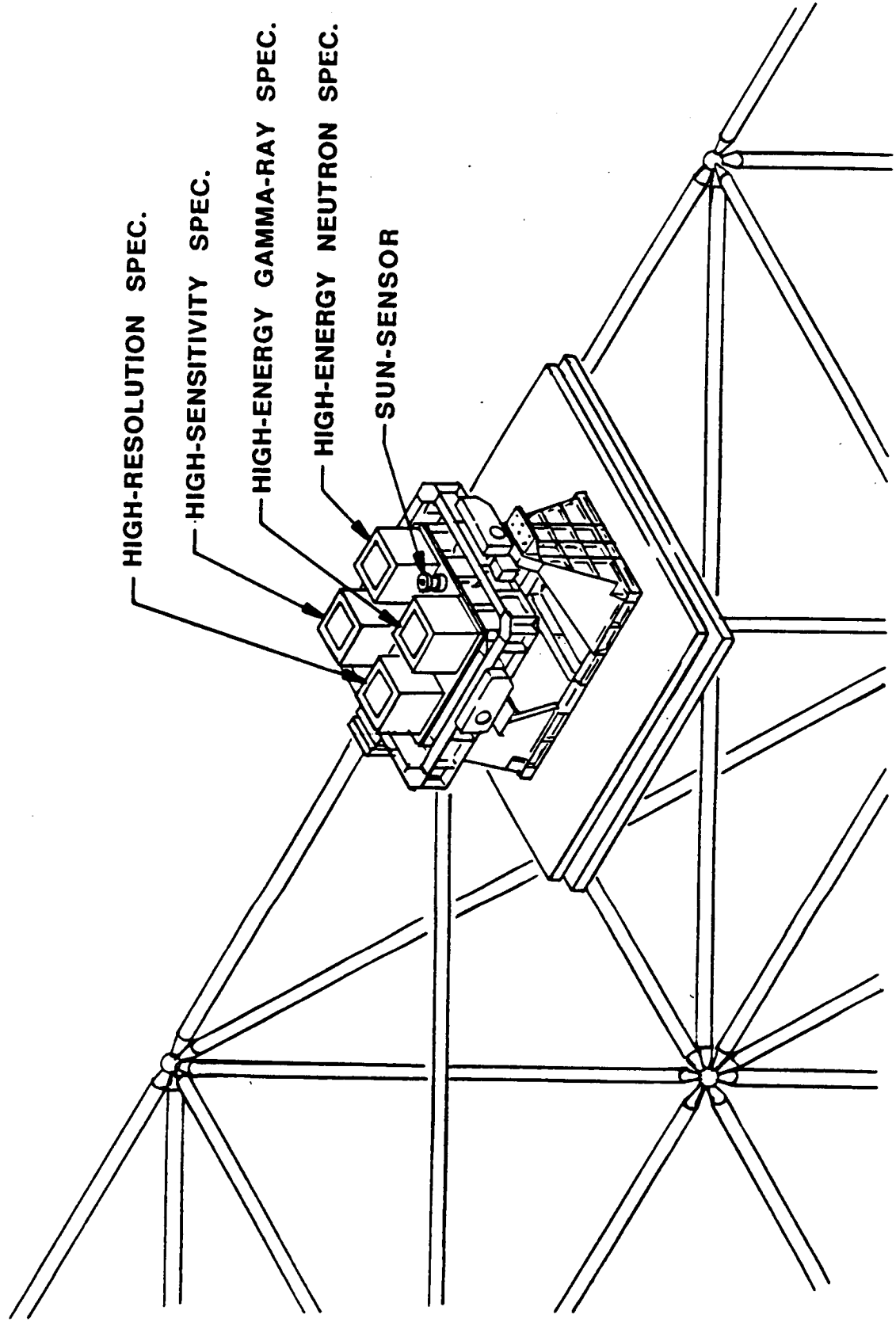
HIGH-ENERGY CLUSTER

	HIGH-RESOLUTION SPECTROMETER	HIGH-SENSITIVITY SPECTROMETER	HIGH-ENERGY GAMMA RAY SPECTROMETER	HIGH-ENERGY NEUTRON SPECTROMETER
Weight	400 kg	1,000 kg	1,000 kg	700 kg
Power	40 W	60 W	40 W	40 W
Telemetry Rate	80 Kbps	120 Kbps	5 Kbps	5 Kbps
Volume	0.7 m. dia x 0.5 m len	1 m dia x 0.5 m len	1 m ³	1 m ³
Detector Area	2,000 cm ²	8,000 cm ²	8,000 cm ²	8,000 cm ³
Spectral Range	10 keV to 10 MeV	100 keV to 10 MeV	5 MeV to 150 MeV	30 MeV to 1,000 MeV
Field of View	Full sun	Full sun	Full sun	Full sun
Spectral Resolution ($\Delta E/E$)	10 keV at 4.4 MeV	200 keV at 4.4 MeV	0.2 at 50 MeV	0.2 at 100 MeV
Temporal Resolution	1 sec	0.25 sec	TBD	TBD
Sensitivity	0.003 at 2.223 MeV	0.005 at 4.437 MeV	0.001 at 10 MeV	0.02 at 500 MeV

HIGH-ENERGY FACILITY

This sketch depicts the High-Energy Facility mounted in a dual-gimbal pointing system. Current PPS capabilities are significantly higher than the High-Energy Facility requires. Some pointing system economies might be achieved by mounting the facility outboard of the alpha gimbal. Coarse sun tracking would then be produced by the space station. However, there are currently no payload accommodations available beyond the alpha gimbals.

HIGH-ENERGY FACILITY



HIGH RESOLUTION TELESCOPE CLUSTER
STRUCTURAL/MECHANICAL

PHYSICAL CONFIGURATION OF THE HIGH RESOLUTION TELESCOPE CLUSTER

Two possible systems of mounting the telescopes were considered. The first involved mounting the telescopes directly on the outer cylinder structure. The second method would mount the telescopes to a cruciform which would be attached to the outer cylinder.

The transfer of power, data, and thermal control were also taken into consideration. It is assumed that these utility systems would be transferred across the gimbals and would be available to each instrument. A standard interface to transfer the utilities to each instrument would need to be developed.

PHYSICAL CONFIGURATION OF HIGH RESOLUTION TELESCOPE CLUSTER

Areas of Consideration

- Telescope placement within outer cylinder
- Transfer of utilities to telescopes
- Use of cruciform for telescope attachment

ASSUMPTIONS

Each telescope was assumed to be of circular cross-section. The given diameters do not include the mounting brackets or any telescope-peculiar instrumentation that may be attached on the outside of the telescope cylinder. The requirement that the telescopes be capable of replacement or removal on-orbit was also investigated.

Four of the telescopes, E-1, X-1, X₂², and X-3, have protrusions that are shown on preliminary sketches as being 180° from each other. To maximize the use of the available space, it is assumed that the Czerny-Turner grating and the focal mirror can be located, by use of optics, other than 180° from each other.

Film canisters and cameras have not been included in this preliminary concept due to the uncertainty of data storage facilities.

The modular nature of the components also implies that any general ASO subsystem would be attached to a cold plate as a single unit. It would be difficult to attain a sufficient thermal bond between cold plate and the component if the component were removed from the cold plate on-orbit and replaced with another unit.

It is assumed that the external cylinder structure is constructed of 2 inch diameter graphite epoxy tubing with multi-layer insulation attached to the outer side.

Assumptions

- Telescopes are of circular cross-section
- Given telescope diameters do not include mounting brackets or telescope-peculiar instrumentation
- Telescopes may be replaced/removed on-orbit
- General ASO subsystems are attached to cold plates, as necessary
- HRTC is attached to PPS on-orbit
- Film canisters and cameras have not been included
- The two protrusions on telescopes E-1, X-1, X-2, X-3 can be located other than 180° from each other
- External cylinder structure constructed of 2 in. dia., 1/8 in. thick graphite epoxy tubing with multi-layer insulation

HRTC STRUCTURE

This chart shows a bottom view of the HRTC structure. The next chart shows a side view.

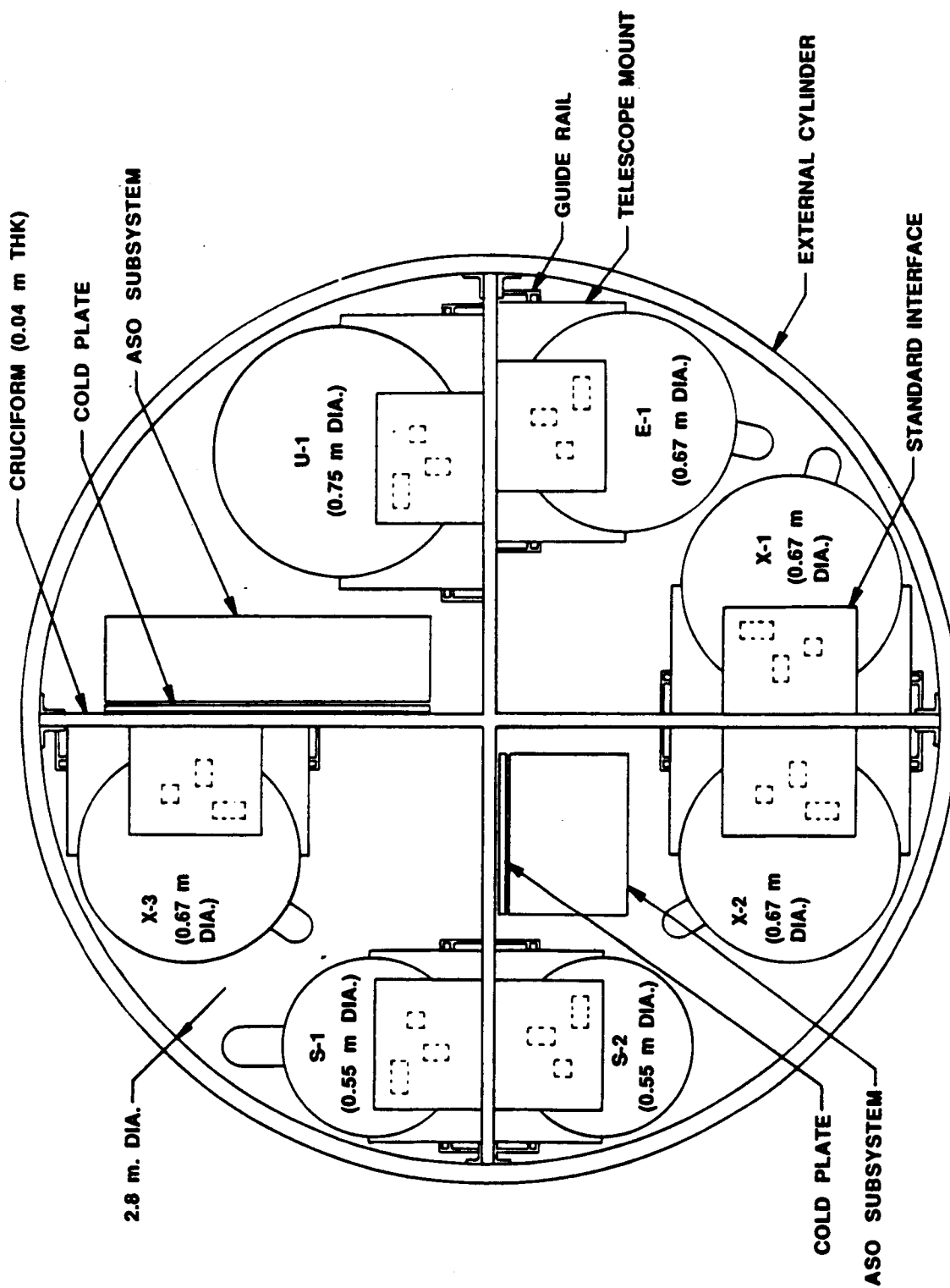
A central cruciform is shown here attached to the outer cylinder structure. The seven telescopes are mounted on this cruciform near the periphery of the cylinder. ASO subsystems, with associated coldplates, if necessary, could possibly be located in the central portion of the cylinder.

A canister length of 7.8 meters with a diameter of 2.8 meters would accommodate the given telescopes with a minimal clearance for removal of instrumentation. A clearance of 0.05 meters would exist between the outer canister and the Payload Pointing System (PPS).

A shield over the top of the canister would prevent excessive solar heating of the interior of the canister as well as prevent contaminants from entering the interior. A sun shield extension is shown, although it's necessity has not yet been determined.

Each telescope would interface with the Space Station power, data, and thermal networks through a standard interface which would need to be developed. This standard interface would be similar to the Standard Interface Adapter (SIA) of the Attached Payload Accommodation Equipment (APAE). The comparable interface on the telescope side would be similar to the Payload Interface Adapter (PIA) of the APAE but would be integral with the telescope. It is assumed that each telescope would need active thermal control for transfer of the electronics heat load out of the telescope cylinder.

HRTC STRUCTURE



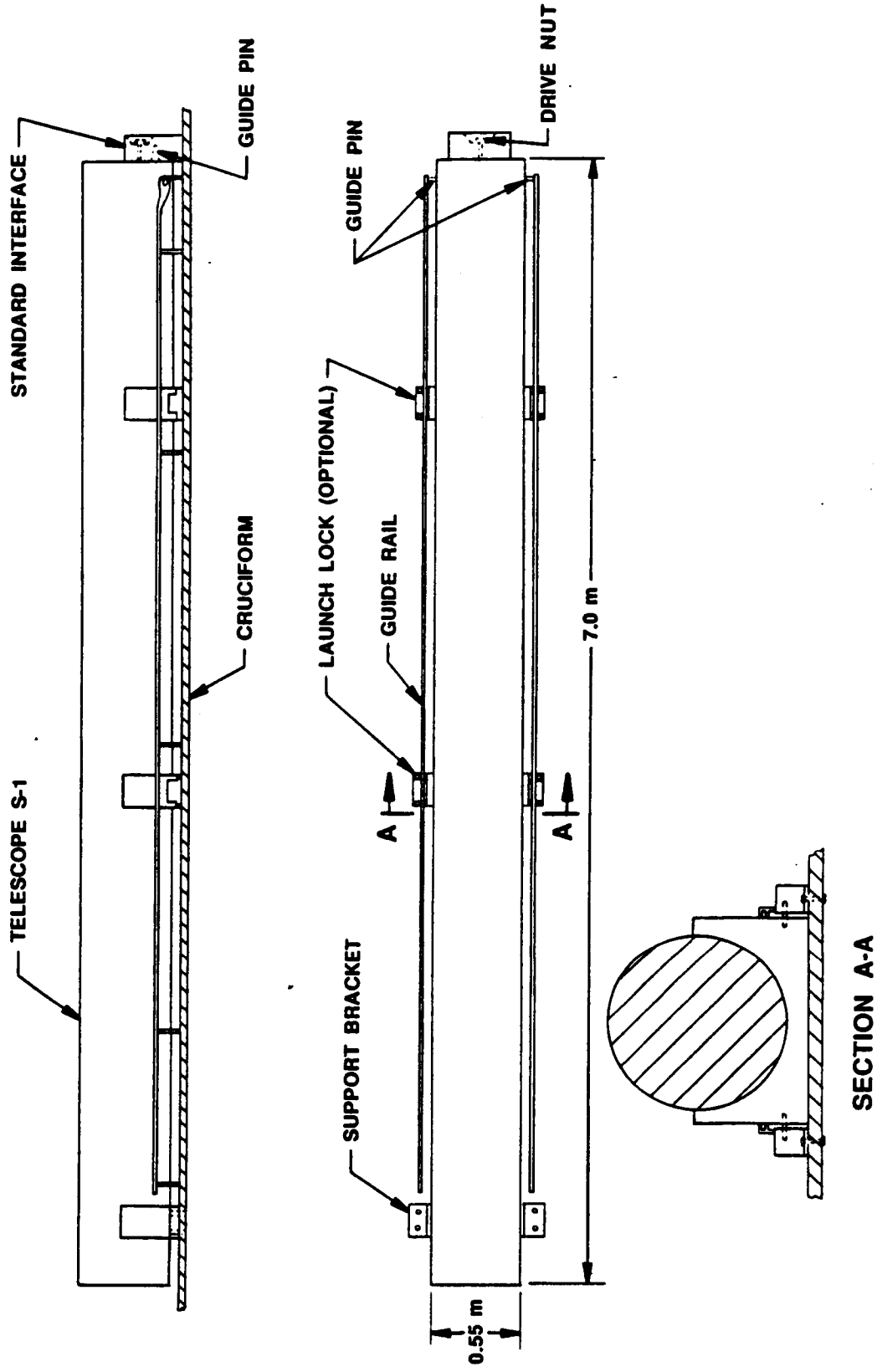
BOTTOM VIEW

HRTC TELESCOPE INSTALLATION

Removal or installation of a telescope would be possible by sliding the telescope along guide rails. Each telescope would be attached by a bracket at the top and by the standard interface at the bottom. For telescope removal, the top telescope bracket would be unbolted. The drive nut on the bottom of the telescope (attaching it to the standard interface) would be reversed; pushing the telescope out of the utility sockets. Guide pins on each side of the telescope would fit into rails running along each side for the major portion of the length of the cruciform. The MSC arm would grasp the top end of the telescope and slide it out with the guide rails preventing it from interfering with other experimentation. Launch locks are shown should they be necessary to reduce vibration loads during launch.

An alternate concept would use rollers positioned at several locations along the length of HRTC, instead of guide rails, as installation guides. The choice between these two implementations can be left for final design.

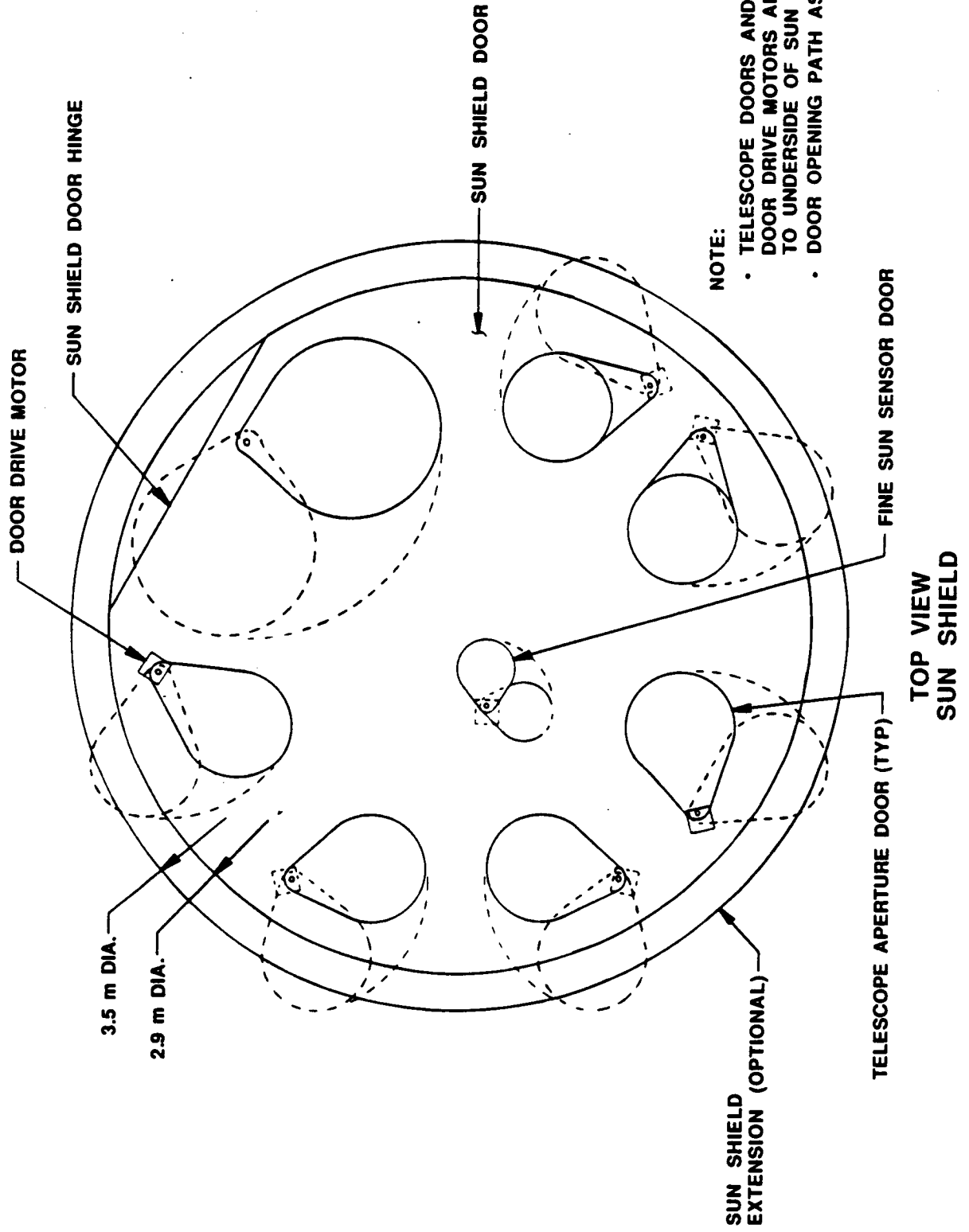
HRTC TELESCOPE INSTALLATION



HRTC SUN SHIELD AND CONTAMINATION COVERS

A sun shield is assumed to be necessary to radiate excess solar radiation and to prevent contaminants from entering the canister. Although the telescope doors are shown mounted on the sun shield, they would most likely be mounted on each telescope. There would be a hole the size of the corresponding aperture for each telescope on the sun shield if this is the case. The sun shield extension is assumed to be located below the top of the cylinder to avoid interference with door opening paths.

HRTC SUN SHIELD AND CONTAMINATION COVERS



ESTIMATED COMPONENT MASSES OF THE HRTC

An estimate of the masses involved for each component of this conceptual layout is presented. The masses listed are rough estimates based on assumed volumes for each component. Material properties for aluminum are used.

**ESTIMATED COMPONENT MASSES OF THE HRTC
(TELESCOPE MASSES NOT INCLUDED)**

ASSUME MATERIAL IS ALUMINUM, $\rho = 2713 \text{ kg/m}^3$

<u>COMPONENT</u>	<u>QUANTITY</u>	<u>ESTIMATED MASS (kg)</u>	<u>ESTIMATED TOTAL MASS (kg)</u>
STANDARD INTERFACE	7	38	266
GUIDE RAIL	14	2.2	31
MOUNTING BRACKET	21	8.9	186
CRUCIFORM	1	1896	1896
OUTER CYLINDER*	1	165	165
TELESCOPE CLUSTER ATTACHMENT RING	1	677	677
SUN SHIELD	1	180	180
SUN SHIELD EXTENSION	1	117	117
			<u>3518</u>

*NOTE: OUTER CYLINDER CONSTRUCTED OF GRAPHITE EPOXY TUBING

CONCLUSIONS

With the configuration shown, the minimum inside canister diameter required is 2.8 meters. The cruciform would facilitate the mounting of the telescopes and would also serve as an optical bench. The cruciform, as a load carrying member, would allow for alternate forms of the outer cylinder. Possible materials for the cruciform would include aluminum and graphite epoxy. The graphite epoxy technology, though, may not be sufficiently developed to be a feasible alternative.

Conclusions

- **Cruciform may be necessary to minimize thermal and mechanical distortions (i.e. serves as an optical bench)**
- **Telescopes cannot be mounted on a cruciform within a 2.5 m dia. envelope**
- **Minimum diameter that can accommodate given telescope diameters is 2.8 m**
- **Possible cruciform materials could be**
 - **Aluminum with weight reduction holes**
 - **Graphite Epoxy**
- **Center of mass can be maintained within given limits by appropriate placement of instrumentation**
- **Limited space available for ASO subsystems**
 - **Max. envelope = 0.4 x 0.55 x 7.0 m**
- **Standard interface to transfer power, data, and thermal control to telescopes needs to be developed**
- **Sun shield with individual telescope doors is necessary for thermal and contamination control**
- **Telescopes removed from top on-orbit**
- **Instrumentation serviced from bottom and side access doors**

PINHOLE OCCULTER FACILITY
STRUCTURAL/MECHANICAL

PINHOLE/OCCULTER FACILITY CONCEPT

This chart summarizes the equipment needed to support P/OF operations, particularly boom pointing and control.

Pointing of P/OF is accomplished by the gimbal system. Flexible boom dynamics are counteracted by angular momentum exchange devices (AMEDs) positioned along the boom. These introduce bending moments into the boom to counteract bending due to P/OF motion. The error signals for the AMEDs are generated in the control computer, based on measurements from rate gyros and the boom tip displacement sensors. Rate gyros are positioned along the boom, while the tip displacement sensor measures the occulter plane motion. The boom tip displacement sensor (TDS) used for this study is the two axis Remote Attitude Measurement System (RAMS) produced by Ball.

During operation, solar pointing of the x-ray instruments can be verified and maintained using a simple pinhole in the occulting plane with visible light detectors. Measurement of the solar limb position in the detector plane will verify pointing of the x-ray instruments to the sun. Alignment of the solar limb imagers with their occulting disks will require more stringent control of the occulting plane with respect to the detector plane, so sun sensors have been included, which are mounted on the detector structure. These sun sensors, with the RAMS, or possibly the pinhole pointing sensor, allow us to control both pointing and alignment of the limb sensors. The sun sensors also provide a degree of redundancy in the dynamics control, also, since in conjunction with the pinhole sun sensor, the boom bending could be determined. We have not investigated the accuracy that could be achieved in this way.

We have also included provision for occulter plane translation and rotation for alignment with the detector plane. There have been indications that this is not necessary. Elimination would simplify the boom tip assembly.

A solar x-ray flare detector was also included, although there are now indications that it is not needed from the science standpoint.

PINHOLE/OCCULTER FACILITY CONCEPT

- o Uses angular momentum exchange devices (AMEDs) and rate gyros to sense and damp boom vibrations
- o Power and signal utilities are supplied to the lower AMED gyro assembly and the entire boom tip assembly by a derotator on the bottom of the canister
- o Boom tip assembly includes electronics, occulter alignment mechanism, power converters, and light x-ray occulter shields
 - integrated AMED/sensor with tip electronics and power
 - occulter alignment system provide ± 30 cm translation and ± 10 deg. rotation about boom axis to 0.1 cm and 0.1 deg. accuracy
 - occulter support/light shield has a mass of 2.2 kg/m^2
 - tungsten x-ray shield has a mass of 9 kg/m^2 minus about 0.26 kg/mask for cut-outs
- o Boom tip displacement sensor (TDS) is the Ball Remote Attitude Measurement System (RAMS) with two axis sensors (X and Y)
 - RAMS sensors placed near center of the umbra with 3.5 deg. FWHM FOV
 - contained in 13 cm cylinder, 25 cm high, mass = 9.1 kg
- o Uses Small Lockheed Sun Sensor with dual star tracker START system to provide inertial reference and up to 1 arc sec accuracy on solar targets
- o Solar x-ray flare sensor
- o Boom Dynamics and Pointing Control Computer

ASO POF ON PPS

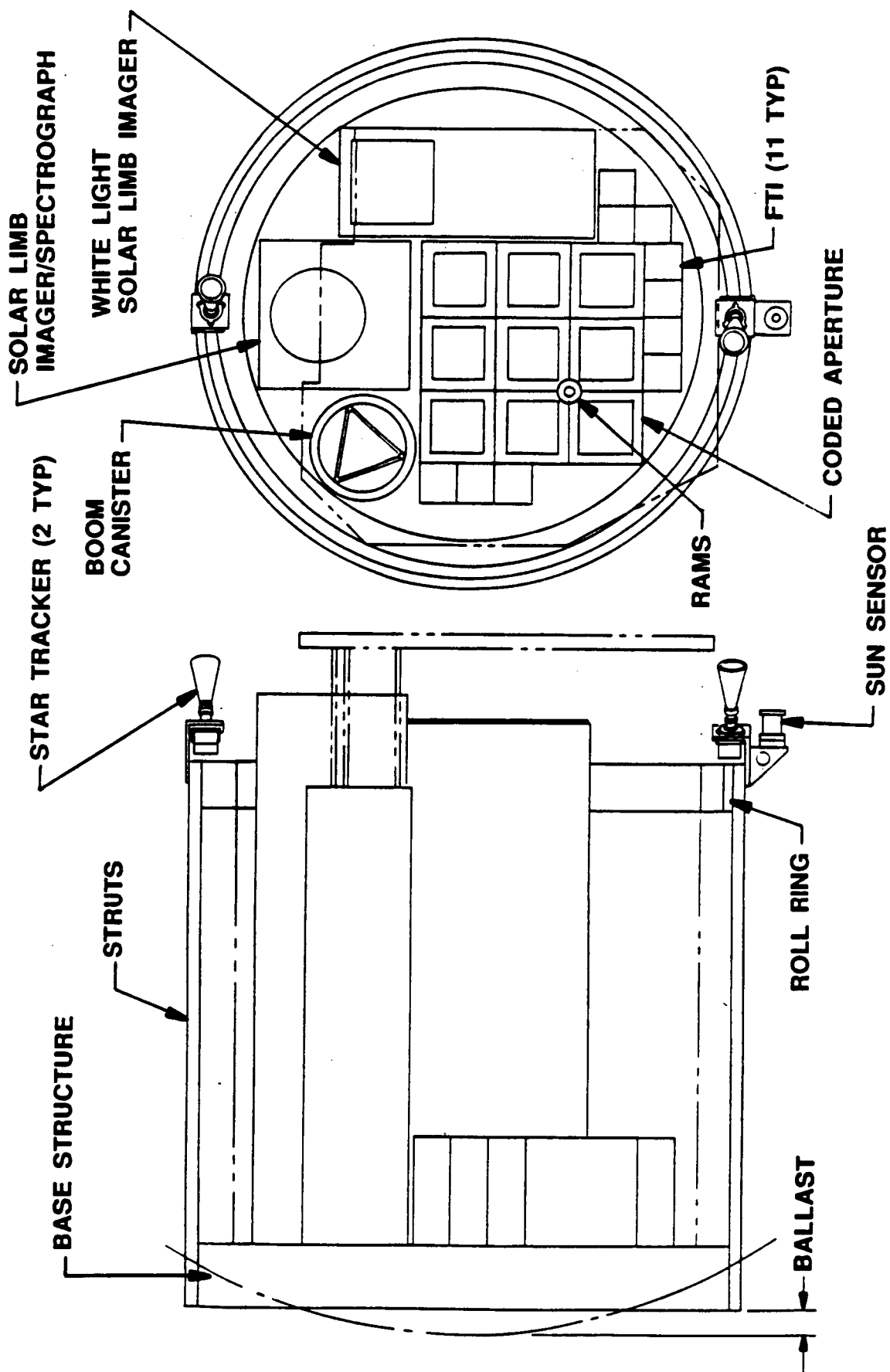
These four charts illustrate possible layouts for P OF instruments which can be accommodated by the Space Station Payload Pointing System (PPS). Two different instrument complements are illustrated: the x-ray instruments (Fourier Transform Imager, FTI, and Coded Aperture Imager, CAI) with two solar limb imagers; and, only the x-ray instruments, which have been scaled up to use the available space. The first chart of each pair shows the detector (lower) end layout, the second chart shows the occulter plane layout.

The roll ring provides a roll axis (around the line of sight) degree of freedom which is not provided by the PPS. It is necessary for the complement including the limb imagers, to position the field of view at the desired limb position. It is probably not needed for the x-ray only complement.

Ballast is shown at the lower end of the P/OF envelope to bring the center of mass within the envelope specified for the PPS. However, if the PPS pointing performance is adequate, the center of mass could be allowed to be forward of the specified envelope, eliminating the need for ballast.

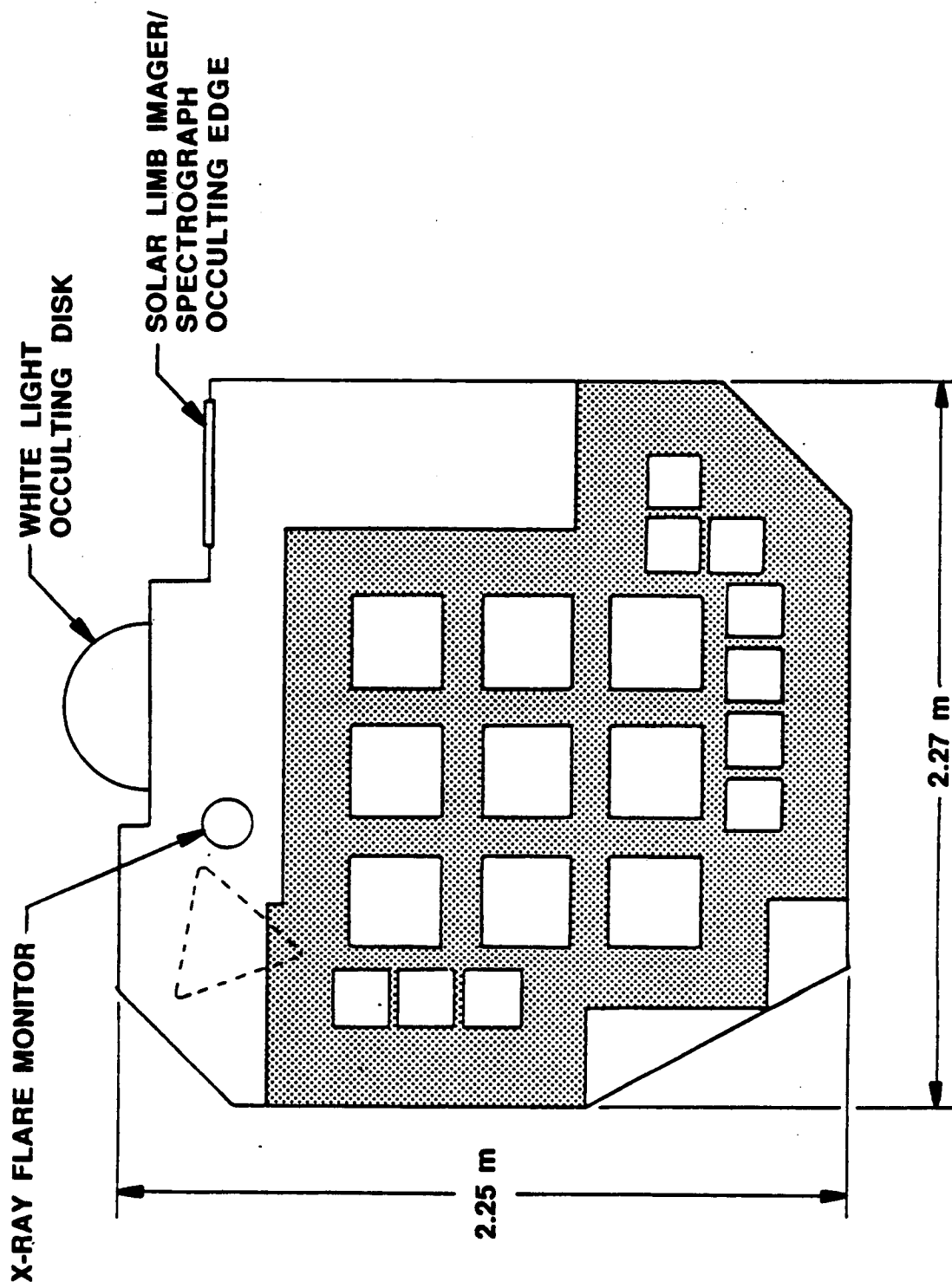
The boom is also shown mounted off-center to optimize instrument layout. This introduces undesirable cross-coupling into the boom dynamics, but preliminary estimates indicate that it is acceptable. More detailed analysis is needed in this area, however.

ASO POF ON PPS X-RAY WITH SOLAR LIMB IMAGERS

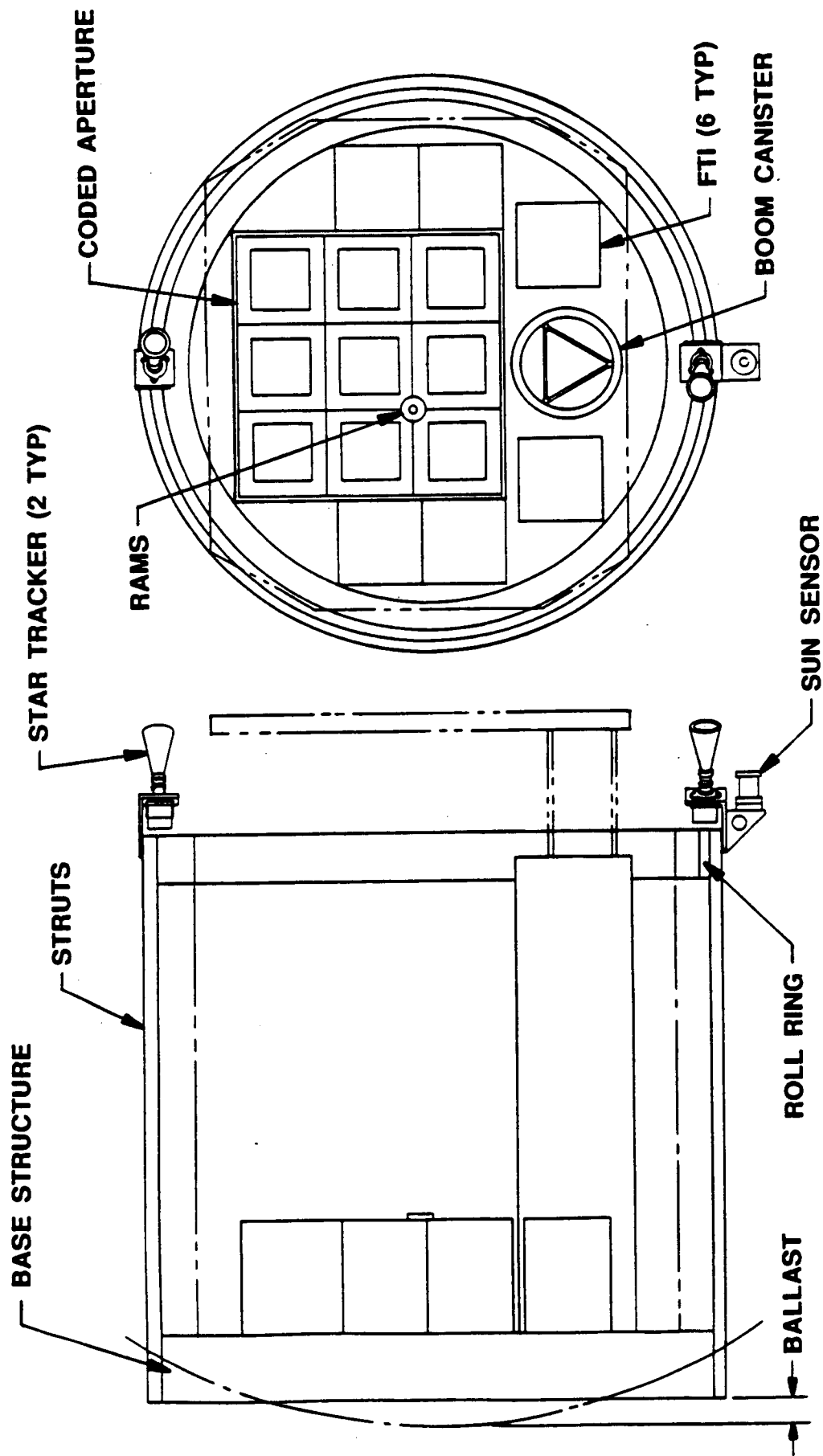


ASO POF ON PPS

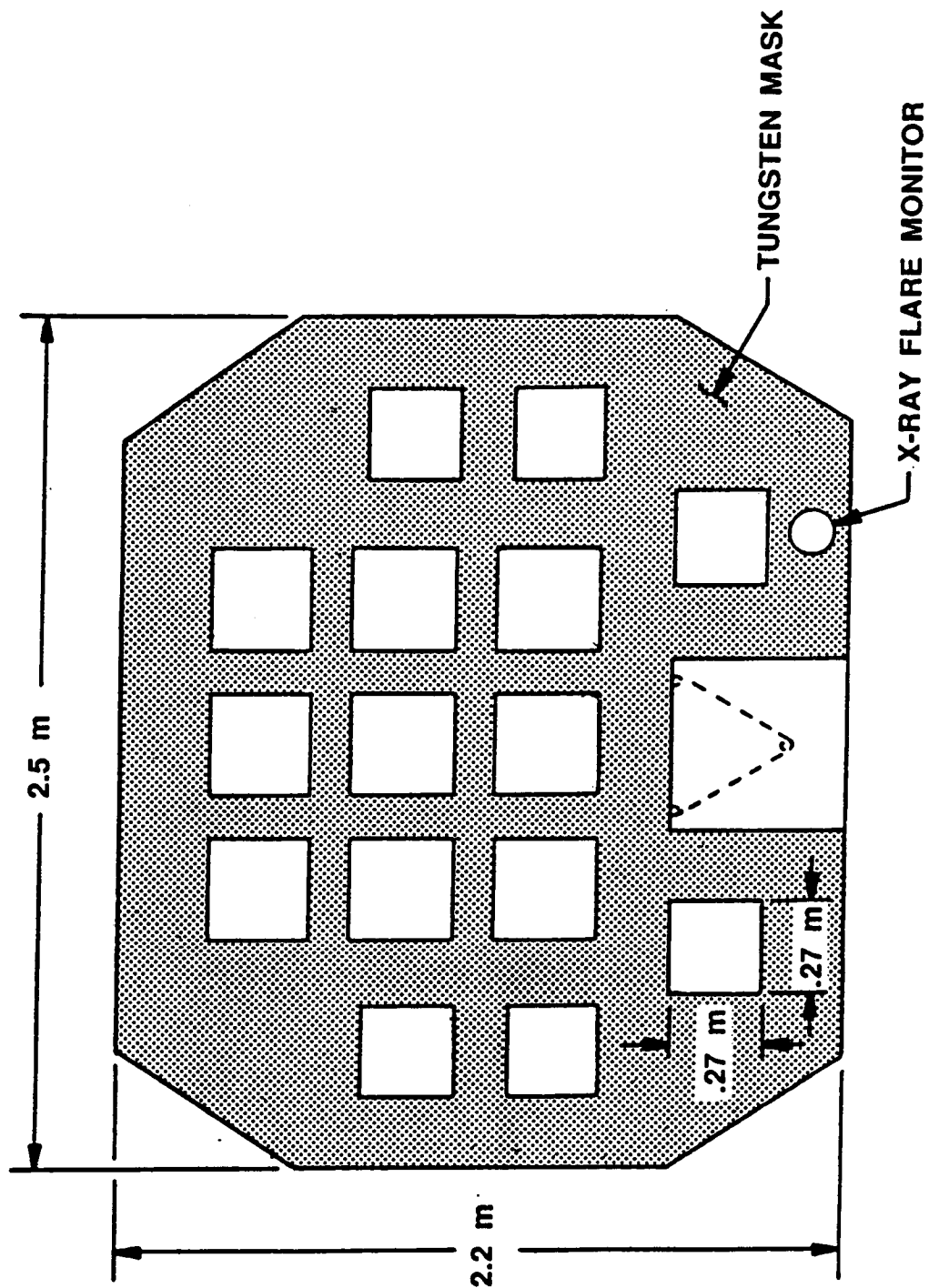
X-RAY WITH SOLAR LIMB IMAGERS OCCULTER LAYOUT



ASO POF ON PPS DEDICATED HARD X-RAY



ASO POF ON PPS
DEDICATED HARD X-RAY OCCULTER LAYOUT

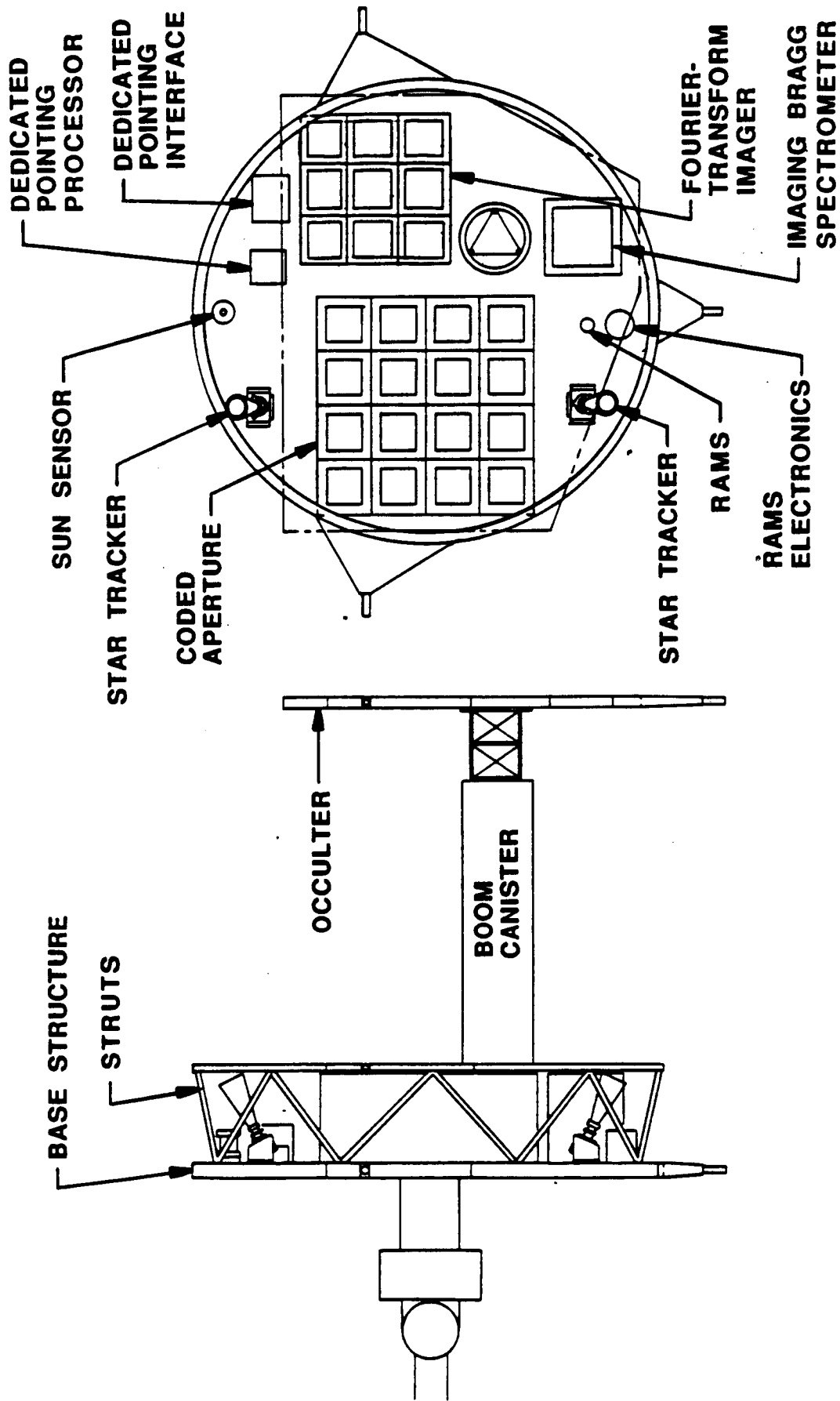


ASO POF ON BPS

The following four charts illustrate mechanical layouts for two different instrument complements using a base-mounted pointing system (BPS), instead of the center of mass mounted PPS. The most significant difference between the two pointing systems, for layout purposes, is the increased diameter available to the instruments which is only constrained by the Shuttle payload bay diameter for launch.

The first instrument complement includes a Fourier Transform Imager (FTI), a Coded Aperture Imager (CAI) and a Bragg crystal imaging spectrometer. The second complement is composed entirely of a rotating modulation collimator imager.

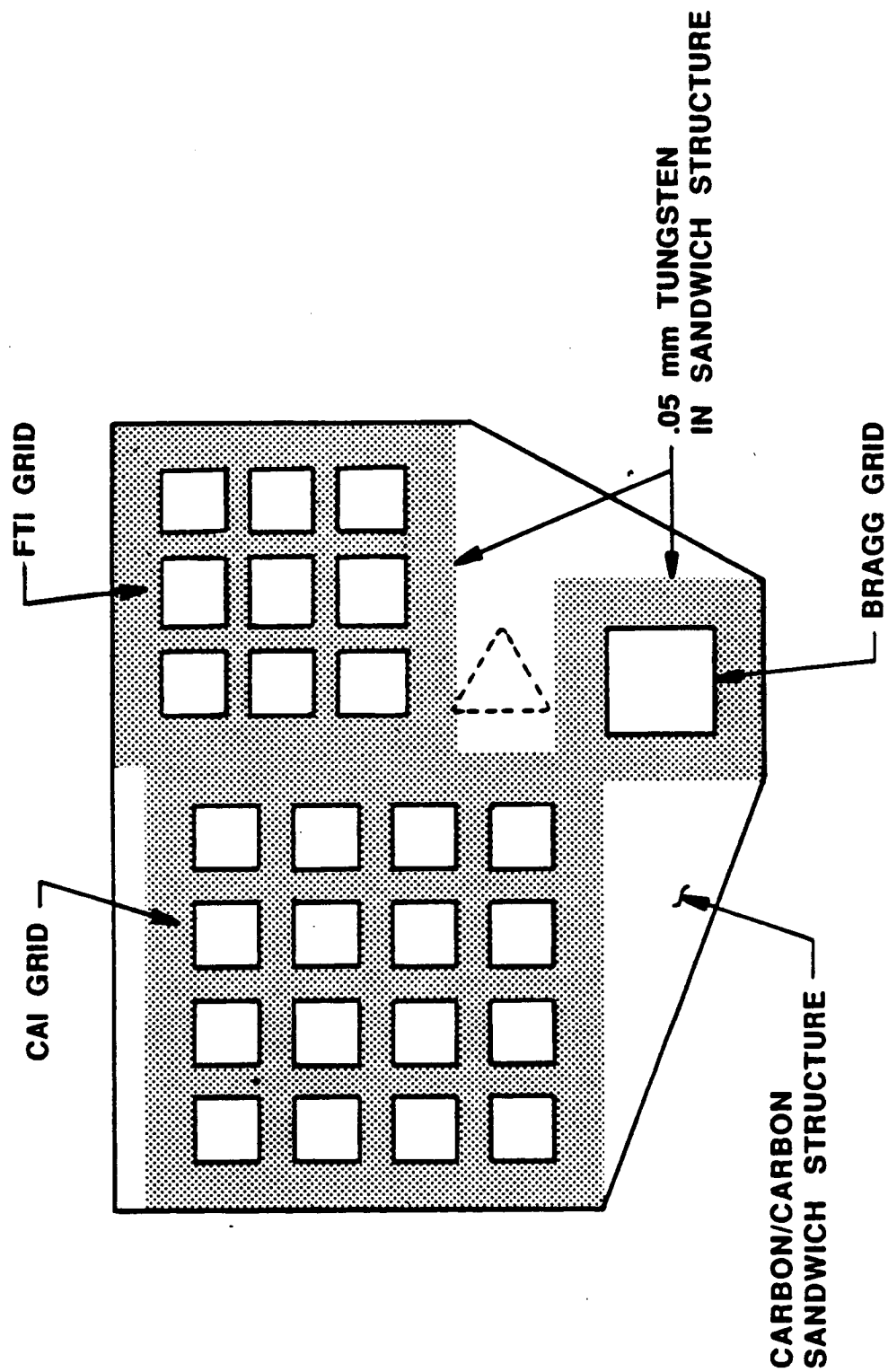
ASO POF ON BPS WITH FTI, CAI, AND BRAGG



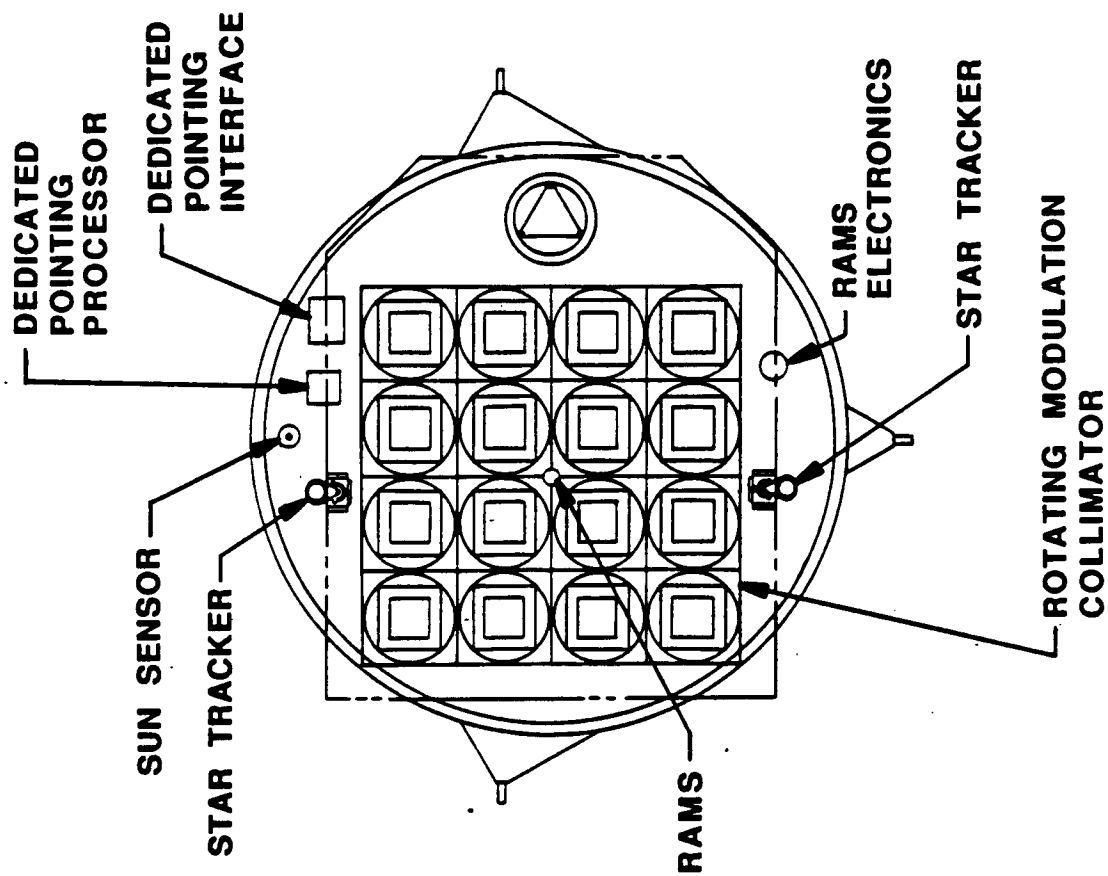
PLAN VIEW

SIDE VIEW

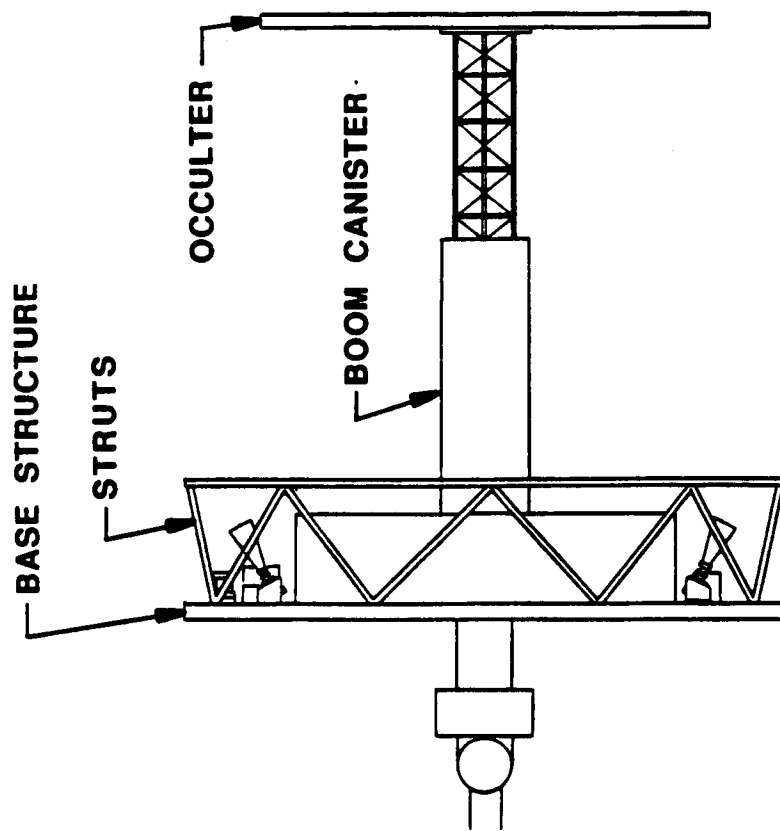
ASO POF ON BPS
WITH FTI, CAI, AND BRAGG OCCULTER ASSEMBLY



ASO POF ON BPS WITH ROTATING MODULATION COLLIMATOR



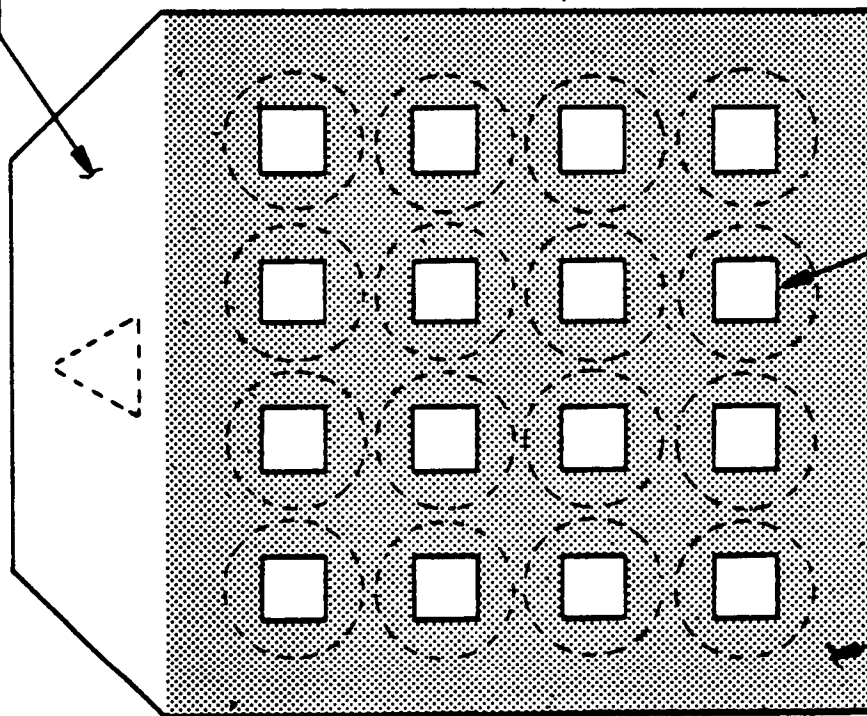
PLAN VIEW



SIDE VIEW

**ASO POF ON BPS
WITH ROTATING MODULATION COLLIMATOR
OCCULTER ASSEMBLY**

**CARBON/CARBON
SANDWICH STRUCTURE**



**.05 mm TUNGSTEN
IN SANDWICH STRUCTURE**

**ROTATING MODULATION
COLLIMATOR GRID**

POF ON PPS

This chart presents the mass properties and various derived quantities for each of the POF configurations analyzed, assuming the use of the Space Station PPS. There are three basic variations: Different experiment complements: Boom or cylindrical shell structure; and lightening of the lower end structure with consequent center of mass located forward of the gimbal. Configurations 1, 2, & 5 use the baseline boom; 3, 4, & 6 use the cylindrical shell. Configurations 5 & 6 are identical to 1 & 3 respectively except that 5 & 6 have lighter support structures and therefore are not cg mounted.

Maximum slew torque (and the corresponding tip displacement) is determined by the requirement to stop, return and accelerate during the shortest orbit dark period.

Maximum tracking torque and tip displacement are determined by the worst case azimuth and elevation accelerations during azimuth-elevation tracking (beta greater than 15 degrees).

Emergency stop conditions assume P/OF angular velocity is limited to less than 1 deg/sec, and shock absorbing mechanical stops are provided that induce less than 1000 newton-meters torque into P/OF. This results in 4.5 degrees of gimbal travel after hitting the stops.

Maximum torque values assume the gimbal drives produce 100 newton-meters torque.

POF ON PPS

CONFIGURATION	1	2	3	4	5 *	6 *
INSTRUMENT	RMC	FT1	RMC	FT1	RMC	RMC
INSTRUMENT MASS (kg)	1200	165	1200	165	1200	1200
INSTRUMENT		CAI		CAI		
INSTRUMENT MASS (kg)		540		540		
INSTRUMENT		WLC		WLC		
INSTRUMENT MASS (kg)		231		231		
INSTRUMENT		UVCS		UVCS		
INSTRUMENT MASS (kg)		410		410		
INSTRUMENT						
INSTRUMENT MASS (kg)						
TIP MASS (kg)	210	109	197	96	210	197
BOOM MASS (kg)	61	61	218	218	61	218
TOTAL MASS (kg)	5950	4195	7613	5681	2073	2159
MOI About Cross-Elevation, Ixx (kg-m ²)	6.26E5	3.56E5	7.40E5	4.69E5	6.03E5	7.07E5
MOI About Elevation, Iyy (kg-m ²)	6.26E5	3.56E5	7.40E5	4.69E5	6.03E5	7.08E5
MOI About Roll, Izz (kg-m ²)	4.52E3	4.68E3	7.52E3	7.56E3	1.49E3	3.26E3
Ixy (kg-m ²)	5.59E-9	1.90	3.33E1	-5.37E1	-1.12E-8	3.33E1
Ixz (kg-m ²)	2.64	-3.98E2	2.64	7.78E2	2.64	2.64
Iyz (kg-m ²)	-2.45E3	5.06E3	-8.55E2	3.58E3	-2.45E3	-8.55E2
MAX SLEW TORQUE (Nm)	7.25	4.12	8.57	5.43	6.98	8.20
MAX SLEW TIP DISPLACEMENT (mm)	21.22	11.45	3.79E-2	2.18E-2	21.24	3.79E-2
MAX TRACKING TORQUE (Nm)	8.08	4.59	9.55	6.05	7.78	9.13
MAX TRACKING TIP DISPLACEMENT (mm)	23.64	12.77	4.23E-2	2.43E-2	23.66	4.23E-2
EMERGENCY STOP TIP DISPLACEMENT (mm)	3556.44	1920.05	6.35	3.66	3556.44	6.35
EMERGENCY STOP MAX BENDING MOMENT (Nm)	1098.86	602.87	1235.33	739.34	1098.86	1235.33
MAX TORQUE TIP DISPLACEMENT (mm)	292.98	278.14	4.43E-1	4.02E-1	304.16	4.63E-1
MAX TORQUE BENDING MOMENT (Nm)	90.52	87.33	86.09	81.30	93.98	89.98

* CONFIGURATIONS 5 AND 6 ARE NOT CG-MOUNTED.

POF ON BPS

This chart is similar to the previous one, except that a base-mounted pointing system is assumed rather than the cg mounted PPS.

POF ON BPS

CONFIGURATION	7	8	9	10	11	12
INSTRUMENT	RMC	RMC	FTI	FTI	FTI	FTI
INSTRUMENT MASS (kg)	1328	1328	680	680	720	720
INSTRUMENT			CAI	CAI	CAI	CAI
INSTRUMENT MASS (kg)			680	680	1280	1280
INSTRUMENT			UVCS	UVCS	Bragg	Bragg
INSTRUMENT MASS (kg)			410	410	240	240
INSTRUMENT			WLUV	WLUV		
INSTRUMENT MASS (kg)			231	231		
INSTRUMENT						
INSTRUMENT MASS (kg)						
TIP MASS (kg)	303	290	169	156	157	144
BOOM MASS (kg)	61	264	61	264	61	264
TOTAL MASS (kg)	3786	3962	4995	5128	4552	4685
MOI About Cross-Elevation, Ixx (kg-m ²)	9.58E5	1.13E6	5.57E5	7.31E5	5.38E5	7.14E5
MOI About Elevation, Iyy (kg-m ²)	9.58E5	1.13E6	5.57E5	7.31E5	5.36E5	7.12E5
MOI About Roll, Izz (kg-m ²)	4.09E3	8.82E3	7.14E3	1.18E4	7.25E3	1.17E4
Ixy (kg-m ²)	2.19E2	2.19E2	5.38E2	5.38E2	-1.58E3	-1.39E3
Ixz (kg-m ²)	-2.00E2	-2.00E2	-7.01E1	-7.01E1	2.65E3	5.16E2
Iyz (kg-m ²)	7.90E3	4.22E3	6.02E3	2.13E3	5.62E3	1.35E3
MAX SLEW TORQUE (Nm)	11.09	13.09	6.45	8.46	6.23	8.27
MAX SLEW TIP DISPLACEMENT (mm)	32.37	5.84E-2	18.53	3.56E-2	17.27	3.35E-2
MAX TRACKING TORQUE (Nm)	----	----	----	----	----	----
MAX TRACKING TIP DISPLACEMENT (mm)	----	----	----	----	----	----
EMERGENCY STOP TIP DISPLACEMENT (mm)	5423.88	9.78	3102.79	5.96	2894.94	5.62
EMERGENCY STOP MAX BENDING MOMENT (Nm)	1668.14	1891.77	964.62	1188.25	901.62	1125.25
MAX TORQUE TIP DISPLACEMENT (mm)	145.99	2.23E-1	143.64	2.10E-1	138.75	2.03E-1
MAX TORQUE BENDING MOMENT (Nm)	44.90	43.17	44.65	41.91	43.21	40.64

P/OF SUPPORT STRUCTURES

Two concepts for a structure to support the P OF occulting plane were investigated. The baseline structure has been a deployable, central boom. We also considered an open, cylindrical, telescoping, outer truss structure.

The boom has the advantages of being lighter, more compact, and is similar to the boom used for the Solar Array Flight Experiment (SAFE) on the Space Shuttle. Its main disadvantage is that it is flexible, and therefore requires active control of vibration.

The telescoping cylinder is much stiffer than the boom, but is more massive, requires considerably more volume during transportation to the Station, is a new design, and is not well adapted to accommodating coronagraph type instruments. This chart summarizes the characteristics of each concept.

P/OF SUPPORT STRUCTURES

o DEPLOYABLE BOOM

- Length 50 meters
- Diameter 20 inches
- Canister Height 88 inches
- Canister Weight 87 lb
- Boom Drive Weight 30 lb
- Boom Weight 110 lb
- Footprint 23.5 inch diameter
- Bending Stiffness (EI) $8.8E7 \text{ lb-in}^2$
- Shear Stiffness (GA) $1.1E5 \text{ lb}$
- Torsional Stiffness (GJ) $5.5E6 \text{ lb-in}^2$
- Axial Stiffness (AE) $1.76E6 \text{ lbs/in}$
- Bending Moment Capacity 15500 lb-in (dbl laced)

o HOLLOW 3 + METER DIAMETER TRUSS

- Length 50 meters
- Number of telescoping sections 5
- Inside diameter 2.5 + meters
- Weight 450 lb
- Bending Stiffness (EI) $5.3E10 \text{ lb-in}^2$
- Bending Moment Capacity $2.7E7 \text{ lb-in}$
- Aluminum coated graphite epoxy structure
- Truss tubing 2 in. O.D., 0.0625 in. wall thickness
- Four longerons

P/OF ROTATING GRID ASSEMBLY

An improved version of the Fourier Transform Imager would use rotating masks. This is referred to as the Rotating Modulation Collimator. Corresponding grids in the upper mask and at the detector must be rotated in synchronization. Synchronization can be accomplished by driving stepper motors from the same source. An index sensor will provide initial collimation of the grids.

In order to rotate the mask it will be necessary to provide a holding fixture, a bearing assembly, and a drive mechanism.

The sketch shown is one of many design concepts that could be used to meet the rotational requirement.

The rotating mask assembly consists of:

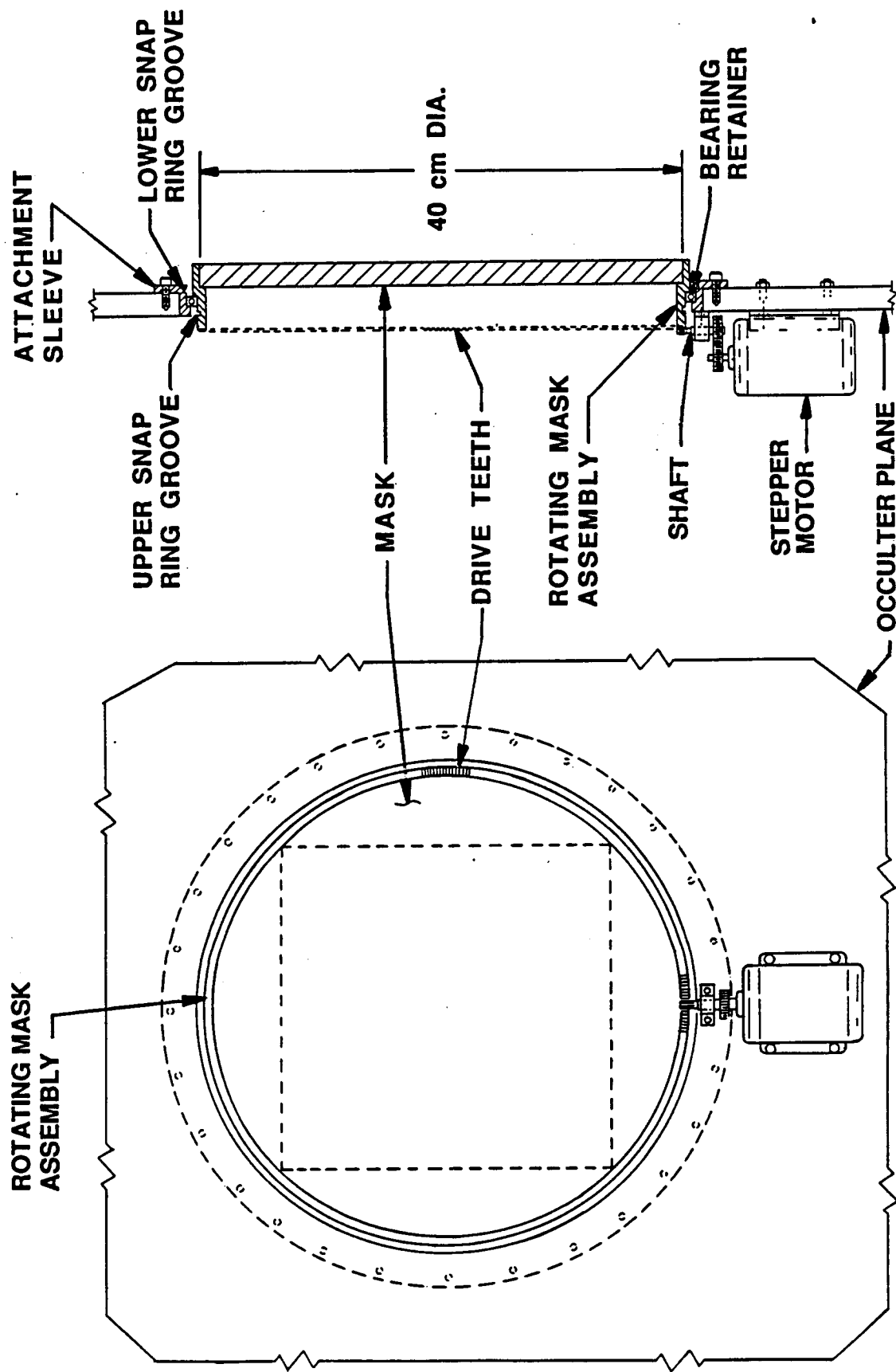
1. An attaching sleeve machined to take a press fit bearing assembly and snap ring. The sleeve would fit into and be fastened to the occulter plane.
2. The rotational portion of the mask assembly would be machined for a press fit inside the bearing assembly with a snap ring groove, a ring gear machined on the bottom for mating with the drive mechanism, and a ledge machined inside to support the mask.
3. The rotating mask is shown being driven by a stepping motor driving a spur gear.

Final selection of material would be made at a later date but plastics, ceramics, and composites look good for the gear assemblies and bearings.

Final selection of a stepping motor can be optimized when detailed design requirements are established. It would be possible to design a stepping motor that used the rotating mask assembly as the its rotor and have the stator windings located in fixed positions around the outside of the assembly. This approach would eliminate the need for a gear drive assembly.

The final design of the rotating mask assembly and drive mechanism should be one integrated unit. This would allow all final adjustments to be made prior to installation on the occulter plane and make changeout of units much simpler.

P/OF ROTATING GRID ASSEMBLY



NOTE: SNAP RINGS PROVIDED FOR POSITIVE RETENTION OF BEARING RETAINER

POINTING/STABILIZATION

SPACE STATION PPS/ASO STRUCTURAL RESPONSE ANALYSIS

The purpose of the pointing/stabilization study task was to identify options for meeting the pointing requirements of the ASO facilities, evaluate the capabilities and requirements of each option, and, if results warrant, develop a pointing and stabilization concept for ASO. The initial baseline pointing system was assumed to be the Space Station Payload Pointing System (PPS). Honeywell Space Systems Division, under subcontract to TBE, analyzed the performance capabilities, and potential additions/modifications, for the PPS and other pointing systems. To provide a disturbance model for their analysis, we obtained NASA Space Station NASTRAN models, and performed an analysis to identify base disturbances at the ASO facilities. This chart summarizes the model and resulting modes.

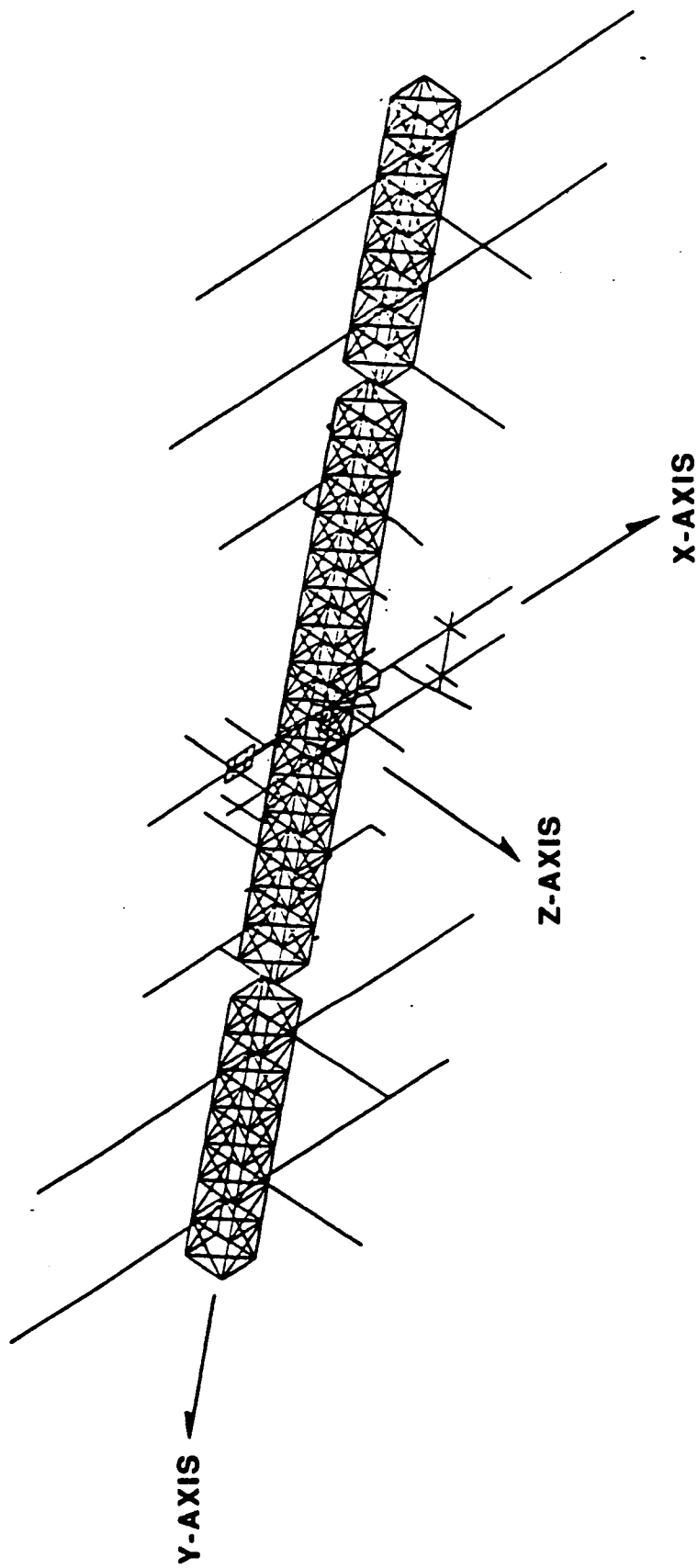
The following two charts illustrate the NASTRAN finite element model, and the Space Station configuration. Detailed NASTRAN results were provided to Honeywell for use in their analysis.

SPACE STATION PPS/ASO STRUCTURAL RESPONSE ANALYSIS

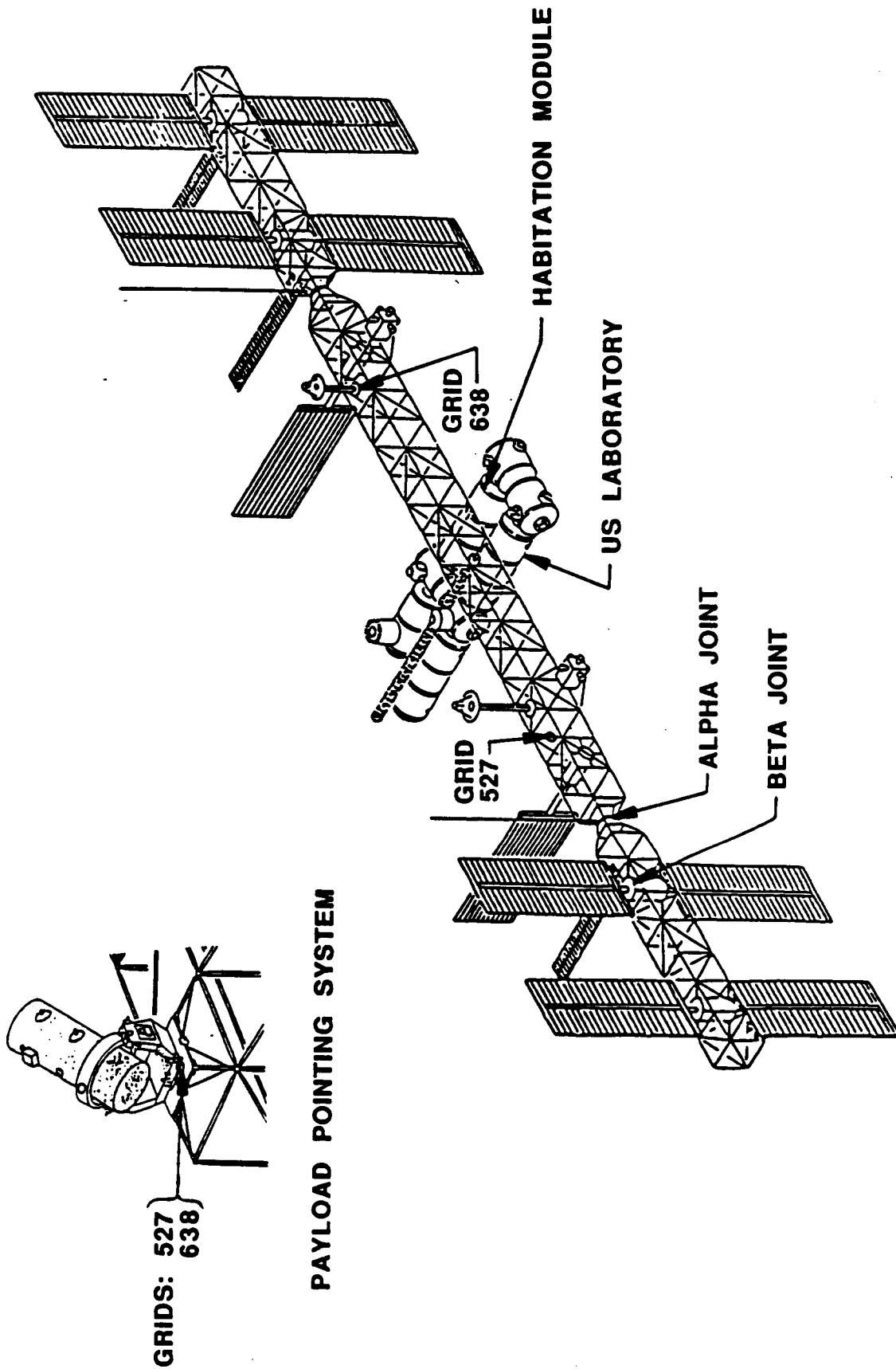
- NASTRAN FINITE ELEMENT MODEL
484 GRIDS 2,900 D.O.F.
- SELECTED OUTPUT AT 30 NODES
TWO PROPOSED PPS LOCATIONS AT GRIDS 527 AND 638
- OUTPUT:
 - 6 - RIGID BODY MODES
 - 172 - ELASTIC BODY MODES: .087 HZ - 5.60 HZ
- STRUCTURAL (TRUSS) MODES - 58 TOTAL
FIRST MODE Z - BENDING @ 0.16 HZ
- APPENDAGE MODES - 114 (MINIMUM)
- SIGNIFICANT PPS MODES (LARGE DISPLACEMENTS)

.28 HZ	.93 HZ
.34 HZ	1.41 HZ
.56 HZ	1.66 HZ
.58 HZ	2.65 HZ
.71 HZ	3.83 HZ
.85 HZ	4.15 HZ

**OF2 CONFIGURATION SPACE STATION
NASTRAN FINITE ELEMENT MODEL**



SPACE STATION



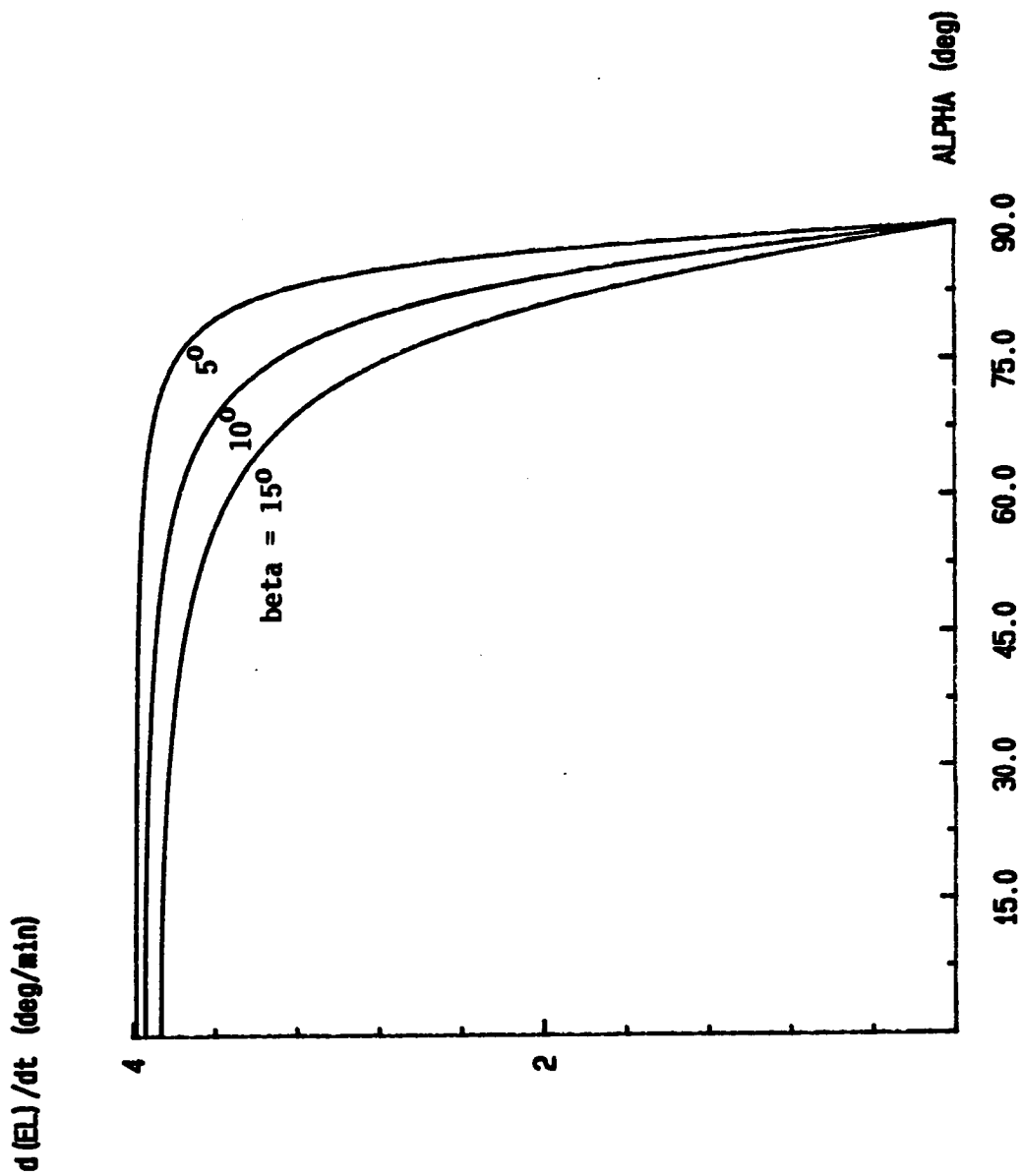
AZIMUTH/ELEVATION TRACKING

The Payload Pointing System (PPS) is a three axis gimbal system (azimuth, elevation, cross-elevation). The simplest method for tracking the sun is to use the azimuth axis to position the elevation axis parallel to the orbit normal, use the elevation gimbal to compensate for the orbit motion, and use cross-elevation to set the beta angle. Sun tracking is then a constant angular rate in elevation (about 4 degrees per minute), with fixed azimuth and cross-elevation.

Since the PPS is limited in cross-elevation to ± 15 degrees, this method of tracking can only be used for beta angles less than 15 degrees. At 28.5 degrees inclination, beta can be as large as 52 degrees.

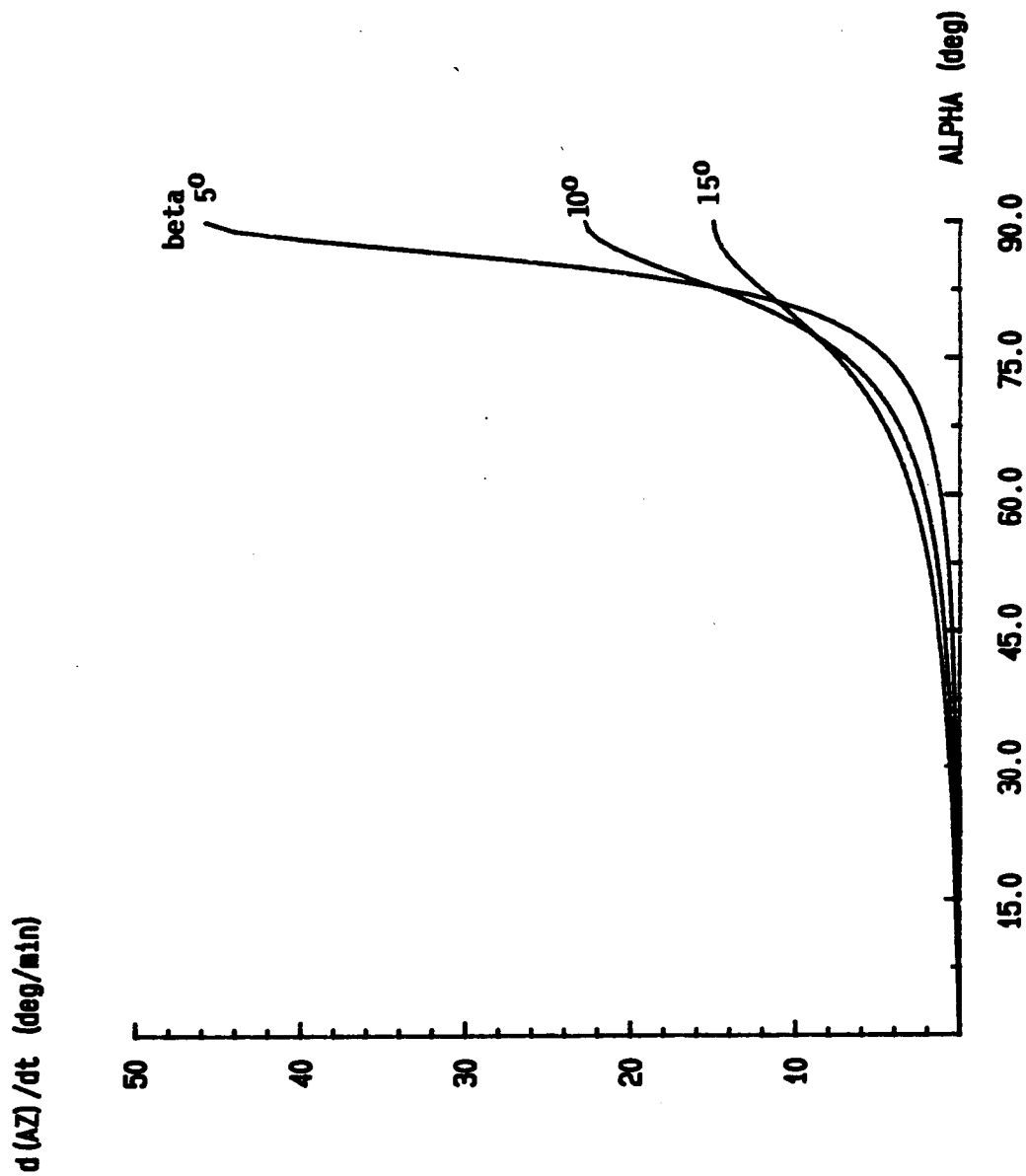
For larger beta, azimuth/elevation tracking must be used. Both the azimuth and elevation gimbals rotate at varying rates. These four charts show the angular rate requirements imposed on the azimuth and elevation gimbals. The angle alpha is a pitch angle (or orbit time angle) which is zero when the rising sun crosses the horizontal plane, 90 degrees at orbit noon, and 180 degrees when the setting sun crosses the horizontal (regardless of beta). Azimuth/elevation tracking cannot be used at low beta because very high azimuth rates and accelerations are required near orbit noon.

AZIMUTH/ELEVATION TRACKING ELEVATION RATE



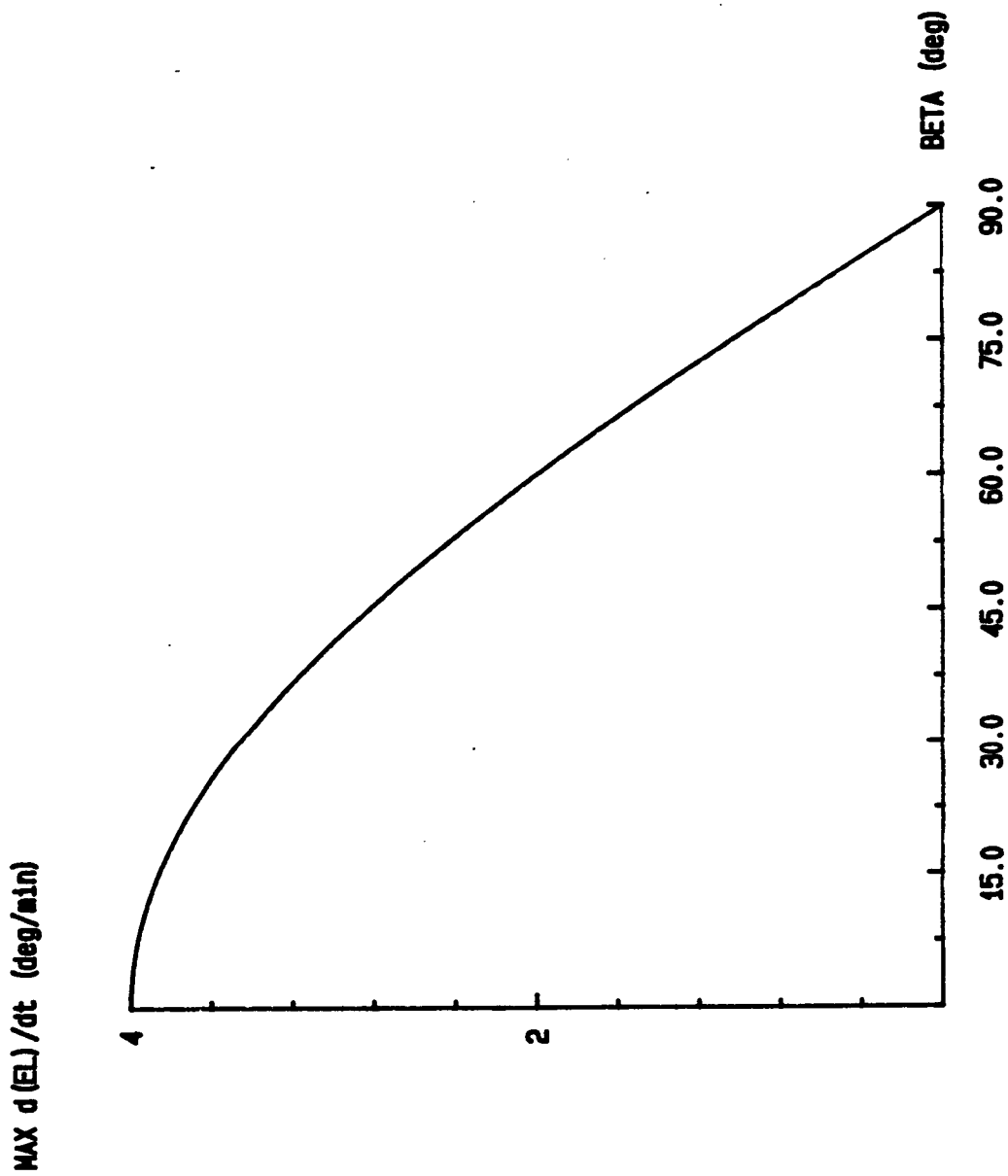
- Sun tracking
- 4 deg/min orbit rate (90 min. period) assumed

AZIMUTH/ELEVATION TRACKING AZIMUTH RATE



- Sun Tracking
- 4 deg/min orbit rate (90 min. period) assumed

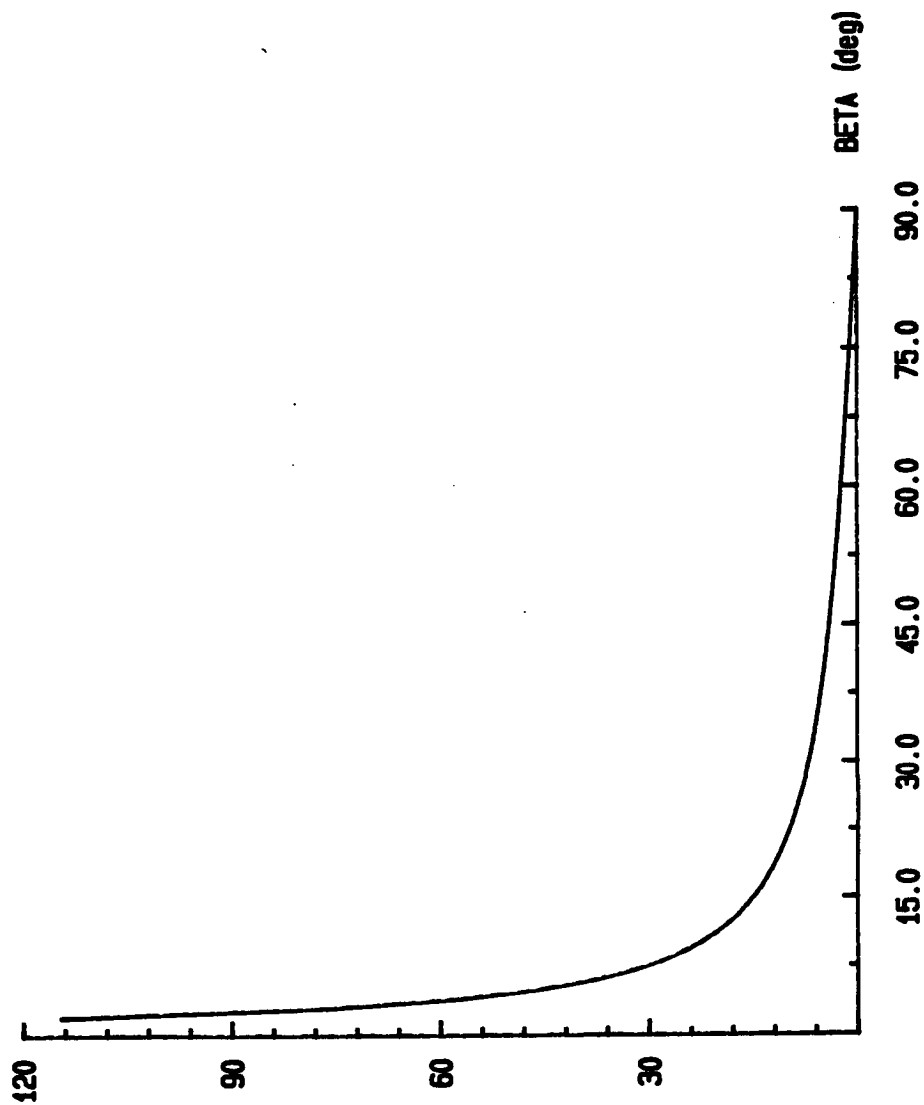
AZIMUTH/ELEVATION TRACKING MAXIMUM ELEVATION RATE



- Sun tracking
- 4 deg/min orbit rate (90 min. period) assumed

AZIMUTH/ELEVATION TRACKING MAXIMUM AZIMUTH RATE

MAX $d(AZ)/dt$ (deg/min)

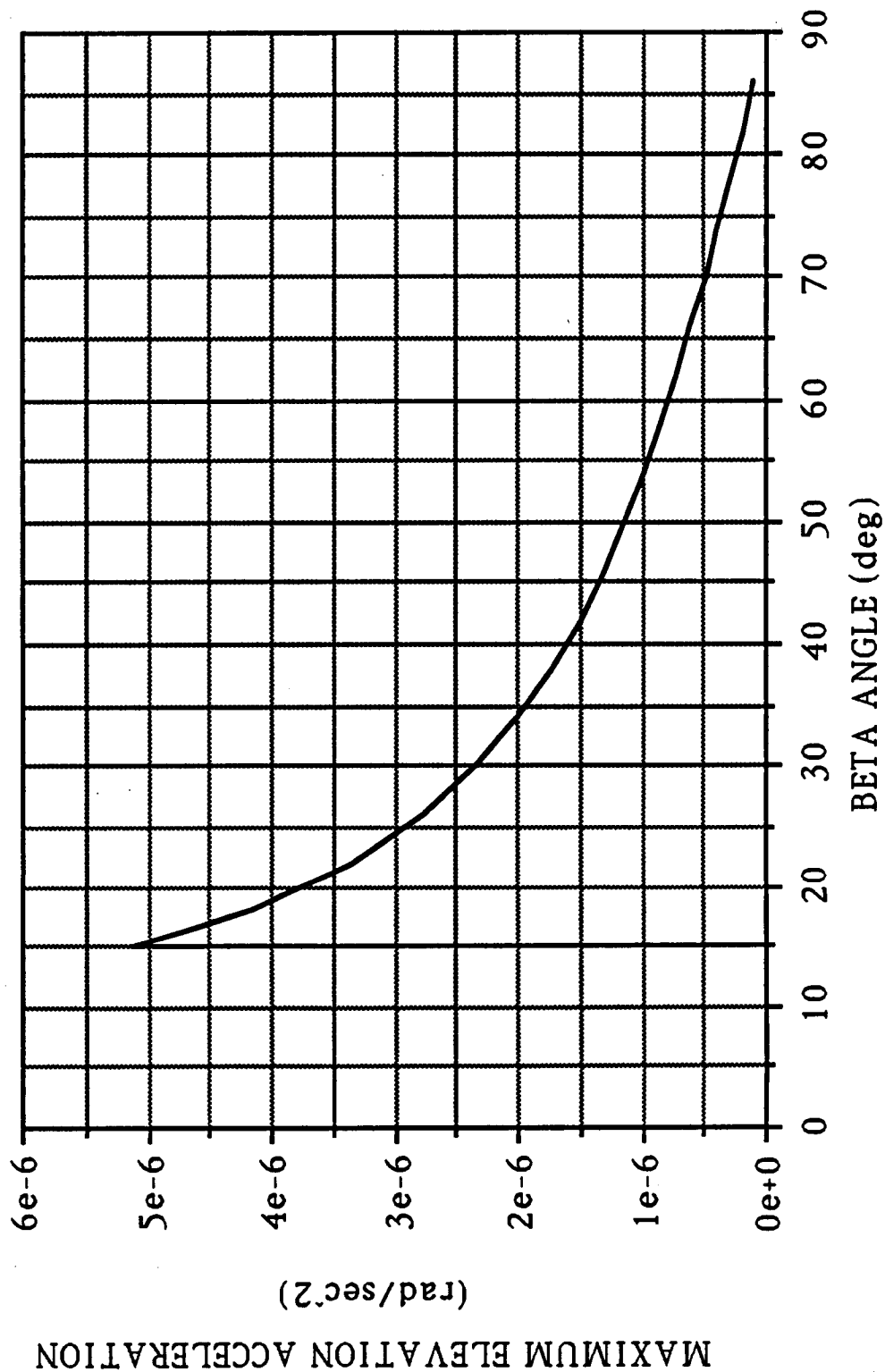


- Sun Tracking
- 4 deg/min. orbit rate (90 min. period) assumed

MAXIMUM ELEVATION ACCELERATION vs. BETA ANGLE

The elevation gimbal acceleration requirements shown in this chart assume that azimuth/elevation tracking is used for beta angles greater than 15 degrees, and elevation/cross-elevation tracking is used for smaller beta. The maximum beta angle possible for the 28.5 degree inclination Space Station orbit is 52 degrees.

MAXIMUM ELEVATION ACCELERATION vs. BETA ANGLE



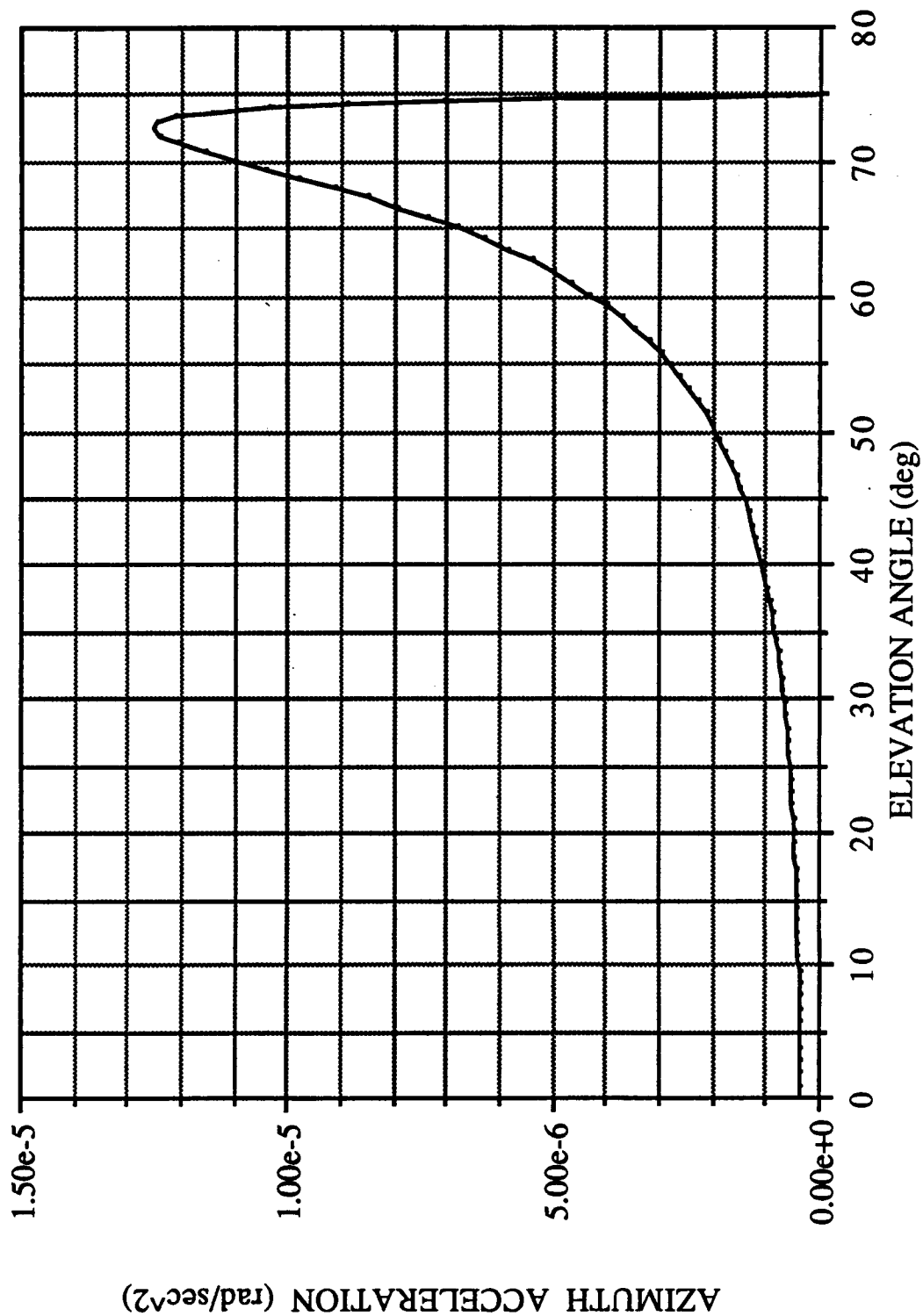
FOR PPS ASSUME ELEVATION-CROSS ELEVATION TRACKING FOR BETA < 15 deg.

AZIMUTH ACCELERATION vs. ELEVATION ANGLE

Maximum azimuth acceleration occurs for low beta angles. This chart shows the azimuth gimbal acceleration profile for 15 degree beta. For smaller beta angles, elevation/cross-elevation tracking would be used.

AZIMUTH ACCELERATION vs. ELEVATION ANGLE

ELEVATION-AZIMUTH TRACKING FOR BETA = 15 deg + epsilon

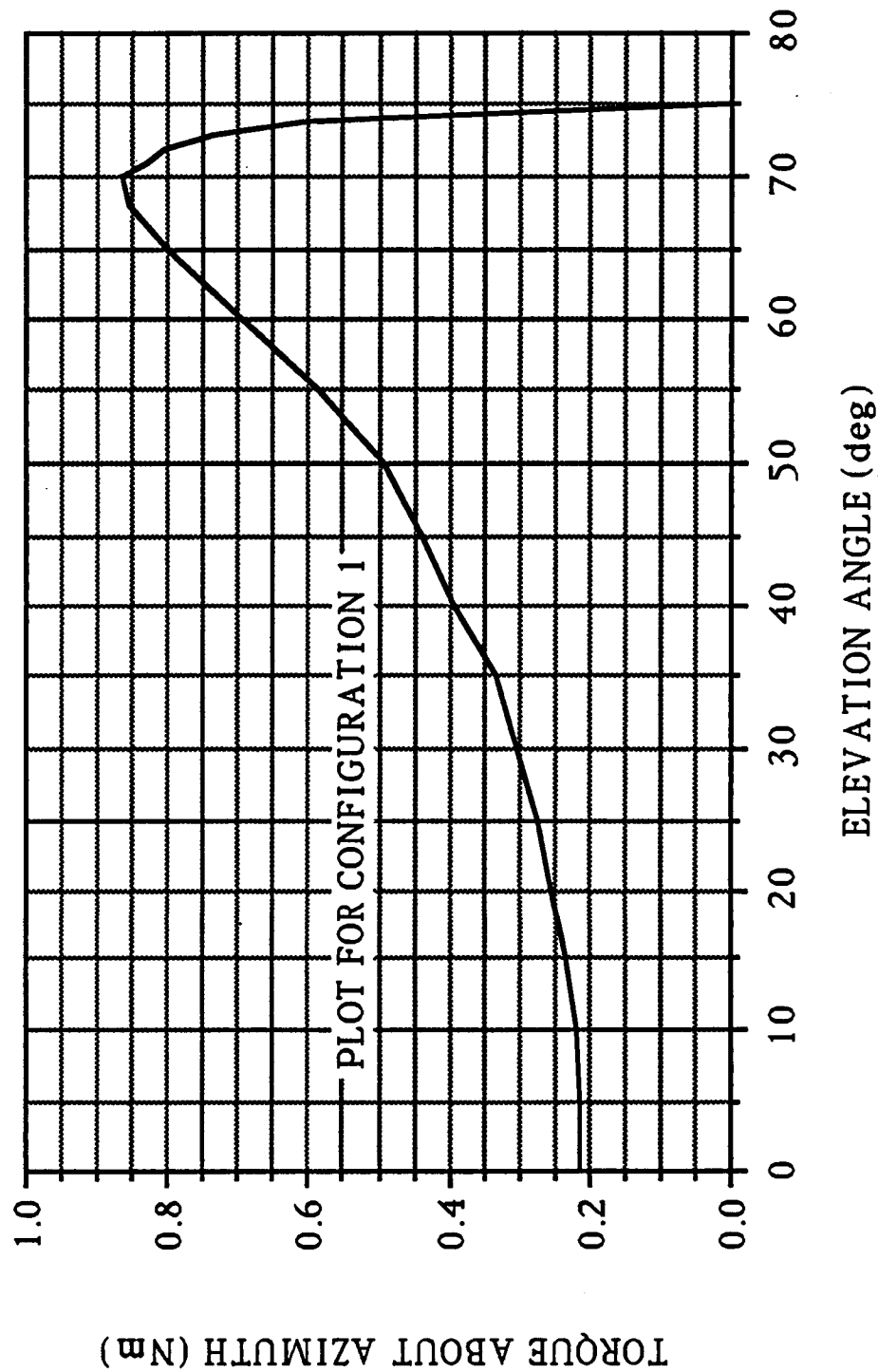


TYPICAL TORQUE ABOUT AZIMUTH vs. ELEVATION ANGLE

This chart shows a typical azimuth gimbal torque profile. This is not a worst case. For small beta, the elevation gimbal torque requirements are larger since the moment of inertia about the azimuth axis depends on beta (through the elevation angle), while the moment of inertia about the elevation axis remains constant.

TYPICAL TORQUE ABOUT AZIMUTH vs. ELEVATION ANGLE

ELEVATION-AZIMUTH TRACKING FOR $\text{BETA} = 15 \text{ deg} + \epsilon$



ASO POINTING STUDY

Honeywell, Space Systems Division, under subcontract, performed detailed simulations of pointing system performance. Various disturbance sources were incorporated using the Space Station dynamics previously described, into models of the pointing system. Variations of the pointing system models included magnetic suspension isolation, and passive vibration damping systems. The results are presented in the following Final Report.

ASO POINTING STUDY

FINAL REPORT

Honeywell, SSD

April 1989

THE ASO POINTING STUDY HAS CONCENTRATED ON ASO PAYLOADS REQUIRING PRECISION POINTING; THE PAYLOAD OCCULTER FACILITY (POF) AND THE HIGH RESOLUTION TELESCOPE CLUSTER (HRTC). DISTURBANCE SOURCE DESCRIPTION'S ARE THE SAME AS THOSE USED IN A RECENT JPL STUDY -

"SPACE SCIENCE/SPACE STATION ATTACHED PAYLOAD
POINTING ACCOMMODATION STUDY"

"POINTING PERFORMANCE ANALYSIS WHITE PAPER: - FEB 1988

MAJOR STUDY OBJECTIVES:

COMPARE POINTING PERFORMANCE (FOR THE HRTC AND POF PAYLOADS) OF SEVERAL SPACE STATION POINTING SYSTEM OPTIONS IN THE PRESENCE OF SPECIFIED SPACE STATION FLEXIBILITY AND DISTURBANCE SOURCES.

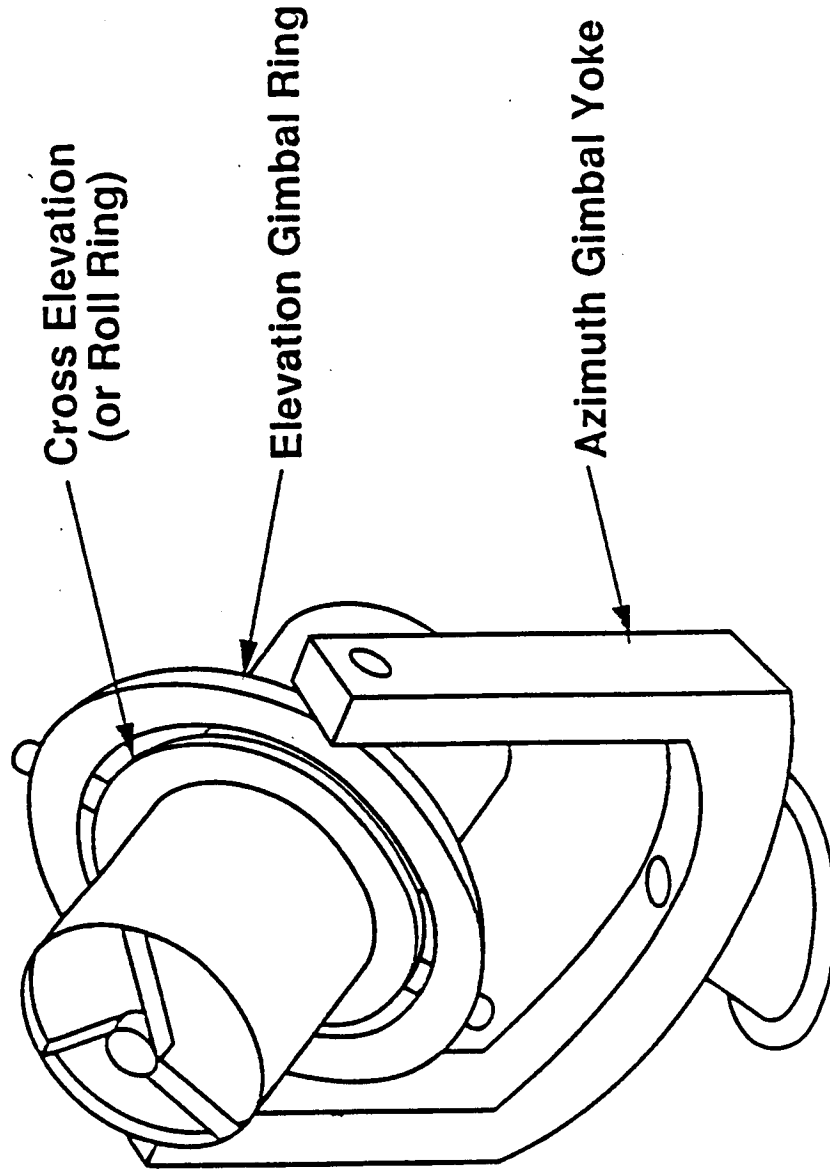
DEFINE RECOMMENDED POINTING SYSTEM IF STUDY RESULTS CLEARLY DEFINE A BEST TECHNOLOGY.

THE GIMBAL SYSTEM SHOWN, ILLUSTRATES THE AZ-EL-CROSS EL GIMBAL ARRANGEMENT OF THE SPACE STATION PPS. IN ADDITION, IT SHOWS THAT A PAYLOAD ROLL RING CAN BE MOUNTED INSIDE THE CROSS-ELEVATION GIMBAL IN ORDER TO PROVIDE ROLL CONTROL. HOWEVER, THE REPORTED STUDY DID NOT INCLUDE SUCH ROLL CONTROL IN THE GIMBAL MODEL

ASO Gimbal Configuration



SATELLITE SYSTEMS
DIVISION



Honeywell

M14167

CONFIGURATION OPTIONS:

- *PPS GIMBAL SYSTEM WITHOUT BASE ISOLATOR
- *PPS GIMBAL SYSTEM WITH BASE ISOLATOR -- 1HZ, 0.1HZ ISOLATORS
- *PPS GIMBAL SYSTEM PLUS VERNIER MAGNETIC POINTER
- *END MOUNTED POINTER WITHOUT BASE ISOLATOR
- *END MOUNTED POINTER WITH BASE ISOLATOR
- *END MOUNTED GIMBAL SYSTEM WITH VERNIER MAGNETIC POINTER

SEVERAL SIMULATION GIMBAL CONFIGURATIONS WERE EXAMINED DURING THE COARSE OF THE STUDY. THREE REPRESENTATIVE CASES ARE INCLUDED IN THIS REPORT. THROUGHOUT THE REMAINDER OF THE REPORT, CASES 1-3 REFER TO THE FOLLOWING GIMBAL ORIENTATIONS -- ILLUSTRATED IN THE OPPOSITE FIGURE.

* CASE 1: 50 DEGREE INCLINATION AT ORBIT NOON

* CASE 2: 5 DEGREE INCLINATION AT ORBIT DAWN

* CASE 3: 5 DEGREE INCLINATION AT ORBIT NOON

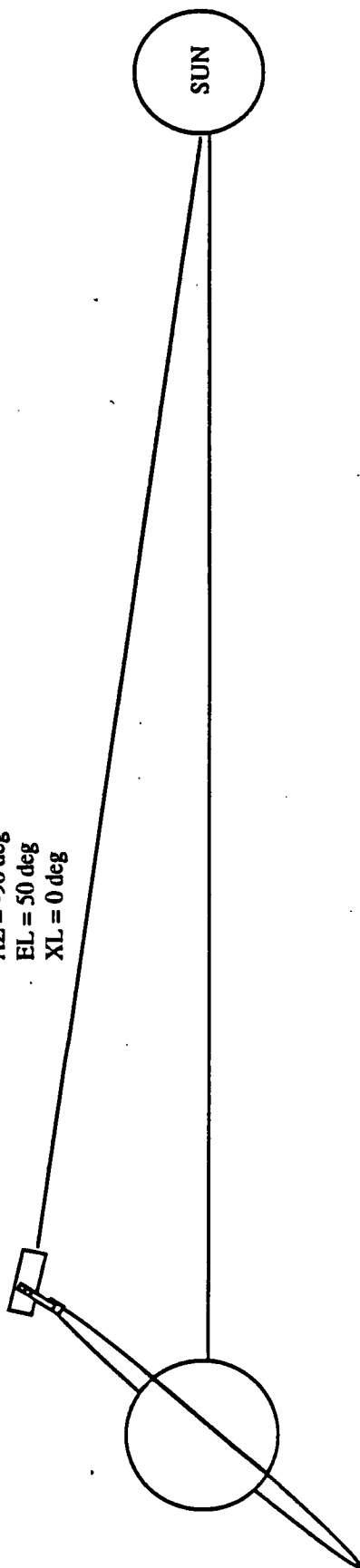
ASO SIMULATION CASE, POINTING ILLUSTRATION

Case 1: 50 degree inclination at orbit noon

AZ = -90 deg

EL = 50 deg

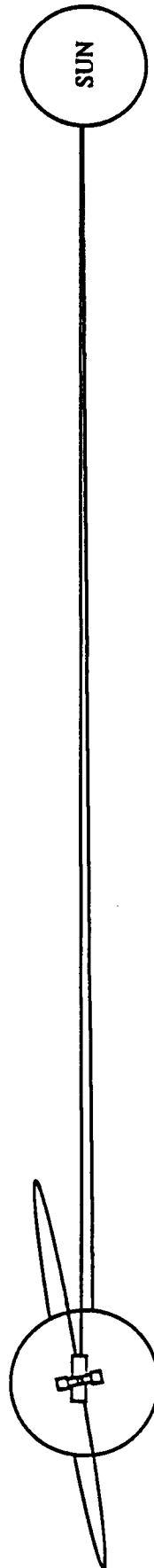
XL = 0 deg



Case 2, 3 Configuration used when inclination is less than 10 degrees

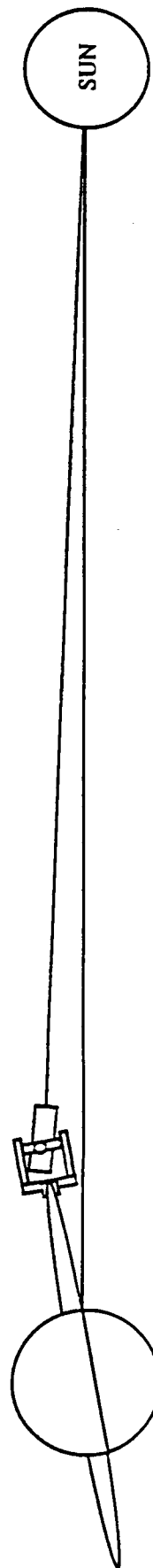
Case 2: 5 degree inclination orbit dawn

AZ = 0 deg; EL = 90 deg; XL = 5 deg



Case 3: 5 degree inclination at orbit noon

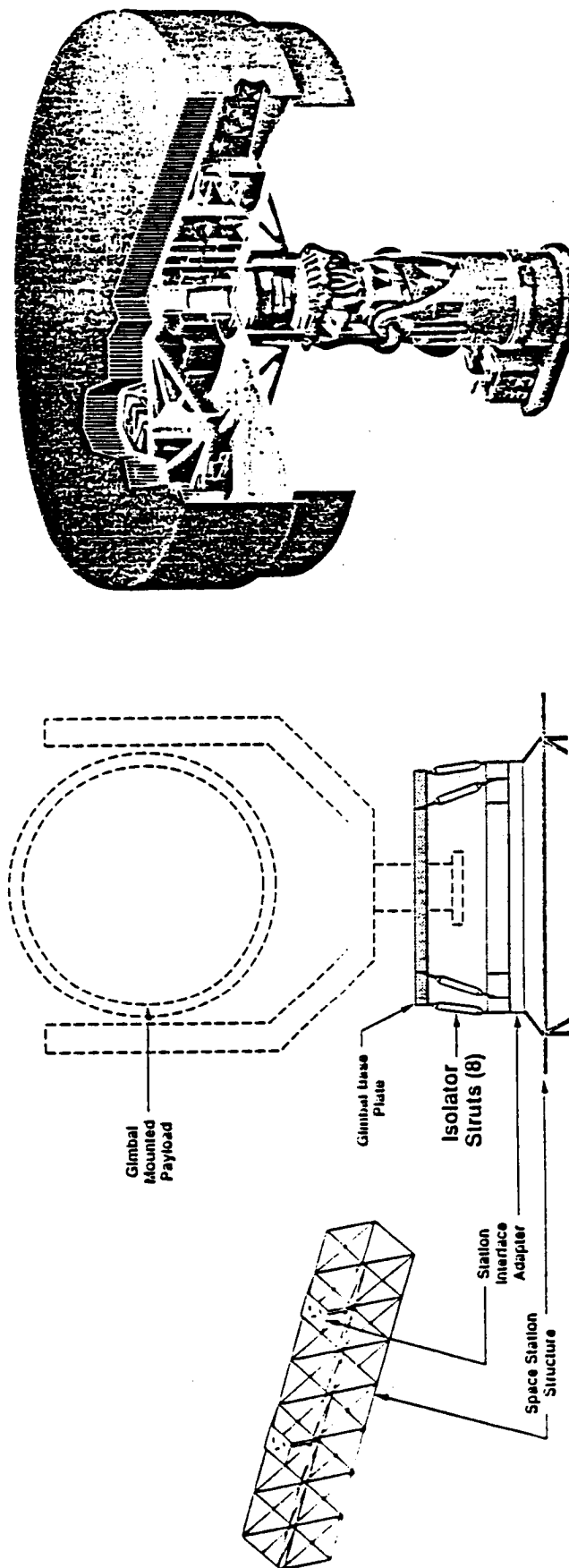
AZ = 0 deg; EL = 0 deg; XL = 5 deg



THE MODEL DESCRIPTIONS ARE BROKEN INTO TWO SECTIONS:

1. ASO/PPS MODEL WITHOUT MAGNETIC SUSPENSION

2. ASO/PPS MODEL WITH MAGNETIC SUSPENSION

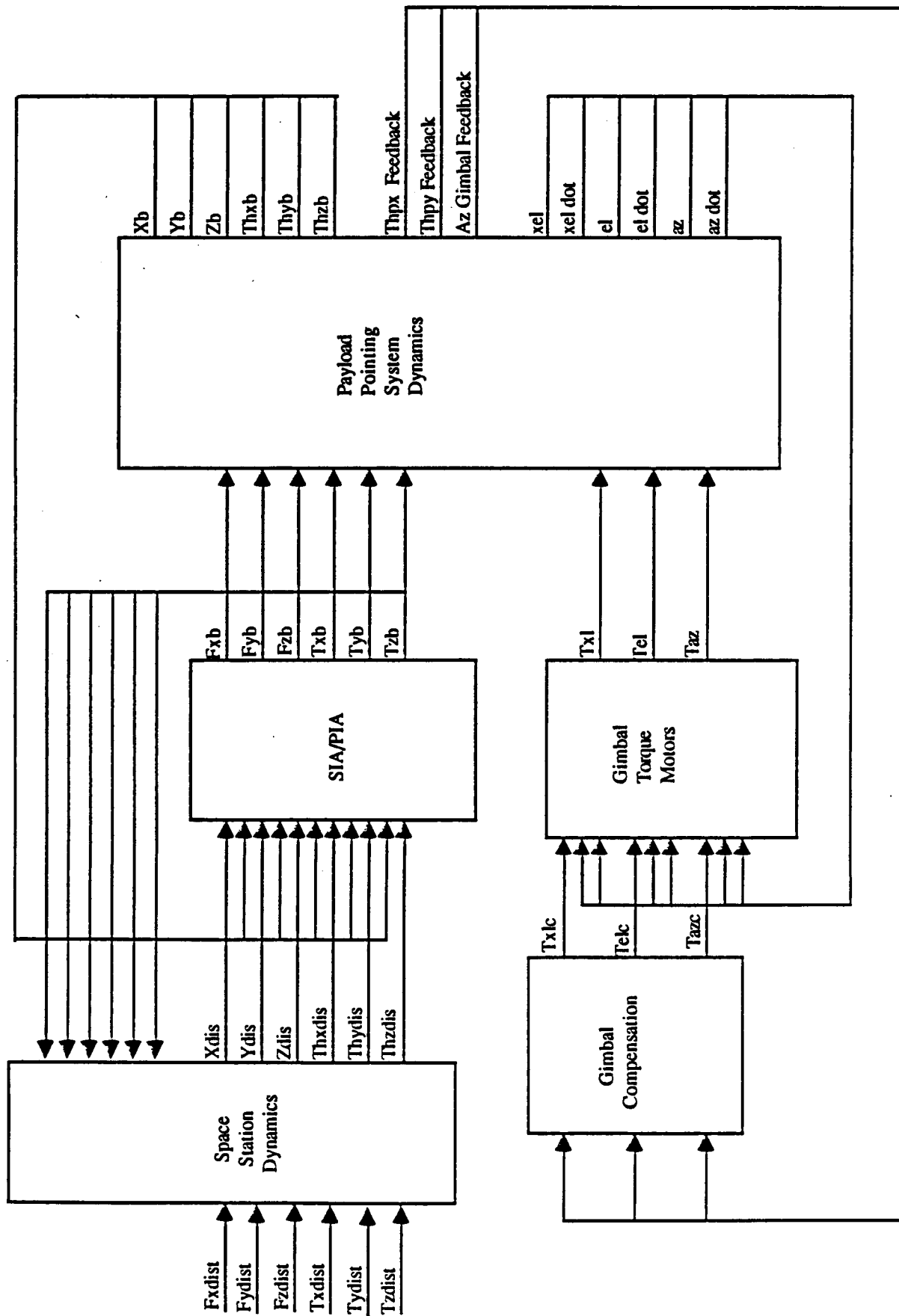


REFER TO THE FOLLOWING ASO MODEL BLOCK DIAGRAM:

SPACE STATION DISTURBANCES (TREADMILL, DOCKING, PUSHOFF AND CENTRIFUGE ASSUMED FOR THIS STUDY), RESULT IN MOTIONS AT THE PPS MOUNTING NODE. THESE MOTIONS ARE DEFINED BY THE SPACE STATION DYNAMICS. THE SPACE STATION DYNAMICS MODEL IS DERIVED FROM NASTRAN DATA PROVIDED BY TELEDYNE BROWN ENGINEERING (TBE). OF THE 196 MODES FROM 0 TO 5.5 HZ SUPPLIED BY TBE, 32 OF THE MOST SIGNIFICANT MODES WERE INCLUDED IN THE MODEL. THESE MODES ARE RESPONSIBLE FOR THE DOMINANT EFFECTS OF THE DISTURBANCES TO BE STUDIED. THE MODE TRUNCATION HAS ALLOWED THE STUDY TO BE CONDUCTED WITHOUT EXPENDING EXCESS COMPUTER TIME EVALUATING EFFECTS OF INSIGNIFICANT MODES.

THE RESULTANT SPACE STATION MOTION AT THE PPS NODE IS INTRODUCED AS A BASE DISTURBANCE TO THE PPS VIA THE SIA/PIA.

ASO MODEL BLOCK DIAGRAM WITHOUT MAGNETIC SUSPENSION



SIGNIFICANT MODAL FREQUENCIES USED IN ASO STUDY

FREQ (hz)	FREQ(rps)	MODE #	FILE ID
0.0	0.0	1	ASO.F06
0.0	0.0	2	ASO.F06
0.0	0.0	3	ASO.F06
0.0	0.0	4	ASO.F06
0.0	0.0	5	ASO.F06
0.0	0.0	6	ASO.F06
0.0	0.0	8	ASO.F06
0.088	0.553	10	ASO.F06
0.094	0.591	12	ASO.F06
0.097	0.609	18	ASO.F06
0.099	0.628	34	ASO.F06
0.102	0.641	36	ASO.F06
0.110	0.691	37	ASO.F06
0.159	0.999	38	ASO.F06
0.174	1.093	39	ASO.F06
0.280	1.759	40	ASO.F06
0.340	2.136	41	ASO.F06
0.450	2.827	1	ASO.F56
0.560	3.519	2	ASO.F56
0.580	3.644	26	ASO.F56
0.660	4.147	29	ASO.F56
0.710	4.461	32	ASO.F56
0.850	5.341	33	ASO.F56
0.930	5.843	34	ASO.F56
1.170	7.351	35	ASO.F56
1.410	8.859	36	ASO.F56
1.460	9.174	42	ASO.F56
1.660	10.43	29	ASO.F96
2.140	13.45	34	ASO.F96
2.650	16.65	3	ASO.F35
3.59	22.56	6	ASO.F35
3.83	24.07	9	ASO.F35
4.15	26.08		

THE INTERFACE ADAPTOR (SIAPIA) IS MODELED AS A PASSIVE SPRING DAMPER. THREE INTERFACES WERE ASSUMED FOR THE ASO STUDY.

1. 4.5 HZ INTERFACE WITH Q OF 50

2. 1 HZ INTERFACE WITH Q OF 1

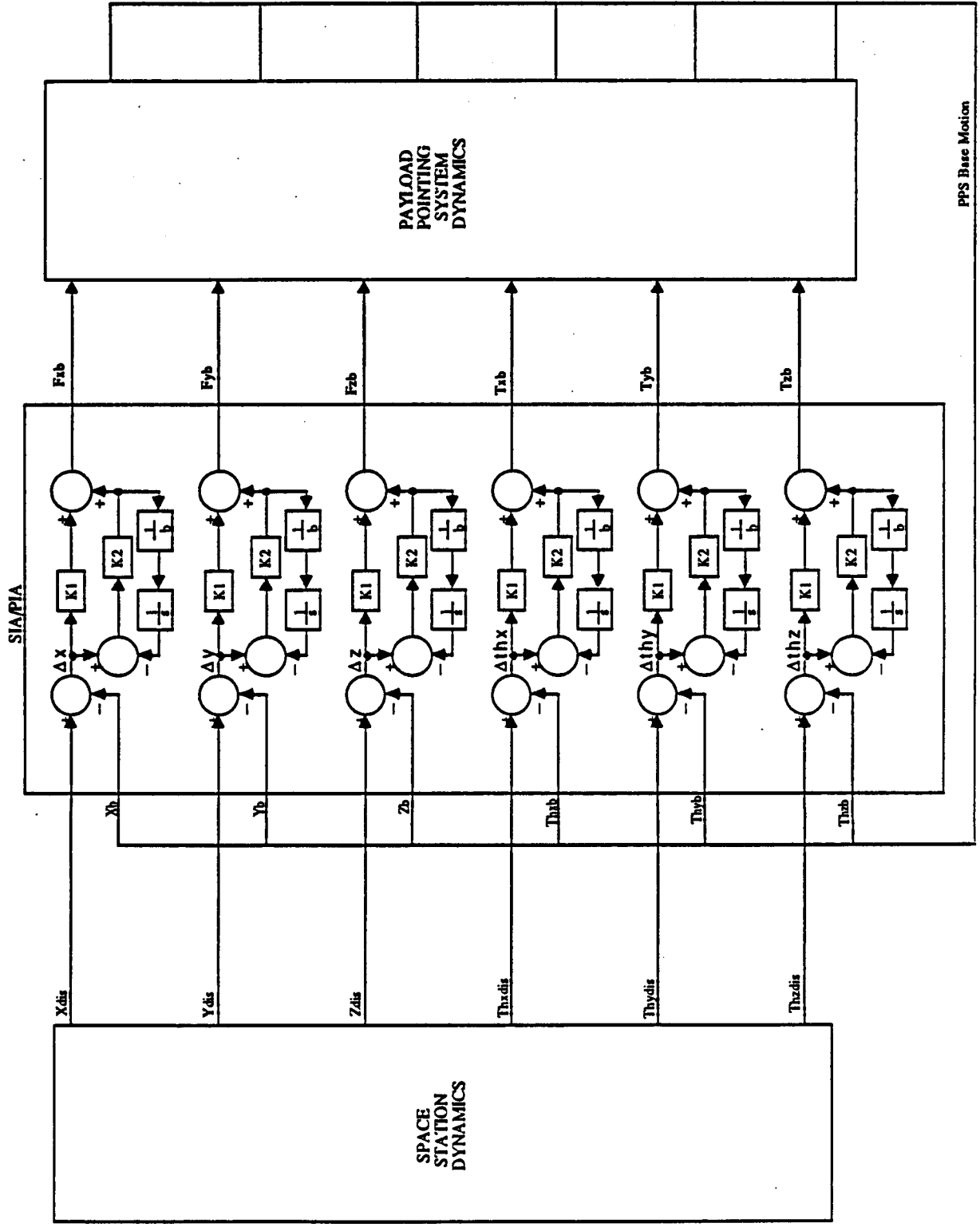
3. 0.1 HZ INTERFACE WITH A Q OF 0.5

THE FOLLOWING FIGURES ILLUSTRATE A CONCEPTUAL INTERFACE, THE SIAPIA MODEL BLOCK DIAGRAM, AND PASSIVE DAMPER CHARACTERISTICS.

IN THE FACING BLOCK DIAGRAM X_{dis} , Y_{dis} --- TH_{dis} , ETC. REFER TO THE SPACE STATION SIA/PIA ATTACHMENT NODE MOTION. X_b , Y_b --- TH_{xb} , ETC. ARE THE CORRESPONDING COMPONENTS OF POINTING SYSTEM MOTION WHILE F_{xb} , F_{yb} --- T_{xb} , ETC. REPRESENT THE INTERFACE FORCES AND TORQUES APPLIED TO THE POINTING SYSTEM.

THESE FORCES AND TORQUES ARE ALSO, OF COURSE, APPLIED TO THE SPACE STATION MODE. HOWEVER, INCLUDING THE REACTION EFFECTS ON THE SPACE STATION MODE SIGNIFICANTLY INCREASES SIMULATION RUN TIME AND, AT THE SAME TIME, HAS LITTLE IMPACT ON POINTING PERFORMANCE. THUS, FOR MOST OF THE DISTURBANCE RUN RESULTS PRESENTED IN THIS REPORT, THESE REACTION FORCES AND TORQUES WERE NOT INCLUDED.

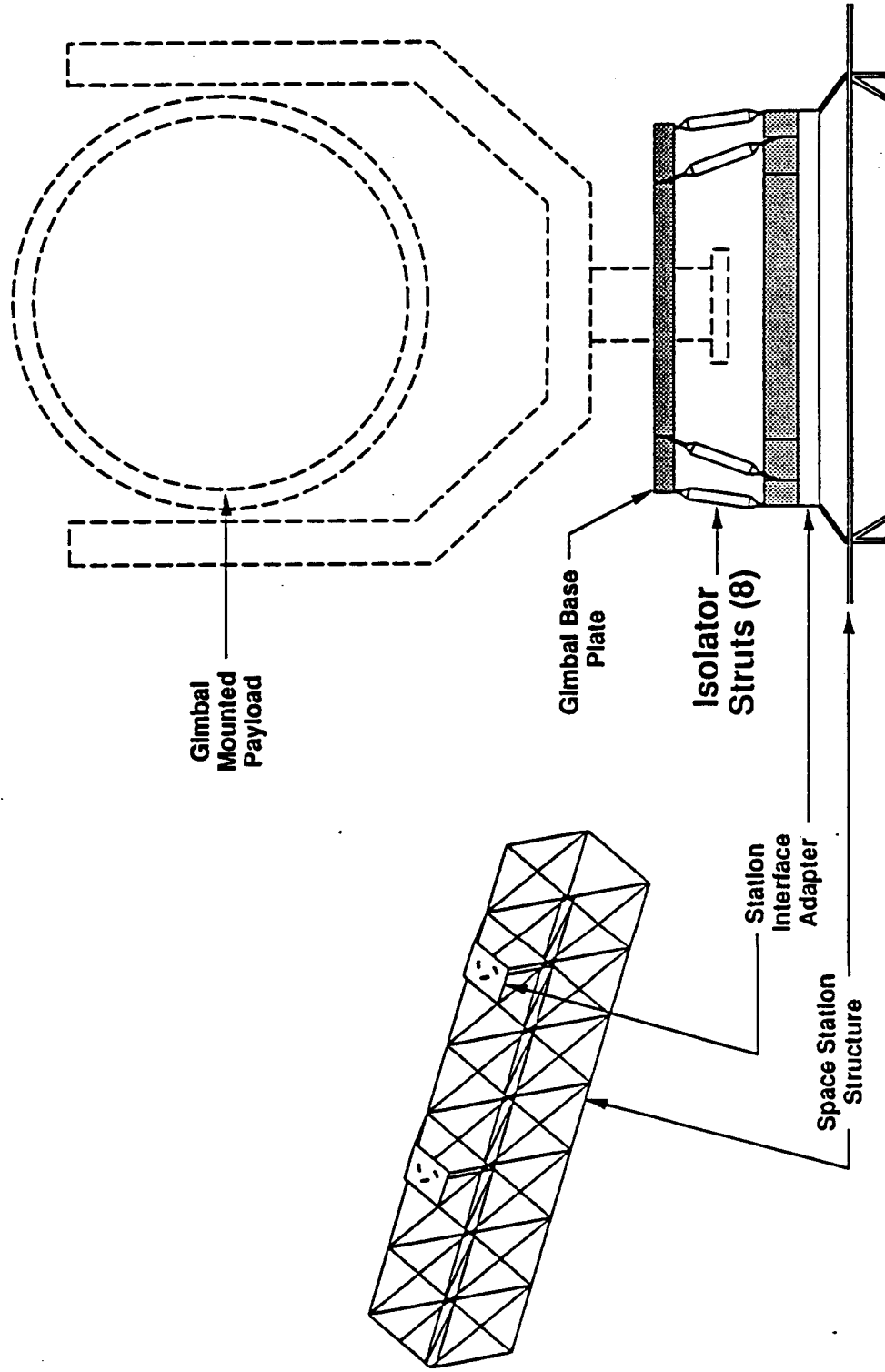
ASO SIA/PIA DYNAMICS BLOCK DIAGRAM



Passive Isolation of Space Station Attached Payload Pointing System



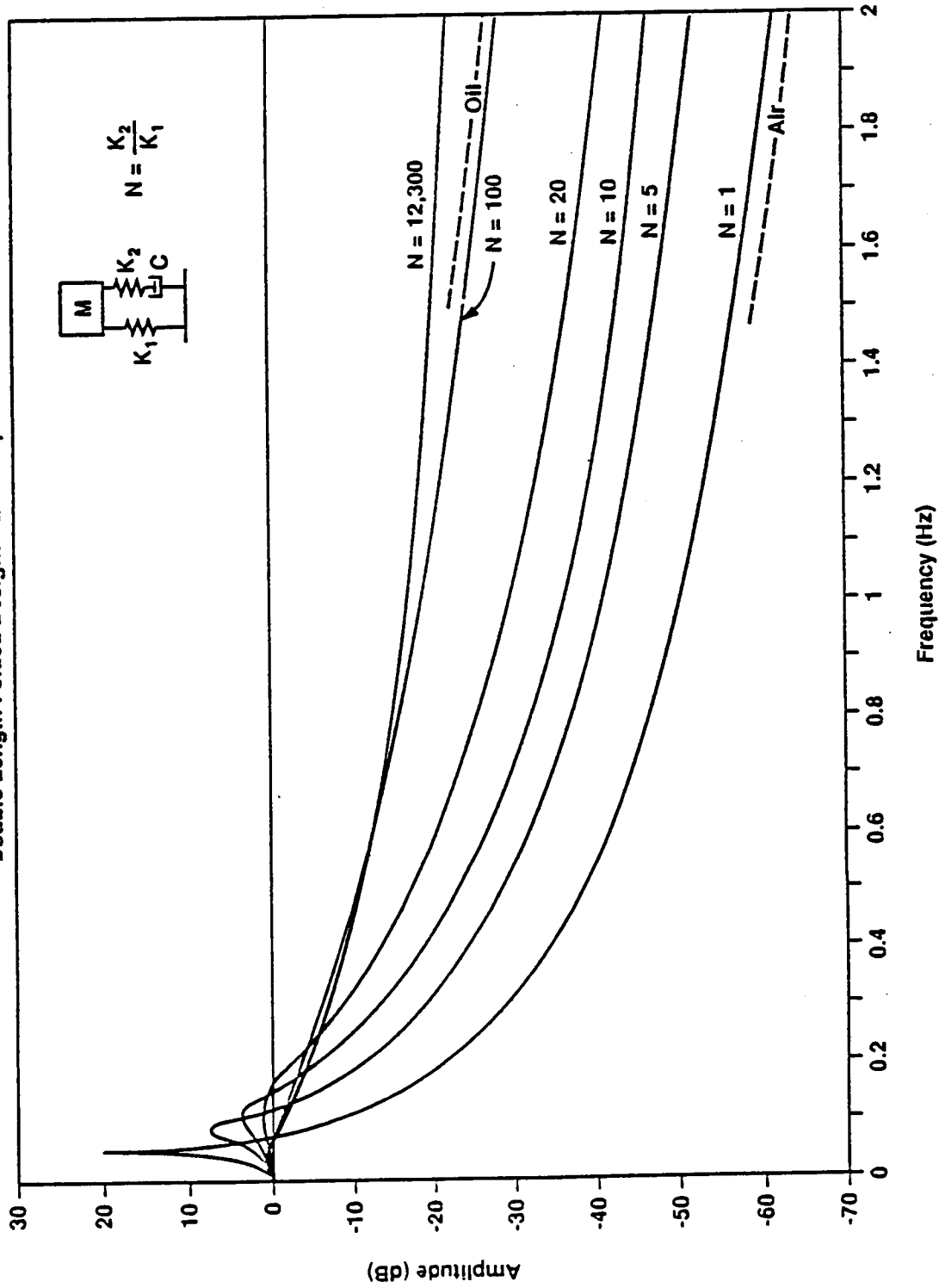
SATELLITE SYSTEMS
DIVISION



Isolator Transfer Function

SATELLITE SYSTEMS
DIVISION

Double Length Folded Design: $Q = 0.26$, $C = 3.4$



Honeywell

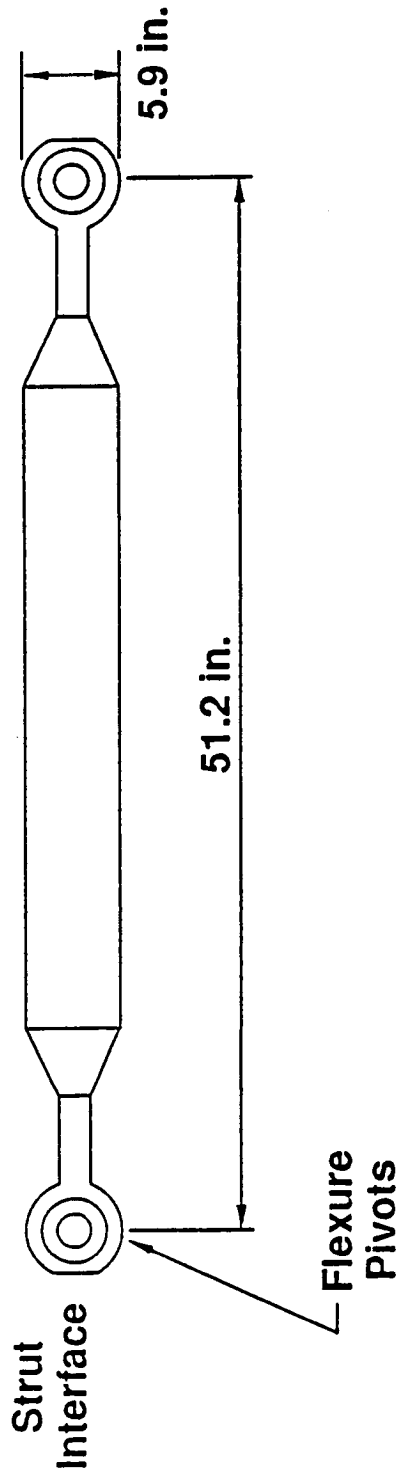
M135124

PPS Strut Specifications

Derived From JPL Requirements



SATELLITE SYSTEMS
DIVISION



Break Frequency	<0.05 Hz
Stroke	±3.15 in.
Effective Mass Load	~3000 lb
Damping	3.4 lb/(in./s)
Stiction	Minimize
Life	>10 years
Linear Performance in μ in. range	

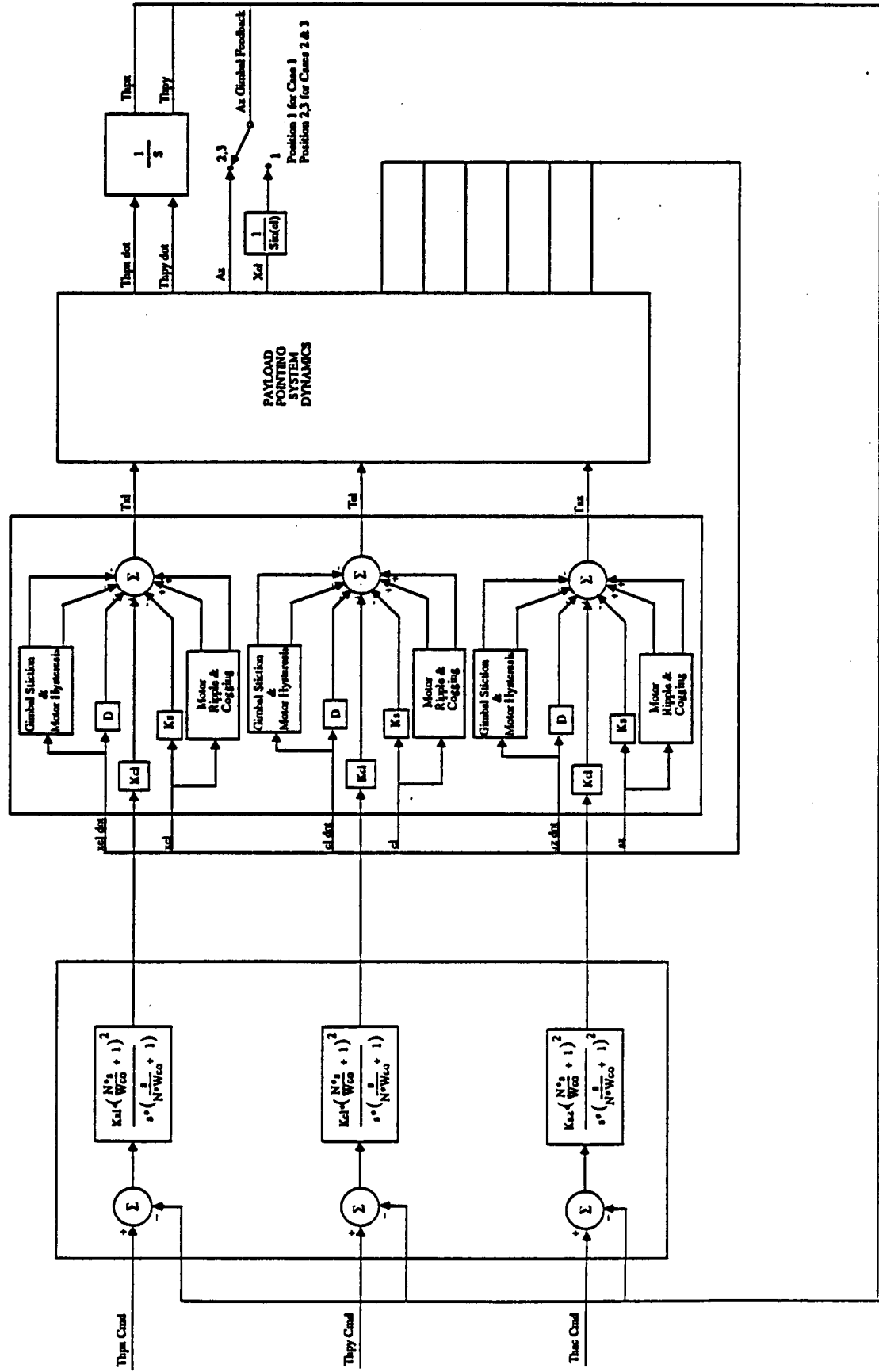
THE COMPENSATION AND TORQUE MOTOR ARE MODELED AS ILLUSTRATED IN THE OPPOSITE FIGURE.

THE POINTING CONTROL COMPENSATIONS CONSIST OF AN INTEGRATOR, A DOUBLE LEAD AND A LAG. THE POINTING CONTROL BANDWIDTHS WERE SELECTED AT 0.5 HZ.

THE AZIMUTH GIMBAL IS USED TO PERFORM ONE OF TWO FUNCTIONS DEPENDING ON THE ORIENTATION OF THE GIMBALS. IF THE INCLINATION IS LESS THAN 10 DEGREES, IT OPERATES IN AN ISOLATION MODE, WHERE THE RELATIVE MOTION OF THE AZIMUTH GIMBAL ANGLE IS CONTROLLED BY CLOSING A CONTROL LOOP ON RELATIVE AZIMUTH GIMBAL MOTION HAVING A MODEST CONTROL BANDWIDTH (0.1 HZ). WHEN THE INCLINATION ANGLE IS GREATER THAN 10 DEGREES, THE AZIMUTH GIMBAL ACTS TO NULL THE CROSS-ELEVATION GIMBAL ANGLE OR TO PRODUCE A SMALL LOW RATE CROSS-ELEVATION MOTION TO MINIMIZE STICKION EFFECTS. THE CONTROL BANDWIDTH IN THIS CASE IS ALSO 0.1 HZ.

THE TORQUE MOTOR MODEL INCLUDES SEVERAL NONLINEARITIES SUCH AS MOTOR HYSTERESIS, GIMBAL STICKION (DAHL MODEL), MOTOR COGGING AND MOTOR RIPPLE. THE TORQUE MOTOR MODEL ALSO INCLUDES LINEAR TERMS FOR SHUNT STIFFNESS (DUE TO HARNESS INTERFACES), AND VISCOUS DAMPING.

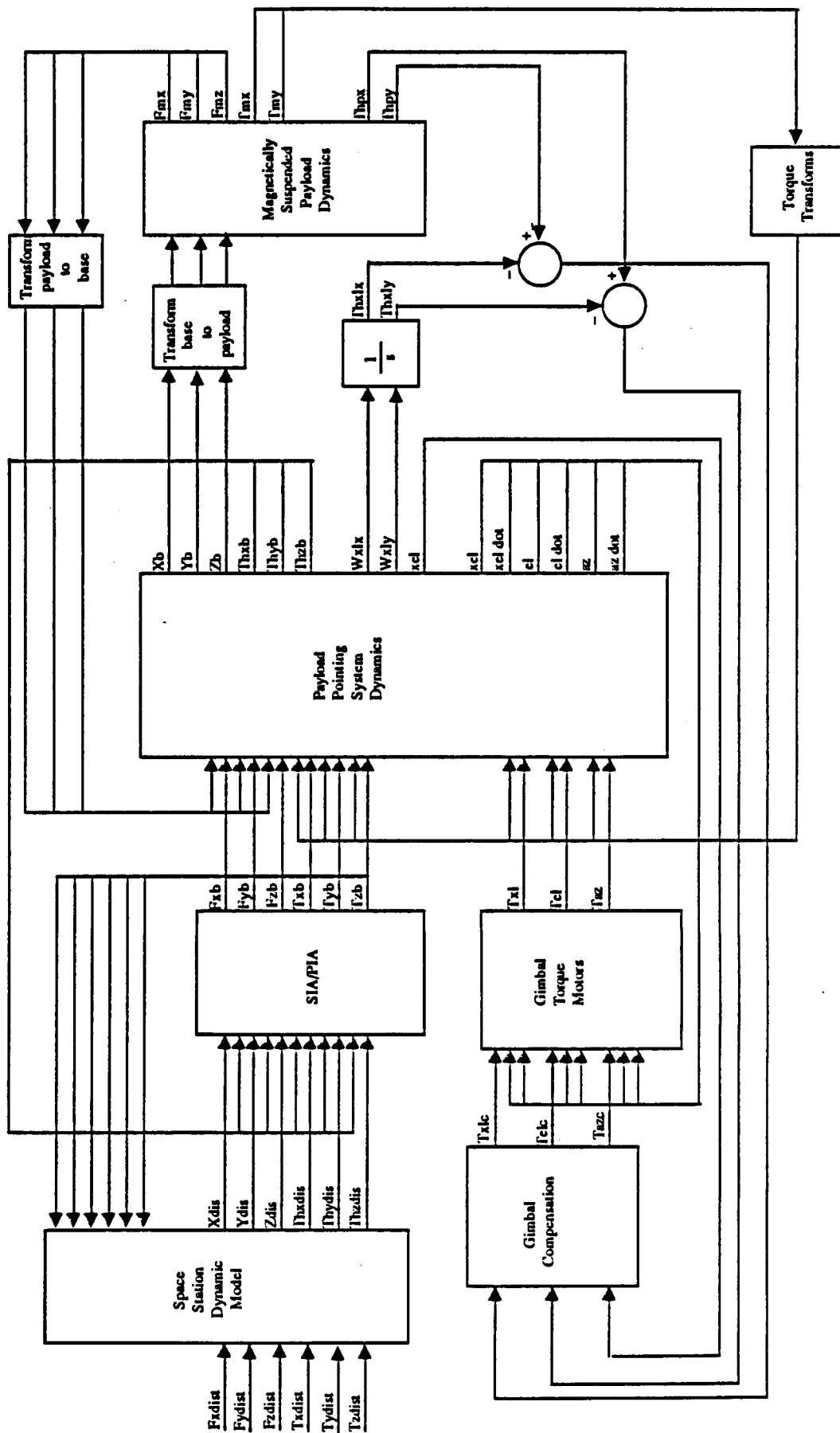
ASO CONTROL COMPENSATION AND TORQUE MOTOR BLOCK DIAGRAMS



THE ASO BLOCK DIAGRAM WITH MAGNETIC SUSPENSION IS SHOWN IN THE FOLLOWING FIGURE.

THE MAJOR BLOCKS OF THIS THIS SYSTEM HAVE THE SAME FORM AS THOSE OF THE MODEL WITHOUT MAGNETIC SUSPENSION, WITH THE OBVIOUS ADDITION OF THE MAGNETIC SUSPENSION DYNAMICS, WHICH INCLUDES THE PAYLOAD DYNAMICS, CONTROL COMPENSATIONS AND SUSPENSION TRANSFORMATIONS. ALSO NOTE THAT THE CROSS ELEVATION AND ELEVATION GIMBALS ARE OPERATING IN A FOLLOW-UP MODE. IN THIS CONFIGURATION, THE MAGNETIC SUSPENSION PROVIDES TRANSLATIONAL ISOLATION AND VERNIER POINTING. THE FOLLOW-UP GIMBALS ENABLE THE PAYLOAD TO REALIZE LARGE ANGULAR MOTIONS WHILE OPERATING IN RELATIVELY SMALL MAGNETIC GAPS.

ASO MODEL BLOCK DIAGRAM WITH MAGNETIC SUSPENSION

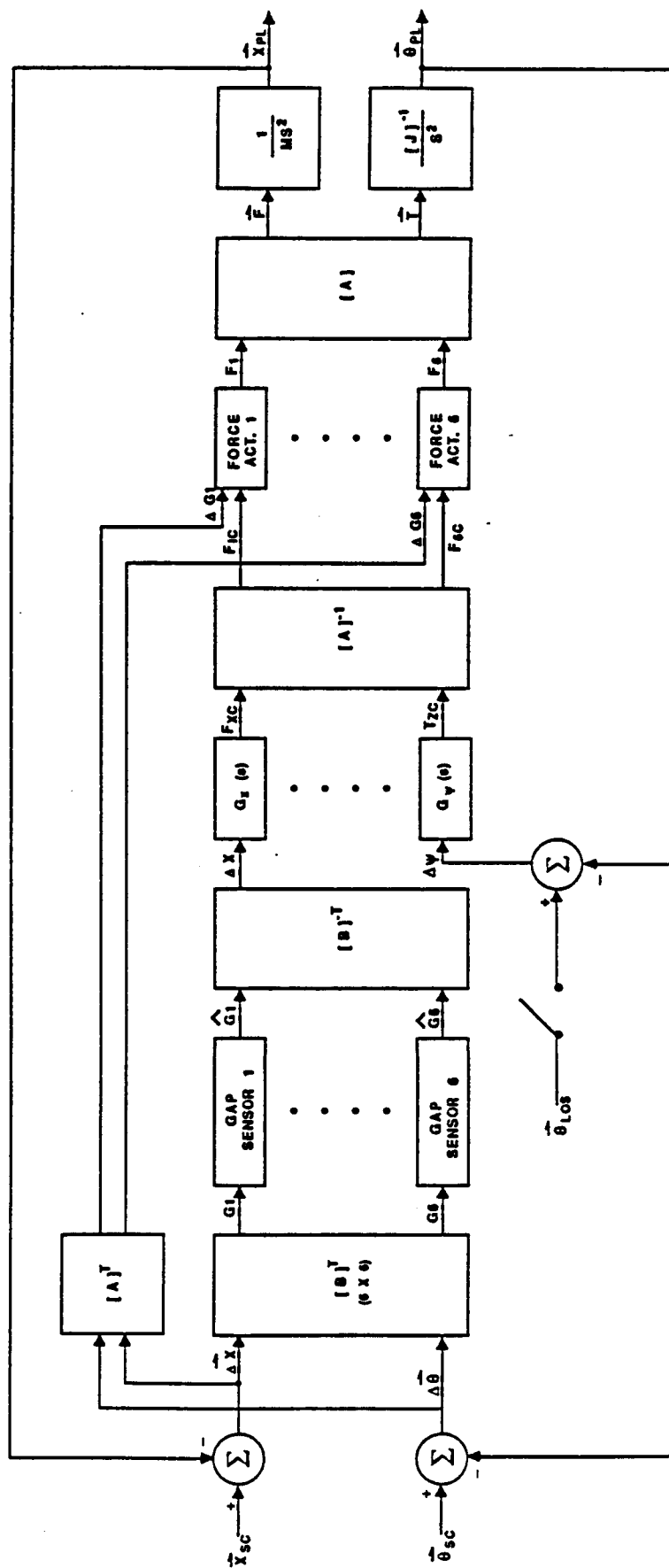


MAGNETIC POINTING & ISOLATION CONTROL



SPACESYSTEMS
GROUP

SATELLITE SYSTEMS
DIVISION



SENSOR
GEOMETRY

SENSORS

ISOLATION CONTROL LAW
(ELECTRONICS / SOFTWARE)

MAGNETIC
ACTUATORS

PAYLOAD
DYNAMICS

$$[B] = \begin{bmatrix} \hat{g}_1 \\ \vdots \\ \hat{g}_6 \end{bmatrix} \quad J = 1:6 \quad [A] = \begin{bmatrix} \hat{f}_1 \\ \vdots \\ \hat{f}_6 \end{bmatrix} \quad J = 1:6$$

Honeywell

M094746

THE FOLLOWING CHART COMPARES PASSIVE MECHANICAL AND ACTIVE MAGNETIC ISOLATION RESPONSES. WHEN DISTURBANCE FREQUENCIES ARE PREDOMINANTLY BEYOND THE ISOLATION BANDWIDTHS, A MAGNETIC ISOLATION SYSTEM WILL REDUCE THEIR EFFECTS MUCH QUICKER DUE TO THE RAPID ROLL-OFF CHARACTERISTICS.

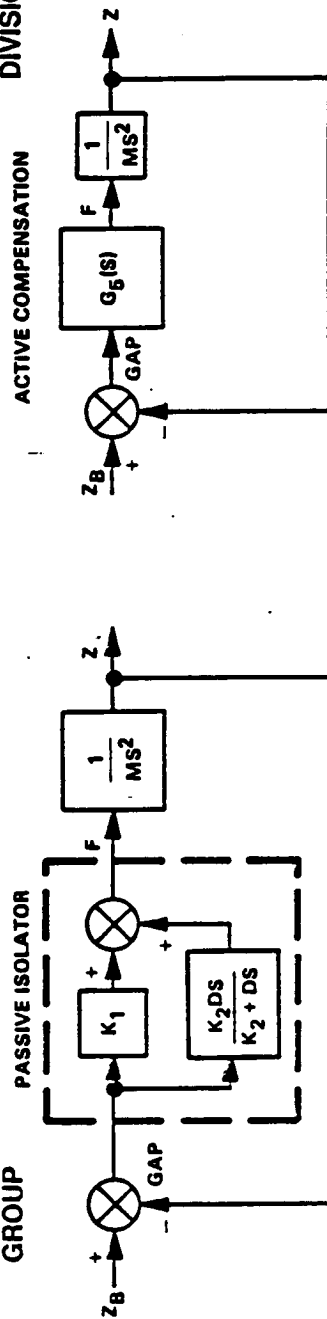
THE ANNULAR SUSPENSION AND POINTING SYSTEM CONCEPT ILLUSTRATES AN END-MOUNTED CONFIGURATION. CG MOUNTED CONCEPTS HAVE ALSO BEEN DEVELOPED.

Comparison of Passive Mechanical to Active Magnetic Isolator

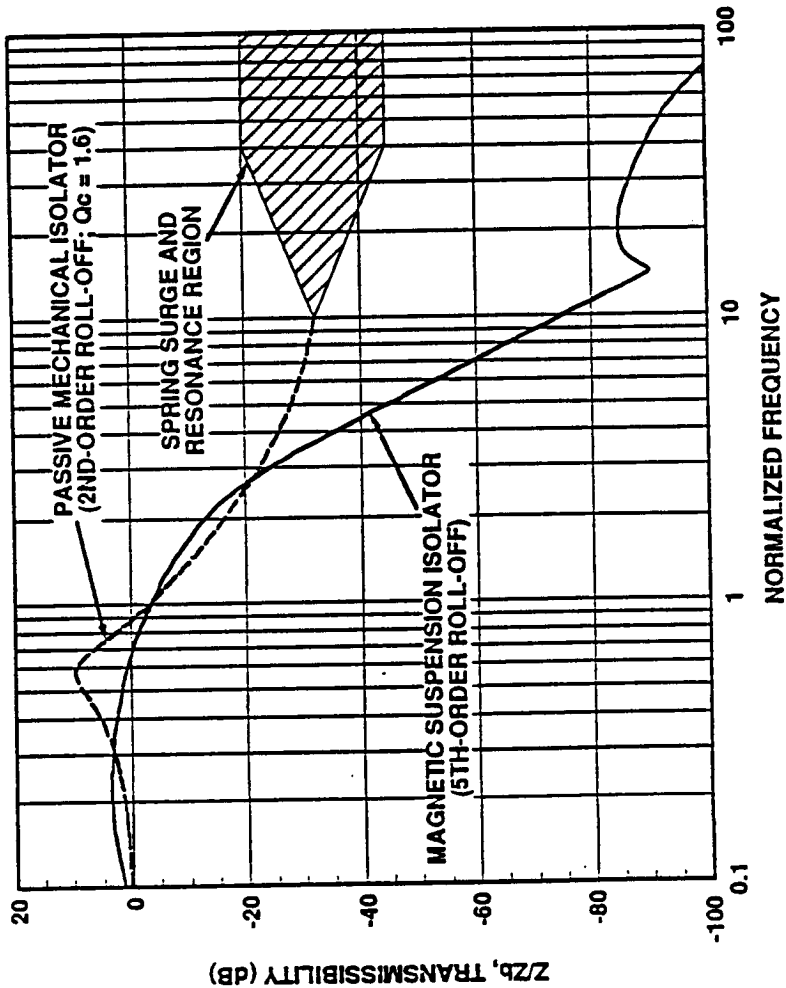


SPACESYSTEMS GROUP

SATELLITE SYSTEMS DIVISION



PS240-18-56



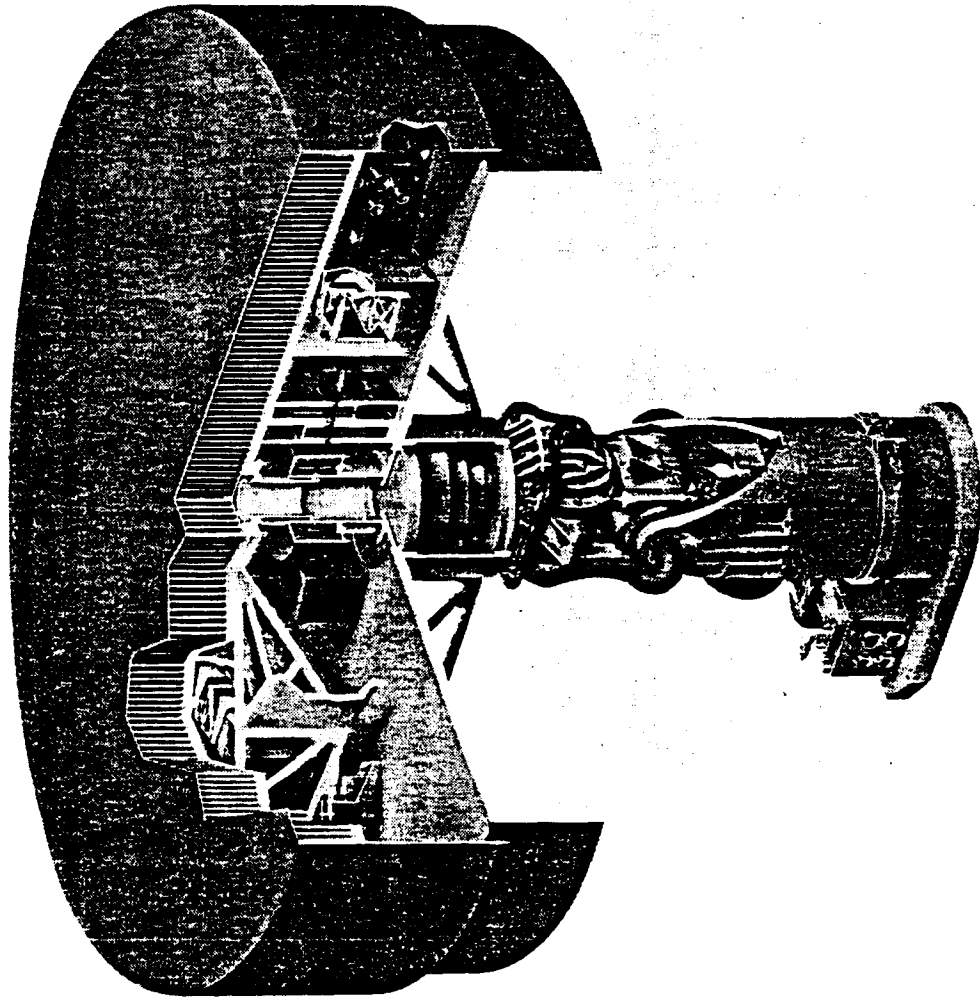
Honeywell

M038084

Annular Suspension and Pointing System

SPACESYSTEMS
GROUP

SATELLITE SYSTEMS
DIVISION



ORIGINAL PAGE
BLACK AND WHITE PHOTOGRAPH

Honeywell

5-15845-C

M03788

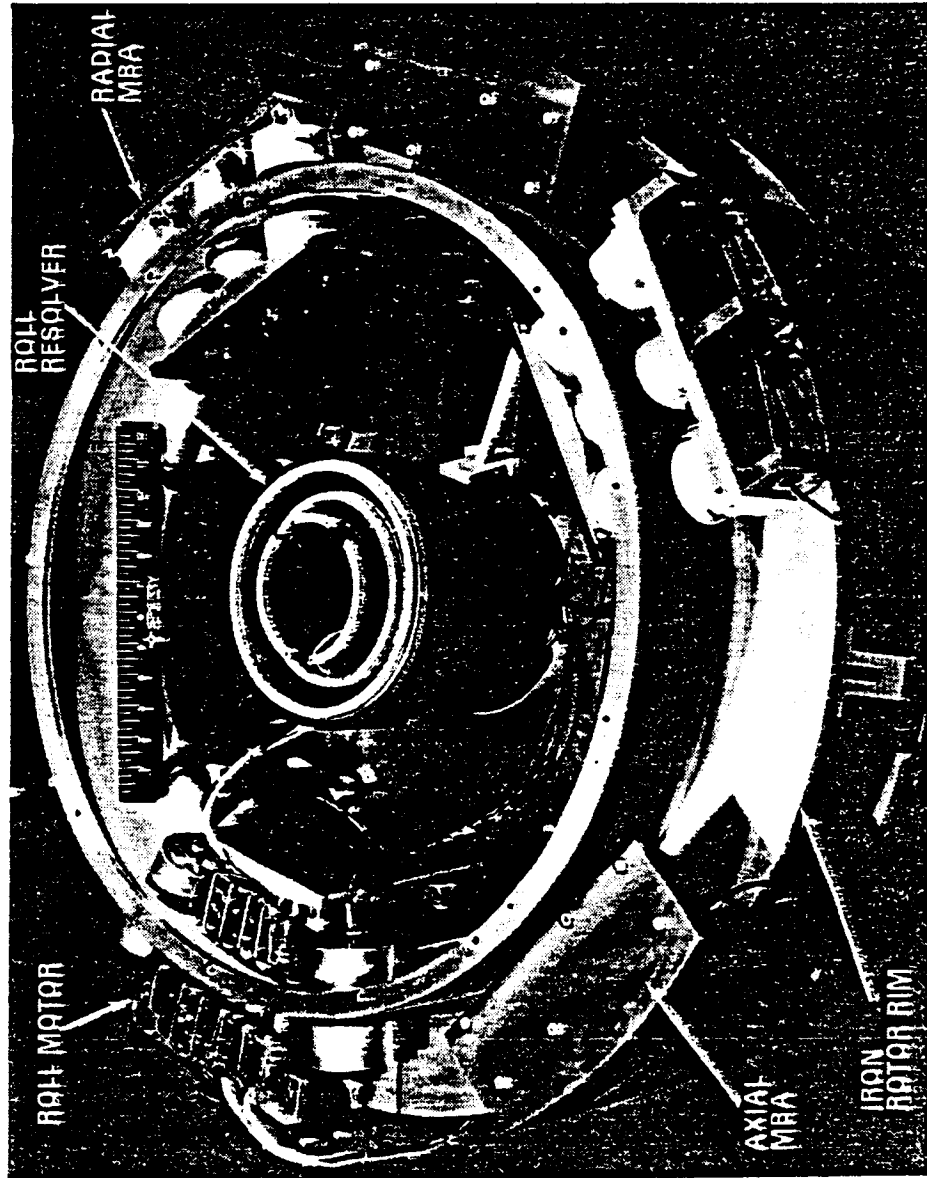
Laboratory Magnetic Isolation & Pointing System ASPS Vernier

SPACESYSTEMS
GROUP

SATELLITE SYSTEMS
DIVISION



ORIGINAL PAGE
BLACK AND WHITE PHOTOGRAPH



3-13066-3C

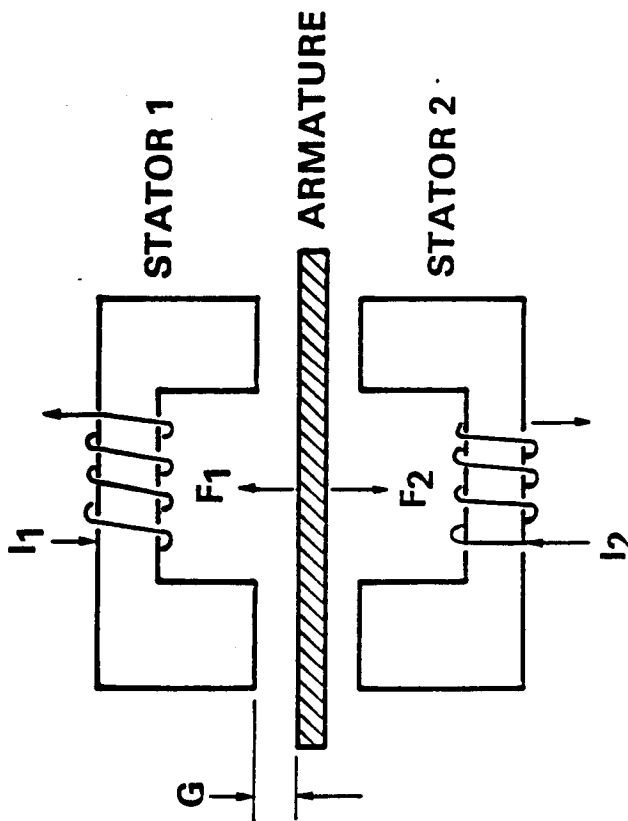
Honeywell

M096184

Magnetic Actuator Description

SPACESYSTEMS
GROUP

SATELLITE SYSTEMS
DIVISION



- Attractive Force F_1 and F_2
- F Insensitive to Armature Rotation and Cross Axes Translation
- Armature Isolated From Stator Disturbance Forces



3-13066-5C

- $F \sim I^2$
- $F \sim G^{-2}$
- Moving Armature Is Passive

Honeywell

PI554 62-3
M09471d

ORIGINAL PAGE
BLACK AND WHITE PHOTOGRAPH

THE REMAINDER OF THIS REPORT PROVIDES INFORMATION AND RESULTS FOR THE ASO SIMULATION ACTIVITY. THE FOLLOWING TERMS DEFINE ABBREVIATED TERMS USED TO IDENTIFY CHARACTERISTICS OF SIMULATED CASES.

PAYLOAD TYPES:

- | | |
|---------|-----------------------------------|
| 1. POF | PINHOLE OCULAR FACILITY |
| 2. EPOF | END MOUNTED POF |
| 3. HRTC | HIGH RESOLUTION TELESCOPE CLUSTER |

GIMBAL ORIENTATION:

- | | |
|----------|----------------------------------|
| 1. CASE1 | 50 DEG INCLINATION AT ORBIT NOON |
| 2. CASE2 | 5 DEG INCLINATION AT ORBIT DAWN |
| 3. CASE3 | 5 DEG INCLINATION AT ORBIT NOON |

SIA/PIA INTERFACES:

- | | |
|----------|-------------------------------|
| 1. 4.5HZ | 4.5 HZ INTERFACE -- $Q = 50$ |
| 2. 1HZ | 1 HZ INTERFACE -- $Q = 1$ |
| 3. LOHZ | 0.1 HZ INTERFACE -- $Q = 0.5$ |

EXAMPLE: POF CASE3 4.5HZ WOULD RELATE TO SIMULATION RESULTS WHEN CONFIGURED WITH THE POF PAYLOAD, WITH THE CASE 3 GIMBAL ORIENTATION AND A 4.5 HZ, LOW DAMPING INTERFACE STRUCTURE.

THE FOUR ASSUMED DISTURBANCE SOURCES ASSUMED FOR THE ASO SIMULATION ARE TREADMILL, MAN-PUSHOFF, CENTRIFUGE AND SHUTTLE DOCKING. THE ASSUMED FORCE VERSES TIME PROFILES OF THESE DISTURBANCES ARE SHOWN IN THE OPPOSITE FIGURE.

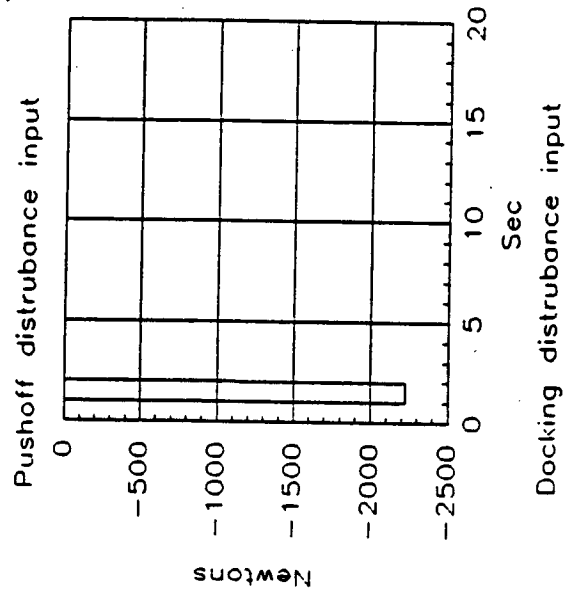
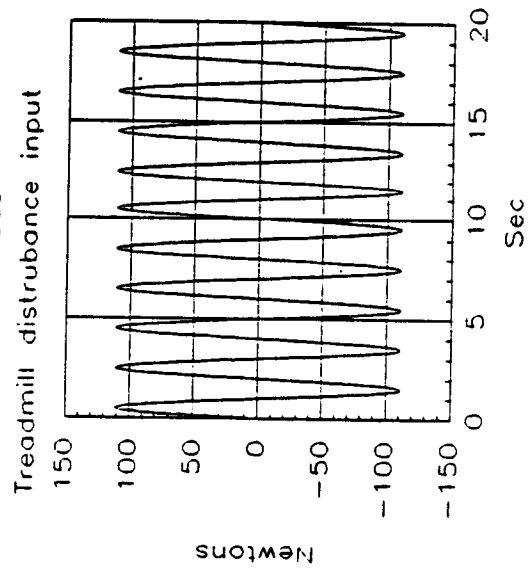
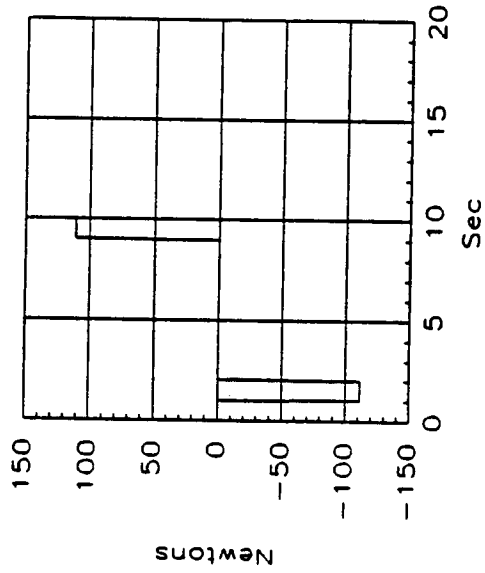
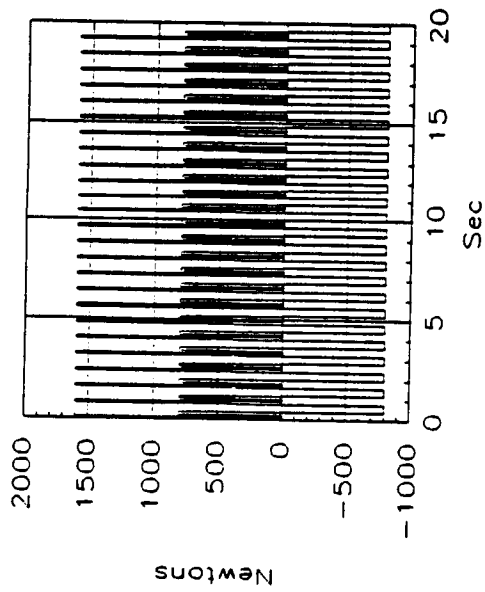
MOST OF THE SIMULATION RESULTS ARE BASED ON A COMBINATION OF THESE DISTURBANCES. THE COMBINED DISTURBANCES USED FOR THE SIMULATION ARE ALSO ILLUSTRATED.

DISTURBANCE DESCRIPTIONS WERE OBTAINED FROM THE JPL REPORT -

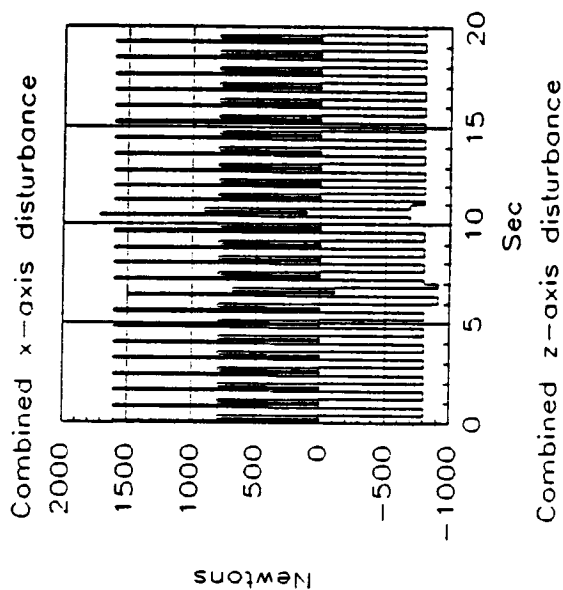
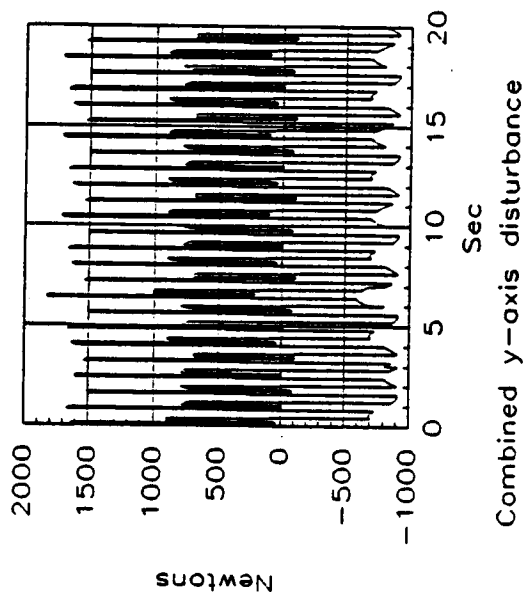
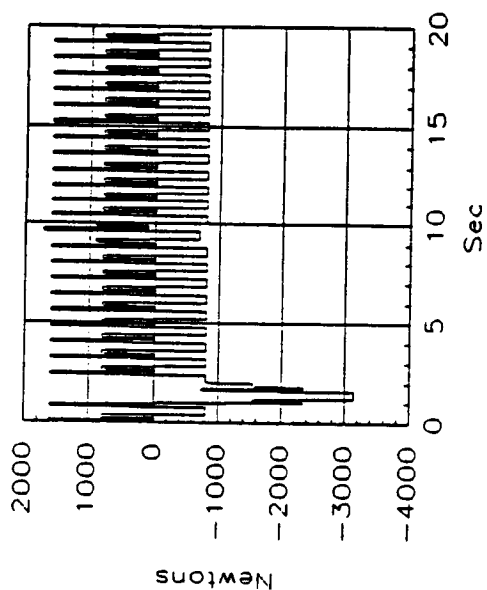
"SPACE SCIENCE/SPACE STATION ATTACHED PAYLOAD
POINTING ACCOMMODATIONS STUDY -

"POINTING PERFORMANCE ANALYSIS WHITE PAPER" FEB 1988

TIME HISTORIES OF SELECTED DISTURBANCE SOURCES



COMBINED DISTURBANCE HISTORIES



THE MASS PROPERTIES USED IN THE ASO SIMULATION ARE TABULATED IN THE FOLLOWING MASS PROPERTIES TABLE.

THE MASS PROPERTIES ARE BROKEN-UP DIFFERENTLY FOR CASES WITH VERSES WITHOUT MAGNETIC SUSPENSION

ALSO INCLUDED ARE THE ASSUMED CG OFFSETS FOR EACH OF THE PAYLOADS. IN THE CASE OF A MAGNETICALLY SUSPENDED POF, THE ASSUMED CG UNCERTAINTY IS ASSUMED TO BE APPROXIMATELY THE SAME AS THE CG OFFSET OF THE POF. THUS POINTING RESULTS WITH A MAGNETICALLY-SUSPENDED END-MOUNTED POF WILL BE THE ROUGHLY THE SAME AS A CG-MOUNTED POF, BUT WOULD REQUIRE HIGHER FORCE ACTUATOR AND FOLLOW-UP TORQUE BUDGETS.

ASO ASSUMED MASS PROPERTIES

Assumed Mass Properties without Magnetic Suspension

	Mass(Kg)	$I_{xx} (Kg-m^2)$	$I_{yy} (Kg-m^2)$	$I_{zz} (Kg-m^2)$
BASE	400	600	600	1000
AZIMUTH YOKE	905	700	700	1000
ELEVATION GIMBAL RING	330	375	375	375
CROSS-ELEVATION ROLL RING + POF PAYLOAD	3788	600110	600110	5100
CROSS-ELEVATION ROLL RING + HRTC PAYLOAD	1786	9879	9794	1185

Assumed Mass Properties With Magnetic Suspension

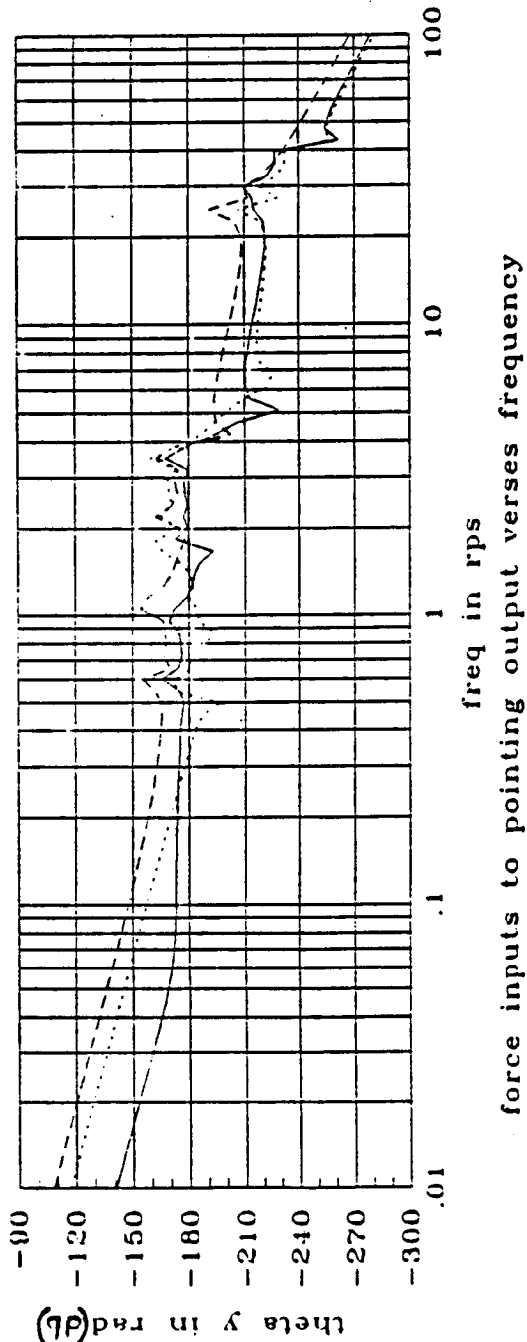
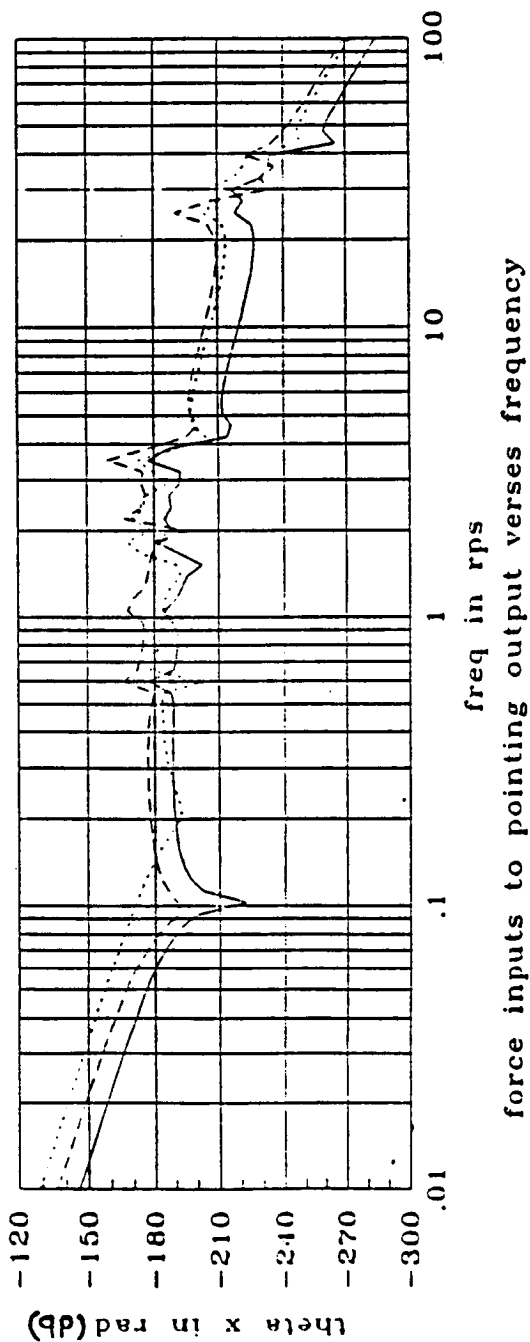
	Mass(Kg)	$I_{xx} (Kg-m^2)$	$I_{yy} (Kg-m^2)$	$I_{zz} (Kg-m^2)$
BASE	400	600	600	1000
AZIMUTH YOKE	905	700	700	1000
ELEVATION GIMBAL RING	330	375	375	375
CROSS-ELEVATION RING	225	300	300	300
SUSPENDED PAYLOAD (POF)	3688	600000	600000	4900
(HRTC)	1800	9880	9800	1190

Assumed cg offset for cg mounted POF cases (control point origin to payload cg): [-0.04, 0.03, 0.05] meters
 Assumed cg offset for end mounted POF cases (control point origin to payload cg): [-0.002, -0.028, 1.875] meters
 Assumed cg offset for cg mounted HRTC cases (control point origin to payload cg): [-0.04, -0.03, 0.05] meters

THE FOLLOWING CHARTS ILLUSTRATE THE FREQUENCY RESPONSE OF POINTING ERRORS (BOTH AXES) TO MODULE FORCE DISTURBANCES.

SPACE STATION MODES UP TO ABOUT 0.5 HERTZ WERE INCLUDED IN THIS PLOT. THE MODAL ACTIVITY BETWEEN 20 AND 50 RPS IS ASSOCIATED WITH THE SIA/PIA. THE INTERFACE WAS SET NOMINALLY FOR 4.5 HZ WITH A Q OF ABOUT 50.

POINTING ERROR TRANSFORMATIONS



THE SIMULATED CASES FOR THE POF PAYLOAD ARE BRIEFLY DESCRIBED IN THE FOLLOWING CHARTS IN TERMS OF MOUNTING, INTERFACE STIFFNESS AND GIMBAL ORIENTATION. THE FILENAME DESCRIPTION WILL BE USED TO IDENTIFY THE SIMULATION CASE IN A SUMMARY TABLE LATER IN THE REPORT.

ASO SIMULATION CASES

POF RUNS: All use combined disturbance inputs.

FILE NAME	DESCRIPTION
POF1_5HZ.DAT	Cg POF--4.5hz interface--case 1
POF1_1HZ.DAT	Cg POF--1 hz interface--case 1
POF1_LOHZ.DAT	Cg POF--0.1 hz interface--case 1
POF2_5HZ.DAT	Cg POF--4.5hz interface--case 2
POF2_1HZ.DAT	Cg POF--1 hz interface--case 2
POF2_LOHZ.DAT	Cg POF--0.1hz interface--case 2
POF3_5HZ.DAT	Cg POF--4.5hz interface--case 3
POF3_1HZ.DAT	Cg POF--1 hz interface--case 3
POF3_LOHZ.DAT	Cg POF--0.1 hz interface--case 3

C-3

THE END MOUNTED POF WAS SIMULATED ONLY WITH A PASSIVE BASE ISOLATOR. A MAGNETIC END MOUNTED SYSTEM SHOULD HAVE SIMILAR POINTING ACCURACY TO A C.G. MOUNTED SYSTEM.

TWO OPTIONS OF THE EPOF HAVE BEEN INCLUDED IN WITH AND WITHOUT REACTIONLESS MOTOR DRIVES.

ASO SIMULATION CASES (Continued)

EPOF RUNS: All use combined disturbance inputs EPOF = End Mounted POF

FILE NAME

DESCRIPTION

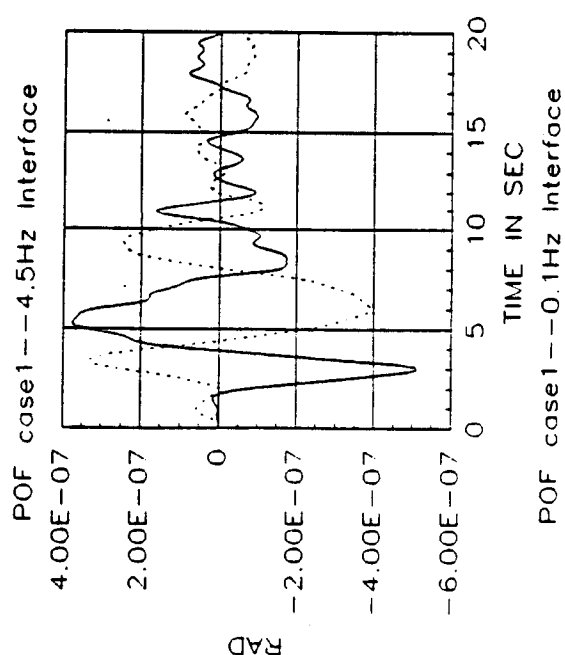
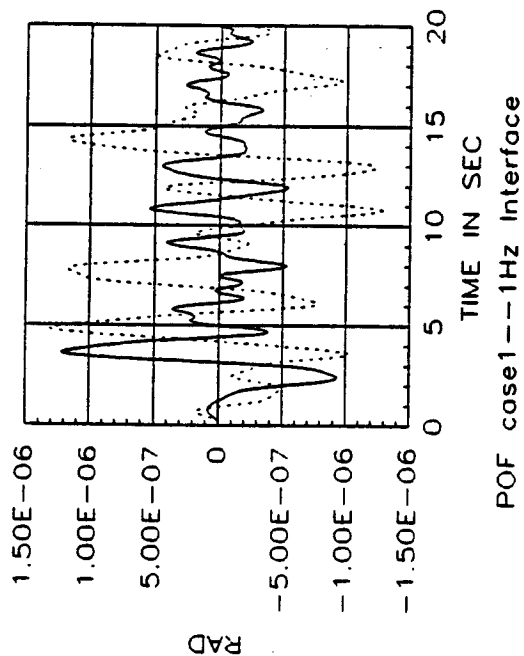
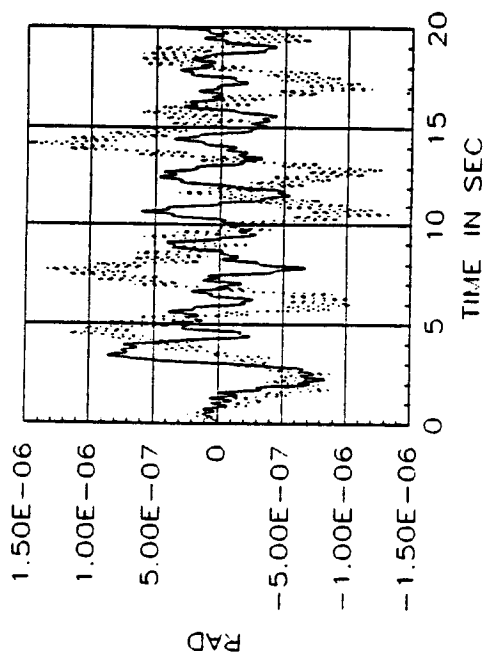
EPOF1_5HZ.DAT	EPOF--4.5-1hz-interface--case1
EPOF1_1HZ.DAT	EPOF--1hz--interface--case1
EPOF1_LOHZ.DAT	EPOF--0.1hz--interface--case1
EPOF2_5HZ.DAT	EPOF--4.5 hz interface--case 2
EPOF2_1HZ.DAT	EPOF--1 hz interface--case 2
EPOF2_LOHZ.DAT	EPOF--0.1 hz interface--case 2
EPOF3_5HZ.DAT	EPOF--4.5 hz interface--case 3
EPOF3_1HZ.DAT	EPOF--1 hz interface--case 3
EPOF3_LOHZ.DAT	EPOF--0.1 hz interface--case 3
EPOF1_REAC5HZ.DAT	EPOF--4.5 hz interface--case 1--reactionless
EPOF1_REAC1HZ.DAT	EPOF--1 hz interface--case 1--reactionless
EPOF1_REACLOHZ.DAT	EPOF--0.1 hz interface--case 1--reactionless
EPOF2_REAC5HZ.DAT	EPOF--4.5 hz interface--case 2--reactionless
EPOF2_REAC1HZ.DAT	EPOF--1 hz interface--case 2--reactionless
EPOF2_REACLOHZ.DAT	EPOF--0.1 hz interface -- case 2--reactionless
EPOF3_REAC5HZ.DAT	EPOF--4.5 hz interface--case 3--reactionless
EPOF3_REAC1HZ.DAT	EPOF--1 hz interface--case 3--reactionless
EPOF3_REACLOHZ.DAT	EPOF--0.1 hz interface--case 3--reactionless

THE POINTING ERROR FOR THE STATED SIMULATION CASES IS PLOTTED IN THE FOLLOWING PLOTS. IN EACH CASE, THE POINTING ERROR ABOUT THE X AXIS IS PLOTTED BY THE SOLID LINE AND THE ERROR ABOUT Y IS PLOTTED BY THE DASHED LINE. THE BORESIGHT VECTOR IS ASSUMED TO LIE ALONG THE PAYLOAD'S Z AXIS.

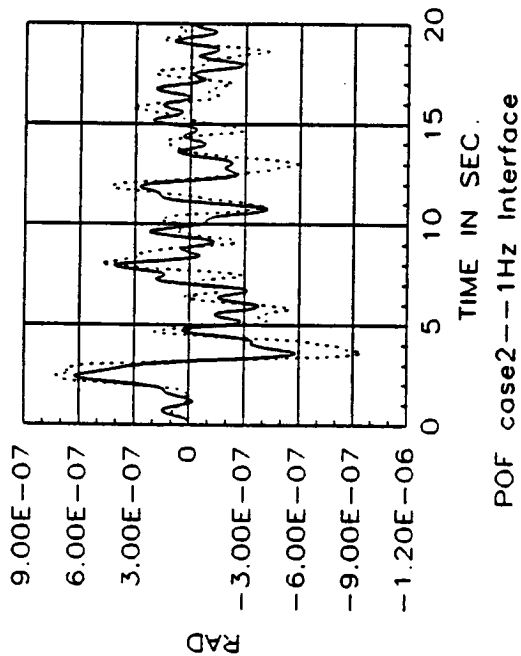
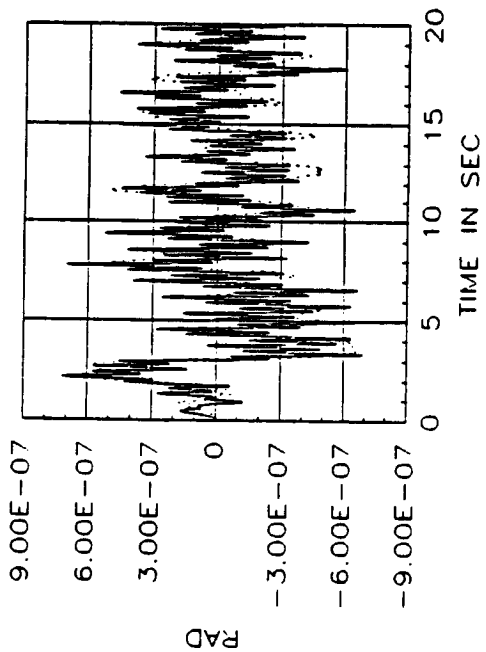
POINTING ERROR RESULTS FOR THE CG-MOUNTED POF ARE INCLUDED IN THE FIRST THREE PLOTS. THESE PLOTS ILLUSTRATE THE POINTING ERROR FOR EACH OF THE THREE INTERFACE STIFFNESSES IN EACH OF THE THREE GIMBAL ORIENTATIONS.

THE LOW FREQUENCY PASSIVE ISOLATOR DOES IMPROVE POINTING ERROR IN ALL THREE GIMBAL CASES, BUT THE WORST CASE POINTING ERROR FOR THE CG-MOUNTED POF (PAYLOAD FLEXIBILITY WAS NOT INCLUDED), IS LESS THAN 1 ARC-SECOND.

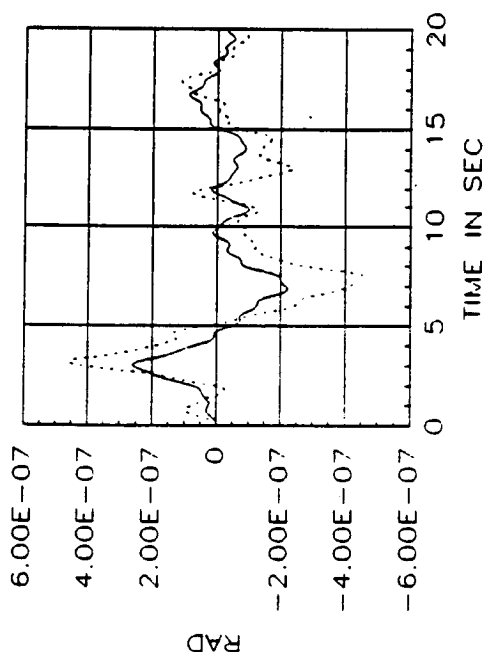
CG MOUNTED POF POINTING ERROR - CASE 1



CG MOUNTED POF POINTING ERROR - CASE 2

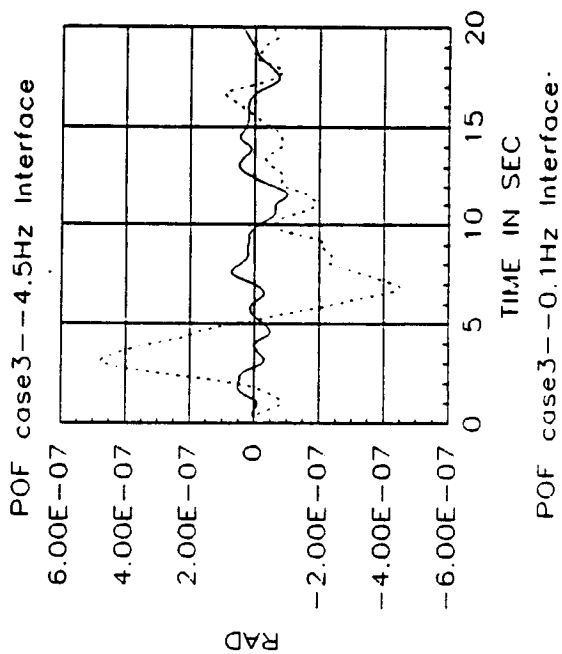
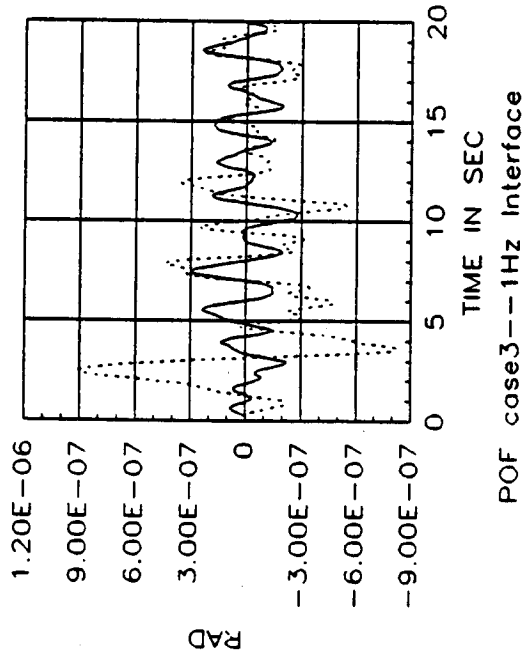
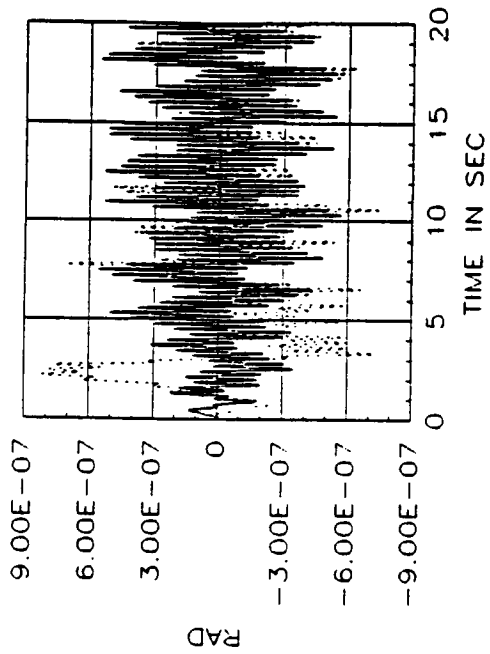


POF case2--4.5Hz Interface



POF case2--0.1Hz Interface

CG MOUNTED POF POINTING ERROR - CASE 3



POINTING PERFORMANCE OF THE POF PAYLOAD IN AN END-MOUNTED CONFIGURATION WAS ALSO STUDIED. ONCE AGAIN, HOWEVER, NO PAYLOAD FLEXIBILITY WAS INCLUDED IN THE MODEL.

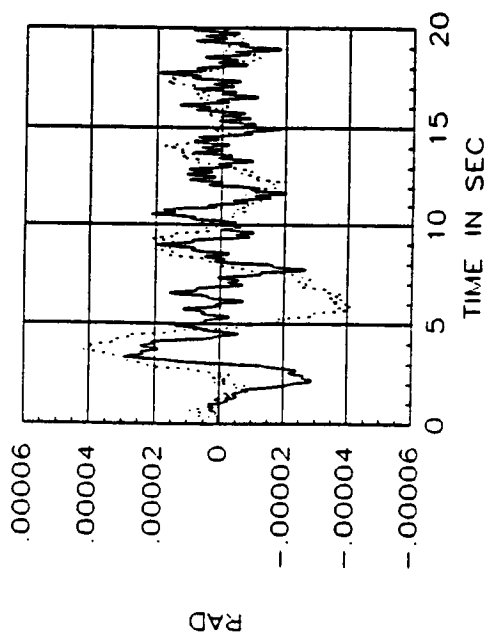
END-MOUNTED POF (EPOF) SIMULATION RESULTS ARE ILLUSTRATED IN THE FOLLOWING PLOTS FOR EACH OF THE AFOREMENTIONED GIMBAL ORIENTATIONS AND INTERFACE STIFFNESSES. ADDITIONALLY, A SIMPLE REACTIONLESS GIMBAL SYSTEM WAS SIMULATED TO EVALUATE ITS IMPACT ON THE SYSTEM PERFORMANCE.

THE WORST CASE POINTING ERROR OCCURS WHEN THE GIMBAL IS IN THE CASE 1 ORIENTATION. THIS ERROR IS ABOUT 10 ARC SECONDS.

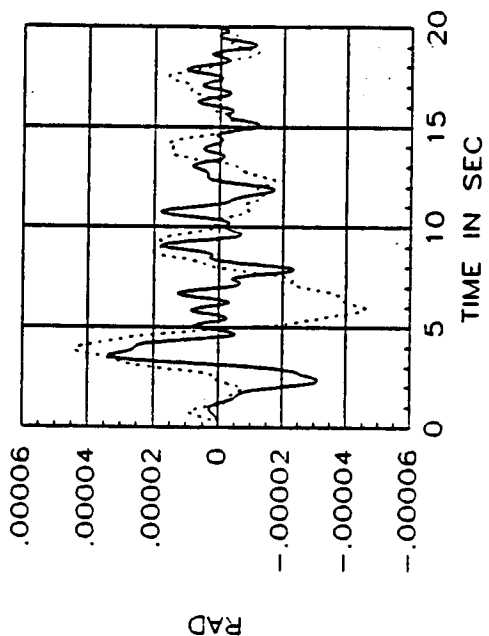
ALTHOUGH THE REACTIONLESS DRIVE SYSTEM HELPED REDUCE THE RELATIVE MOTION IN THE SIA/PIA INTERFACE AND REDUCED POINTING ERRORS IN SOME CASES, IT DID NOT HAVE A DOMINANT EFFECT ON THE ASO/POF SYSTEM.

AS ILLUSTRATED IN THE SUMMARY TABLE AT THE END OF THIS REPORT, THE RELATIVE MOTION OF THE SIA/PIA ISOLATORS SEEM REASONABLE IN TERMS OF PASSIVE ISOLATOR TECHNOLOGY.

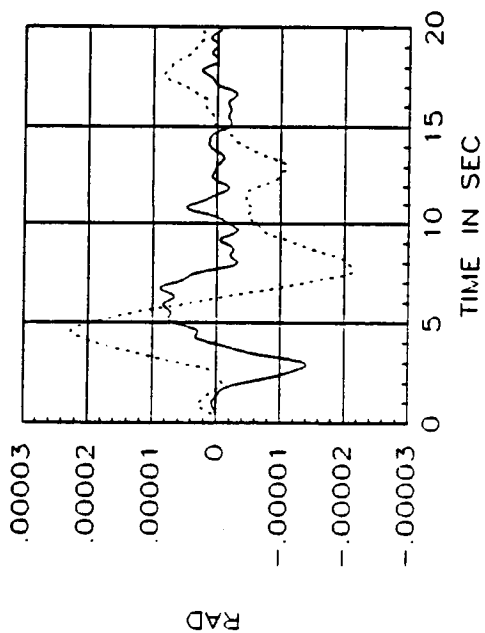
END MOUNTED POF - CASE 1



Epof case 1 -- 4.5Hz Interface

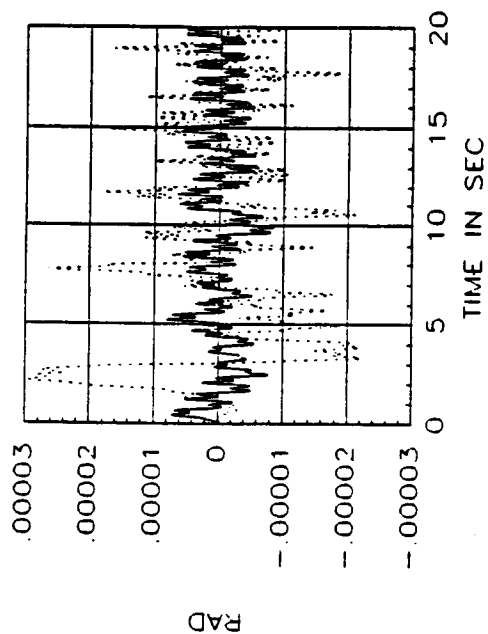


Epof case 1 -- 1Hz Interface

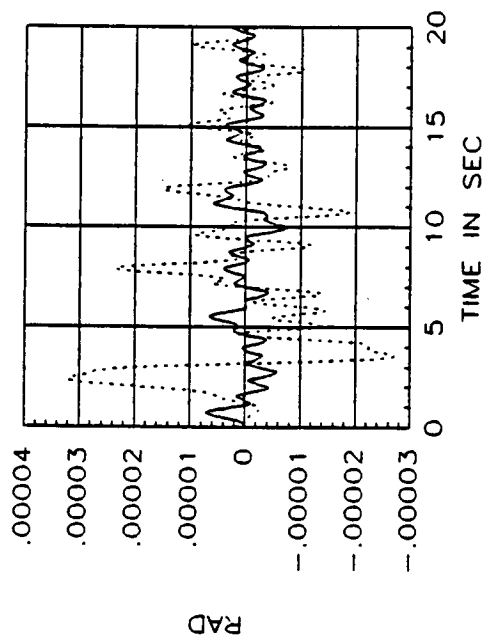


Epof case 1 -- 0.1Hz Interface

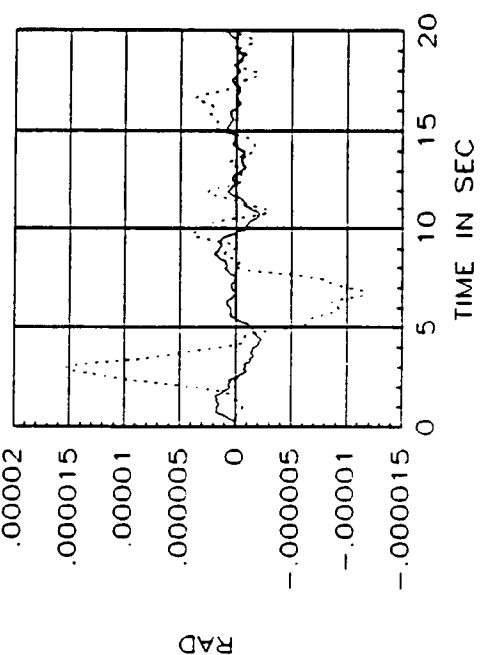
END MOUNTED POF - CASE 3



Epof case3--4.5Hz Interface

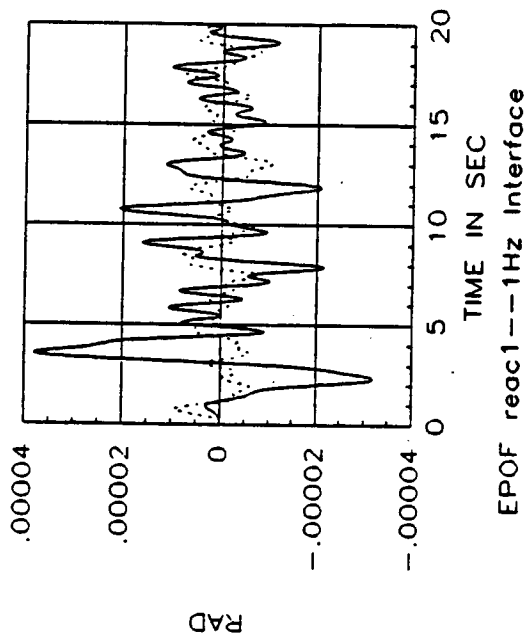
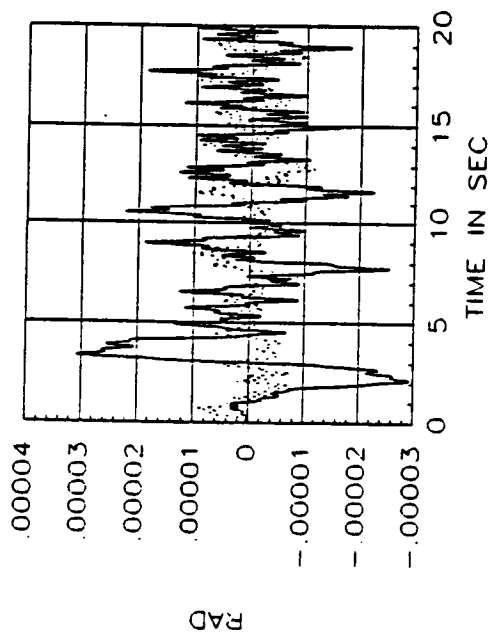


Epof case3--1Hz Interface

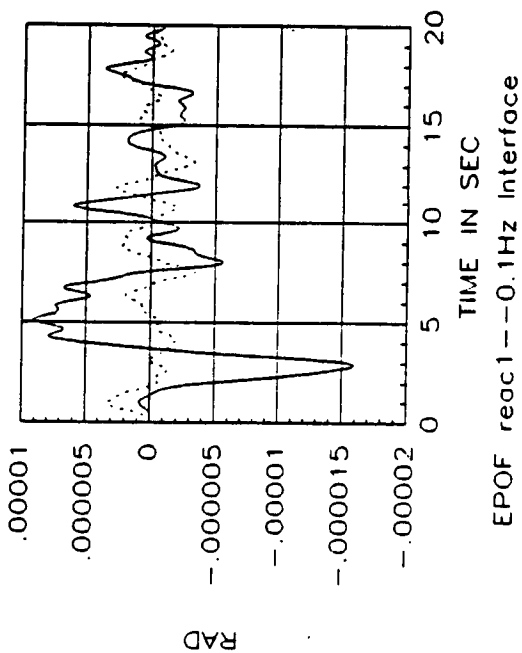


Epof case3--0.1Hz Interface

END MOUNTED POF WITH REACTIONLESS GIMBAL DRIVE - CASE 1

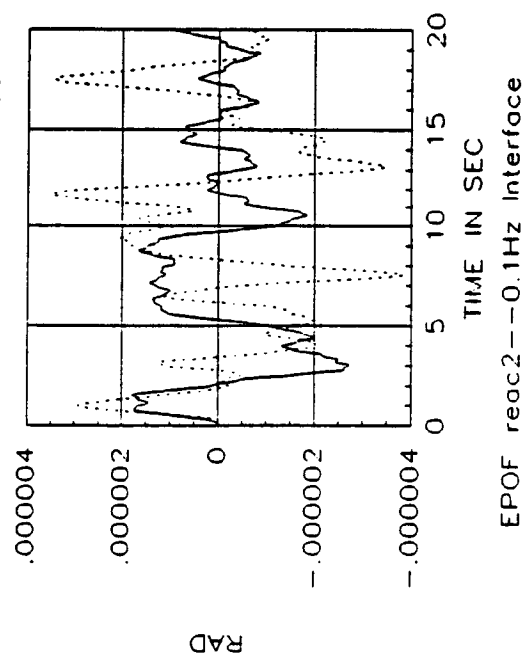
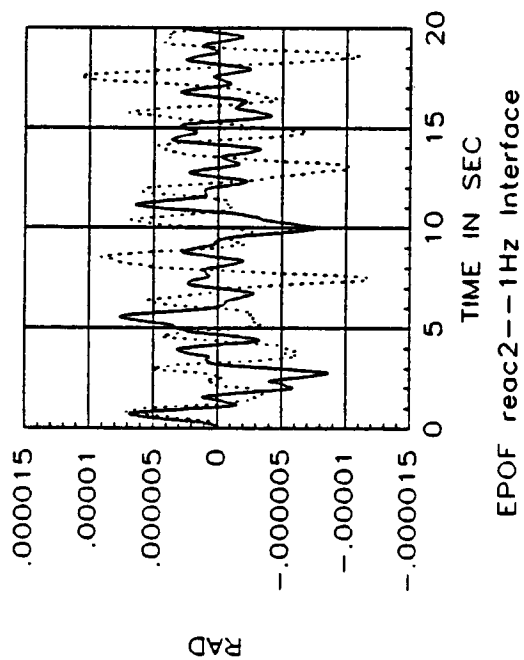
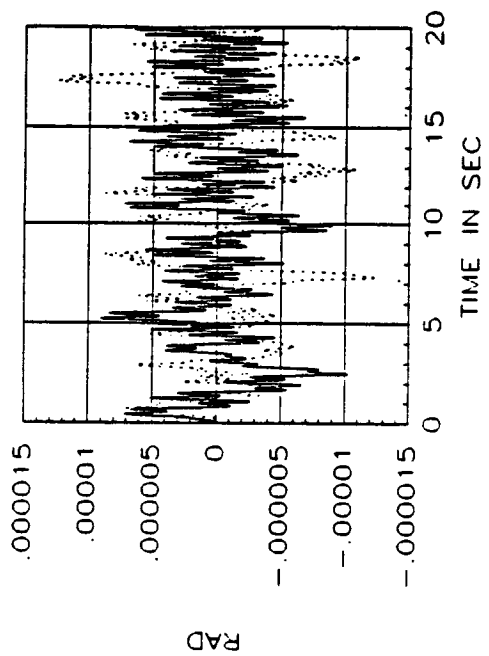


EPOF reac1--4.5Hz Interface

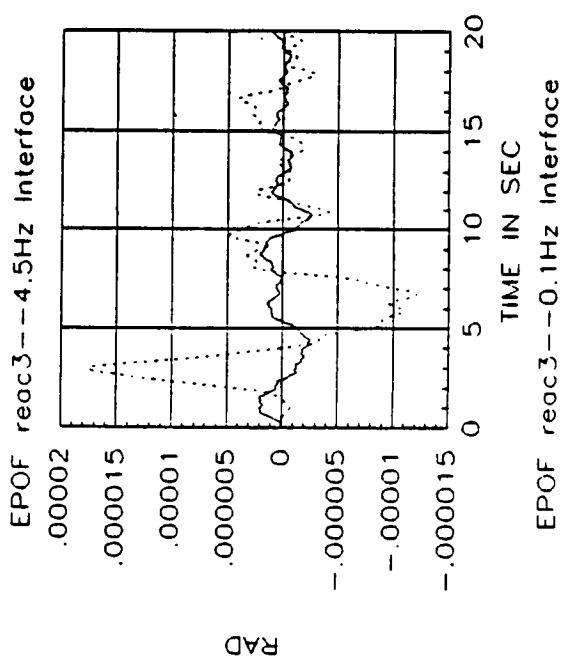
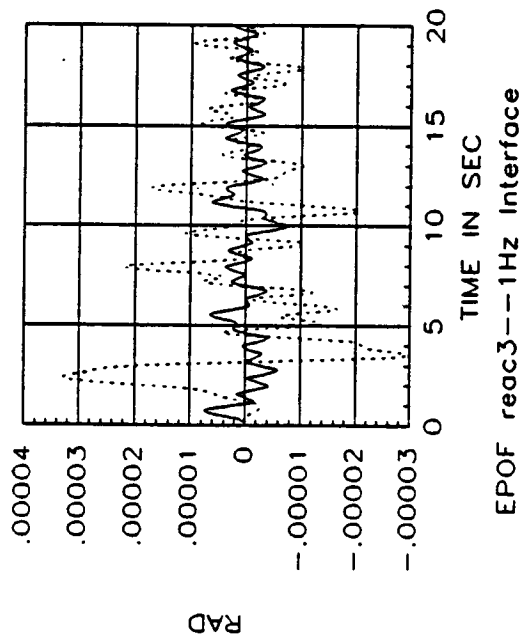
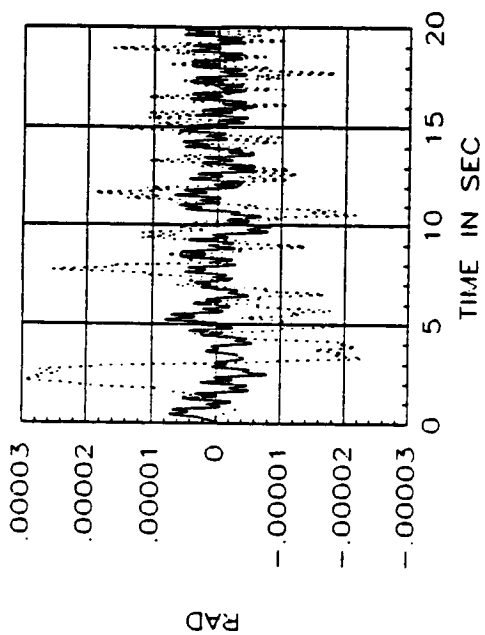


EPOF reac1--0.1Hz Interface

END MOUNTED POF WITH REACTIONLESS GIMBAL DRIVE - CASE 2



END MOUNTED POF WITH REACTIONLESS GIMBAL DRIVE - CASE 3



THE HIGH RESOLUTION TELESCOPE CLUSTER (HRTC) SIMULATION CASE SUMMARY IS TABULATED IN THE FOLLOWING TABLE.

19 SIMULATION CASES ARE SUMMARIZED IN THE ENSUING PLOTS:

THE FIRST FOUR CASES COMPARE THE IMPACT OF EACH ASSUMED DISTURBANCE SOURCE, ASSUMING THE HRTC PAYLOAD IN THE CASE 1 GIMBAL ORIENTATION WITH A 4.5 HZ NOMINAL SIA/PIA INTERFACE STIFFNESS.

THE NEXT NINE CASES EVALUATE HRTC POINTING IN EACH OF THE THREE GIMBAL ORIENTATIONS WITH EACH OF THE THREE INTERFACE STIFFNESS.

THE FINAL 6 CASES DEMONSTRATE THE HRTC PERFORMANCE WHEN MOUNTED ON A MAGNETIC ISOLATION/VERNIER POINTING SYSTEM. PERFORMANCE FOR TWO ISOLATION BANDWIDTHS ARE INCLUDED IN THIS REPORT.

ASO SIMULATION CASES (Continued)

HRTC RUNS: HRTC= High Resolution Telescope Cluster
Unless Otherwise noted, Cases Use Combined Disturbance Inputs

FILE NAME	DESCRIPTION
HRTC1_5HZTREAD.DAT	HRTC--4.5 hz--case1--treadmill disturbance
HRTC1_5HZPUSH.DAT	HRTC--4.5 hz--case1--pushoff disturbance
HRTC1_5HZCENT.DAT	HRTC--4.5 hz--case1--centrifuge disturbance
HRTC1_5HZDOCK.DAT	HRTC--4.5 hz--case1--docking disturbance
HRTC1_5HZ.DAT	HRTC--4.5 hz interface--case 1
HRTC1_1HZ.DAT	HRTC--1 hz interface--case 1
HRTC1_LOHZ.DAT	HRTC--0.1 hz interface--case 1
HRTC2_5HZ.DAT	HRTC--4.5 hz interface--case 2
HRTC2_1HZ.DAT	HRTC--1.0 hz interface--case 2
HRTC2_LOHZ.DAT	HRTC--0.1 hz interface--case 2
HRTC3_5HZ.DAT	HRTC--4.5 hz interface--case 3
HRTC3_1HZ.DAT	HRTC--1.0 hz interface--case 3
HRTC3_LOHZ.DAT	HRTC--0.1 hz interface--case 3

ASO SIMULATION CASES (Continued)

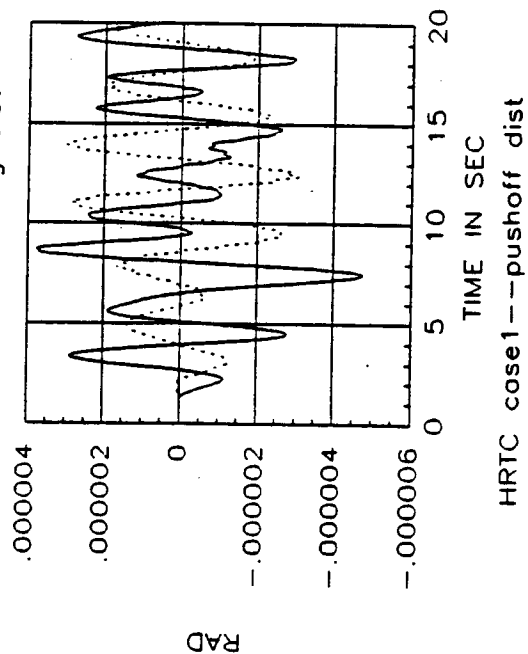
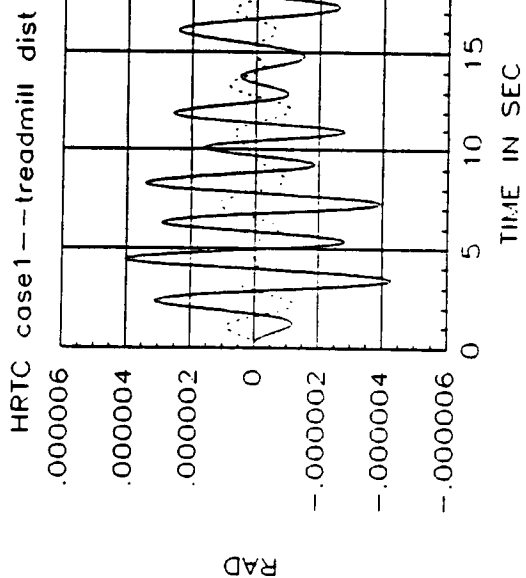
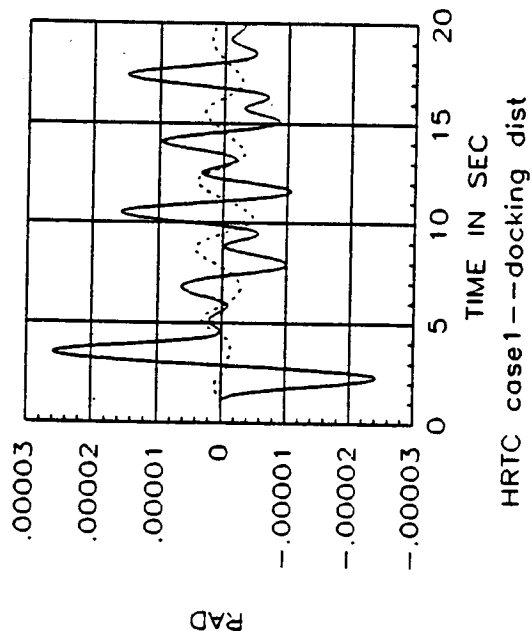
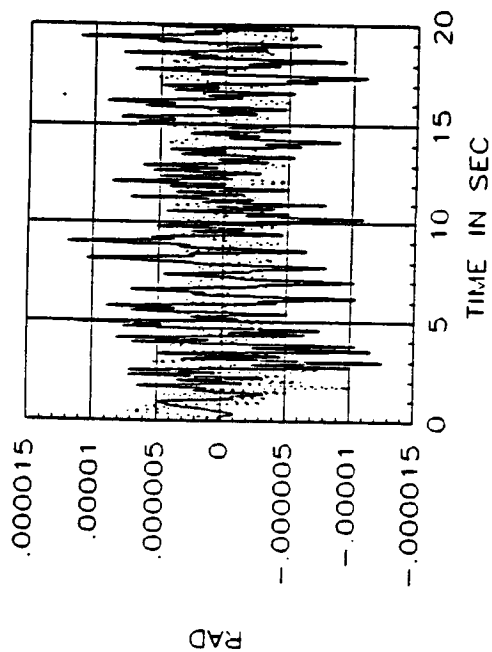
HRTC MAG-ISOLATED RUNS:

MHRTC1_LO.DAT
MHRTC2_LO.DAT
MHRTC2_LO.DAT
MHRTC1_VLO.DAT
MHRTC2_VLO.DAT
MHRTC3_VLO.DAT

MHRTC--0.1hz isolation bandwidth -- case 1
MHRTC--0.1hz isolation bandwidth -- case 2
MHRTC--0.1hz isolation bandwidth -- case 3
MHRTC--0.03hz isolation bandwidth --case1
MHRTC--0.03hz isolation bandwidth--case2
MHRTC--0.03hz isolation bandwidth--case3

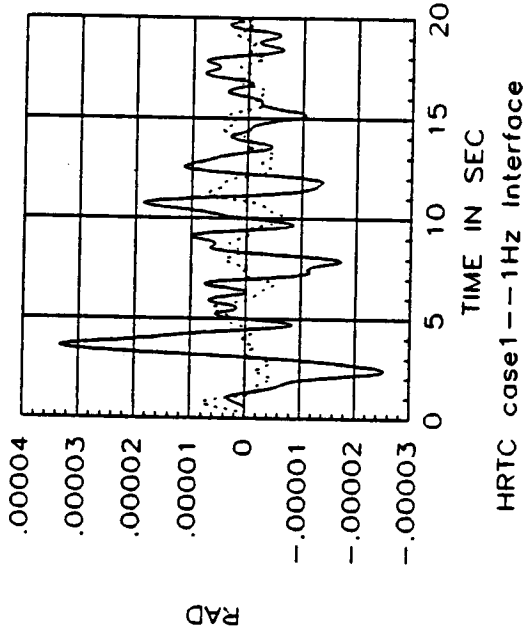
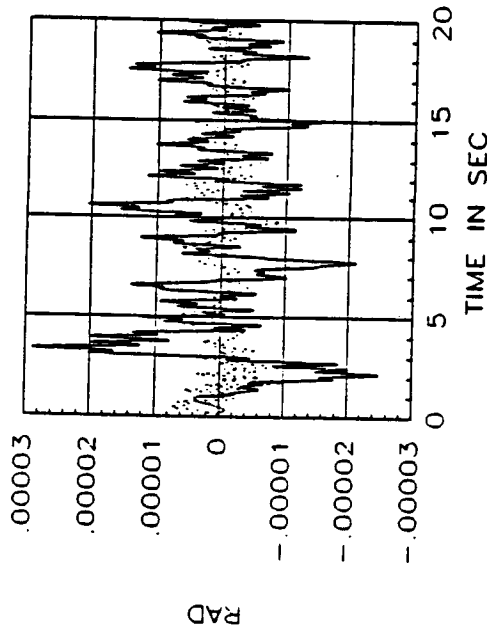
THE FOLLOWING HRTC POINTING RUNS WERE MADE WITH INDIVIDUAL DISTURBANCE SOURCES AND THE 5. HZ SIA/PIA INTERFACE STIFFNESS. EVIDENTLY, THE DOCKING DISTURBANCE HAS THE GREATEST IMPACT ON POINTING ERROR.

HRTC POINTING ERROR CAUSED BY SEPARATE DISTURBANCE SOURCES



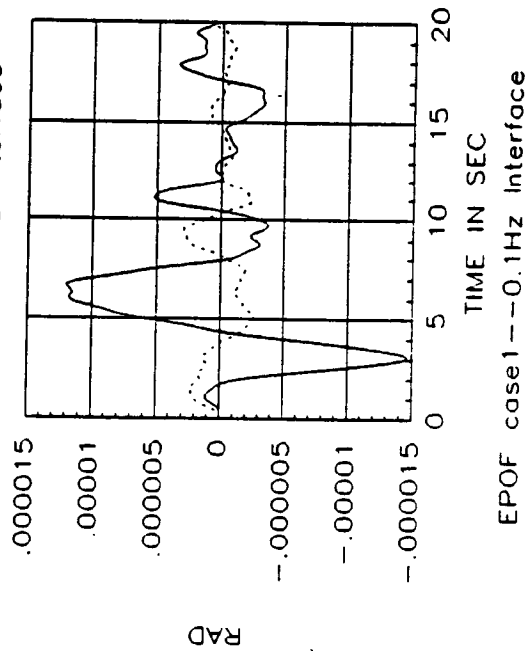
THE PLOTS ON THE FOLLOWING CHARTS INDICATE THAT THE 1 HZ PASSIVE ISOLATOR IS NOT ADEQUATE TO REDUCE PEAK. POINTING ERROR (ALTHOUGH HIGH FREQUENCY JITTER IS ATTENUATED). A 0.1 HZ ISOLATOR DOES RESULT IN A 2 TO 1 (OR MORE) REDUCTION IN DISTURBANCE INDUCED POINTING ERROR.

HRTC POINTING ERROR - CASE 1 PASSIVE BASE ISOLATOR OPTIONS



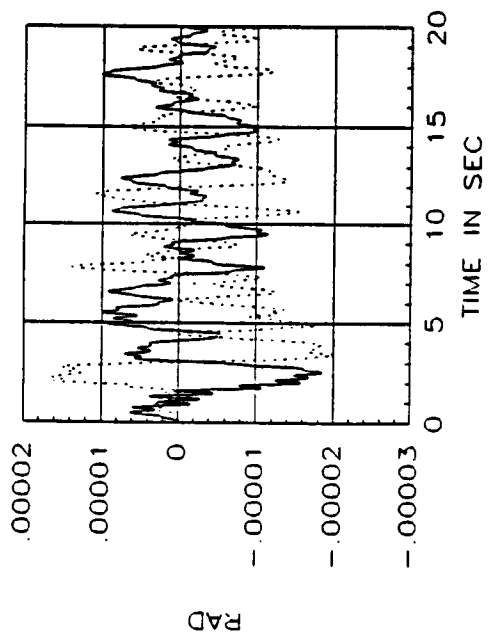
HRTC case1--4.5Hz Interface

HRTC case1--1Hz Interface

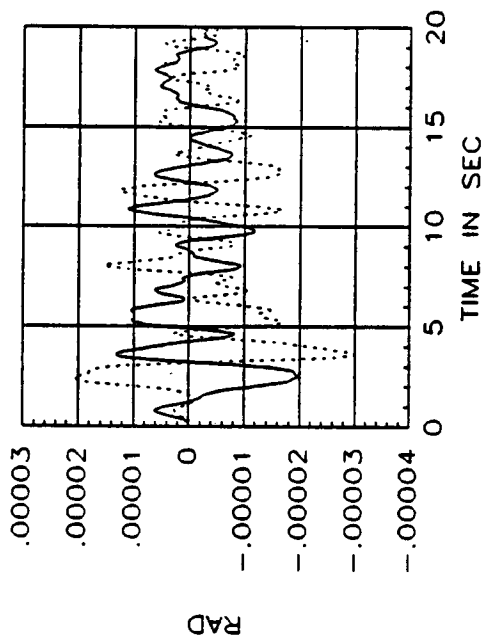


EPOF case1--0.1Hz Interface

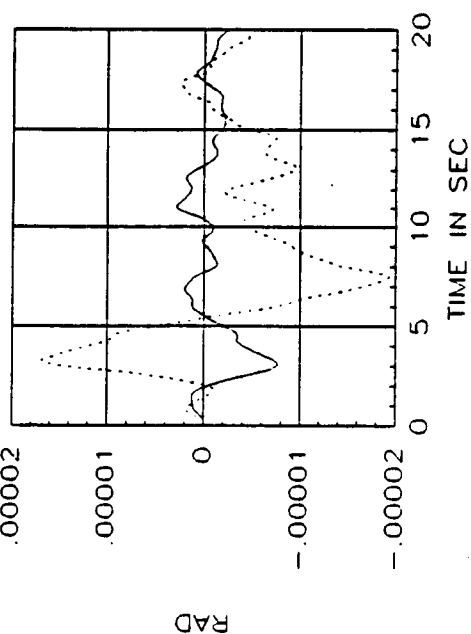
HRTC POINTING ERROR - CASE 2 PASSIVE BASE ISOLATOR OPTIONS



HRTC case2--4.5Hz Interface

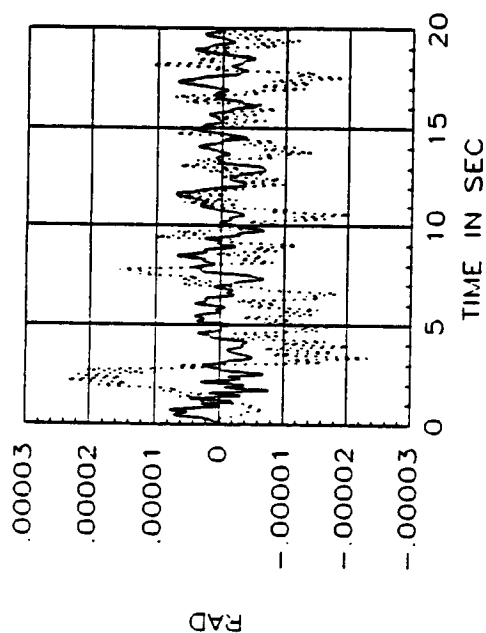


HRTC case2--1Hz Interface

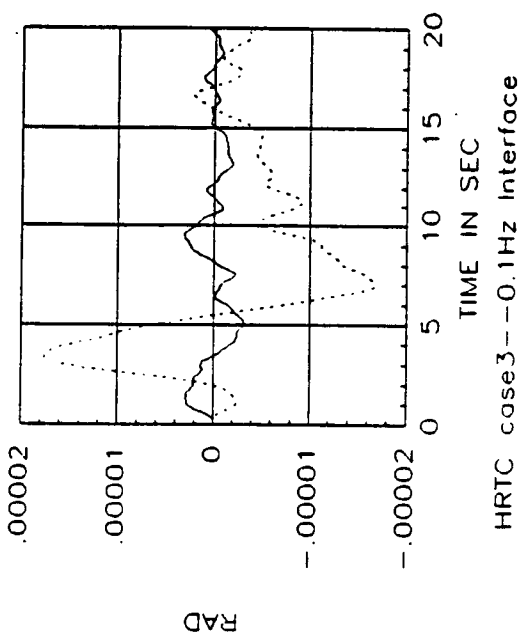


HRTC case2--0.1Hz Interface

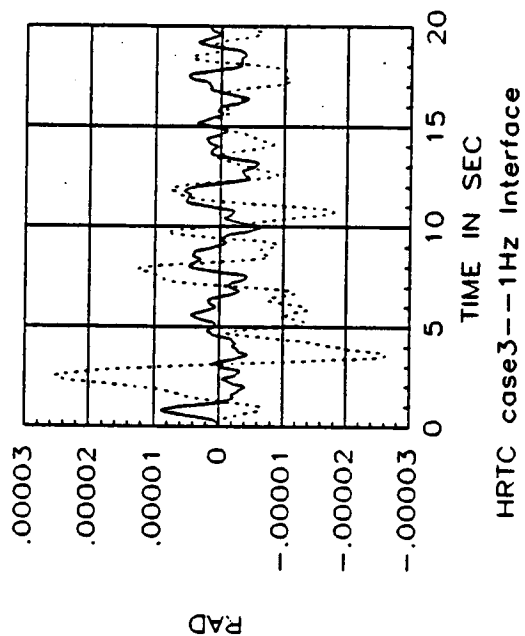
HRTC POINTING ERROR - CASE 3 PASSIVE BASE ISOLATOR OPTIONS



HRTC case3--4.5Hz Interface



HRTC case3--0.1Hz Interface

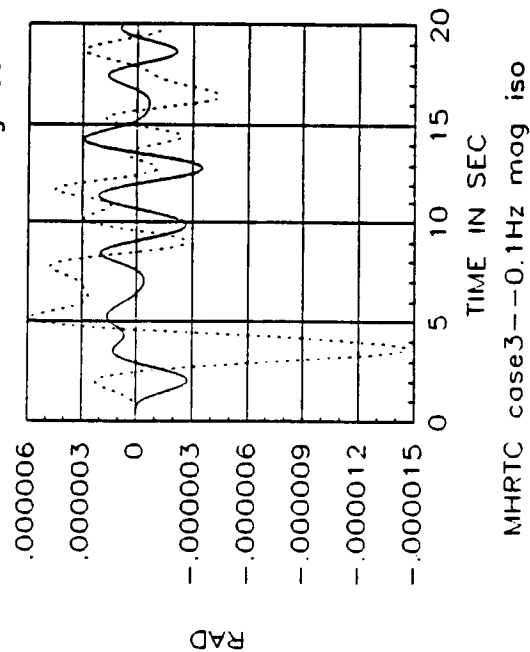
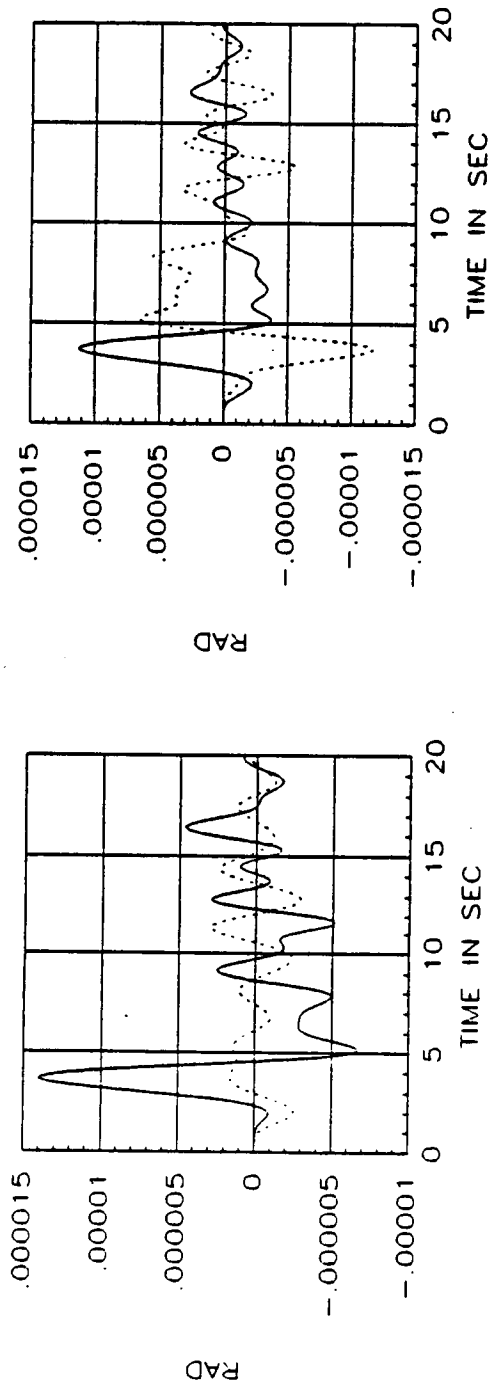


HRTC case3--1Hz Interface

HRTC POINTING ERROR - USING A MAGNETIC POINTING AND ISOLATION SYSTEM WITH A 0.5 HZ POINTING LOOP BANDWIDTH AND 0.3 HZ ISOLATION BANDWIDTH ARE SHOWN IN THE FOLLOWING PLOT FOR THE 3 GIMBAL ORIENTATIONS. THE 0.1 HZ DESIGNATION REFERS TO THE OPEN LOOP Crossover FREQUENCY OF THE ISOLATION LOOP.

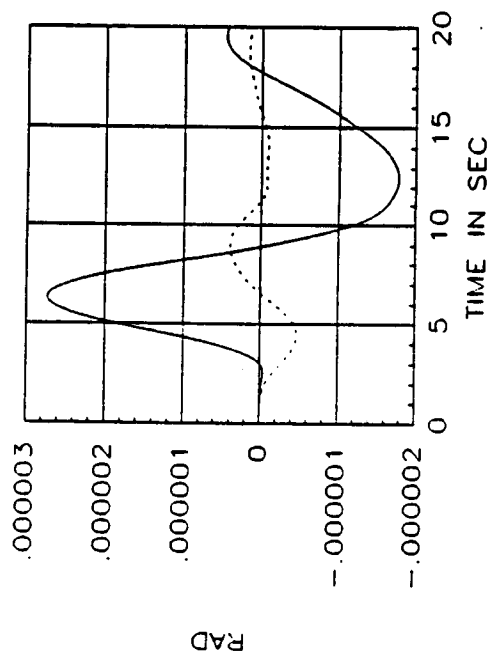
HRTC POINTING ERROR -

0.1 HZ MAGNETIC ISOLATION & POINTING SYSTEM - EFFECTIVE 0.3 HZ ISOLATION BANDWIDTH

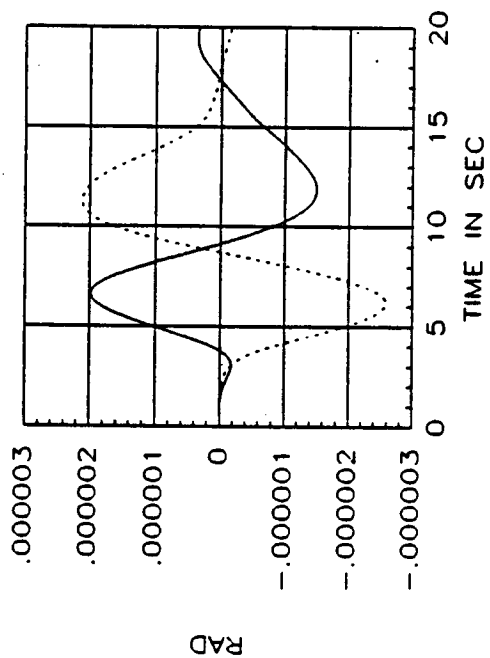


HRTC POINTING ERROR -

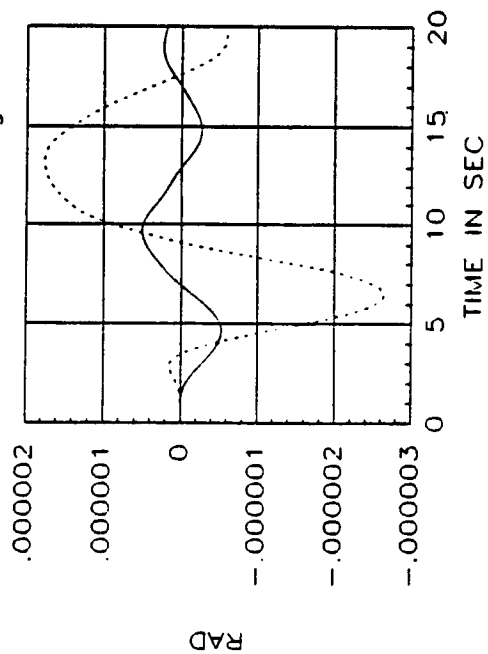
0.3 HZ MAGNETIC ISOLATION & POINTING SYSTEM - EFFECTIVE 0.1 HZ ISOLATION BANDWIDTH



MHRTC case1--0.03Hz mag iso



MHRTC case2--0.03Hz mag iso



MHRTC case3--0.03Hz mag iso

DESCRIPTION OF TABLE TERMS:

THX: POINTING ERROR ABOUT X-AXIS

THY: POINTING ERROR ABOUT Y-AXIS

DELX-DELZ RELATIVE DISPLACEMENT THROUGH THE SIA/PIA INTERFACE

DTHX-DTHZ RELATIVE ROTATIONS THROUGH THE SIA/PIA INTERFACE

TXL-TAZ GIMBAL TORQUER REQUIREMENTS

* * ALL TABLE ENTRIES REPRESENT PEAK VALUES FOR THE SIMULATION CASE THEY DESCRIBE.

SIMULATION SUMMARY FOR CG MOUNTED POF PAYLOAD

DATA FILE	Thx(rad)	Thy(rad)	Delx(nm)	Dely(nm)	Delz(nm)	dthx(rad)	dthy(rad)	dthz(rad)	Txl(nm)	Tel(nm)	Taz(nm)
POF1_5HZ	0.8μrad	1.2μrad	0.25	0.41	0.15	200μrad	140μrad	20μrad	5.5	10	4.5
POF1_1HZ	1μrad	1.4μrad	0.6	0.16	0.35	80μrad	290μrad	180μrad	5.5	6.5	5
POF1_LOHZ	0.55μrad	1.8μrad	5.1	0.55	1.25	300μrad	2.6μrad	2.5μrad	1.7	1.4	6.5
POF2_5HZ	0.65μrad	0.7μrad	0.25	0.31	0.16	180μrad	150μrad	10μrad	7	4.5	4
POF2_1HZ	0.6μrad	0.9μrad	0.61	0.15	0.32	100μrad	290μrad	190μrad	3.5	5.5	3
POF2_LOHZ	0.25μrad	0.45μrad	5.1	0.55	1.2	300μrad	2.6μrad	800μrad	0.9	1.5	1.2
POF3_5HZ	0.56μrad	0.8μrad	0.25	0.45	0.15	250μrad	150μrad	11μrad	7.5	7	1.5
POF3_1HZ	0.3μrad	0.9μrad	0.61	0.15	0.32	90μrad	300μrad	150μrad	1.5	3.8	1.6
POF3_LOHZ	0.1μrad	0.5μrad	5.1	0.55	1.2	300μrad	2.6μrad	700μrad	0.4	1.1	0.8

SIMULATION SUMMARY FOR END-MOUNTED POF PAYLOAD

DATA FILE	Thx(rad)	Thy(rad)	Delx(nm)	Dely(nm)	Delz(nm)	dthx(rad)	dthy(rad)	dthz(rad)	Txl(nm)	Tel(nm)	Taz(nm)
EPOF1_5HZ	30μrad	41μrad	0.25	0.15	0.10	30μrad	50μrad	60μrad	160	190	65
EPOF1_1HZ	35μrad	45μrad	0.55	0.22	0.35	90μrad	160μrad	1.3μrad	175	180	70
EPOF1_LOHZ	14μrad	23μrad	5.8	1.7	1.2	2.3μrad	1.5μrad	25μrad	55	100	32
EPOF2_5HZ	10μrad	12μrad	0.25	0.14	0.1	30μrad	50μrad	50μrad	100	90	45
EPOF2_1HZ	8μrad	12μrad	0.6	0.2	0.32	50μrad	110μrad	800μrad	40	75	40
EPOF2_LOHZ	3μrad	3.8μrad	5.5	0.65	1.2	160μrad	1.2μrad	3.5μrad	11	20	9
EPOF3_5HZ	8μrad	30μrad	0.25	0.14	0.1	30μrad	50μrad	25μrad	90	180	5
EPOF3_1HZ	7μrad	32μrad	0.55	0.2	0.3	45μrad	140μrad	150μrad	40	170	5
EPOF3_LOHZ	3μrad	15μrad	5.5	0.6	1.2	210μrad	1.7μrad	2.3μrad	10	50	1.6
EPOF1_REAC5HZ	30μrad	10μrad	0.25	0.1	0.1	30μrad	50μrad	120μrad	160	90	130
EPOF1_REAC1HZ	38μrad	10μrad	0.6	0.3	0.3	45μrad	120μrad	2.5μrad	190	55	140
EPOF1_REACLOHZ	15μrad	3.5μrad	5.5	1.2	1.2	150μrad	1.1μrad	21μrad	65	17	50
EPOF2_REAC5HZ	10μrad	12μrad	0.25	0.14	0.1	30μrad	50μrad	100μrad	100	90	100
EPOF2_REAC1HZ	9μrad	11.5μrad	0.6	0.2	0.3	45μrad	120μrad	700μrad	40	70	40
EPOF2_REACLOHZ	2.7μrad	3.8μrad	5.5	0.6	1.2	160μrad	1.1μrad	3μrad	11	20	20
EPOF3_REAC5HZ	8μrad	29μrad	0.25	0.14	0.1	30μrad	50μrad	25μrad	90	170	5
EPOF3_REAC1HZ	7μrad	32μrad	0.6	0.2	0.3	45μrad	120μrad	80μrad	40	170	5
EPOF3_REACLOHZ	3μrad	17μrad	5.5	0.65	1.2	150μrad	1.1μrad	650μrad	10	60	3.5

SIMULATION SUMMARY FOR CG-MOUNTED HRTC

DATA FILE	Thx(rad)	Thy(rad)	Delx(nm)	Dely(nm)	Delz(nm)	dthx(rad)	dthy(rad)	dthz(rad)	Txl(nm)	Tel(nm)	Taz(nm)
HRTC1_5HZIRD	13μrad	6μrad	0.25	0.25	0.24	110μrad	120μrad	25μrad	1	0.5	0.3
HRTC1_1HZPUSH	6μrad	3μrad	**	**	**	6μrad	2.8μrad	0.6μrad	0.25	0.18	0.2
HRTC1_LOHZCENT	4.5μrad	1.4μrad	**	**	**	0.4μrad	2μrad	0.3μrad	0.3	0.08	0.1
HRTC1_5HZDOCK	26μrad	5μrad	**	**	**	2.4μrad	11μrad	1.2μrad	1.6	0.2	0.5
HRTC1_5HZ	29rad	7μrad	0.24	0.24	0.24	120μrad	130μrad	25μrad	3.5	2.0	0.9
HRTC1_1HZ	33μrad	8μrad	0.18	0.7	0.4	80μrad	300μrad	140μrad	2.4	0.8	1.6
HRTC1_LOHZ	15μrad	7μrad	0.75	6.0	1.4	300μrad	2.5μrad	130μrad	0.6	0.2	1.6
HRTC2_5HZ	18μrad	19μrad	0.24	0.24	0.24	110μrad	130μrad	30μrad	1.9	2.2	0.8
HRTC2_1HZ	20μrad	23μrad	0.18	0.7	0.4	90μrad	300μrad	130μrad	1.6	2.7	0.8
HRTC2_LOHZ	8μrad	13μrad	0.75	6.0	1.3	300μrad	2.5μrad	450μrad	0.5	0.7	0.3
HRTC3_5HZ	8μrad	20μrad	0.24	0.24	0.24	120μrad	130μrad	25μrad	1.6	3.5	0.5
HRTC3_1HZ	9μrad	21μrad	0.18	0.71	0.4	90μrad	300μrad	130μrad	0.8	1.8	0.5
HRTC3_LOHZ	4μrad	16μrad	0.75	6.0	1.3	300μrad	2.5μrad	390μrad	0.2	0.5	0.3

RELATIVE TRANSLATIONAL MOTIONS ARE ACROSS THE MAGNETIC GAPS RATHER THAN ACROSS THE SIA/PIA

MHRTC1_LO	14μrad	2.9μrad	2.3	12	1.6				1.2	0.7	1.2
MHRTC2_LO	12μrad	11μrad	2.3	1.4	12				0.13	0.5	1.2
MHRTC3_LO	3.2μrad	14.5μrad	12	1.6	2.1				0.1	0.2	0.6
MHRTC1_VLO	2.7μrad	0.5μrad	7.5	42	2				0.04	0.04	0.4
MHRTC2_VLO	2μrad	2.5μrad	6.5	1.8	42				0.03	0.05	0.5
MHRTC3_VLO	0.5μrad	2.6μrad	42	3.8	6.2				0.03	0.07	0.5

* ⇒ LESS THAN 1μrad
 ** ⇒ LESS THAN 0.1nm

STUDY SUMMARY

- **THE POINTING ERRORS FOR THE RIGID BODY CG MOUNTED POF ARE SO LOW THAT AN ISOLATOR, ACTIVE OR PASSIVE, SHOULD NOT BE REQUIRED. PAYLOAD FLEXIBILITY SHOULD BE THE DRIVING ERROR SOURCE.**

- **THE MAGNETIC ISOLATION AND POINTING SYSTEM OFFERS A SIGNIFICANT IMPROVEMENT IN POINTING PERFORMANCE FOR AN END MOUNTED POF.**

(1)

STUDY SUMMARY

- **FOR THE HRTC PAYLOAD, AN ACTIVE MAGNETIC ISOLATION AND POINTING SYSTEM HAS BETTER POINTING PERFORMANCE THAN THE PPS WITH A BASE ISOLATOR IF THE TWO SYSTEMS HAVE THE SAME ISOLATION BANDWIDTH. - BUT THE MAGNETIC SYSTEM REQUIRES GREATER RELATIVE MOTION AT THE ISOLATOR INTERFACE.**
- **A 0.1 HZ PASSIVE BASE ISOLATOR PROVIDES A TWO TO ONE IMPROVEMENT IN POINTING PERFORMANCE WITH ISOLATOR INTERFACE MOTION WELL WITHIN THE LIMITS OF THE HONEYWELL PROPOSED ISOLATOR ELEMENT.**

STUDY SUMMARY

- **AN ACTIVE MAGNETIC SYSTEM PROVIDES COMPARABLE
IMPROVEMENT WITH AN ISOLATION BANDWIDTH OF
0.3 HZ.**

RECOMMENDATIONS

- **THE ASO POINTING STUDY SHOULD BE UPDATED AND PERHAPS EXPANDED TO MORE CASES WHEN MORE DETAILED INFORMATION ON DISTURBANCE SOURCES, SPACE STATION CHARACTERISTICS, AND PPS CHARACTERISTICS ARE AVAILABLE.**
- **THE SIMULATION GENERATED FOR THE ASO POINTING STUDY OFFERS THE BASIS OF A SIMULATION FOR ASSESSING POINTING CONTROL OPTIONS FOR A FLEXIBLE POF PAYLOAD**

THERMAL

ASO THERMAL STUDY

A top level thermal study of the ASO concept was undertaken to identify potential problem areas and possible solutions.

When considering HRTC the major objectives were to minimize the amount of trapped heat within the HRTC, and maintain to electronics temperatures within operational limits. Thermal distortion of the structure should not be a major problem since the HRTC is normally pointed to the sun an exterior insulation will minimize thermal gradients. The optical design of the telescopes will need to incorporate baffles and a heat dump window to reflect unneeded sunlight out of the tube before it is absorbed. For the shorter wavelength telescopes the possibility also exists covering the aperture with material that is transparent at the observing wavelength, but reflective in the visible, to prevent entrance of most solar energy. Electronics boxes will be thermally isolated from the structure to minimize induced distortion. The PPS coolant loop will also be used to actively control temperatures at critical points.

During normal operation, the only part of P/OF exposed to the sun is the occulting plane. The only components of the occulting plane that are thermally sensitive are the rotating modulation collimator's bearings and drive motors. A front surface coating which is reflective in the visible but transparent at the observing wavelengths will minimize solar heating. If necessary, heaters could be used to maintain temperatures above minimum. The lower end detectors and electronics will be in shadow during normal operation, and may require heaters. Active cooling using the fluid loop will be used for local control.

Thermal data was not available for the High Energy Facility, but we expect a combination of fluid loop control and integral heat pipes and radiators to suffice.

ASO THERMAL STUDY

CONCERNS:

Minimization of trapped heat inside canister

Maintaining electronics temperatures within operational limits

CONSIDERATIONS:

Baffles to block and reflect excess radiation

Optical properties and coatings for thermal protection

Electronics mounting schemes to control conduction

Heat pipes to distribute heat over surfaces used as radiators

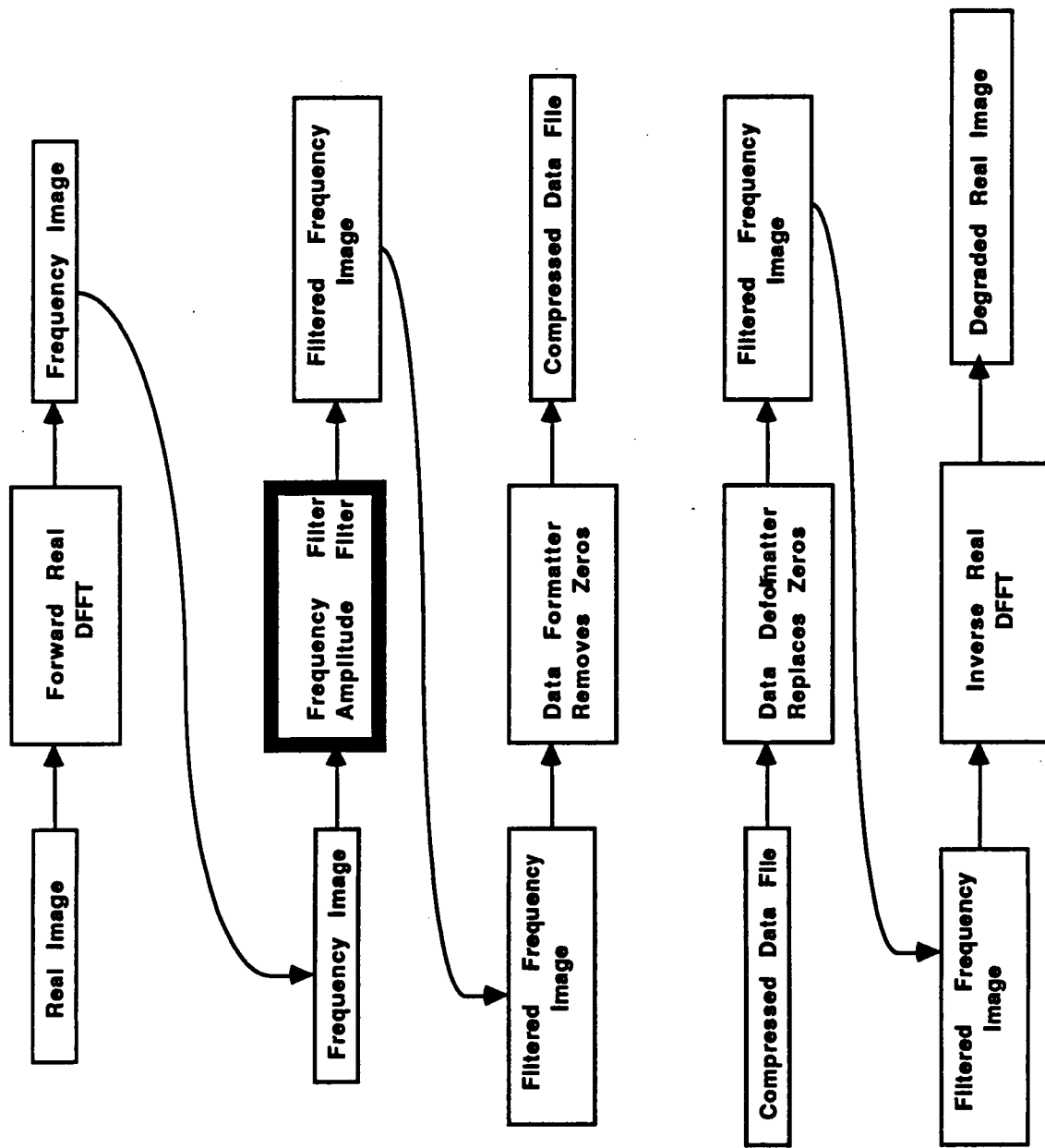
Windows in telescope tube to dump excess radiation

DATA COMPRESSION

DISCRETE FAST FOURIER TRANSFORM (DFFT) DATA COMPRESSION

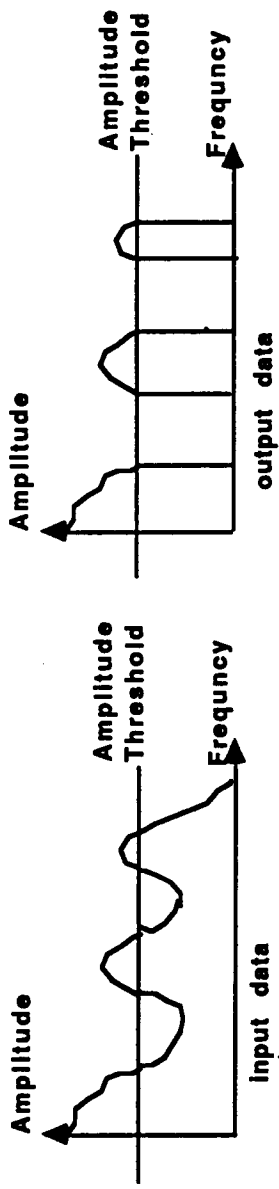
A simple image compression method can be implemented using a DFFT. The basic concept is to convert an image to its fourier transform image, or frequency image, where frequency domain processing can be done. In the frequency domain, operations to any point of the image correspond to distributed operations in the real domain. By application of simple frequency and/or amplitude filtering one can remove terms from the frequency image. The loss of these terms results in a smaller representation of the image at the price of a reduced overall image quality when it is reconstructed. The DFFT can be performed in real time with current technology.

SIMPLE DISCRETE FAST FOURIER TRANSFORM (DFFT) DATA COMPRESSION

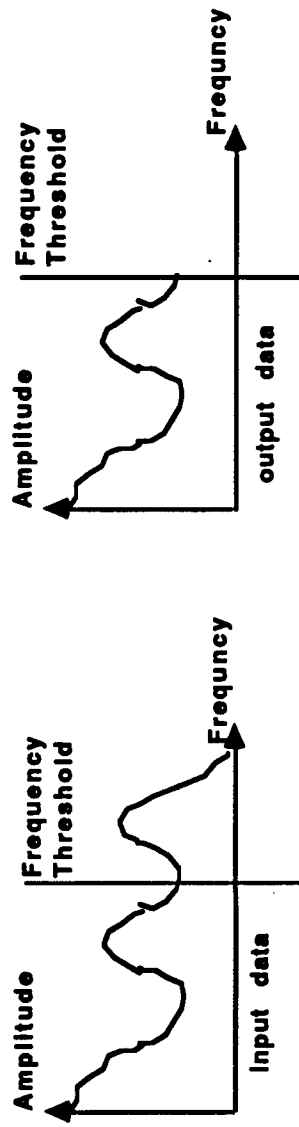


Frequency Domain Filtering : Simple Operators for compression

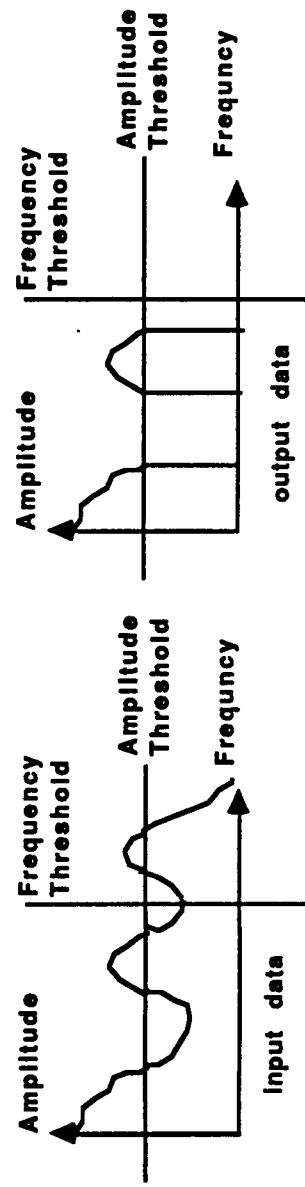
* Amplitude Filter:



* Frequency Filter:



* Amplitude & Frequency Filter:



DFFT compression examples

A one-dimensional real DFFT was implemented on each pixel row of a 512X480 input image. Reconstructed images are shown after respective amplitude and/or frequency filtering. In cases 1&2 amplitude filtering was done. In cases 3&4 frequency filtering was done. And in cases 5&6 amplitude and frequency filtering was performed. The black to white inversion of some pixels is the result of the reconstructed image having gray scale values exceeding the display computer's limits. Compression ratios were estimated by:

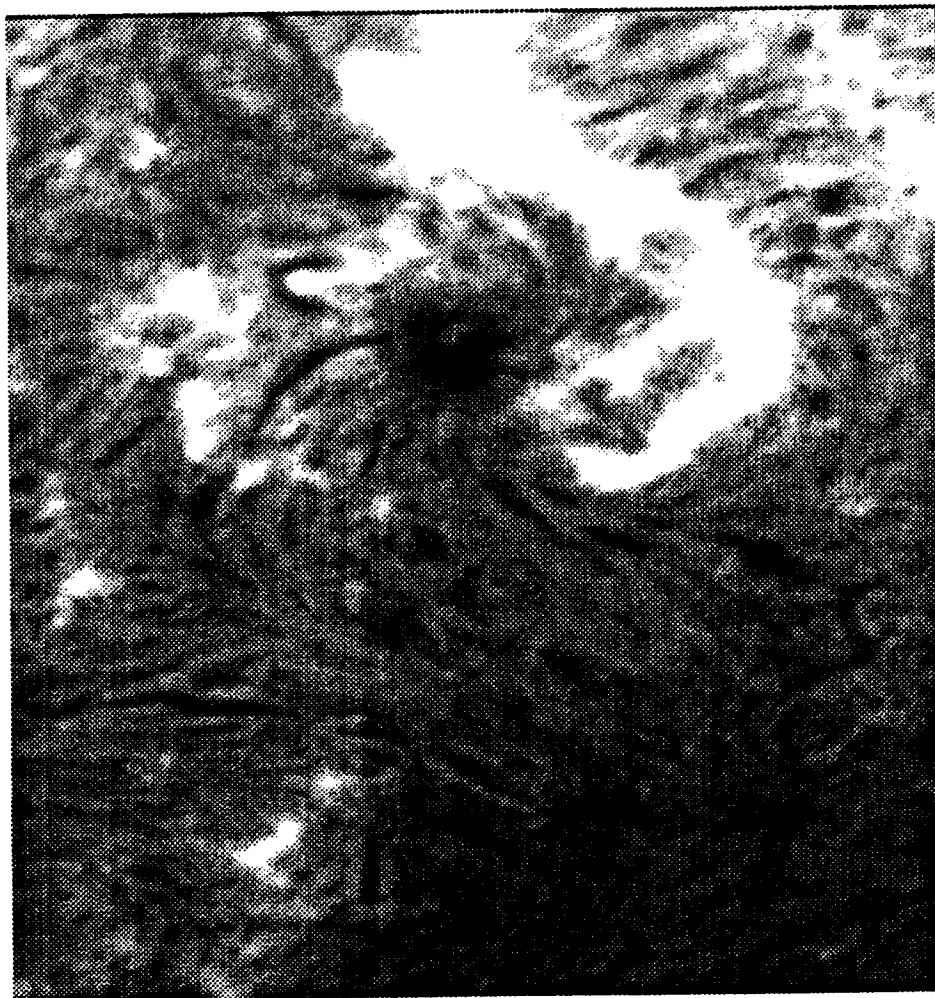
$$\text{Compression} = \frac{1}{N} \sum_{i=1}^N \frac{1}{1 + \frac{Z_i}{N}}$$

Z_i = Number of terms which were removed
from the pixel row frequency image. (i.e. the number of zeros)

N = Number of pixels in the row

ORIGINAL PAGE
BLACK AND WHITE PHOTOGRAPH

Input Image: Solar surface



TELEDYNE
BROWN ENGINEERING
CUMMINGS RESEARCH PARK
HUNTSVILLE, ALABAMA 35807

ORIGINAL PAGE
BLACK AND WHITE PHOTOGRAPH

case 1: Amplitude Filter
compression ratio: 1.969:1



TELEDYNE
BROWN ENGINEERING
CUMMINGS RESEARCH PARK
HUNTSVILLE, ALABAMA 35807

ORIGINAL PAGE
BLACK AND WHITE PHOTOGRAPH

case 2: Amplitude Filter
compression ratio: 4.894:1



TELEDYNE
BROWN ENGINEERING
CUMMINGS RESEARCH PARK
HUNTSVILLE, ALABAMA 35807

ORIGINAL PAGE
BLACK AND WHITE PHOTOGRAPH

case 3: Frequency Filter
compression ratio: 2.003:1



TELEDYNE
BROWN ENGINEERING
CUMMINGS RESEARCH PARK
HUNTSVILLE, ALABAMA 35807

ORIGINAL PAGE
BLACK AND WHITE PHOTOGRAPH

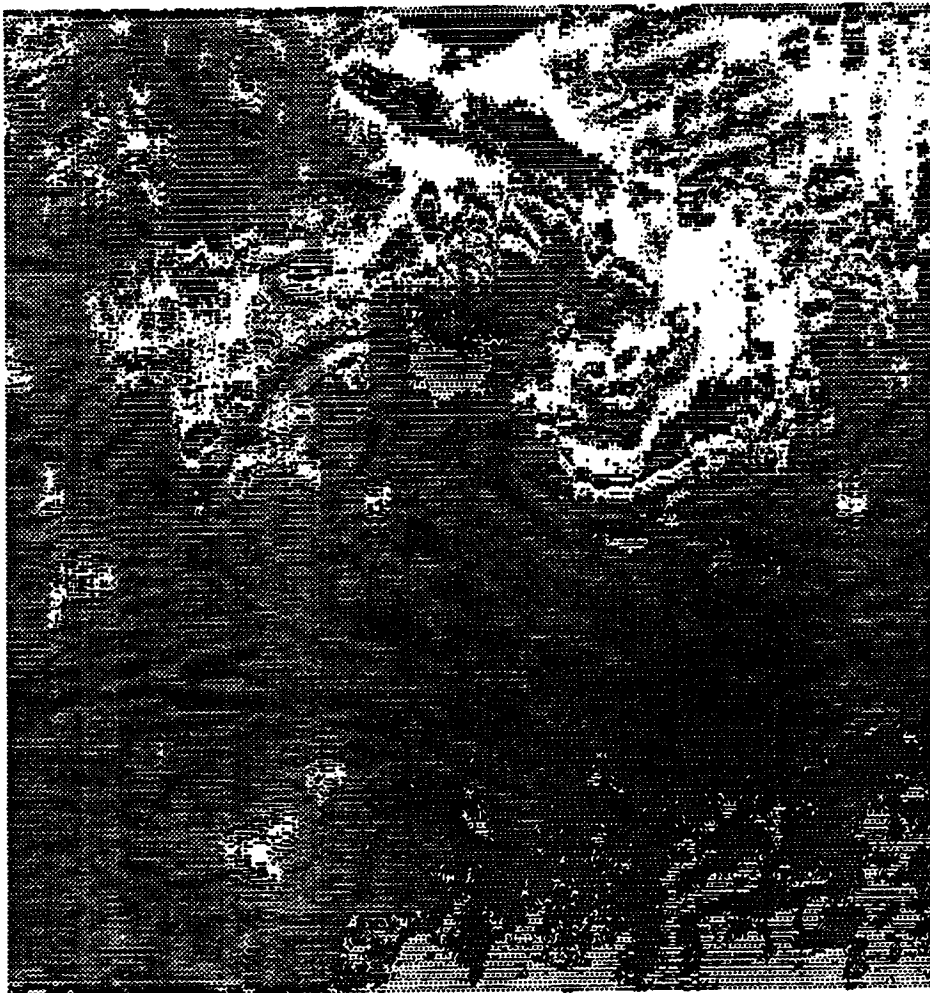
case 4: Frequency Filter
compression ratio: 4.577:1



TELEDYNE
BROWN ENGINEERING
CUMMINGS RESEARCH PARK
HUNTSVILLE, ALABAMA 35807

ORIGINAL PAGE
BLACK AND WHITE PHOTOGRAPH

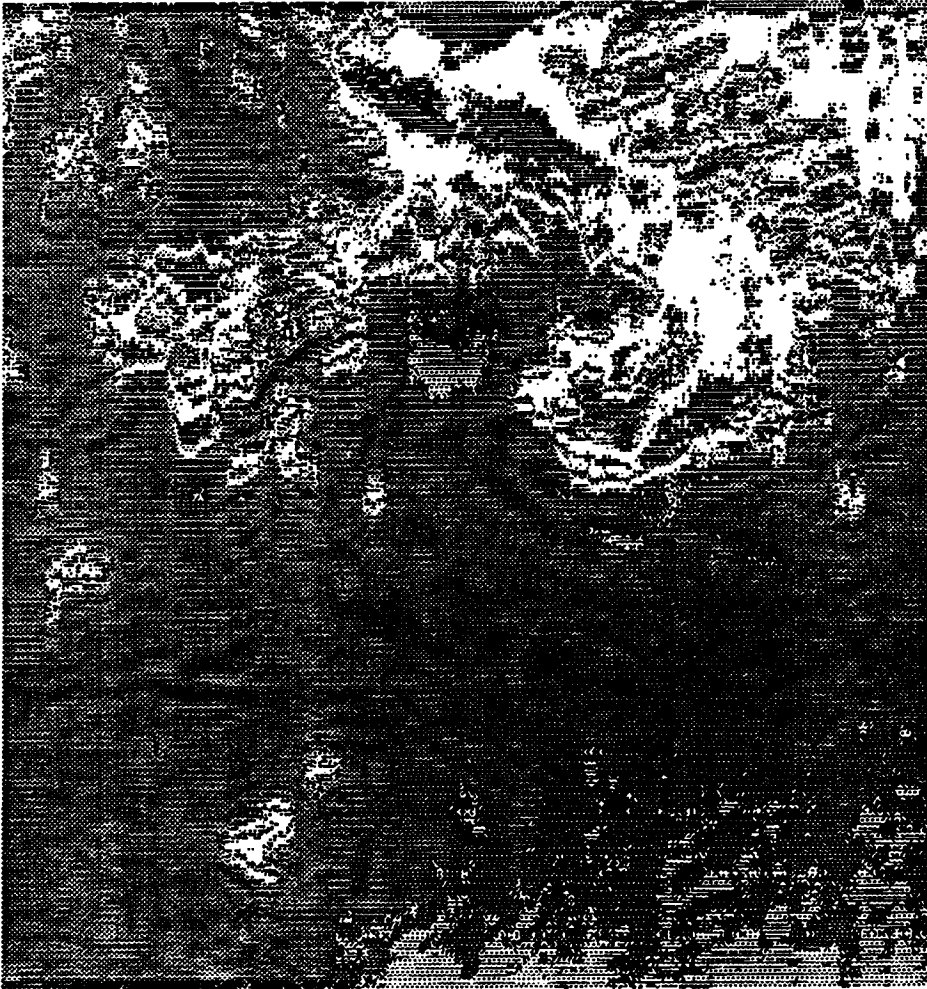
case 5: Frequency & Amplitude Filter
compression ratio: 2.077:1



TELEDYNE
BROWN ENGINEERING
CUMMINGS RESEARCH PARK
HUNTSVILLE, ALABAMA 35807

ORIGINAL PAGE
BLACK AND WHITE PHOTOGRAPH

case 6: Frequency & Amplitude Filter
compression ratio: 5.025:1



TELEDYNE
BROWN ENGINEERING
CUMMINGS RESEARCH PARK
HUNTSVILLE, ALABAMA 35807

IMAGE COMPRESSION USING IFS TECHNIQUES

An examination was made of the feasibility of using iterated function systems (IFS) for image compression. IFS's are used to make fractals which imitate natural textures with minimal information. By appropriate choice of function, reconstruction can be exact. However, no automated method of choosing the function currently exists. Considerable advances in automation and speed of the process are needed before it would be suitable for scientific data. However, IFSs show promise for use on data used for real-time monitoring. The data compression ratio that is potentially achievable with IFS's is extremely large (several orders of magnitude).

IMAGE COMPRESSION USING IFS TECHNIQUES

- o A preliminary experiment was done to explore the application of Iterated Function Systems to image compression
- o The goal of the experiment was to use a simple BASIC program to build an IFS which produced a fractal representing a solar feature. The derivation of the IFS was not automated
- o Result, 46 IFS codes that closely resemble a sunspot family

WHAT ARE IFS's?

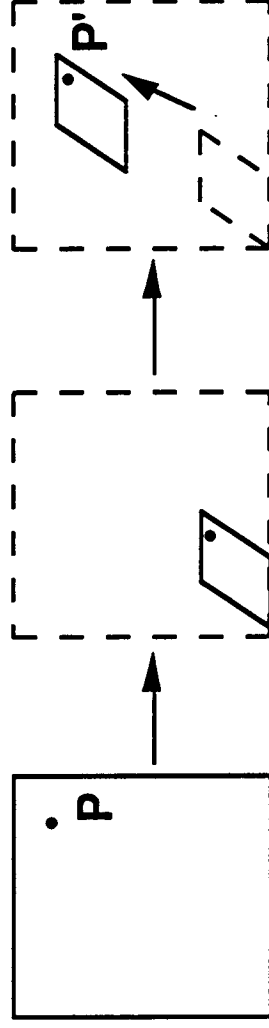
Iterated function systems are simply collections of transforms each of which re-maps the points within a space. The image compression experiment used all 2D linear transforms.

By choosing a starting point and acting on it by a long sequence of transforms from the IFS in random order one makes the point dance around in the space. The computer records on the screen the places where the dancing point touches.

WHAT ARE IFS'S ?

- o Iterated Function Systems are collections of transforms that operate in some space

Example: a linear transform in 2D



... the action of the transform on the rectangle shrinks it and then translates it. Point P is mapped to P'

- o An IFS makes a fractal. Pick a starting point and use a randomly chosen transform of the IFS to map it back into the space. Repeat the procedure for the new point. Continue in this fashion to build up an attractor of a dynamic system. A fractal

AN IFS IMAGE COMPRESSION EXAMPLE

This shows the image we modeled with IFS's. The output image is the actual record of locations visited by the dancing point. Since the original image was essentially black and white the output image was made just black and white (1 bit per pixel). However, the frequency with which the dancing point visits a screen pixel can be used to create a grey scale image, allowing the encoding of digital images with more than 1 bit per pixel.

AN IFS IMAGE COMPRESSION EXAMPLE



Mukul R. Kundu, University of Maryland, College Park

Original image



Output image

- o The example output image was ~600x200 pixels, 120000 bits. It's IFS code was contained in a ~4500 bit binary file, yielding a compression ratio of 27/1. More efficient storage of IFS codes and encoding of multi bit-plane images will yield even higher compression

SUNSPOT FAMILY IFS PARAMETERS

These are the actual linear transforms that produced the output image of the preceding page.

SUNSPOT FAMILY IFS PARAMETERS

a	b	e	c	d	f	a	b	e	c	d	f
0.620	0.000	170	0.000	0.660	118	0.120	0.020	99	-0.060	0.070	89
-0.590	-0.160	773	0.150	-0.590	303	0.090	0.000	159	-0.010	0.060	83
0.200	-0.610	486	0.510	0.230	-26	0.150	0.000	146	0.000	0.150	29
0.520	0.250	117	-0.350	0.610	245	0.070	-0.090	219	0.090	0.120	-21
0.600	0.000	221	0.000	0.700	91	0.140	0.130	133	-0.050	0.140	24
0.680	0.270	104	-0.040	0.740	59	0.180	0.000	163	0.000	0.190	0
-0.730	0.340	707	-0.360	-0.700	594	0.120	0.070	171	-0.050	0.160	17
0.100	-0.050	-20	0.030	0.120	12	0.120	0.050	188	-0.050	0.080	51
0.000	-0.020	194	0.000	0.000	278	0.100	0.000	147	-0.040	0.100	85
0.000	-0.020	197	0.010	0.000	218	0.070	0.000	-10	-0.010	0.050	67
0.000	-0.020	35	0.000	0.000	291	0.180	0.010	170	0.090	0.160	-11
0.000	-0.020	274	0.020	0.000	280	0.000	0.160	253	-0.040	-0.010	73
-0.010	-0.030	260	0.020	-0.010	243	-0.020	-0.500	574	0.420	0.010	27
0.010	-0.030	111	-0.020	-0.010	246	-0.050	0.000	205	0.010	0.130	69
0.000	-0.040	142	0.030	0.000	243	0.050	0.000	176	0.000	0.100	72
-0.420	0.000	463	0.000	0.460	-55	0.100	0.000	198	0.000	0.060	17
0.640	0.000	411	0.000	0.440	-49	0.050	0.000	176	0.000	0.100	61
0.180	0.000	-46	0.000	0.180	20	0.000	-0.020	185	0.020	0.000	278
0.050	0.000	-3	0.000	0.050	55	0.000	-0.080	82	0.020	0.010	235
0.280	0.000	-46	0.000	0.280	11	0.000	-0.020	195	0.020	0.000	245
0.150	0.020	55	-0.030	0.100	31	0.500	0.000	330	0.000	0.500	-98
0.300	0.000	23	-0.040	0.150	69	0.500	0.000	460	0.000	0.540	-24
0.190	-0.010	58	-0.010	0.130	74	0.180	0.000	93	0.000	0.200	208

$$\begin{pmatrix} a & b \\ c & d \end{pmatrix} \begin{pmatrix} x \\ y \end{pmatrix} + \begin{pmatrix} e \\ f \end{pmatrix}$$

The values a-f represent the linear transform

OPERATIONS

OPERATIONS OBJECTIVES

The basic objective of the operations analysis was to identify any problem areas associated with accommodating the activities required to operate ASO.

The analysis proceeded by developing functional objectives for each of the operating modes specified; determining the role of the on-board crew and ground operators; analyzing the interactions between crew and ground; analyzing the data flows required for operation, monitoring, and science; evaluating the adequacy of on board standard accommodations; and assessing the potential benefits of automation.

OPERATIONS OBJECTIVES

Develop functional objectives for each operating mode

Analyze each step to determine the role of the on-board crew and ground operators

Analyze the crew-operator interactions

Analyze the data flows for data handling and display equipment

Evaluate on-board requirements with respect to standard accommodations to determine ASO-unique equipment

Assess the potential benefits of automated functions

SPACE STATION ACCOMMODATIONS

This chart summarizes the accommodations provided by Space Station to payloads. In particular, note that there are four utility ports on the truss which are potential payload attachment points, but only two sets of Attached Payload Accommodation Equipment (APAE), and only one pointing system. Only two utility ports are on the truss upper face. ASO is composed of three facilities, each of which requires pointing.

SPACE STATION ACCOMMODATIONS

The Space Station Program (SSP) provides a permanently manned research facility pre-launch, launch and post-landing services.

The basic structure of the SS is a traverse truss, 4 pressurized modules, four connecting nodes and an airlock

SPECIFIC ACCOMMODATIONS

- . Eight crew max (2 shift, 4/shift operation)
Four utility ports on the truss
- . Two APAE (one with a pointing control system) for use at the utility ports
- . Support Subsystems
 - . Data Management and Information Processing
 - . Power
 - . Thermal Control
 - . Communications and Tracking
 - . Guidance, Navigation and Control
 - . Human Life Support
 - . Fluid Management
- . Transport, installation, and removal, while at the station, of attached payloads
- . Normal payloads operations, including routine maintenance servicing and repair
- . Contingency Maintenance and Servicing
- . Grapple fixtures
- . Mobile Servicing Center (MSC)
- . Flight Telerobotic Servicer (FTS)
- . Crew Support Station in the Laboratory Module to monitor/control attached payloads
- . EVA/IVA

SUMMARY OF STATION-PROVIDED RESOURCES

This chart summarizes the resources provided by the Space Station to attached payloads.

SUMMARY OF STATION-PROVIDED RESOURCES

Services	Standard Capacity each port	Optional Capacity each port
POWER	208 Vac, 20 kHz, 10 kW max (PPS - 5 kW)	120/208 Vac, 60 Hz 28 Vdc (Converters and losses are charged to users)
THERMAL	Cold Plate (24 deg F) 10kW max. (PPS 5kW max)	TBD
COMMAND & DATA HAND.	10 Mbps LAN Real Time commands Data Return Storage and Buffering	100 Mbps P/L LAN Increased storage
MONITORING DATA	Contamination Altitude Orbit Ephemeris	TBD

DATA MANAGEMENT ACCOMMODATIONS

This chart summarizes the data management accommodations provided to attached payloads. Note that use of maximum resources impacts other Space Station users. Also, continuous use of maximum data rate will exceed the daily volume of data.

DATA MANAGEMENT ACCOMMODATIONS

Data management services provided by the SSP during the on-orbit phase of the mission on-board storage and display of experiment data and video images, payload system diagnostics, payload servicing end-to-end checkout, internal audio and video, hard copy presentation of single frame imagery (including video) uplink and downlink transmission services

SPECIFIC CAPACITIES

- . Transmit at least 275 MBPS of user data to ground
- . Daily volume of at least 1 terabyte
- . Capability to handle data rates of 100 MBPS and analog video at each APAE attached payload location
- . On-line, rapid access mass storage capability of (TBD) bits
- . Buffer storage capability and removable media capability, with total on-board storage of 1 terabyte
- . Handle high data rate payload data rates for data transfer to buffer storage, prior to transmission to ground
- . Electronic reallocation capability to interconnect input/output signals for payload communications
- . Command and control support.

APAE ACCOMMODATIONS

Attached Payload Accommodation Equipment (APAE) is equipment and services provided by the Space Station for users. Not all the equipment is required by all payloads, and the user can provide substitute equipment if necessary.

APAE ACCOMMODATIONS

The APAE provides

accommodations for external user payloads attached to the truss. all hardware and software interfaces required for the installation, check-out, operation, maintenance, repair and removal of payloads attached to the traverse truss. access to the power, data and thermal resources of the Space Station. mechanical attachment and structural support for payloads for selected launch configurations and all on-orbit environmental conditions

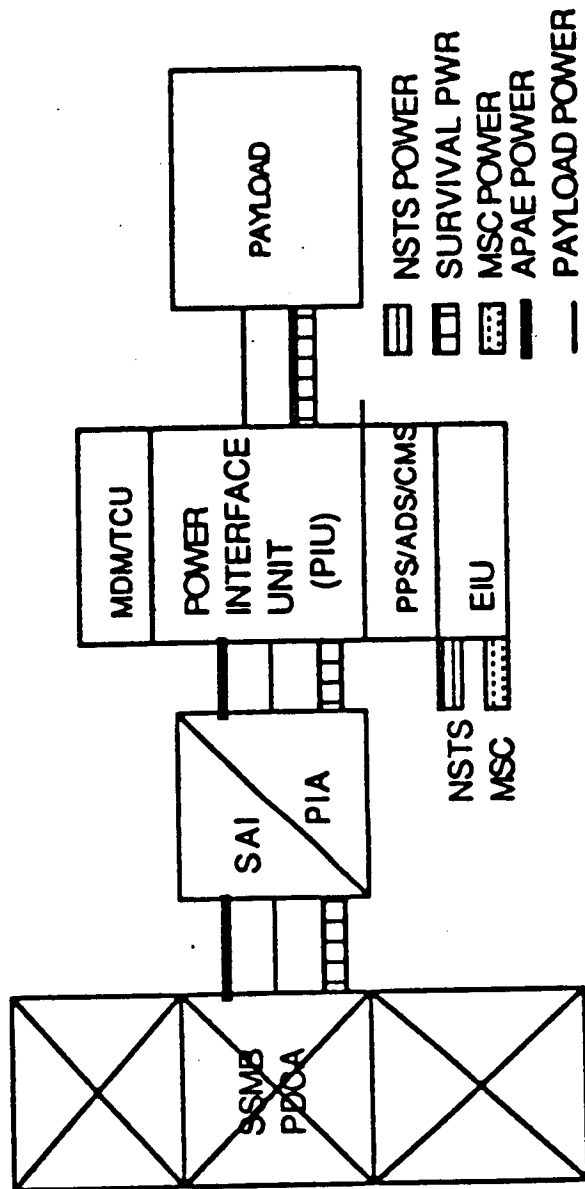
MAJOR SUBELEMENTS

- . Payload Attach System (PAS)
- . Station Interface Adapter (SIA)
- . Payload Interface Adapter (PIA)
- . System Support Module (SSM)
- . Deck Carrier
- . Multiple Payload Adapters (MPSS)
- . Payload Cold Plates
- . Contamination Monitoring System (CMS)
- . Payload Pointing System (PPS)
- . Attitude Determination System (ADS)
- . Payload related coordinate system information
 - . APAE reference coordinate system
 - Antenna/Instrument coordinate system

APAE/EPS FUNCTIONAL BLOCK DIAGRAM

This chart illustrates the functional structure of the electrical power system APAE.

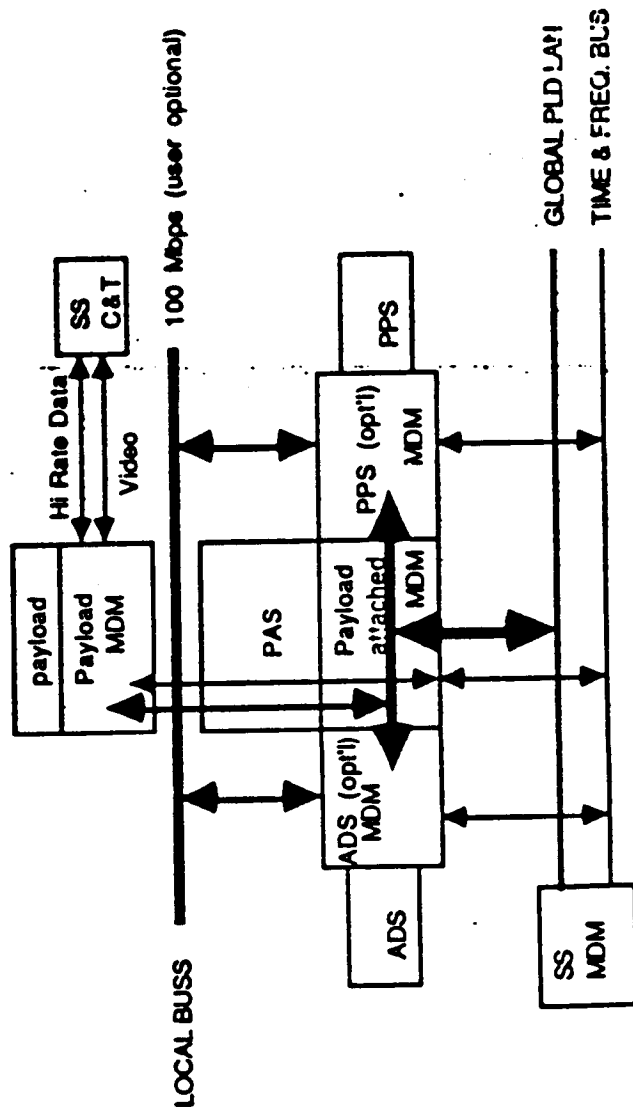
APAE/EPS FUNCTIONAL BLOCK DIAGRAM



APAE/DMS FUNCTIONAL BLOCK DIAGRAM

This chart illustrates the functional structure of the data management system APAE.

APAE/DMS FUNCTIONAL BLOCK DIAGRAM



DEVELOPMENT OF FUNCTIONAL OBJECTIVES

AND

REPRESENTATIVE FLOWS

SUMMARY OF ACCOMMODATIONS REQUIREMENTS DESIGN DATA

Accommodations requirements for the HRTC and P.OF are summarized on this chart. Uplink (control) data requirements have not been defined, but should be well within the Space Station capabilities if the ASO command and data system is capable of interpreting high level commands. The crew manhours assume the data downlink is not capable of supporting sufficient data for real time control from the ground. There appear to be techniques to minimize the downlink rate requirements that will permit operation from the ground. A realistic estimate is that the crew will only be required intermittently.

SUMMARY OF ACCOMMODATIONS REQUIREMENTS DESIGN DATA

	HRTC	POF	TOTAL ASO
POINTED MASS (kg)	7,000	2,400	9,400
PWR ACROSS GIMBAL (KW)	2.8	1.3	4.1
HK DATA ACROSS GIMBAL (kbps)	18.2	2.4	20.6
SCIENCE DATA ACROSS GIMBAL (MBPS)	38	1.4	39.4
THERMAL LOAD ACROSS GIMBAL (KW)	2.8	1.3	4.1
TOTAL POWER (KW)	5	3.5	8.5
TOTAL THERMAL LOAD (KW)	5	3.5	8.5
TOTAL HK DATA (kbps)	45.2	29.4	74.6
TOTAL DOWNLINK DATA (MBPS)	38.05	1.43	39.48
TOTAL UPLINK DATA (MBPS)	TBD	TBD	TBD
CREW MANHOURS PER DAY			
S'VEILLANCE MODE	TBD	TBD	TBD
FLARE MODE	16	16	16
CAMPAIGN MODE	16	16	16
FACILITY SERVICING RQMTS			
EVA CREW M'HOURLS	TBD	TBD	TBD
IVA CREW M'HOURLS	TBD	TBD	TBD
MASS (KG)	TBD	TBD	TBD
VOLUME (CU. M)	TBD	TBD	TBD
FREQUENCY (MOS)	TBD	TBD	TBD

TELESCOPE OPERATING MODES

The ASO has defined three unique operating modes: Campaign mode; Surveillance mode; and Special Event mode.

Campaign mode is intensive operations in support of an investigation of a well-defined scientific problem. Typically, this will involve a group of scientists, all working simultaneously on various aspects of an investigation. It will include a lengthy period (typically one month) of planned, coordinated observations. Operations can be defined well in advance, but ASO usage will be high, and the resources required correspondingly high.

Surveillance mode is, in a sense, the default mode. Whenever a campaign is not in progress, and a special event has not occurred, surveillance mode will be in use. In this mode, observation rate is reduced to only monitor the sun, watching for special events, and possibly collecting routine data. This is the minimum resource requirement mode.

Special Event mode is used whenever an unpredicted transient event (such as a flare) occurs. It uses all observational capabilities of the ASO and requires the maximum resources. Special Event mode may be triggered either automatically or manually.

TELESCOPE OPERATING MODES

CAMPAIGN

SURVEILLANCE

FLARE (SPECIAL EVENT)

STEPS IN TELESCOPE OPERATION

Operating steps for the telescope were identified to develop functional objectives for ASO operation. This chart summarizes the individual steps identified.

This chart is not an ordered listing.

STEPS IN TELESCOPE OPERATION

STARTUP
INITIAL CALIBRATION
RE-CALIBRATION
ANALYZE
MONITOR
SLEW TELESCOPES
COARSE SLEW
FINE SLEW
COMMAND
SHUTDOWN
STANDBY
TAKE DATA
SEND DATA
ARCHIVE DATA
DISTRIBUTE DATA
WARMUP
DOWNLINK

STEP PERFORMANCE LOCATION

The operation steps were analyzed to determine the roles of the Discipline Operation Center (DOC), on-board crew, and automation, in performance of the step.

STEP PERFORMANCE LOCATION

STEP	DOC	ON-BOARD	AUTOMATIC
DEVELOP PASS COMMANDS	P	--	--
VERIFY COMMANDS	P	--	--
UP-LINK COMMANDS	P	--	--
START-UP	CB	P	--
WARMUP	M	M,B	A
INITIAL CALIBRATION	M,B	P	--
SLEW TELESCOPES	M	M,B	A
VERIFY	P	S	--
SHUTDOWN	C	P	--
ANALYZE PROBLEMS	P	C	--
OPERATIONS	P,M	M,B,S	A
ANALYZE DATA (1)	P	S	--
DISTRIBUTE DATA	P	--	--
RECALIBRATE	M	P	--
STANDBY	M	M,B	A
DOWNLINK DATA	M	M,B	A
ANALYZE DATA (2)	P	--	--
ARCHIVE DATA	P	--	--

LEGEND

P PRIMARY
 B BACKUP
 S SECONDARY
 C CONSULTATION
 M MONITOR
 A AUTOMATIC

OPERATION BLOCK DIAGRAMS

This and the following four charts present strawman operation block diagrams for ASO. They apply to any of the facilities individually or in combination.

CHART 1--PRE-OPERATE PHASE

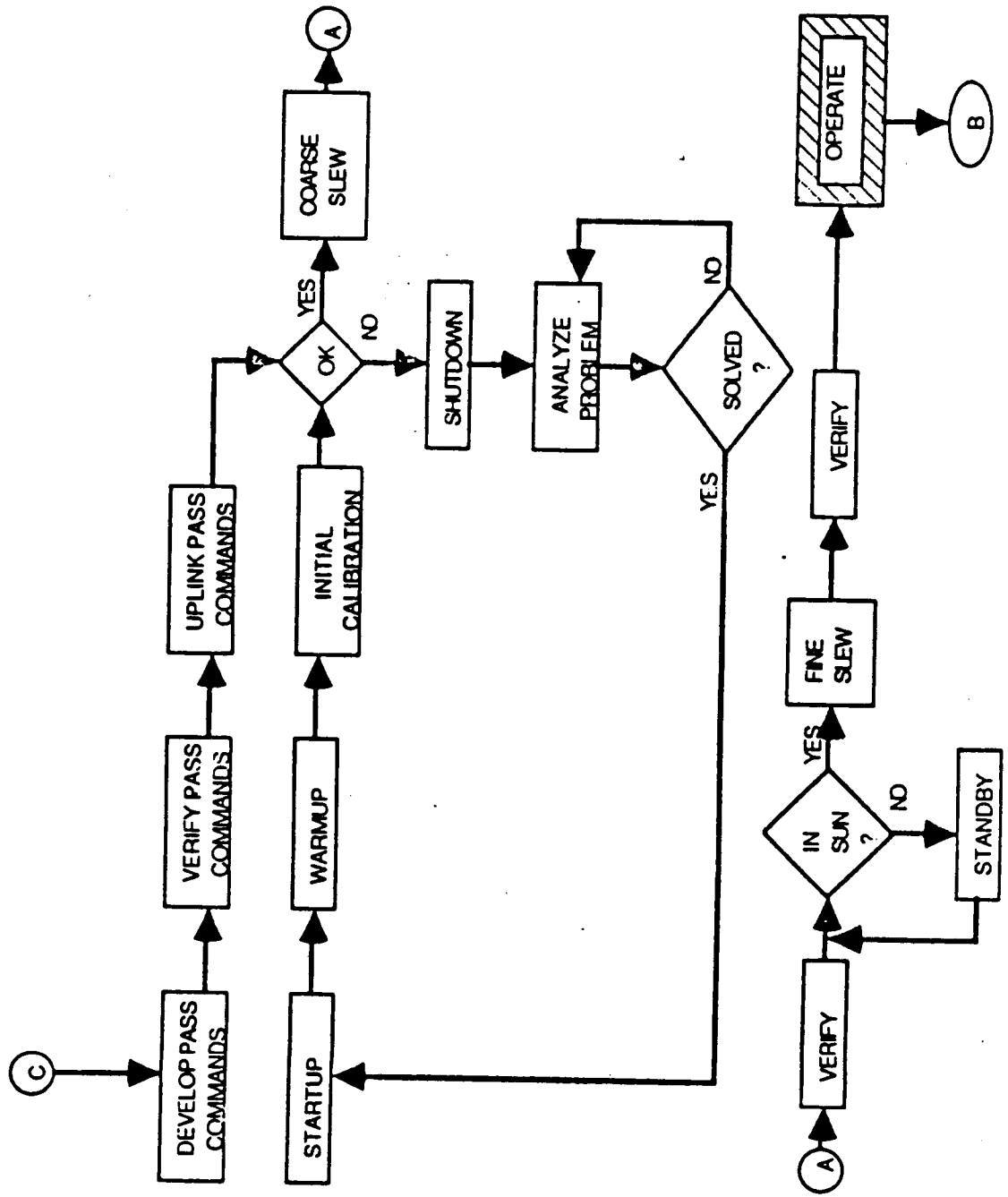


CHART 2-- OPERATE PHASE

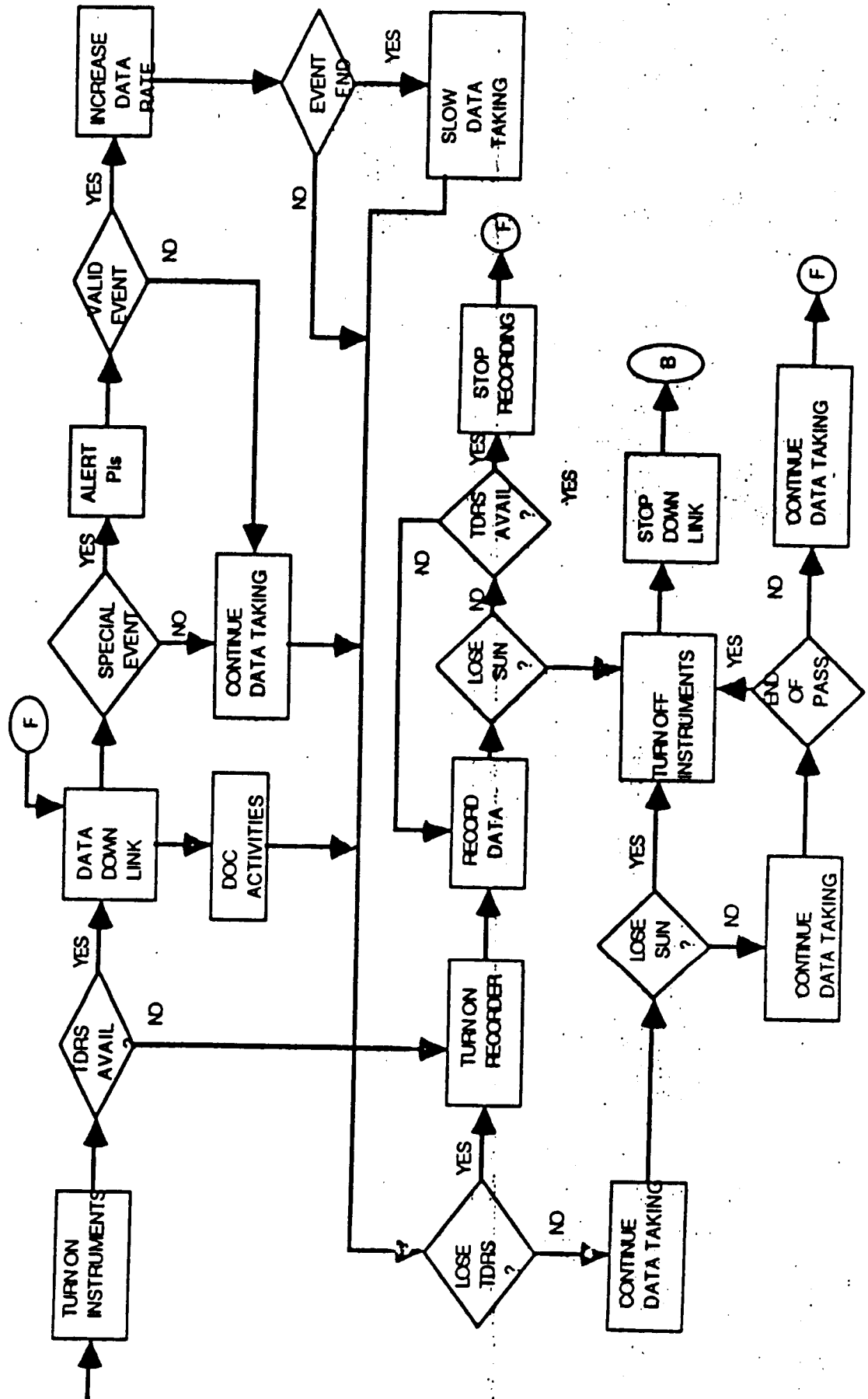


CHART 3-- POST-OPERATE PHASE

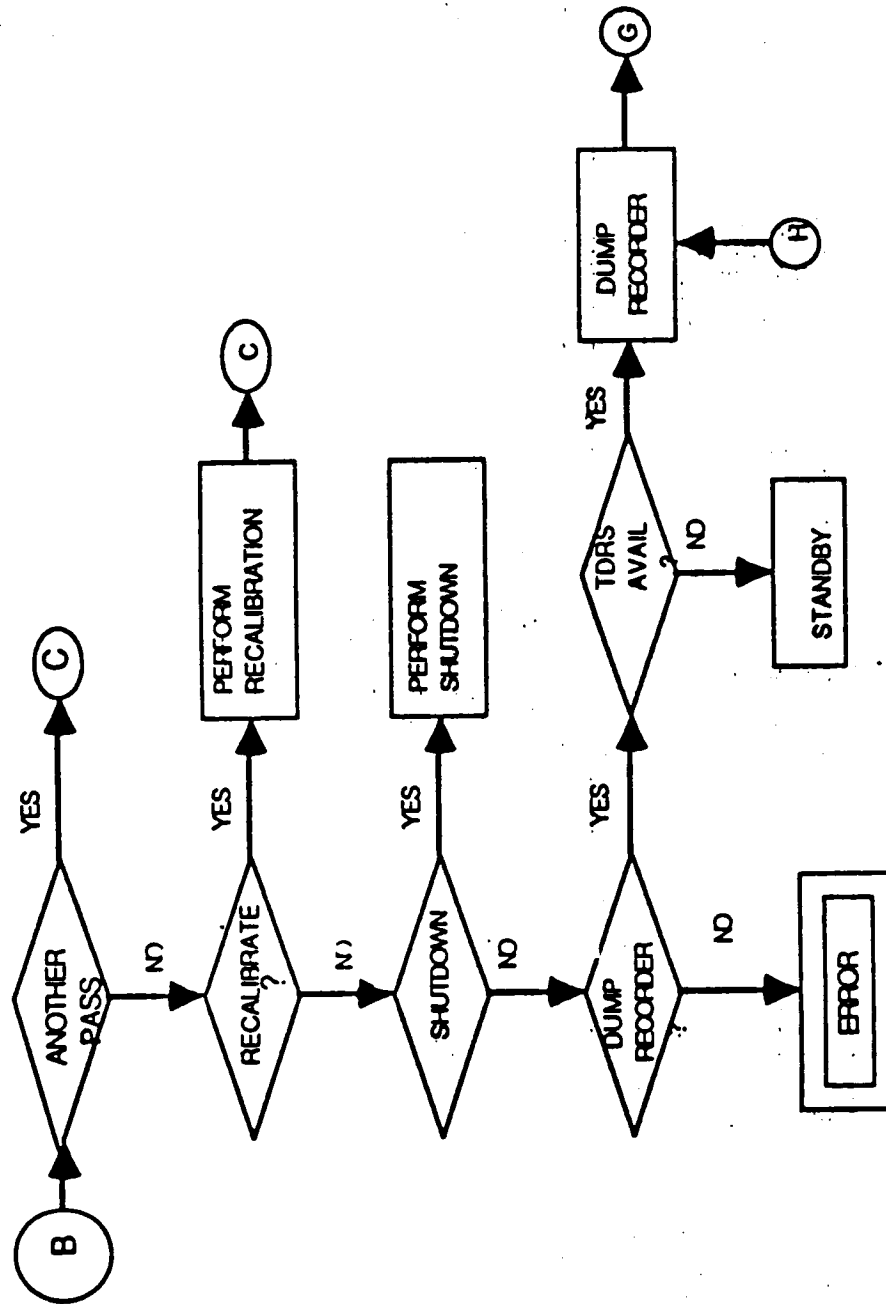


CHART 3-- POST-OPERATE PHASE (con't)

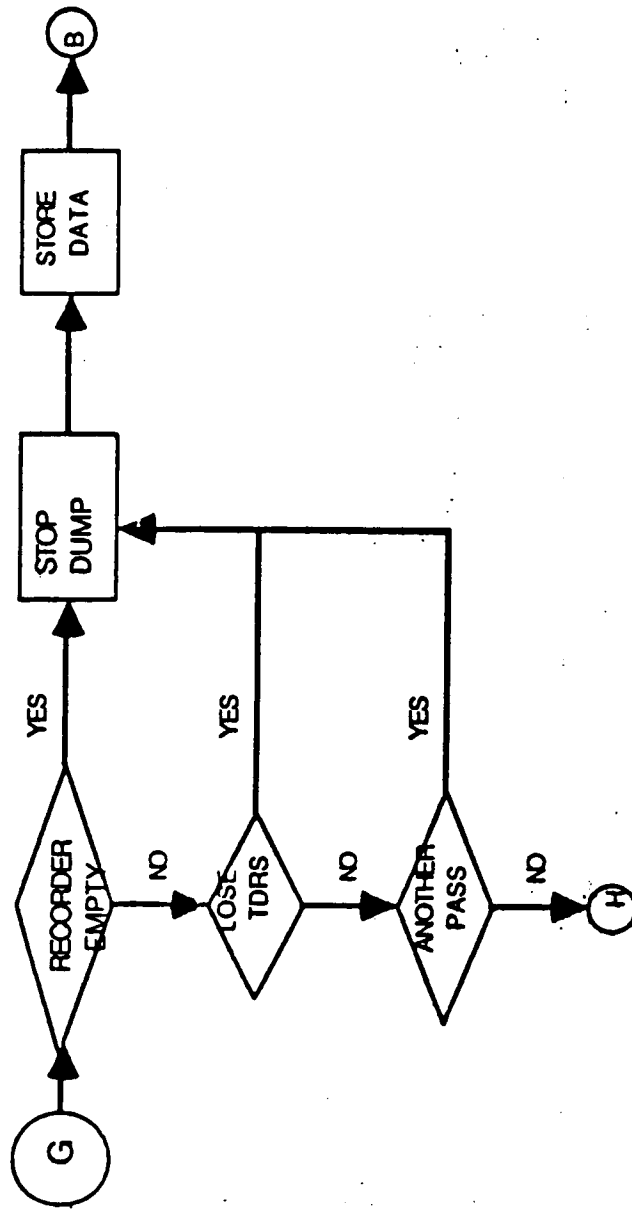
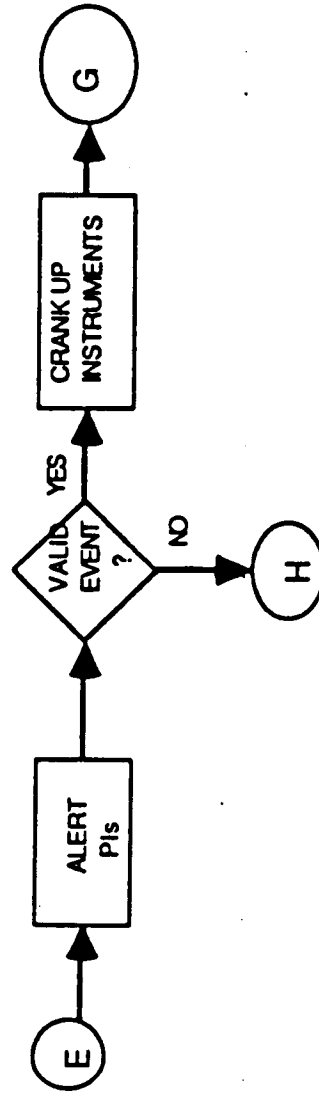


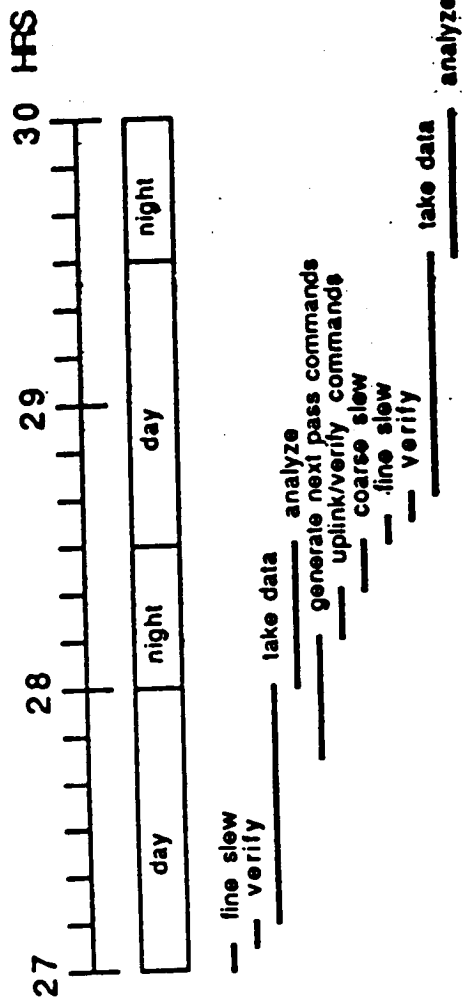
CHART 4-- MISCELLANEOUS FLOWS



TYPICAL OPERATION TIMELINE

Typical sequencing of operations is shown on this chart. The differences between operating modes primarily occur within the "take data" portion of the timeline. Every step may not be required on every orbit, of course.

TYPICAL OPERATION TIMELINE



DATA/COMMUNICATIONS

ASO CONTROL AND DATA RETRIEVAL CONSIDERATIONS

Considered in defining the ASO HRTC control and data retrieval system were the HRTC telemetry requirements to determine if they were compatible with the systems planned for the Space Station and TDRSS.

Data compression was evaluated to determine if it could be used as an acceptable method of reducing the HRTC telemetry requirements.

Recording capabilities were investigated as an alternate means to real time telemetry.

Consideration was given to using film as an alternate method of storing information. The successful use of film on the ATM demonstrated its acceptability.

The ATM control and display console and related schematics were reviewed to identify typical functions that would be used on the HRTC. These functions were then used to evaluate the Space Station multipurpose application console capabilities to determine if it could control and monitor the HRTC without the addition of any peculiar hardware.

ASO CONTROL AND DATA RETRIEVAL CONSIDERATIONS

- **ASO HRTC TELEMETRY REQUIREMENTS**
- **SPACE STATION/TDRSS DATA MANAGEMENT/
TELEMETRY CAPABILITY**
- **DATA COMPRESSION**
- **RECORDING CAPABILITIES
TAPE RECORDERS
OPTICAL DISK**
- **FILM AVAILABILITY/EXPOSED ON THE APOLLO
TELESCOPE MOUNT**
- **ATM CONTROL AND DISPLAY CONSOLE**

REQUIREMENTS/CAPABILITY COMPARISON

TDRSS is listed as having a down link capability of up to 300 Mbps. Up to one half of its total capability is used in encoding the data to assure proper retrieval and identification of the useful data on the ground. A portion of the remaining capability will be used for Space Station housekeeping, caution and warning functions, navigation and tracking, etc. The remaining 100 to 150 Mbps will be made available for payload use.

Two fiber optics links connect the HRTC mounted in the payload pointing system to the Space Station. One link is used for high rate payload data and is capable of 100 Mbps. The second fiber optics link is part of the payload network and is capable of 10 Mbps from the HRTC to the Space Station. This network can be used to control and monitor payloads from the Space Station multipurpose application console or from the ground stations.

The HRTC telemetry requirements in the as shown raw form far exceed the Space Station, TDRSS capability. Dr. Walker is considering using data compression, data selection, etc. to reduce the data requirements to the 10 to 20 Mbps range. This would bring the HRTC requirements more in line with the planned capabilities.

REQUIREMENTS/CAPABILITY COMPARISON

ASO HRTC TELEMETRY REQUIREMENTS				SPACE STATION CAPABILITY		TDRSS CAPABILITY
TELE- SCOPE	SPECTROHELIOGRAPHIC		WIDE FIELD FOCUS		SLIT JAW IMAGES BITS PER IMAGE	
	FOCUS	BITS PER IMAGE	BITS PER IMAGE	FOCUS		
U1	1.2×10^9		1.5×10^8		10^7	UP TO 300 MBPS
E1	3.0×10^8		1.5×10^8		10^7	UP TO ONE HALF USED TO ENCODE DATA
X1	1.5×10^8		1.5×10^8		10^7	APPROX. 150 MBPS
X2	1.5×10^8		1.5×10^8		10^7	USABLE DATA
X3	1.5×10^8		1.5×10^8		10^7	PORTION USED FOR HOUSE- KEEPING
S1	0.4×10^8		0.4×10^8		10^7	NAVIGATION CAUTION AND WARNING, ETC.
S2	NA		1.5×10^8		10^7	
						HI-RATE PAYLOADS DATA LINK 100 MBPS
						PAYLOADS NETWORK 10 MBPS

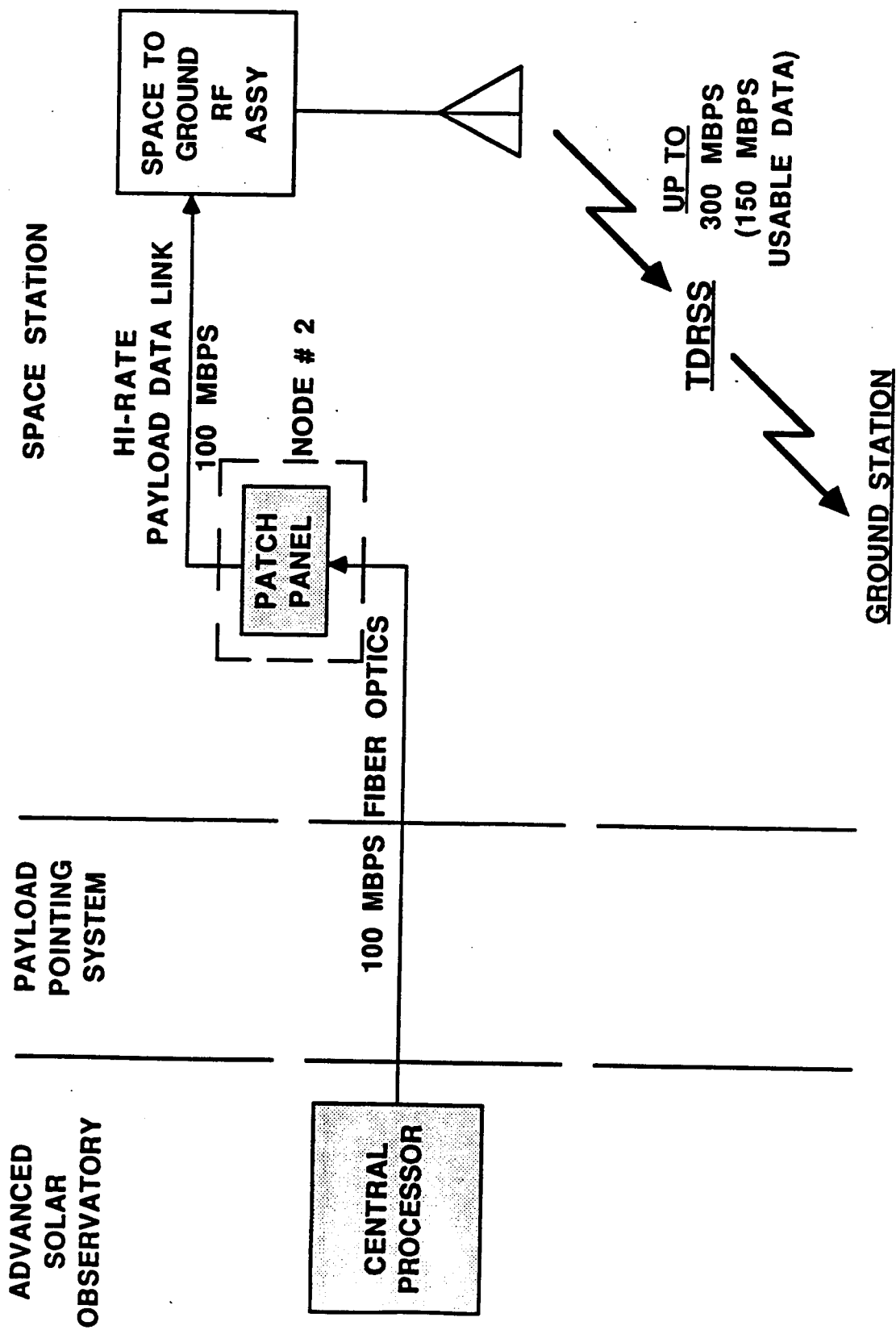
WITHOUT DATA COMPRESSION

DATA FLOW

Data flow is from the ASO HRTC central processor through the fiber optics high rate payload data link to the patch panel in node number two. From the patch panel the data flows to the communication and tracking signal processor to the RF assembly through TDRSS to ground.

The high rate payload data link does not interface with the Space Station payload network. This means that none of the data on the high rate payload data link can be displayed on the Space Station multipurpose application console for real time viewing and can only be monitored on the ground.

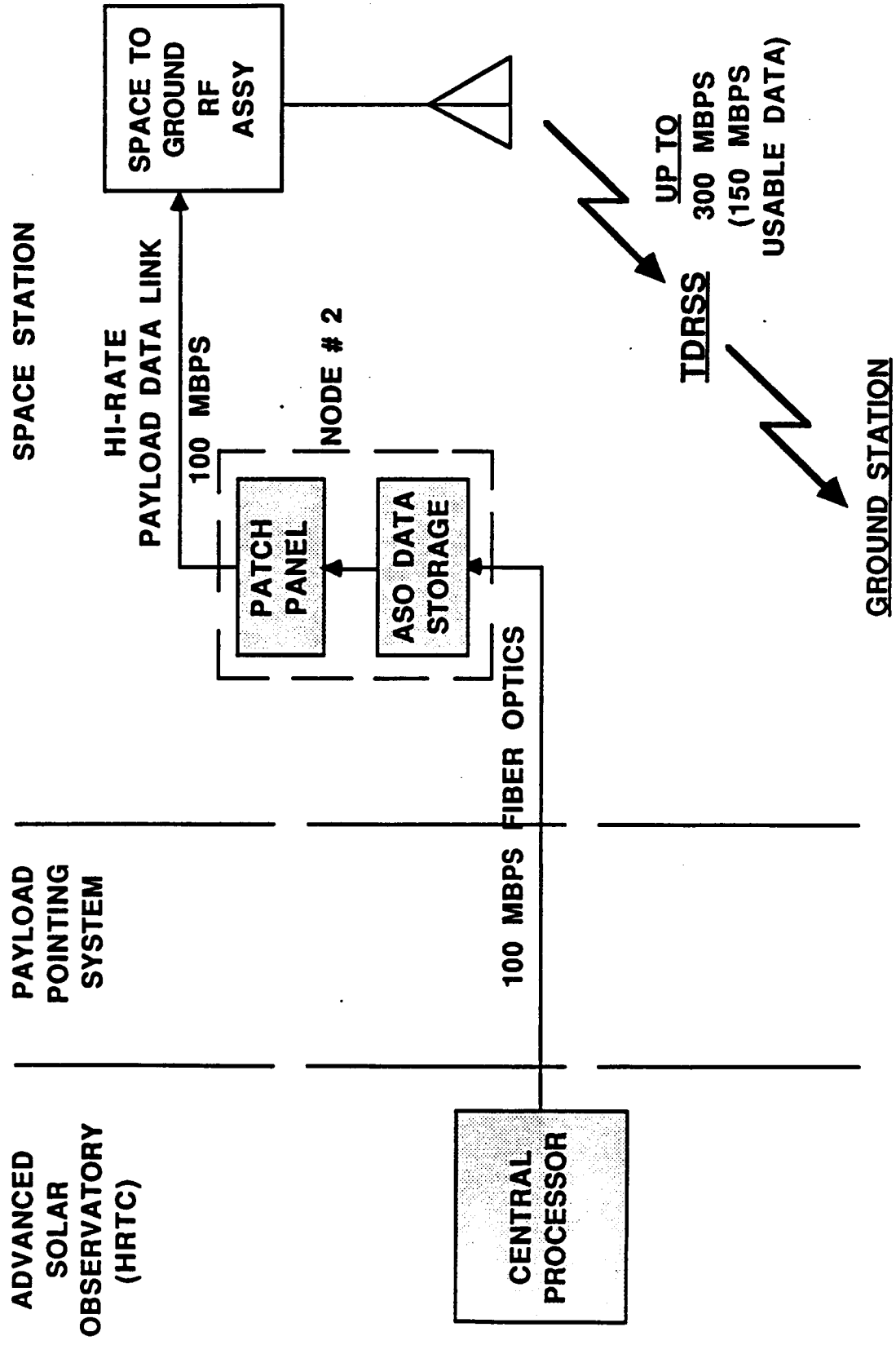
DATA FLOW



DATA FLOW WITH STORAGE CAPABILITY

It is recognized that even with a reduced HRTC telemetry data requirement (10 to 20 Mbps) there will be times when TDRSS will not be available for use by the HRTC. In order to work around this condition consideration was given to placing a HRTC dedicated data storage device in the high rate payload data link just prior to the patch panel in node number two. This would allow storage of data for a short period of time while down linking a small amount of data for review and analysis. The results of the review would determine if the data should be stored and brought back on a resupply mission at a later date or recorded over on the next data taking session. The decision to store or write over data and the storage capability of the recording device would influence the amount of time required by the crew to change and store data tapes. If the data could be reduced to an average of 10 Mbps for a 40 to 45 minute data taking session per orbit the Odetics recorder could store data for approximately 10 orbits. This would require changing tape reels no more than twice in a twenty four hour period. Two reels of one inch wide by fifteen inch diameter tape in a protective container would take up no more than one half cubic foot of storage space.

DATA FLOW WITH STORAGE CAPABILITY



TAPE RECORDING CAPABILITY

In reviewing tape recorders for use on the HRTC the two most promising units found were built by Odetics and Data Tape. Odetics is building a unit for use on the Space Station and Data Tape builds units for the Solid Rocket Booster. The Odetics unit has a fixed head, long life expectancy, but less storage capability than the rotary head unit built by Data Tape.

TAPE RECORDING CAPABILITY

	<u>ODETICS</u>	<u>DATA TAPE</u>
TAPE SIZE	1 INCH 9200 FEET/REEL	1 INCH 10,800 FEET/REEL
RECORD RATE	3 to 300 MBPS	12.5 TO 100 MBPS
RECORD TIME	45 MIN AT 100 MBPS	330 MIN AT 100 MBPS
STORAGE CAPACITY	2.5×10^{11} BITS PER REEL	1.88×10^{12} BITS PER REEL
WEIGHT	165 LBS	65 LBS
VOLUME	5.3 CUBIC FEET	1.5 CUBIC FEET
	BEING BUILT FOR SS USE	

U.S.

OPTICAL DISK RECORDING CAPABILITY

Optical disk recording devices are available from RCA and Kodak. However, there is no flight qualified hardware available. The storage media are somewhat more compact than magnetic tape. Other capabilities are comparable to, or slightly inferior to magnetic tape.

OPTICAL DISK RECORDING CAPABILITY

- 14 INCH DIAMETER DISK
- RECORD RATE 300 MBPS 150 MBPS ON EACH SIDE OF DISK
- STORAGE CAPACITY 80×10^9 BITS 40×10^9 ON EACH SIDE OF DISK
- RECORD TIME 13 MIN AT 100 MBPS
- NO FLIGHT HARDWARE AVAILABLE

QUANTITY OF SKYLAB MISSION ATM SCIENTIFIC DATA

Film is an option that could be used as a backup or complement to the digital data. This could probably be best used during crew operation of the HRTC from the multipurpose application console. This would give the crew member the option to select film exposure on a real time basis.

The telescopes could be designed for film changeout using robotics with crew EVA as a backup.

The chart showing the film exposed on three ATM missions indicates the large amount of data that can be stored on film.

QUANTITY OF SKYLAB MISSION ATM SCIENTIFIC DATA

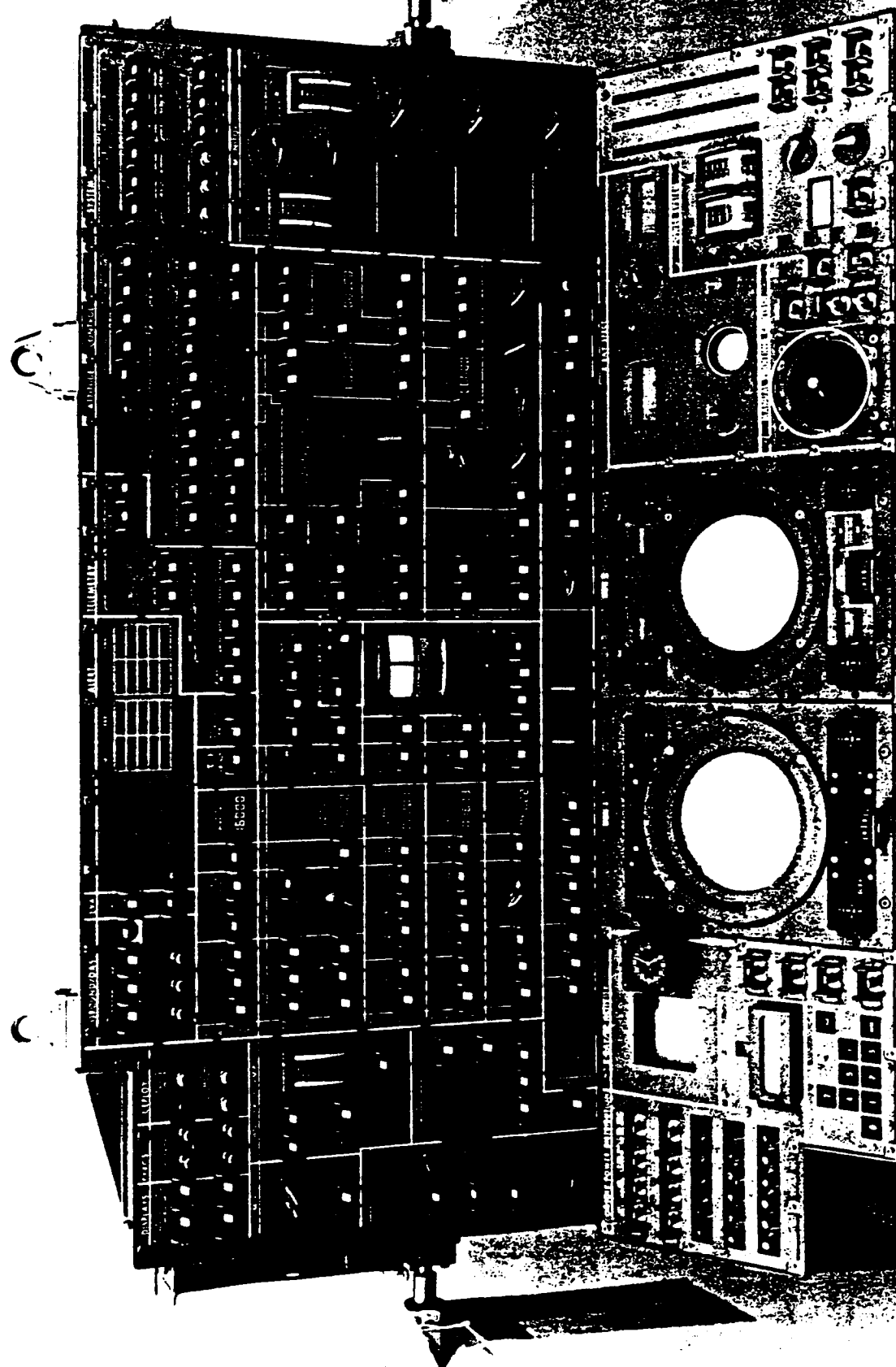
EXPERIMENT	FRAMES AVAILABLE PER LOAD	FRAMES EXPOSED			
		Skylab 2	Skylab 3	Skylab 4	TOTAL
S052	8,025	4,381	15,735	15,802	35,918
S054	6,970	5,155	13,325	13,305	31,785
S056	6,000	4,184	11,493	12,098	27,775
S082A	201	220	402	402	1,024
S082B	1,608	1,608	3,195	1,608	6,411
H-Alpha 1	15,400	12,998	30,787	24,400	68,185
TOTAL	38,204	28,546	74,937	67,615	171,098

ATM CONTROL AND DISPLAY CONSOLE

The ATM control panel layout and the related electrical schematics were reviewed to determine what functions were necessary to control and monitor the ATM telescopes. It is assumed that typical functions would be necessary to control and monitor the HRTC telescopes. After reviewing the capabilities of the Space Station multipurpose application console (MPAC) and comparing them to the projected HRTC requirements it appears that the HRTC can be controlled and monitored from the MPAC using a keyboard, hand controller, and cathode ray tubes provided as standard hardware.

ORIGINAL PAGE
BLACK AND WHITE PHOTOGRAPH

ATM CONTROL AND DISPLAY CONSOLE



DATA AND CONTROL NETWORKS

A data and control network similar to the one shown could be used to control, monitor, and retrieve data from the ASO HRTC. The control and monitoring portion could be built from Space Station developed hardware similar to that used throughout the payload network.

Commands to control the HRTC could be sent from the MPAC in the Space Station, uplinked from ground control, or be preprogrammed into each telescope embedded data processor (EDP) or into the HRTC standard data processor (SDP). The amount of automation could vary depending on the availability of the crew.

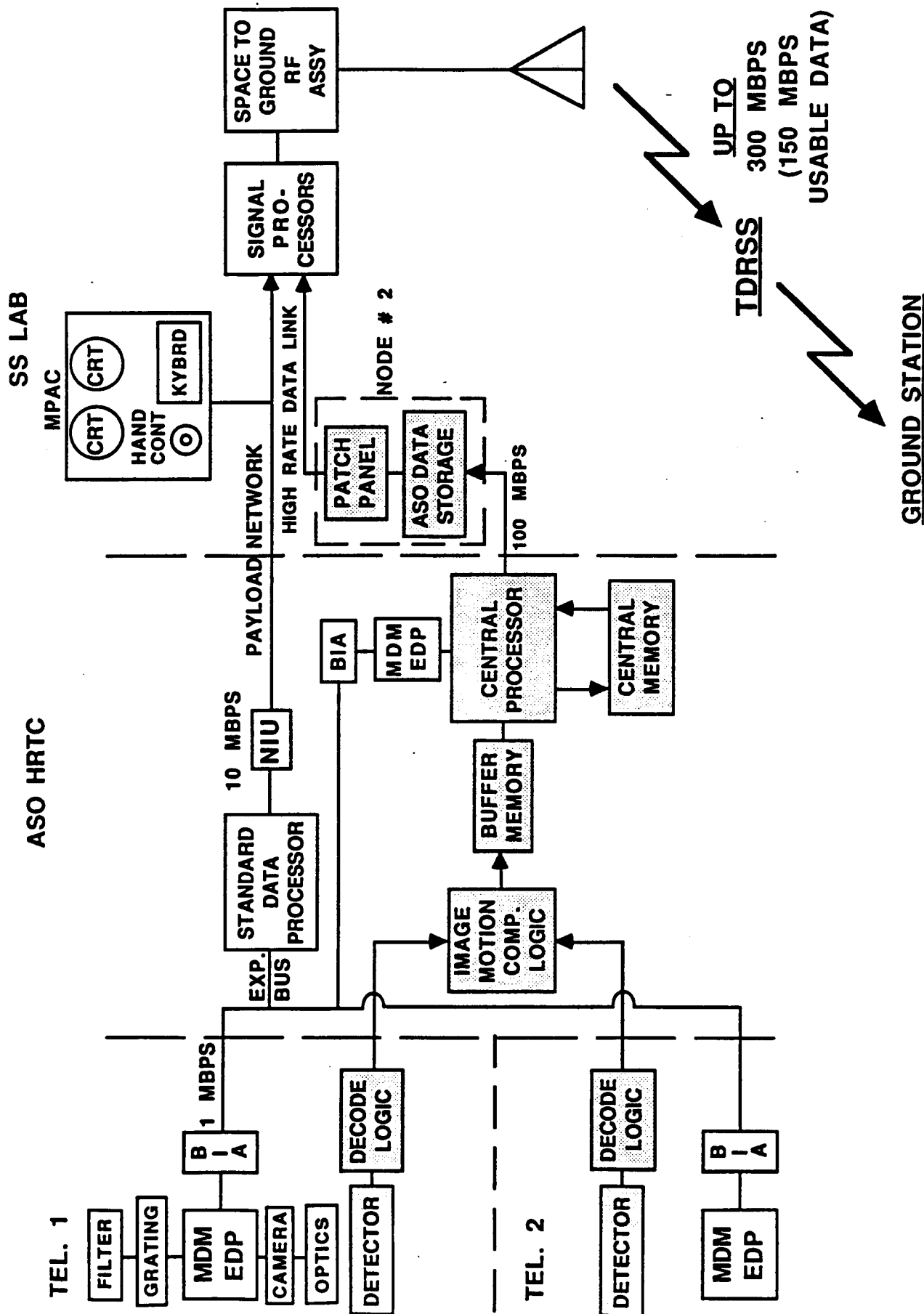
Monitoring of the HRTC would be accomplished by the EDP and SDP with out of tolerance conditions being presented on the MPAC and down linked to the ground station. All measurements could be displayed on command to both MPAC and ground.

Pointing of the HRTC would be accomplished by the payload pointing system (PPS). The PPS would use inputs for pointing from its own instruments, the HRTC and commands from MPAC and the ground station.

Since the high rate data link has no interface with the payload network any data put on the high rate data link cannot be viewed on the MPAC cathode ray tubes. In order to overcome this and let the crew member monitor the pointing a signal can be transmitted from the HRTC central processor through the multiplexer demultiplexer (MDM) to the payload network and the MPAC CRT. The signal would transmit the output of the selected telescope and allow the crew member to decide if the image being received is originating from the desired location on the sun or if another location should be selected. If another location is desired the crew member would use the hand controller on the MPAC to input a signal into the PPS to drive the system to the new location. The progress would be followed by monitoring the output from the telescope on the CRT. A similar approach could be used to control the PPS from the ground station.

The system shown would allow data to be collected by storage on tape, downlinking through TDRSS or exposure on film.

DATA AND CONTROL NETWORKS



RECOMMENDATIONS

- **REFINE DATA COMPRESSION**
- **DEVELOP DATA RECORDER WITH GREATER STORAGE CAPABILITY**
- **USE COMBINATION OF RECORDER AND FILM TO STORE DATA**
- **DESIGN ASO FOR CREW EVA AND ROBOTICS FILM REPLACEMENT**
- **DOWNLINK ENOUGH DATA TO MANAGE VIEWING PROGRAM
NEGOTIATE ADDITIONAL DATA ON A DAY TO DAY BASIS**
- **DON'T DEPEND ON ACCESS TO TDRSS FOR SUCCESS OF
MISSION**

COLLISION AVOIDANCE

POF ON PPS

This chart presents the mass properties and various derived quantities for each of the P/OF configurations analyzed, assuming the use of the Space Station PPS. There are three basic variations: Different experiment complements; Boom or cylindrical shell structure; and lightening of the lower end structure with consequent center of mass located forward of the gimbal. Configurations 1, 2, & 5 use the baseline boom; 3, 4, & 6 use the cylindrical shell. Configurations 5 & 6 are identical to 1 & 3 respectively except that 5 & 6 have lighter support structures and therefore are not cg mounted.

Maximum slew torque (and the corresponding tip displacement) is determined by the requirement to stop, return and accelerate during the shortest orbit dark period.

Maximum tracking torque and tip displacement are determined by the worst case azimuth and elevation accelerations during azimuth-elevation tracking (beta greater than 15 degrees).

Emergency stop conditions assume P/OF angular velocity is limited to less than 1 deg/sec, and shock absorbing mechanical stops are provided that induce less than 1000 newton-meters torque into P/OF. This results in 4.5 degrees of gimbal travel after hitting the stops.

Maximum torque values assume the gimbal drives produce 100 newton-meters torque.

POF ON PPS

CONFIGURATION	1	2	3	4	5 *	6 *
INSTRUMENT	RMC	FTI	RMC	FTI	RMC	RMC
INSTRUMENT MASS (kg)	1200	165	1200	165	1200	1200
INSTRUMENT		CAI		CAI		
INSTRUMENT MASS (kg)		540		540		
INSTRUMENT		WLC		WLC		
INSTRUMENT MASS (kg)		231		231		
INSTRUMENT		UVCS		UVCS		
INSTRUMENT MASS (kg)		410		410		
INSTRUMENT						
INSTRUMENT MASS (kg)						
TIP MASS (kg)	210	109	197	96	210	197
BOOM MASS (kg)	61	61	218	218	61	218
TOTAL MASS (kg)	5950	4195	7613	5681	2073	2159
MOI About Cross-Elevation, Ixx (kg-m ²)	6.26E5	3.56E5	7.40E5	4.69E5	6.03E5	7.07E5
MOI About Elevation, Iyy (kg-m ²)	6.26E5	3.56E5	7.40E5	4.69E5	6.03E5	7.08E5
MOI About Roll, Izz (kg-m ²)	4.52E3	4.68E3	7.52E3	7.56E3	1.49E3	3.26E3
Ixy (kg-m ²)	5.59E-9	1.90	3.33E1	-5.37E1	-1.12E-8	3.33E1
Ixz (kg-m ²)	2.64	-3.98E2	2.64	7.78E2	2.64	2.64
Iyz (kg-m ²)	-2.45E3	5.06E3	-8.55E2	3.58E3	-2.45E3	-8.55E2
MAX SLEW TORQUE (Nm)	7.25	4.12	8.57	5.43	6.98	8.20
MAX SLEW TIP DISPLACEMENT (mm)	21.22	11.45	3.79E-2	2.18E-2	21.24	3.79E-2
MAX TRACKING TORQUE (Nm)	8.08	4.59	9.55	6.05	7.78	9.13
MAX TRACKING TIP DISPLACEMENT (mm)	23.64	12.77	4.23E-2	2.43E-2	23.66	4.23E-2
EMERGENCY STOP TIP DISPLACEMENT (mm)	3556.44	1920.05	6.35	3.66	3556.44	6.35
EMERGENCY STOP MAX BENDING MOMENT (Nm)	1098.86	602.87	1235.33	739.34	1098.86	1235.33
MAX TORQUE TIP DISPLACEMENT (mm)	292.98	278.14	4.43E-1	4.02E-1	304.16	4.63E-1
MAX TORQUE BENDING MOMENT (Nm)	90.52	87.33	86.09	81.30	93.98	89.98

* CONFIGURATIONS 5 AND 6 ARE NOT CG-MOUNTED.

POF ON BPS

This chart is similar to the previous one, except that a base-mounted pointing system is assumed rather than the cg mounted PPS.

POF ON BPS

CONFIGURATION	7	8	9	10	11	12
INSTRUMENT	RMC	RMC	FTI	FTI	FTI	FTI
INSTRUMENT MASS (kg)	1328	1328	680	680	720	720
INSTRUMENT			CAI	CAI	CAI	CAI
INSTRUMENT MASS (kg)			680	680	1280	1280
INSTRUMENT			UVCS	UVCS	Bragg	Bragg
INSTRUMENT MASS (kg)			410	410	240	240
INSTRUMENT			WLUV	WLUV		
INSTRUMENT MASS (kg)			231	231		
INSTRUMENT						
INSTRUMENT MASS (kg)						
TIP MASS (kg)	303	290	169	156	157	144
BOOM MASS (kg)	61	264	61	264	61	264
TOTAL MASS (kg)	3786	3962	4995	5128	4552	4685
MOI About Cross-Elevation, Ixx (kg-m ²)	9.58E5	1.13E6	5.57E5	7.31E5	5.38E5	7.14E5
MOI About Elevation, Iyy (kg-m ²)	9.58E5	1.13E6	5.57E5	7.31E5	5.36E5	7.12E5
MOI About Roll, Izz (kg-m ²)	4.09E3	8.82E3	7.14E3	1.18E4	7.25E3	1.17E4
Ixy (kg-m ²)	2.19E2	2.19E2	5.38E2	5.38E2	-1.58E3	-1.39E3
Ixz (kg-m ²)	-2.00E2	-2.00E2	-7.01E1	-7.01E1	2.65E3	5.16E2
Iyz (kg-m ²)	7.90E3	4.22E3	6.02E3	2.13E3	5.62E3	1.35E3
MAX SLEW TORQUE (Nm)	11.09	13.09	6.45	8.46	6.23	8.27
MAX SLEW TIP DISPLACEMENT (mm)	32.37	5.84E-2	18.53	3.56E-2	17.27	3.35E-2
MAX TRACKING TORQUE (Nm)	----	----	----	----	----	----
MAX TRACKING TIP DISPLACEMENT (mm)	----	----	----	----	----	----
EMERGENCY STOP TIP DISPLACEMENT (mm)	5423.88	9.78	3102.79	5.96	2894.94	5.62
EMERGENCY STOP MAX BENDING MOMENT (Nm)	1668.14	1891.77	964.62	1188.25	901.62	1125.25
MAX TORQUE TIP DISPLACEMENT (mm)	145.99	2.23E-1	143.64	2.10E-1	138.75	2.03E-1
MAX TORQUE BENDING MOMENT (Nm)	44.90	43.17	44.65	41.91	43.21	40.64

SOLAR POINTING VOLUME

This chart shows the computer model used to evaluate the potential for collision between P/OF and Space Station elements. Following this chart are four sets of three charts showing the results of the analysis. The same computer model of the Space Station is used as was used for the view analysis.

The first chart in each set of three (labeled P/OF Collision Potential) shows the view from the PPS center of rotation after a sphere of 50 m radius is centered on the PPS center of rotation. This sphere blocks the view of anything not reachable by the P/OF boom, so that anything visible is a candidate for collision.

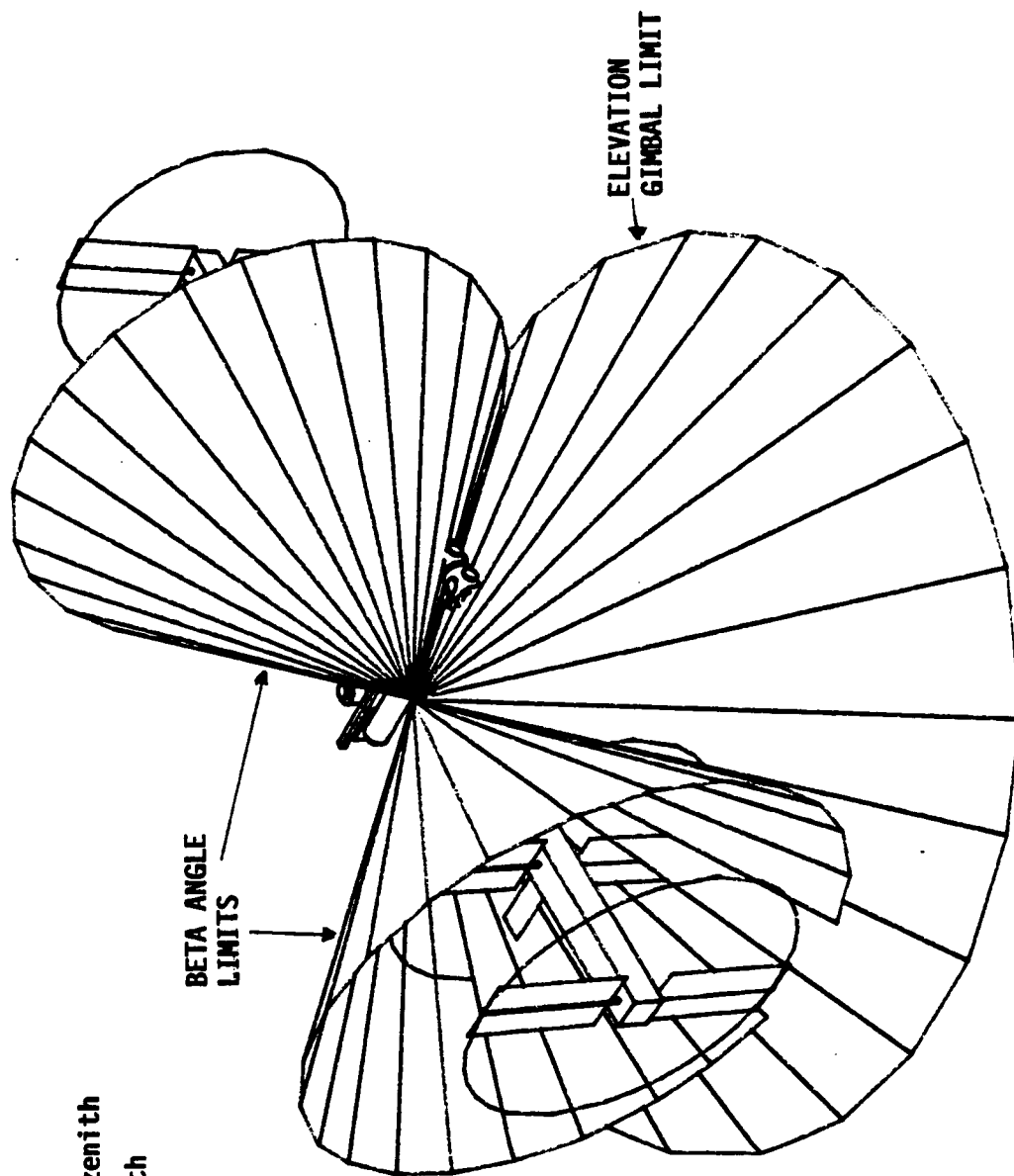
The second chart in each set (labeled Limited by Gimbal Stops) shows the view after adding a 60 degree half angle cone centered on the nadir, which excludes the region protected by proposed mechanical gimbal stops, allowing for the maximum predicted bending of the P/OF boom. It should be noted here that if sun tracking is terminated when the tangent point altitude is 90 km, P/OF travel would normally stop 8 degrees above this cone at approximately 112 degrees from the zenith.

The third chart in each set (labeled Normal Operating Range) also excludes the two horizontal cones which correspond to the maximum possible beta angle for 28.5 degrees inclination.

The four sets of charts correspond to starboard and port views from starboard and port mounting locations, as labeled.

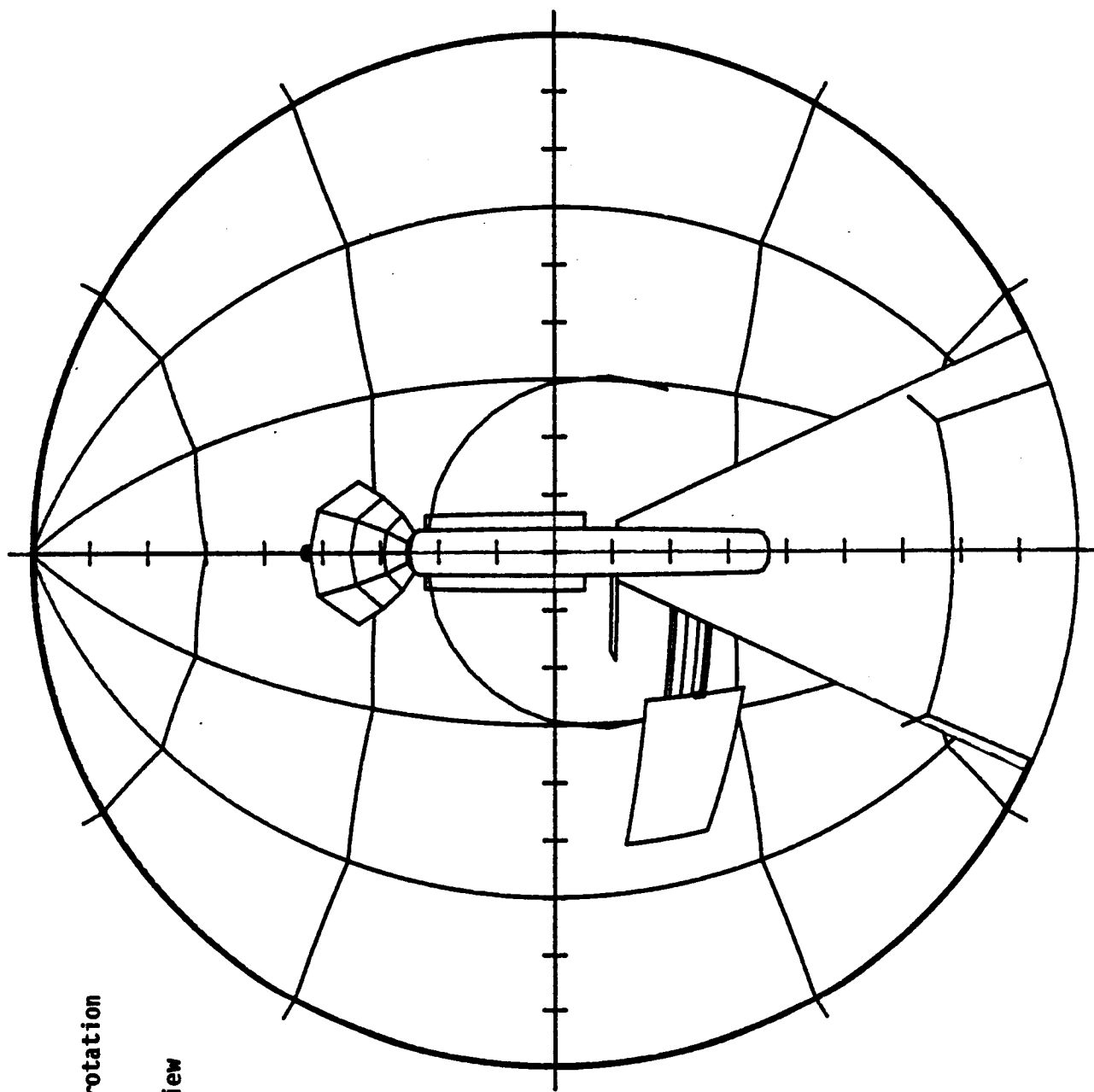
SOLAR POINTING VOLUME

- 28.5 degree orbit inclination
- Maximum beta angle 52°
- Gimbal limit 120 degree from zenith
- Horizon 112 degrees from zenith



P/OF COLLISION POTENTIAL

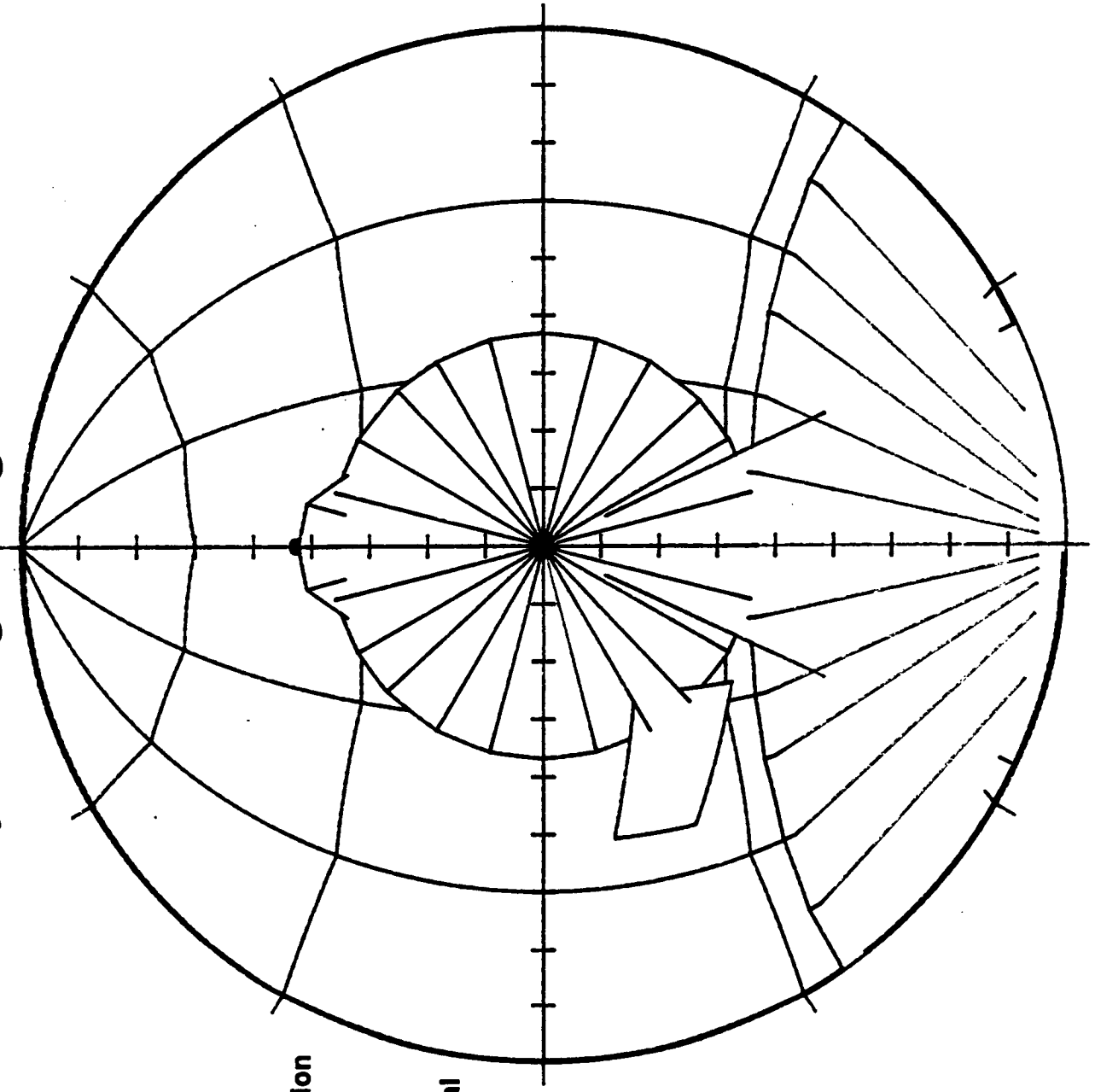
- View from PPS center of rotation to port
- Hemispherical field-of-view
- Port mounting
- Everything visible is within reach of 50-m boom



-

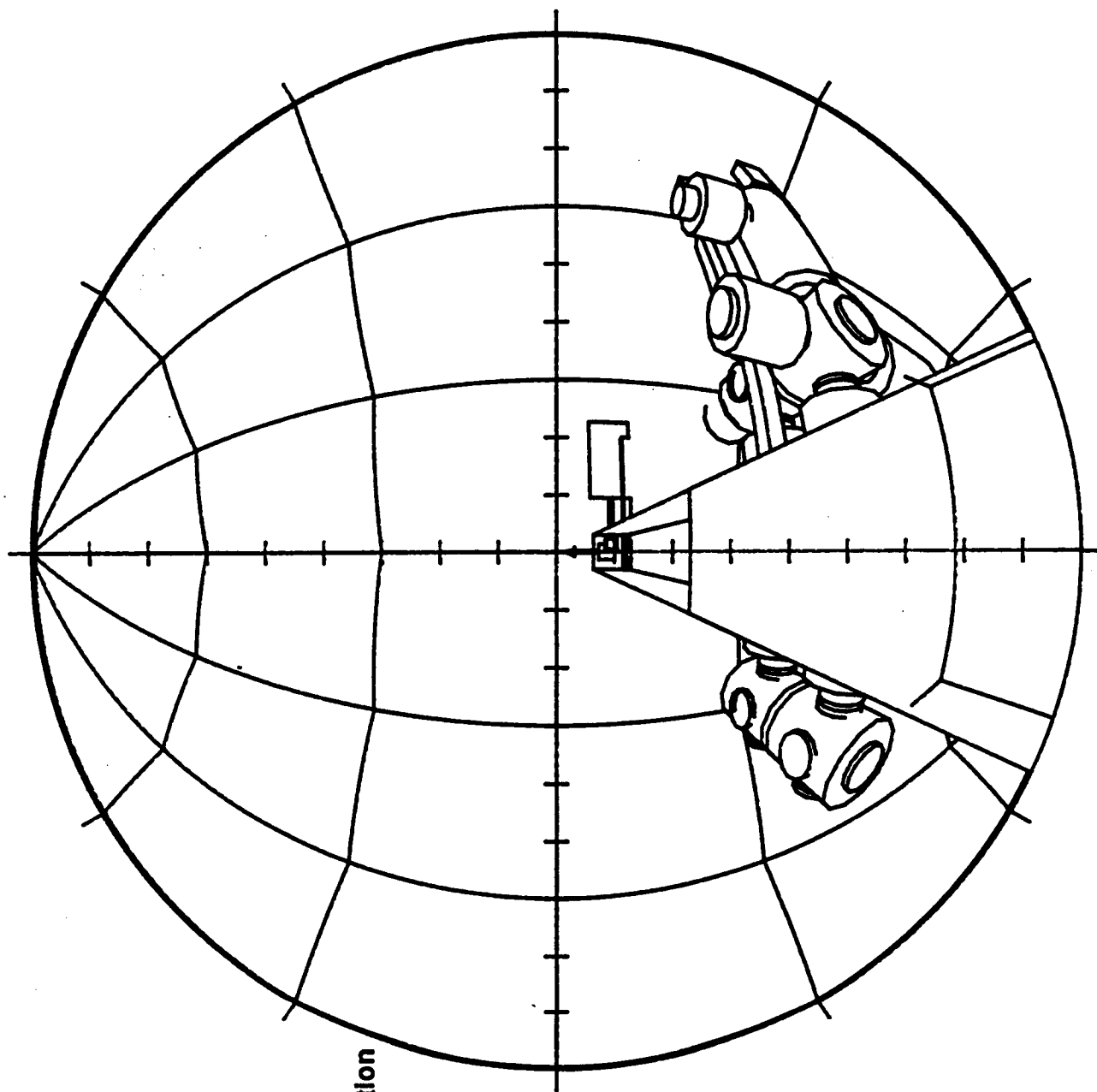
P/OF COLLISION POTENTIAL

Normal Operating Range



- View from PPS center of rotation to port
- Hemispherical field-of-view
- Port mounting
- Limited by 50-m radius, gimbal stops plus contingency, and maximum beta

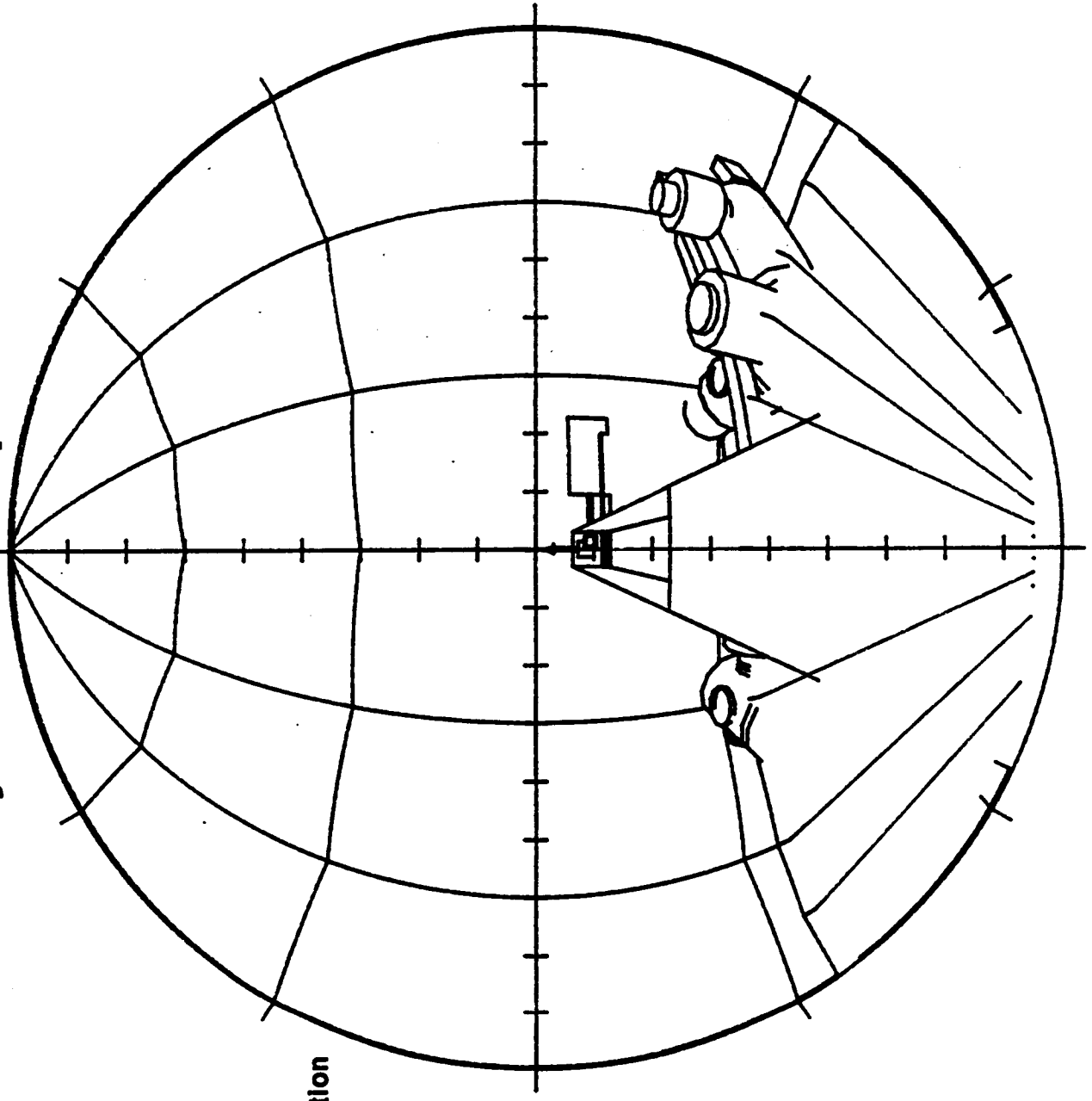
P/OF COLLISION POTENTIAL



- View from PPS center of rotation to starboard
- Hemispherical field-of-view
- Port mounting
- Everything visible is within reach of 50-m boom

P/OF COLLISION POTENTIAL

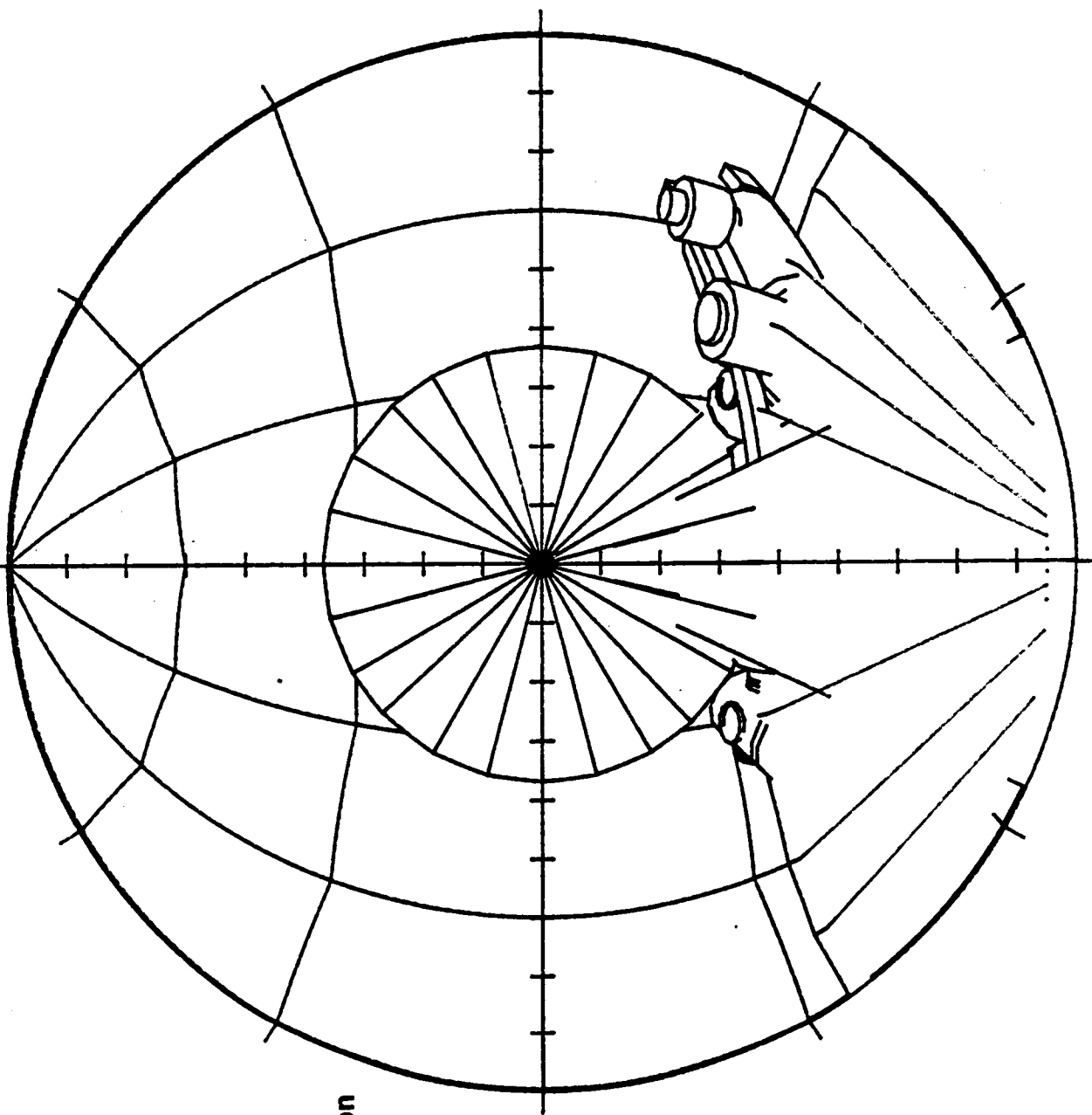
Limited by Gimbals Stops



- View from PPS center of rotation to starboard
- Hemispherical field-of-view
- Port mounting
- Limited by 50-m radius and 120-deg. gimbal stops (plus 4-m contingency tip motion)

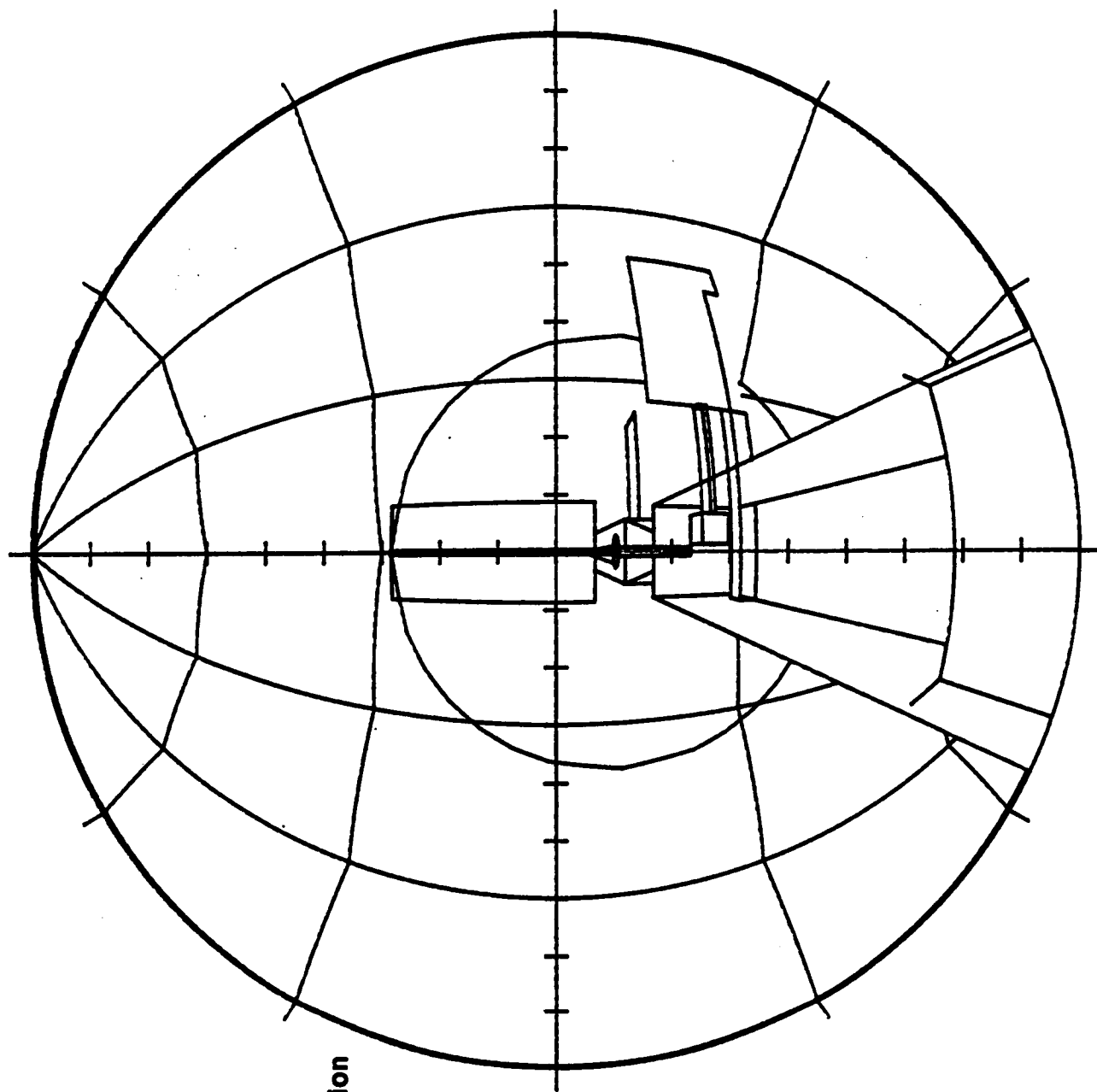
P/OF COLLISION POTENTIAL

Normal Operating Range



- View from PPS center of rotation to starboard
- Hemispherical field-of-view
- Port mounting
- Limited by 50-m radius, gimbal stops plus contingency, and maximum beta

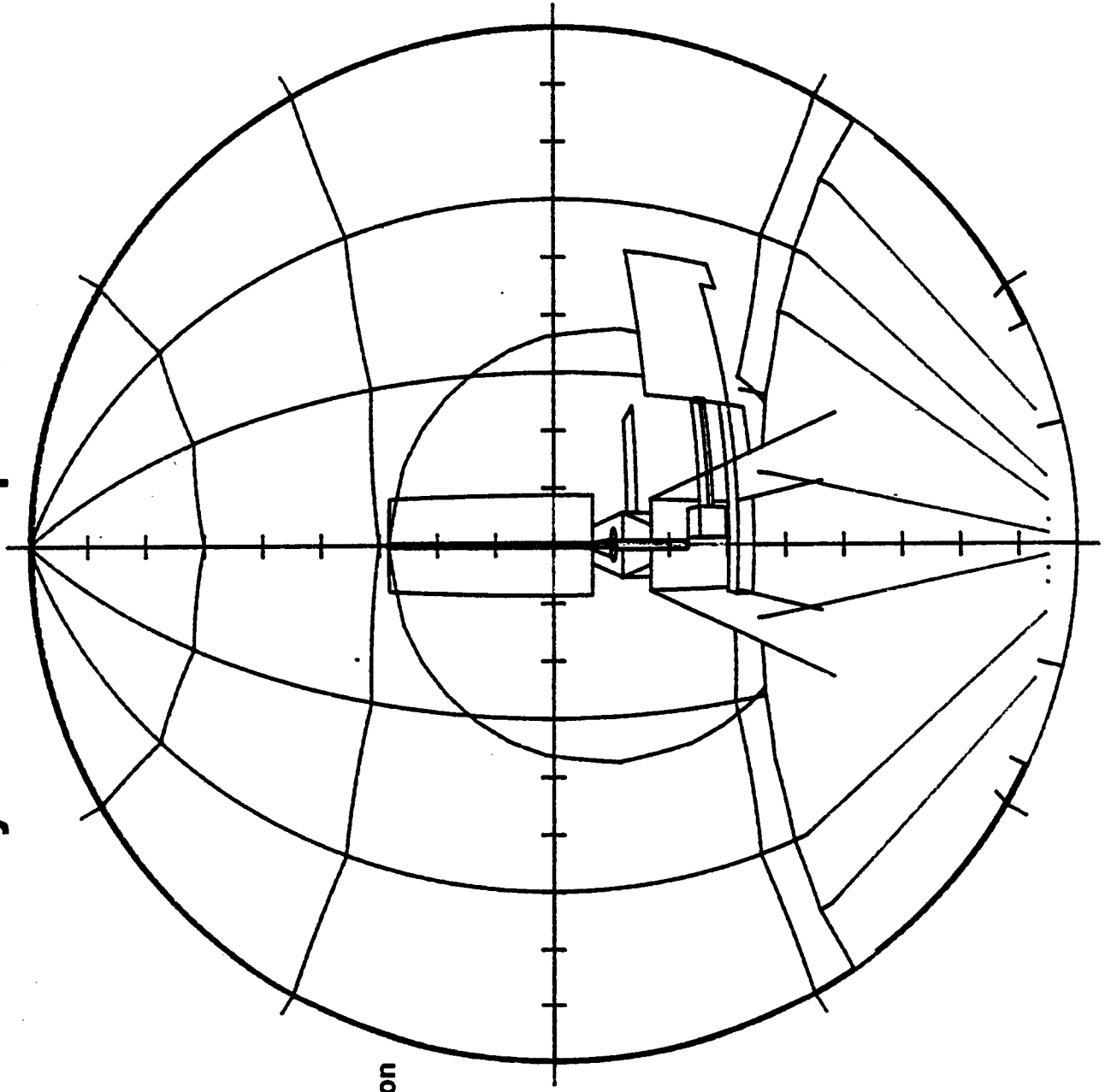
P/OF COLLISION POTENTIAL



- View from PPS center of rotation to starboard
- Hemispherical field-of-view
- Starboard Mounting
- Everything visible is within reach of 50-m boom

P/OF COLLISION POTENTIAL

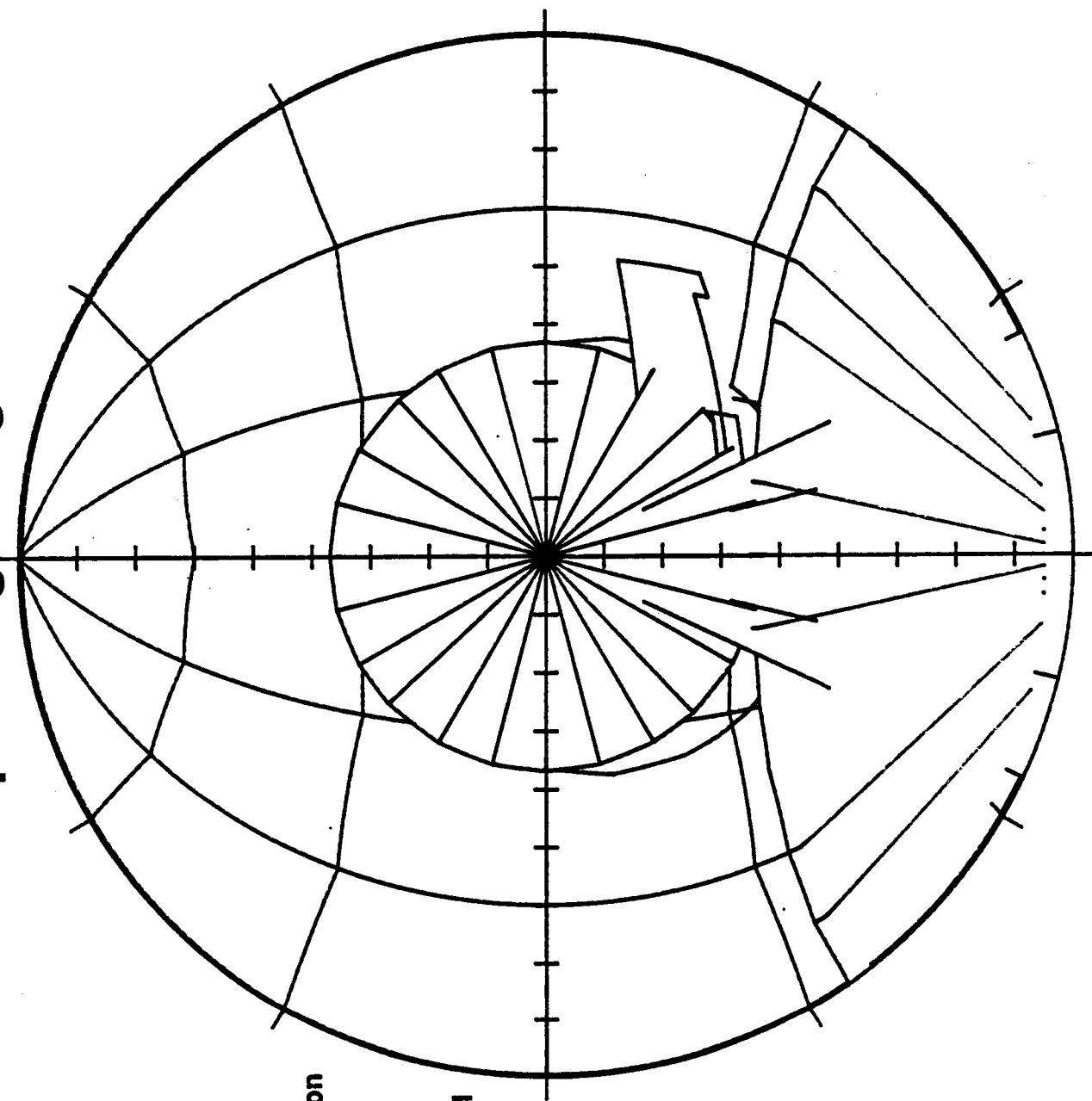
Limited by Gimbal Stops



- View from PPS center of rotation to starboard
- Hemispherical field-of-view
- Starboard mounting
- Limited by 50-m radius and 120-deg. gimbal stops (plus 4-m contingency tip motion)

P/OF COLLISION POTENTIAL

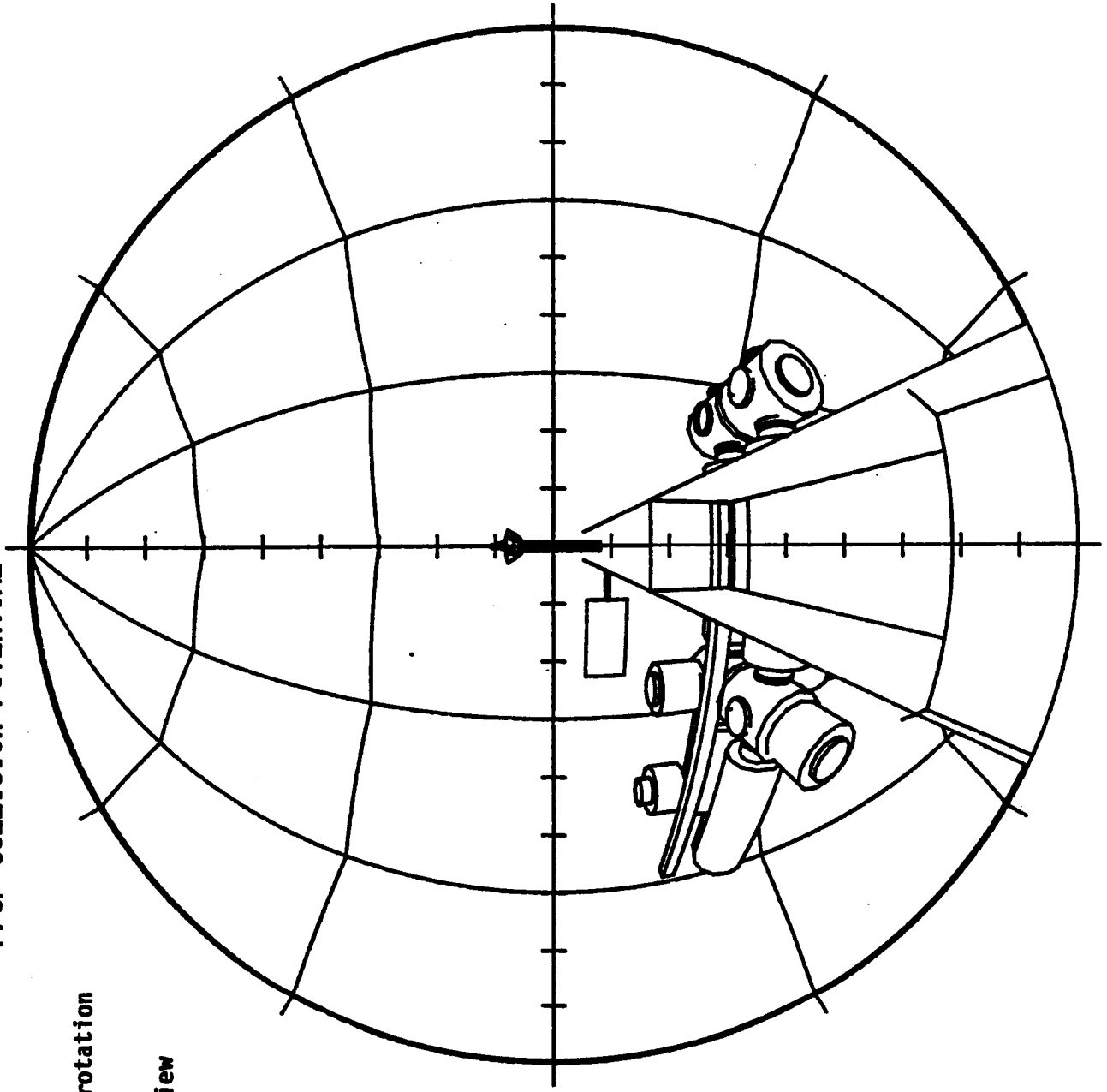
Normal Operating Range



- View from PPS center of rotation to starboard
- Hemispherical field-of-view
- Starboard mounting
- Limited by 50-m radius, gimbal stops plus contingency, and maximum beta

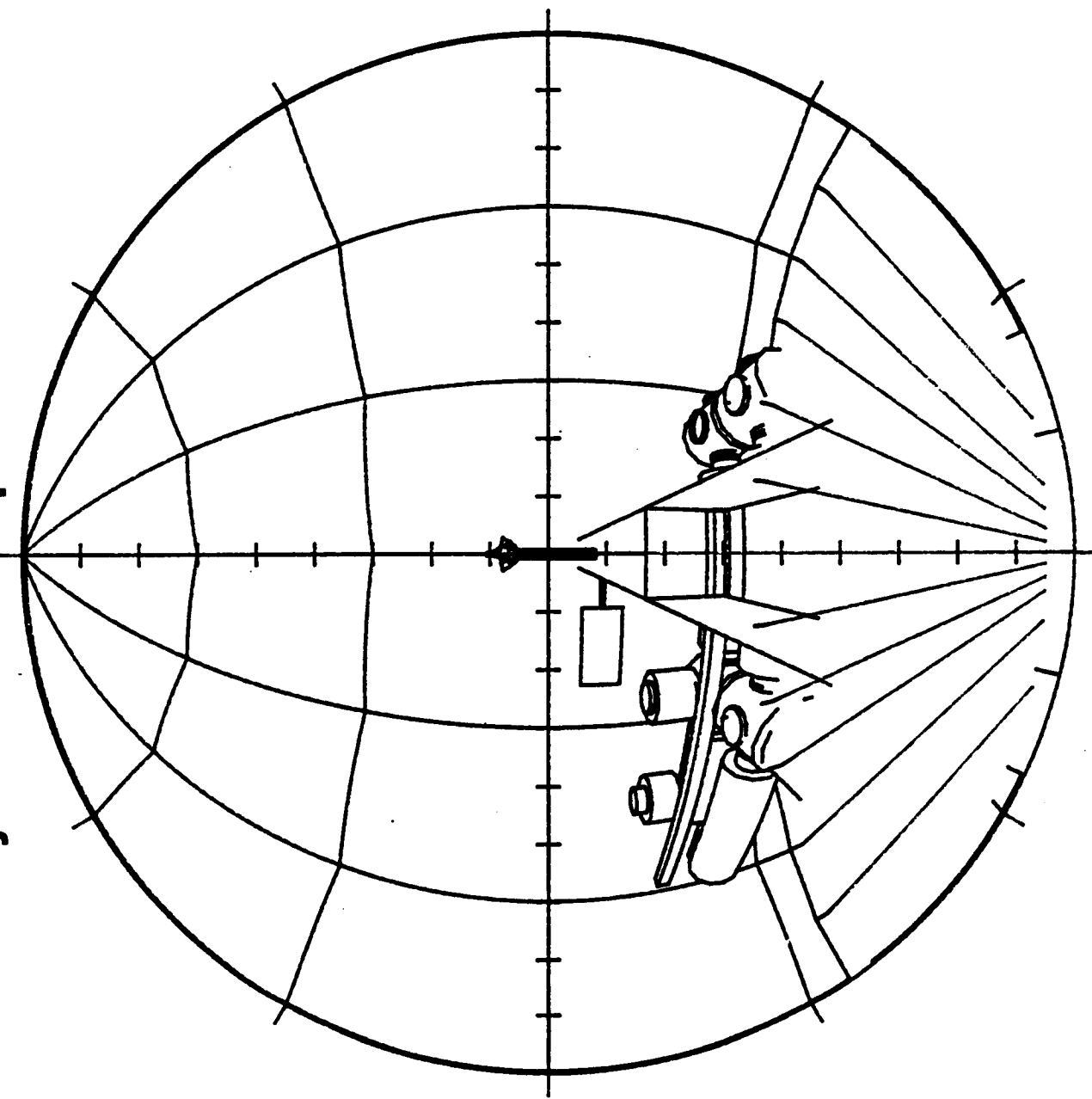
P/OF COLLISION POTENTIAL

- View from PPS center of rotation to port
- Hemispherical field-of-view
- Starboard mounting
- Everything visible is within reach of 50-m boom



P/OF COLLISION POTENTIAL

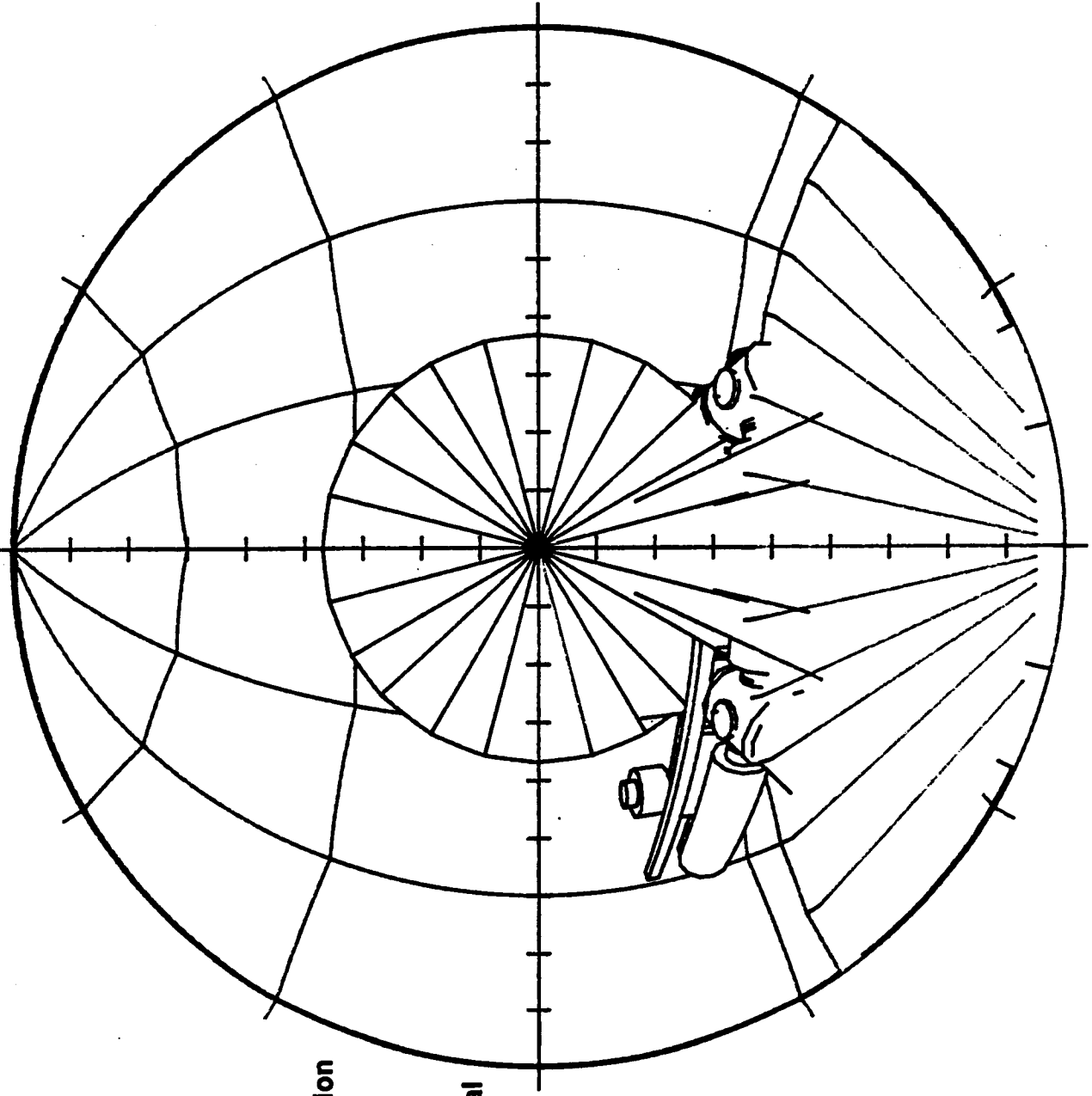
Limited by Gimbals Stops



- View from PPS center of rotation to port
- Hemispherical field-of-view
- Starboard mounting
- Limited by 50-m radius and 120-deg. gimbal stops (plus 4-m contingency tip motion)

P/OF COLLISION POTENTIAL

Normal Operating Range



- View from PPS center of rotation to port
- Hemispherical field-of-view
- Starboard mounting
- Limited by 50-m radius, gimbal stops plus contingency, and maximum beta

SUMMARY

CRITICAL ISSUES

This chart summarizes the approaches available to alleviate concerns over critical issues.

Several approaches to handle the high rate and large volume of HRTC data are possible. On board storage and return only affects the scientists through the limitation on real time data availability. Data compression, if limited to techniques which can be exactly reversed, also does not affect the scientists. However, no exact compression technique currently exists which will completely eliminate the data rate problems. Film will affect operation scenarios as well as data storage, primarily because it is not erasable and reusable, and because it must be physically located within the instrument. The remaining two possibilities involve selective retention of data, and therefore require the active participation of the scientists.

P/OF boom dynamics and control are not a major concern. Either the pointing mount, or boom mounted angular momentum exchange devices can be used to damp out vibrations. Gimbal motor torques are not capable of damaging the boom. As an alternative to the boom, we have investigated a concept for a cylindrical shell which is stiffer than the boom. The shell concept appears viable, but unnecessary.

Contamination/debris protection can be achieved using standard techniques. Contamination monitors are desirable to supplement knowledge of scheduled contamination producing events. Since many of the instruments operate in the x-ray and gamma-ray range, transparent windows to protect the telescope interiors are feasible.

Although the Space Station PPS will not directly satisfy the pointing requirements of HRTC, optical or electronic image motion compensation techniques exist which will bridge the gap. Comparing the High Energy Facility requirements to the Gamma Ray Observatory currently being built, we expect the pointing requirements to increase substantially before implementation.

Collision avoidance is a prime concern for P/OF, since the 50 m boom is potentially capable of reaching most components of the Space Station. Only small parts of the Space Station protrude into the volume which would be swept out by P/OF during normal operations. Other payloads may be a more significant problem. Off-nominal operation is the major problem. This will require a combination of software and hardware constraints on gimbal operation. Gimbal range limits will need to be implemented, and gimbal rates must be limited to avoid buckling of the boom when a hard stop is encountered. Gimbal torque alone is not capable of buckling (or even excessively bending) the boom.

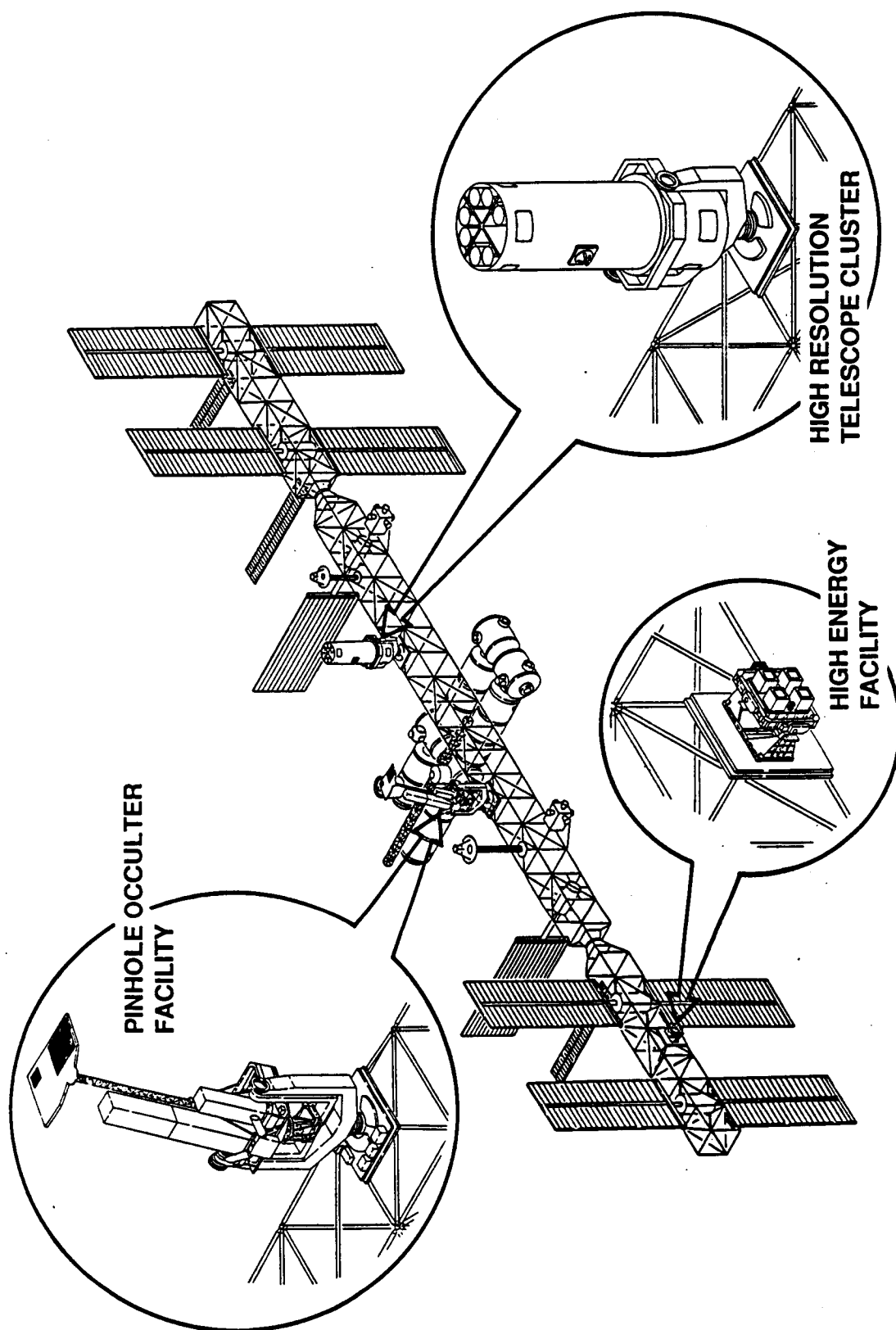
CRITICAL ISSUES

- o HRTC Data Rate and Volume
 - Temporary storage on board with selective archiving
 - Active selection and editing of images
 - Data compression
 - On board storage and return
 - Film
- o P/OF Boom Dynamics and Control
 - Effect of off-center boom
 - Cylindrical shell structure
- o Contamination/Debris Protection
 - Motorized doors
 - Transparent windows
 - Sandwich construction for P/OF mask
 - Contamination monitors
- o Pointing
 - Active mirrors and/or electronic IMC for HRTC
 - PPS for P/OF (roll ring may be added)
 - Moderate accuracy gimbal adequate for High Energy Facility
 - Single axis tilt table adequate for High Energy Facility outside alpha joint
- o Collision Avoidance
 - Operational constraints
 - Software limits on gimbal range and rate
 - Hardware stops on gimbal

ADVANCED SOLAR OBSERVATORY

A viable concept for ASO on the Space Station is shown in this chart. Note that the P/OFF boom is shown in a retracted position.

ADVANCED SOLAR OBSERVATORY



DUAL KEEL SPACE STATION

The dual keel Space Station concept was briefly examined to identify the differences in accommodations that should be expected. In most areas, the results are that the characteristics of the upper boom are different than the transverse boom, but not grossly different.

Dynamics is the one area where the upper boom could potentially be significantly inferior to the transverse boom for a large pointed payload such as P/OF. This is not certain, but the dynamics are unlikely to be significantly better on the upper boom.

Field of view is not noticeably different for solar viewing payloads. Both locations will be constrained primarily by other payloads.

Contamination should be better on the upper boom since it is further from the major sources. Other payloads may affect this conclusion, however.

If servicing capability is provided by the Space Station, the only difference appears to be transit time. This could be significant for EVA, however.

While the thermal environment will be different on the upper truss, there is no indication that it will be significantly more stressful.

The upper truss only eliminates the possibility of P/OF contacting the modules. The solar arrays, station structure, other payloads, and antennas on the truss are still within reach.

DUAL KEEL SPACE STATION

- o Dynamics
 - Center of gravity mounting more critical
 - P-OF boom disturbances more severe
- o Field of View
 - Upper boom location better than main truss
- o Contamination
 - Further from contamination sources on upper boom
 - No change in natural or debris environment
- o Servicing
 - Further from modules
 - More time required
- o Thermal
 - Environment different on upper truss
 - No more stressful
- o Collision Avoidance
 - Collision with module not possible
 - All other collision potentials remain

CONCLUSIONS

The conclusion of this study is that all three components of ASO could be accommodated on the Space Station. Some very interesting engineering challenges will be encountered in the implementation, but multiple concepts exist for alleviating concerns. Each of these concepts appears feasible from an engineering standpoint.

CONCLUSIONS

- o All three facilities are possible
 - Interesting engineering challenges exist
 - All appear to be solvable
 - Multiple implementation concepts exist for the most severe challenges
- o High Energy Facility
 - Easiest to accommodate, no accommodation drivers
 - Best location is outboard of alpha joint
 - if resources can be obtained
 - single axis tilt table needed
 - Requirements expected to grow before implementation
- o High Resolution Telescope Cluster
 - Data is the major accommodation driver
 - Several accommodation concepts appear feasible
- o Pinhole/Occulter Facility
 - Boom dynamics are the major accommodation driver
 - Dynamics will be significantly worse on upper boom
 - Significant safety concerns can be alleviated



Report Documentation Page

1. Report No.		2. Government Accession No.		3. Recipient's Catalog No.	
4. Title and Subtitle Advanced Solar Observatory (ASO) Accommodations Requirements Study Final Report				5. Report Date May 1989	
				6. Performing Organization Code	
7. Author(s)				8. Performing Organization Report No.	
				10. Work Unit No.	
9. Performing Organization Name and Address Teledyne Brown Engineering 300 Sparkman Drive NW P.O. Box 070007 Huntsville, AL 35807-7007				11. Contract or Grant No. NAS8-37128	
				13. Type of Report and Period Covered Final	
12. Sponsoring Agency Name and Address George C. Marshall Space Flight Center National Aeronautics and Space Administration Marshall Space Flight Center, AL 35812				14. Sponsoring Agency Code	
15. Supplementary Notes					
16. Abstract This report presents the results of an accommodations analysis for the Advanced Solar Observatory on Space Station Freedom. Concepts for the High Resolution Telescope Cluster, Pinhole/Occluder Facility, and High Energy Cluster were developed which can be accommodated on Space Station Freedom. It is shown that workable accommodations concepts are possible. Areas of emphasis for the next stage of engineering development are identified.					
17. Key Words (Suggested by Author(s)) Advanced Solar Observatory, Solar Physics, Sun, Space Station, HRTC, P/OF				18. Distribution Statement Unclassified - Unlimited	
19. Security Classif. (of this report) Unclassified		20. Security Classif. (of this page) Unclassified		21. No. of pages 426	22. Price A19*